DEVELOPMENT AND EVALUATION OF HUMAN *EX VIVO* NORMOTHERMIC MACHINE LIVER PERFUSION FOR VIABILITY TESTING AND INVESTIGATION OF THE ROLE OF TWEAK/FN14 IN ISCHAEMIA REPERFUSION INJURY.

by

BARNABY T. F. STEPHENSON

A thesis submitted to
The University of Birmingham
for the degree of
DOCTOR OF PHILOSOPHY

School of Immunology and Immunotherapy
College of Medical and Dental Sciences
The University of Birmingham
January 2018

Abstract

Liver disease is characterised by ongoing inflammation and regeneration the mechanism of which is incompletely understood, although the Fn14/TWEAK receptor-ligand system may play a role in cholangiopathies. Currently, the only treatment for end stage disease is transplantation.

This thesis describes the development of *ex vivo* Normothermic Machine Liver Perfusion of discarded human livers for viability testing, before validation by transplantation and assessment as a novel model of ischaemia-reperfusion injury. Biliary epithelial cells were isolated, Fn14 expression determined and functional activity of Fn14 stimulation by TWEAK established using existing *in vitro* modelling. *Ex vivo* Normothermic Machine Liver Perfusion was evaluated as a model of Fn14 expression. Perfusate lactate $<$2.0mmol/L after 2 hours of normothermic perfusion and delta lactate concentrations were key determinants in the viability of discarded human livers. Viability could be predicted earlier using proteomics at commencement of perfusion. Evolution of this model included using a bovine haemoglobin-based oxygen carrier as the perfusate and successful liver splitting with concurrent perfusion. This *ex vivo* human system then investigated the potential role of Fn14 in this newly established, validated model.

Normothermic Machine Liver Perfusion has a significant role in determining viability of discarded human livers and establishing the Machine Criteria Donor.

This thesis is dedicated to my Mum and Dad (1931-2012). Only with your sustained presence in body, mind and spirit has this been achieved.

ACKNOWLEDGEMENTS

I would like to thank Professor Philip Newsome and Mr. Simon Bramhall for giving me the opportunity to conduct research at the University of Birmingham in addition to Mr. Michael Hallissey for his support as the Training Programme Director. I am grateful to my Supervisors, Dr. Simon Afford and Professor David Adams, for all their expertise and mentorship throughout this period of research as well as Dr. Linda Burkley for collaborating on Fn4/TWEAK. I am indebted to Bridget Gunson and the NIHR Birmingham Liver Biomedical Research Unit & Centre for Liver Research, the College Research and Development Fund at the University of Birmingham, The Liver Foundation, Queen Elizabeth Hospital Birmingham Charities and the Medical Research Council for the logisitical and financial support these organisations have provided during my studies.

I am grateful to the Machine Perfusion Group led by Dr. Simon Afford and Professor Darius Mirza including: Mr. Ricky Bhogal, Mr. Yuri Boteon, Dr. Anna Casey, Dr. Rob Cramb, Dr. Miruna David, Miss. Janine Fear, Professor Stefan Hübscher, Dr. Elizabeth Humphreys, Miss. Amanda Kirkham, Mr. Richard Laing, Dr. Anna Massey, Mr. Hynek Mergental, Dr. Desley Neil, Mr. Thamara Perera, Dr. Gary Reynolds, Miss. Andrea Schlegel, Ms. Amanda Smith and Miss. Jeannette Widmer; with significant contributions from Professor Paolo Muiesan, Mr. John Isaac, Mr. Keith Roberts, Mr. Manuel Abradelo, Mr. Robert Sutcliffe, Mr. Ravi Marudanayagam and Mrs. Sarah Banks, for their assistance during my endeavours to develop and nuture normothermic machine liver perfusion. Photographs in Figure 2.1 were provided by the Machine Perfusion Study Group. Plots of individual parameters and secondary statistical anal-

ysis of the perfusion data in Chapter 2 were kindly performed by Amanda Kirkham, statistician at the University of Birmingham, and relevant graphs generated from that analysis have been presented in this thesis. There is special thanks to Professor Stefan Hübscher, Dr. Simon Afford, Dr. Desley Neil and Dr. Gary Reynolds for facilitating the histological assessment and analysis. Mr. Yuri Boteon, Mr. Richard Laing and Mrs. Lorraine Wallace kindly performed ATP experiments. Mr. Ricky Bhogal performed the preclinical element of the perfusions using the acellular fluid. Support in developing cell surface proteomics analysis is directly attributed to Dr. Ashley Martin, whilst perfusate proteomics and metabolomics would not have possible without the contributions of Mrs. Lorraine Wallace and Dr. Warwick Dunn respectively. The technical assistance from Mr. Scott Davies, Mr. Tom Bean and Dr. Robert Shaw with respect to slide scanning has been invaluable.

Specifically, I would like to thank Professor Lola Reid at the University of North Carolina, Chapel Hill, her laboratory staff and her family, for their kindness, generosity and intellectual discussions surrounding the future of liver research both during and since my Travel Award gifted by the College of Medical and Dental Sciences Research Development Fund. Mr. Ricky Bhogal has not only been a colleague but also a friend during my research, providing scientific and clinical expertise as well as a working relationship that will continue throughout our careers. To my work colleagues, thank you for your flexibility. To my close friends and chums, thank you for your conversations of all types, pastoral care and above all kindness. I will always remember you.

This work would not have been possible without the incredible gift from our organ donors and their families, the donor hospitals, transplant coordinators, retrieval teams and transplant surgeons, as well as the anaesthetic, theatre, nursing and administrative staff from the Liver Unit at the Queen Elizabeth Hospital Birmingham. Good luck for the next 5000 liver transplants.

CONTENTS

LIST OF FIGURES

LIST OF TABLES

LIST OF ABBREVIATIONS

7-AAD 7-Aminoactinomycin D

ABG Arterial Blood Gases

AFP Alpha-feto Protein

AGC Automatic Gain Control

AIC Akaike Information Criterion

AKN-1 Andreas K Nussler-1

ALD Alcoholic Liver Disease

ALM Actual Liver Mass

ALT Alanine Aminotransferase

ANCOVA Analysis of Covariance

ANOVA Analysis of Variance

AP-1 Activator Protein-1

AST Aspartate Aminotransferase

ATP Adenosine Tri-Phosphate

BAR Balance of Risk

BE Base Excess

BEC Biliary Epithelial Cells

BMI Body Mass Index

BTS British Transplant Society

CD Cluster of Differentiation

CDB Cell Dissociation Buffer

CID Collision Induced Dissociation

CIT Cold Ischaemic Time

CK Cytokeratin

CLM Calculated Liver Mass

CLOD Clinical Lead for Organ Donation

CO_2 Carbon Dioxide

CT Computed Tomography

D-MELD Donor Age and Recipient Model for End stage Liver Disease

DAB 3,3'-Diaminobenzidine

DAMPs Damage Associated Molecular Patterns

DAPI 4',6-diamidino-2-phenylindole

DBD Donation after Brainstem Death

DCD Donation after Circulatory Death

DCF Dichlorodihydrofluorescein

DGF Delayed Graft Function

DLI Donor Liver Index

DMEM Dulbecco's Modified Eagle's Medium

DNA Deoxyribose Nucleic Acid

DPX Distyrene Polystyrene Xylene

DRI Donor Risk Index

DTT Dithiothreitol

EAD Early Allograft Dysfunction

ECD Extended Criteria Donors

ECM Extracellular Matrix

EpCAM Epithelial Cell Adhesion Molecule

ESI Electrospray Ionisation

ET-DRI Eurotransplant Donor Risk Index

FFP Fresh Frozen Plasma

FGF-b Fibroblast Growth Factor-basic

FiO_2 Fraction of Inspired Oxygen

FITC Fluorescein Isothiocyanate

Fn14 Fibroblast Growth Factor-inducible protein 14

GLM Generalised Linear Model

GO Gene Ontology

GTN Glyceryl Trinitrate

H-R Hypoxia-Reperfusion

H&E Haematoxylin & Eosin

HA Hepatic Artery

HAS Human Albumin Solution

HCC Hepatocellular Carcinoma

HEA125 Human Epithelial Antigen 125

HILIC Hydrophilic Interaction Liquid Chromatography

HMP Hypothermic Machine Perfusion

HOPE Hypothermic oxygenated machine perfusion

HRP Horse Radish Peroxidase

HSC Hepatic Stellate Cells

HSEC Human Sinusoidal Epithelial Cells

HTK Histidine-Tryptophan-Ketoglutarate

IC Ischaemic Cholangiopathy

ICAM-1 Intercellular Adhesion Molecule 1

IDA Industrial Denatured Alcohol

IFN-γ Interferon Gamma

ILC Innate Lymphoid Cell

INR Internationalised Normal Ratio

IQGAP1 Ras GTPase-activating-like Protein

IRI Ischaemia Reperfusion Injury

ITBL Ischaemic Type Biliary Lesions

ITU Intensive Therapy Unit

IU International Units

IVC Inferior Vena Cava

JNK c-Jun-N-terminal Kinases

KIM-1 Kidney Injury Molecule-1

LC Lactate Clearing

LOESS Locally Estimated Scatterplot Smoothing

LPC Liver Progenitor Cell

MAPKs Mitogen-Activated Protein Kinases

MCD Machine Criteria Donor

MDC Monodansylcadaverine

MELD Model of End Stage Liver Disease

MFI Median Fluorescent Intensity

MRCP Magnetic Resonance Cholangio-Pancreatogram

MRI Magenetic Resonance Imaging

MUP Minimum Unit Price

NAFLD Non-Alcoholic Fatty Liver Disease

NASH Non-Alcoholic Steato-Hepatitis

NCAM Neural Cell Adhesion Molecule

NF-κB Nuclear Factor-kappa B

NGAL Neutrophil Gelatinase-associated Lipocalin

NHSBT National Health Service Blood and Transplant

NMLP Normothermic Machine Liver Perfusion

NMR Nuclear Magnetic Resonance

Non-LC Non-Lactate Clearing

NORS National Organ Retrieval Service

O2ER Oxygen Extraction Ratio

ODR Organ Donor Register

OLT Orthotopic Liver Transplantation

PAM Partitioning Around Medoids

PAMP Pathogen-Associated Molecuar Pattern

PAS Periodic Acid-Schiff

PBC Primary Biliary Cirrhosis

PBS Phosphate Buffered Saline

PCA Principle Component Analysis

pCO_2 Partial Pressure of CO_2

PECAM-1 Platelet Endothelial Cell Adhesion Molecule-1

PLS Partial Least Squares

PLS-DA Partial Least Squares Discriminant Analysis

PNF Primary Non-Function

PPI Protein-Protein Interaction

PRC Packed Red Cell

PSC Primary Sclerosing Cholangitis

PSM Peptide Spectrum Matches

PV Portal Vein

RGB Red Green Blue

ROS Reactive Oxygen Species

SCD Standard Criteria Donor

SCS Static Cold Storage

SDC Sodium-deoxycholate

SNOD Specialist Nurse in Organ donation

SV40 Simian Vacuolating Virus 40

TBS Tris Buffered Saline

TCA Tricarboxylic Acid Cycle

TEAB Tetraethylammonium Bromide

TEM Transmission Electron Microscopy

TFA Trifluoroacetic Acid

Thy-1 Thymocyte Differentiation Antigen-1

TLR Toll-Like Receptor

TNF Tumour Necrosis Factor

TNF-α Tumour Necrosis Factor-alpha

TNFRSF TNF Receptor Superfamily

TNFSF Tumour Necrosis Factor Superfamily

TRAFs TNF Receptor Associated Factors

TRAIL TNF-Related Apoptosis-Inducing Ligand

TWEAK Tumour Necrosis Factor Weak Inducer of Apoptosis

TXRD Texas Red

UCP2 Uncoupling Protein 2

UKELD United Kingdom Model for End-Stage Liver Disease

UPLC-MS Ultra Performance Liquid Chromatography Mass Spectrometry

UW University of Wisconsin

VAP-1 Vascular Adhesion Protein-1

VCAM-1 Vascular Cell Adhesion Molecule 1

VG Van Gieson

WIT Warm Ischaemic Time

XIC eXtracted Ion Chromatogram

CHAPTER 1

INTRODUCTION

1.1 Liver Anatomy and Physiology

To investigate liver disease it is important to understand the fundamentals of liver anatomy and pathophysiology. Below is a summary to enable an understanding of the data presented later in this thesis.

1.1.1 Gross Anatomy and Physiology

The liver weighs approximaetly 1500 grammes and is located in the upper quadrants of the abdomen, mainly on the right side, where is is protected by the spine posteriorly, diaphragm superiorly and abdominal musculature and ribs anteriorly.[1, 2] The diaphragmatic surface of the liver is covered with visceral peritoneum except posteriorly where it lies in direct contact with the diaphragm, known as the bare area, that is demarcated by the reflection of teh peritoneum from the diaphragm forming the upper and lower layers of the coronary ligament.[2] The liver is suspended from the aorta and Inferior Vena Cava (IVC) by the left and right triangular ligaments as well as the falciform ligament.[1] The liver is enveloped by the capsule made of connective tissue and is largely surrounded by the peritoneum on its visceral surface, except in the gallbaldder fossa.[2] The liver consists of four non-functional anatomical lobes, the left lobe, right lobe, quadrate and caudate lobes. The left and right lobes are separated by the falciform ligament, whilst the caudate lobe lies superoposteriorly and the quadrate lobe inferoposteriorly.[2] The liver receives its dual blood supply predominantly from the nutrient rich but oxygen deplete portal vein, itself the confluence of the splenic and superior mesenteric veins that drain the spleen and bowel respectively.[3] This accounts for approximately 70% of the blood flow. The remaining 30% is supplied by the oxygenated hepatic artery, itself a branch of the coeliac artery arising from the aorta superior to the superior mesenteric and two renal arteries.[1, 3] Of surgical importance is the variation in the vascular anatomy, itself a result of the emryological origins of the midgut that undergoes a 270^{o} *in utero*. The liver itself can be divided functionally into eight segments, originally described by Couinaud, with segments II,III and IV in the functional left lobe and segments V-VIII in the functional right lobe, demarcated

by Cantlie's line running through the gallbladder fossa to the IVC.[4, 5] Segment I is largely counted as an independent functioning segment. Each of these segments receives blood supply from branches of the portal vein and hepatic arteries whilst venous drainage is to the hepatic veins that drain directly in to the IVC and onto the right atrium.[2] Drainage of bile from each segment converges into the left and right hepatic ducts form the common hepatic duct and, after storage in the gallbladder, passes into the common bile duct subsequently the duodenum.[2] The bile duct, hepatic artery and portal vein together form the portal triad that extends from the porta hepatis to the duodenum encased within the lesser omentum, known as the hepatoduodenal ligament.[2] The discovery of this segmental anatomy was pivotal in allowing the planning and execution of radical resections of liver lesions so permitting onocological clearance whilst minimising haemorrhage .[6]

The liver performs a number of complex tasks but overall they can be divided into three main categories. These comprise resorption the storage as well as synthesis and secretion of carbohydrates, lipids, amino acids and proteins.[7] Such proteins include albumin, ceruloplasmin, acute phase proteins and clotting factors.[7] Additionally, the liver detoxifies bilirubin, alcohol and ammonium as well as excreting primary bile acids cholic acid and chenodeoxycholic acid as components of bile.[7] The liver produces approxiamtely 600-750ml of bile per day that is stored in the gallbladder before being excreted in to the duodenum to facilitate digestion and subsequent absorption of dietary fat by micelle formation.[7]

1.1.2 Microarchitecture and Function

The functional unit of the liver parenchyma is the hexagonal liver lobule which has the hepatic vein at its centre with the portal triad of a bile ductule, terminal branch of the heptic artery and terminal branch of the portal vein at each of its six corners.[7, 8] Heptic arterial and portal venous mix as it enters the lobule before draining in to the central hepatic vein, whilst bile travels through the bile canniculus before entering the bile ductules and eventually bile duct.[9] The most fucntioanly relevant unit of the liver is the liver acinus, composed of the two portal triads

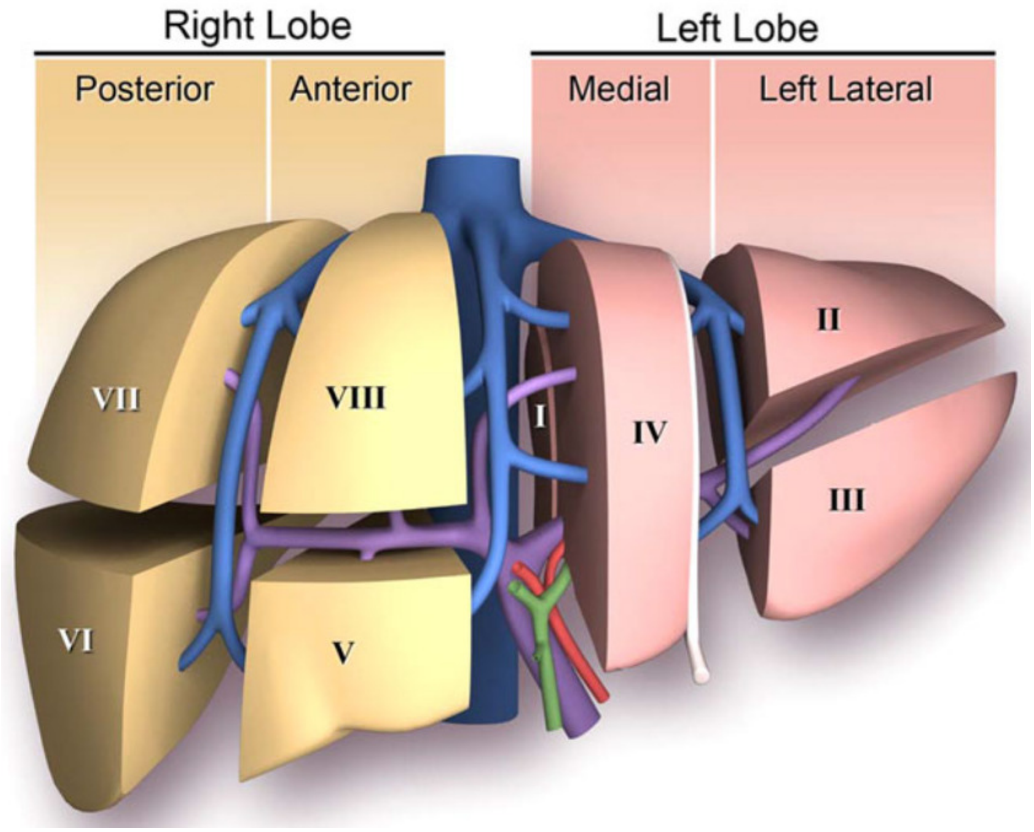

Figure 1.1: Segmental anatomy of the liver. The functional left lobe of the liver contains segments II, III (left lateral), IV (medial) whilst the functional right lobe contains segments V & VIII (anterior), VI & VII (posterior). Segment I is an independent functioning segment.[5]

and their neighbouring central veins in a diamond shape and reflects metabolic activity.[7, 8] Split in to three zones, each zone receives differently oxygenated blood with periportal zone I exposed to the highest oxygen concentrations and zone III the lowest oxygen concentraion.[10] Each lobule contains all of the cells described below.

Hepatocytes

Hepatocytes are the functioning unit of each lobule and form more than 75% of the weight of the liver. They are arranged in plates around a hepatic sinusoid. Their primary function is the detoxification of blood that has drained from the portal venous system from the gut as well as critical liver function including protein synthesis, coagulation factor production and immune responses. They have a high metabolic rate with hepatocytes in zone I specialising in oxidative energy metabolism, amino acid catabolism and fatty acid oxidation. Conversely, lipogenesis, ketogenesis and metabolism of xenobiotics mainly occurs in zone III, where hepatocytes are more prone to hypoxic damage.[10] Hepatocytes are derived from foregut hepatic progenitor cells on exposure to fibroblast growth factors 1 & 2, bone morphogenic proteins 2 & 4 and the Wnt signalling pathway.[11, 12] It is thought that transforming growth factor β limits the extent of differenitation.[13] These progenitor cells appear to bipotent with the abilty to differenitate into either hepatocytes or cholangiocytes btu is dependent on the complex interplay of six transcription factors HNF1a, HNF1β, FoxA2, HNF4a1, HNF6 and LRH-1.[14] Once matured, hepatocytes are some fo the largest cells in the body, rich in organelles, can contain two and more nuclei that reach polyploidy with increasing age and reduced nutrient supply.[7] Hepatocytes are polarized with the basolateral domain facing the sinusoid, the apical domain facing the same domain from the opposite heaptcyte forming the bile canniculus containing the ATP-dependent excretion pump ABC transporter superfamily and the lateral domain containing a series of tight junctions and cell adhesion molecules used in direct cell to cell communication.[15, 16, 17]

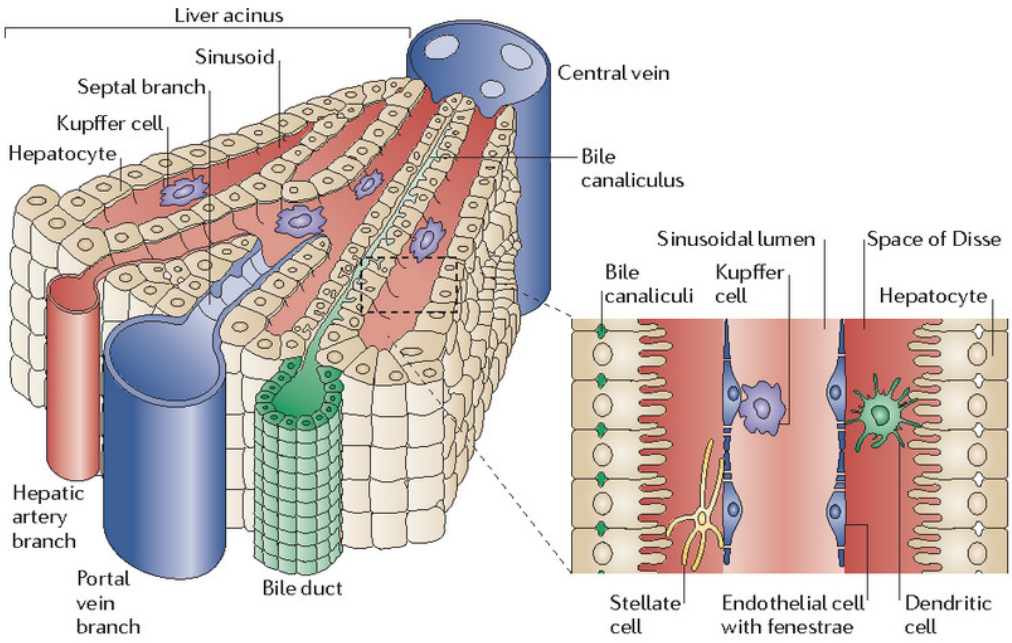

Figure 1.2: Representation of the structure of the liver lobule. The portal veins and hepatic arteries terminate in the intrahepatic portal tracts, which contain bile ducts that transport bile from the canaliculus through the extrahepatic biliary system.[9]

Hepatic Sinusoidal Endothelial Cells

Human Sinusoidal Epithelial Cells (HSEC) are a morphologically distinct popuation of cells that line the sinuoids and have multiple fenestrae and lack a basement membrane.[18] They are separated from the hepatocytes by the perisinusoidal Space of Disse and are often the first cells to come into contact with blood from the portal triad. One of their cellular functions is filtration using the fenestrae that have a diameter of approximately 100nm and so serve as a mechanical sieve.[19, 20] HSEC have an important role in the attraction of leukocytes that bind to the adhesion molecules on HSEC, such as Vascular Adhesion Protein-1 (VAP-1) that promotes adhesion and transmigration of leukocytes, particularly as the sinusoid is a low blood flow environment.[21] Other adhesion molecules such as Vascular Cell Adhesion Molecule 1 (VCAM-1) and Intercellular Adhesion Molecule 1 (ICAM-1) are upregulated during liver injury.[22] HSEC also have a role in nitric oxide signalling for the autoregulation of blood flow, endocytosis, bacterial processing and liver regeneration.[7]

Cholangiocytes

Biliary epithelial cells, also known as cholangiocytes constitute approxiamately 5% of the mass of the liver. They line the lumen of the biliary tree and are polarized with apical and basolateral domains but are largely mitotically dormant.[23, 24] They play an important role in the formation of bile by altering the contents of the primary cannicular bile via secretion and absorption in addition to the detoxification of xenobiotics.[23] Cholangiocytes express numerous G and non-G protein-coupled receptors including the tyrosine kinase receptors in addition to components of the Notch and Hedgehog signialling pathways.[7] Development of cholangiocytes stems from the differentiation of bipotent hepatoblasts under the influence of the six transcription factors above.[14] Ductal plate formation necessary for cholangiogyte expansion appears to be dependent on the TGF-β gradient and possibly the Notch pathway.[25] The expression of Sox-9, starting in the periportal region, is an early marker for cholangiocyte differentiation.[26]

Hepatic Stellate Cells

Hepatic Stellate Cells (HSC) are located in the Space of Disse and store retinyl esters and are important in the metabolism and storage of retinoids.[27] Activated HSC display a number of phenotypes including proliferation, migration, contraction, chemoattraction and cross-talk with the immune system, cancer cells and biliary cells. However, much attention has been paid to the myofibroblast-like phenotype that produces excessive amounts of collagen types I and III over the predominant synthesis of collagen IV and the different sources of activation are being studied to distinguish between differential activated phenotypes.[28] The stiffness of the extracellular matrix may influence activation as suspension or culturing on matrix similar to basement membrane inhibits proliferation and collagen deposition.[29]

Kupffer Cells

Kuppfer cells are the resident liver macrophages that reside in the hepatic sinusoids and are the first immune cells to encounter the antigens and microbe-derived toxins from the portal vein.[7] Lipolysaccharide, IL-12 and Interferon Gamma (IFN-γ) polarizes Kupffer cells to produce proinflammatory cytokines such as CCL2 that recruit Ly6C positive monocytes to the liver as well as Reactive Oxygen Species (ROS) and Tumour Necrosis Factor-alpha (TNF-α) to result in anti-microbial and tumourocidal activity. The effect of these recruited monocytes is to potentiate the initial response of the Kupffer cells by producing TNF-α, IL-1β, IL-12 and IL-6. These are known as Classic M1 type Kupffer cells. The alternaitvely activated M2 type Kupffer cells produce antiinflammatory cytokines such as IL-10, arginase-1 and CD206 and are involved with tissue repair and modelling, tumour progression and resolution of inflammation.[30, 31, 32]

Extracellular Matrix

The Extracellular Matrix (ECM) is not only an important structural scaffold but also dynamically reguates cell and organ function using signals that are transduced via cellular receptors, the most widely studied being the integrin family. ECM is composed of a large number of collagens,

non-collagenous glycoproteins such as laminin and fibronectin, glycoaminoglycans, proteoglycans and matricellular proteins that may be released by the degrading matrix proteases.[33] There is evidence to suggest that the ECM plays a role in the directing teh stem cell niche during liver regeneration.[34]

1.2 Principles of Inflammation and Its Relationship to Liver Disease

Chronic inflammation of the liver leads to end stage liver disease and cirrhosis, resulting in over 1 million deaths worldwide each year.[35] Risk factors are the chronic pathological liver diseases such as chronic viral infection, in particular hepatitis B and C, Alcoholic Liver Disease (ALD), Non-Alcoholic Steato-Hepatitis (NASH), autoimmune disease and cholangiopathies, diseases of the bile ducts, such as Primary Biliary Cirrhosis (PBC) and Primary Sclerosing Cholangitis (PSC), characterised by destruction of the intrahepatic bile ducts.[36, 37, 38, 39] Different liver injuries elicit several mechanisms that trigger potentially chronic immune reactions and subsequent fibrosis. These are highly conserved with all diseases involving cell death but ultimately lead to activation of HSCs producing myofibroblasts, contributing to the production of ECM and inflammatory signalling pathways.[40, 41] The HSC interact with other liver resident cells, such as hepatocytes, HSEC and cholangiocytes, as wel as infiltrating immune cells to control the development and regression of fibrosis.[42] During extensive hepatocellular death, fibrosis can be seen to be beneficial by providing mechanical stability, the inflammatory cells removing cellular debris and inflammatory cells promoting liver regeneration with the aim of creating normal liver architecture.[43] However, if left unchecked, extensive hepatocellular deaths results in progressive fibrosis and cirrhosis.

1.2.1 Cell Types That Link Inflammation and Fibrosis

As described previously, HSC are the main effector of fibrosis and interact with hepatocytes, HSEC, cholangiocytes and Kupffer cells to promote fibrosis, although termination of the re-

sponse can be achieved when HSCinteract with natural killer cells.[44, 45] The HSC are responsive to lipopolysaccharide and, once activated via the Nuclear Factor-kappa B (NF-κB) pathway and AP-1, signal in either an autocrine fashion or recieve signals form immune cells to maintain their activation.[46] The expression of Toll-Like Receptor (TLR)s provides a link between the gut either using the portal venous system or lymphatics and the liver.[44, 47]

Hepatocellular death is significantly promotes chromic liver inflammation with necrotic hepatocytes and apoptotic bodies releasing pro-inflammatory and profibrogenic cytokines to activate HSCs. Cytokine release from hepatocytes under oxidative stress in addition to Damage Associated Molecular Patterns (DAMPs) are aso implicated[48, 49] Cholangiopathies, such as PBC and PSC are strongly associated with inflammation and fibrosis but the relationship between cholangiocytes and HSCs is not clear.Cholangiocytes are a source of cytokine and chemokines that interact in particular with T lypmhocytes as well as being responsive to TLRs.[50] The ductular reaction seen in many cholangiopathies might be related to cholangiocyte proliferation resulting from the activation of the hyaluronan receptor Cluster of Differentiation (CD)44 following deposition of hylauronan.[51] There is a close relationship between HSEC and HSCs, with suppression of HSCs by HSEC during normal liver function, but the inability to suppress HSC activity following liver injury.[52] This might be mediated by CXCR4, FGFR-1 and TLR.[42]

In addition to the large number of Kupffer cells, the resident liver macrophages, liver injury promotes the recruitment of macrophages from the bone marrow that subsequently promote liver fibrosis by releasing profibrogenic cytokines and maintain activation of HSCs. Polarisation of these macrophages to M2 macrophages can promote resolution of fibrosis via the degradation of of ECM via increased matrix metalloprotease expression.[41] It is reported that M2 macrophages can also promote resolution by the deactivation and removal of HSCs via TRAIL.[53]

Natural killer cells and natural killer T cells constitute a high proportion of liver lymphocytes and are important in exerting an anti-firotic effect.[45, 54] This is mediated via IFN-γ and

the destruction of HSC via TRAIL and FasL, but this effect is suppressed through elevated TGF-β concentrations.[55, 56] There does not appear to be a clear role for neutrophils in the fibrogenesis although they are recruited to the liver.[57] A subset of Innate Lymphoid Cell (ILC), the ILC2 appear to have a role in fibrosis and epand in response to secretion of IL-33 from hepatocytes that results in activation of HSCs in a IL-13 and STAT6 dependent fashion but independent of the TGFβ pathway.[58] Although microthrombi are seen in the hypercoaguable injured liver, suggesting the release of growth factors such as PDGF resulting in the activation of profibrotic coagulation cascasdes, there are potentially antifibrotic effects exerted by platelets that is an ongoing active area of research.[59]

1.2.2 Pathways Modulating Hepatic Inflammation

There are a number of different pathways that modulate hepatic inflammation. Triggers of inflammatory signalling include the gut microbiota-TLR pathway, the inflammatory cytokines, chemokines, interferons, inflammatory and fibrogenic signals from dead cells.[60]

The gut microbiota-TLR pathway is mediated by bacterial molecules Pathogen-Associated Molecuar Pattern (PAMP)s via the activation of TLR4. Induction of TLR4, particularly on HSCs induces expression of chemokines and adhesion molecules to recruit macrophages.[44] Stimulation of HSEC by TLR4 can induce portal hypertension via fibronectin production from HSCs.[61] when acting on Kupffer cells, TLR4 elicits expression of pro-inflammatory cytokines such as TNF-α, IL-β1, CCL2 and CCL20.[62]

Inflammatory cytokines implicated in fibrosis include IL-1β, produced by macrophages and is of particular relevance in toxic alcohol and NASH induced fibrosis.[63] The cytokine TNF-α has diverse effects but may contribute to fibrosis preventig HSC apoptosis in addition to promoting hepatocyte apoptosis, immune cell activation and HSC activation.[64] IL-17, produced from CD4+ Th17 T cells stimulate Kupffer cells and HSCs via activation of NF-κB and STAT3, inducing HSC activation.[65] In the liver IL-22 suppresses fibrosis by inducing HSC senescence in a STAT3-p53-p21 dependent manner and can be used clinically as a biomarker to predict the

prognosis of cirrhosis.[66, 67] TGF-β, produced hepatic macrophages but needing to be activated by fr example ROS plays an important role in fibrosis and induces the transcripton of collagen types I and III in HSC[68]

The function of chemokines and their receptors is the recruitment of immune and non-immune cells in to the inflammed areas. In particular, CCL2 which is mainly produced by Kupffer cells and HSCs receruits monocytes and macrophages to the liver and promotes HSC activation.[69] CCL5 and its receptors CCR1 and CCR5 promote liver fibrosis via mcrophage and HSC respectively.[70] In comparison, interaction of CX3CL1 with its receptor CX3CR1 on macrophages enhances macrophage survival, with CX3CL1 expressed on HSC suggesting its anti-inflammatory properties.[71]

Both type I (IFNα and IFNβ) interferon and type II (IFNγ) interferon are increased in chronic liver disease.[60] The latter suppresses HSCproliferation directly whilst IFNα reduces collagen gene transcription in HSCs.[55]

1.2.3 Downstream Signalling Pathways Linking Inflammation and Fibrosis

The transcription factor NF-κB acts as a key regulator of inflammation and cell death and is of importance in chronic liver diseases.[60] It is activated by TLRs, IL-1β and TNF-α and whilst physiological activation of NF-κB is protective by preventing hepatocyte apoptosis, overactivation in hepatocytes or inflammatory cells induces production of pro-inflammatory cytokines such as TNF-α, IL-1β and IL-6.[60] Activation of NF-κB in HSCs promotes HSC survival and thus continuing fibrogenesis that is mediated by IL-1β and TNF-α from Kupffer cells.[72] Furthermore, activation of NF-κB in HSCs initiates chemokine secretion to promote recruitment and interaction with inflammatory cells, so perpetuating fibrosis.[73]

The c-Jun-N-terminal Kinases (JNK)s are Mitogen-Activated Protein Kinases (MAPKs) activated by stimuli including TLR, IL-1β, TNF-α, ROS and saturated free fatty acids.[60] In the liver, substrates for JNK1 and JNK2 are components for the transcription factor AP-1 that in-

clude c-Jun, Jun B, Jun D and Fos.[60] The JNKs promote fibrogensis by HSC proliferation via PDGF, TGF-β and angiotensin II as well as collagen production.[74] JNK also modulates hepatic fibrosis by regulating hepatic steatosis, hepatocyte cell death and inflammatory gene expression, consolidating its role in liver fibrosis.[75]

1.3 The Tumour Necrosis Factor Receptor Superfamily

The Tumour Necrosis Factor (TNF) receptor cytokines form a superfamily that bind with their cognate receptors, the TNF Receptor Superfamily (TNFRSF), that are found on the cell surface of a variety of cells including those involved with immune function.[76] The TNF superfamily is composed of 19 structurally related ligands that bind to one or more molecules from the TNF receptor superfamily, a total of 29 structurally similar receptors.[77, 78] A number of these ligands can be grouped according to chromosomal loci.[76] However, there is complexity to this receptor-ligand signalling system. Although each ligand, acting in its trimeric form, was initially thought to bind to its cognate receptor there is considerable crossover between ligands interacting with various receptors, as summarised in Figure 1.3.[76, 79] Additionally, ligands are either membrane-anchored or soluble trimers that cluster their cognate receptors to iniate signal transduction.[80] Activation of the intracellular signalling pathway is initiated via receptor clustering of the extracellular cysteine-rich domains that utilises a series of adapter mechanisms that subsequently activates a number of intracellular enzymatic complexes (Figure 1.4).[76, 80]

Generally, the Tumour Necrosis Factor Superfamily (TNFSF) promote either survival or inflammatory signalling, for example TNF, lymphotoxin, nerve growth factor, CD40 ligand, OX40 ligand and B cell activating factor.[80] Alternatively, they can induce apoptotic cell death, such as FAS ligand and TNF-Related Apoptosis-Inducing Ligand (TRAIL).[80] The functional outcome of TNF ligand engaging with its receptor can include cellular proliferation, death and differentiation although the mechanisms that determine which fates cells take are yet to be fully characterised and is dependent on the specific receptor-ligand interaction.[76] The transcription

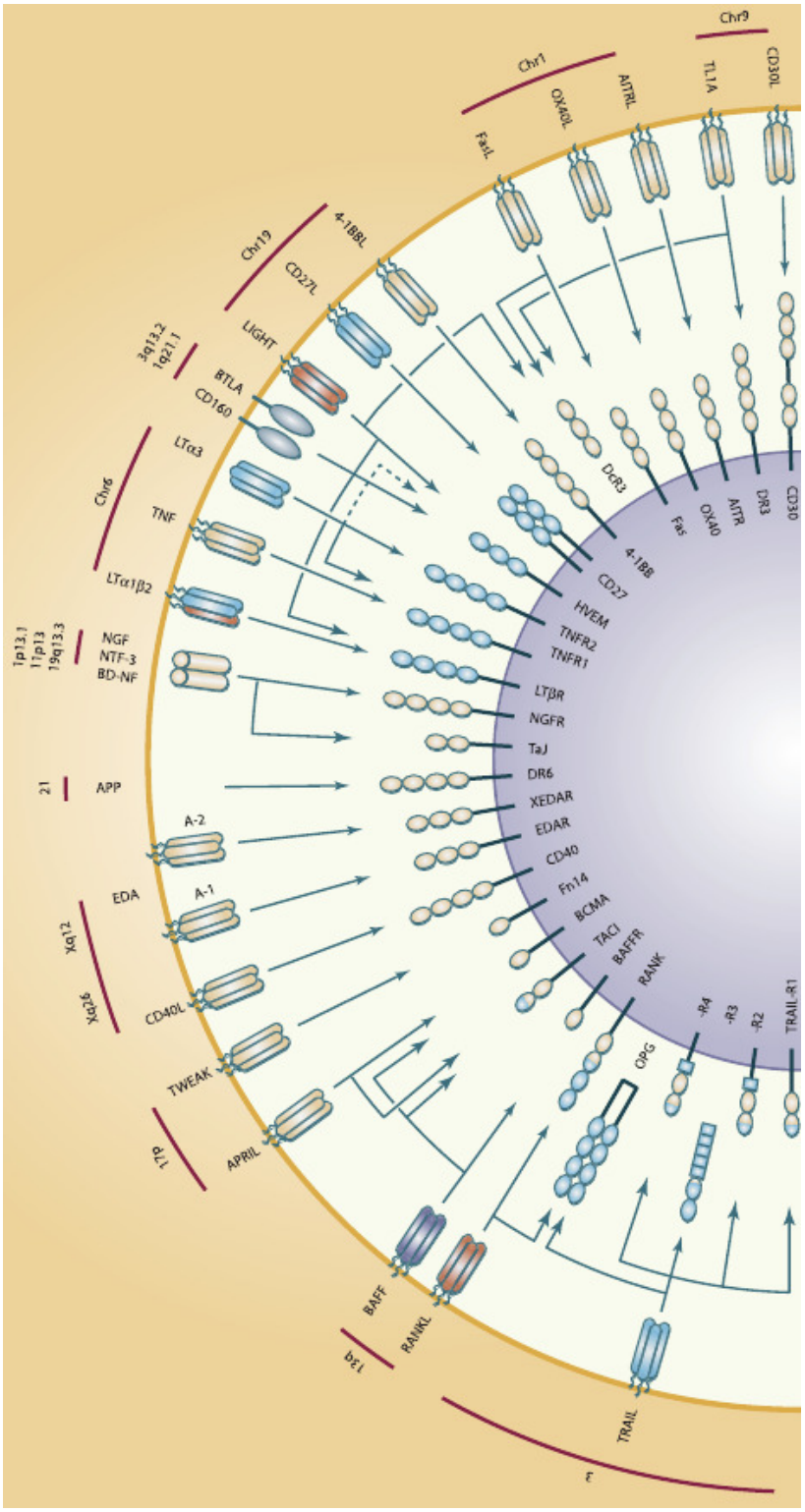

Figure 1.3: Summary of the TNF Superfamily. Members of the TNF cytokine superfamily are represented on the outer aspects (amber ring) and grouped according to chromosomal location (mauve segments). Members of the TNF receptor superfamily are represented on the inner aspect (blue ring) and vary in size according to the number of cysteine domains. The blue arrows represent the specific ligand and cognate receptor interaction, which may include cross-over as shown.[79]

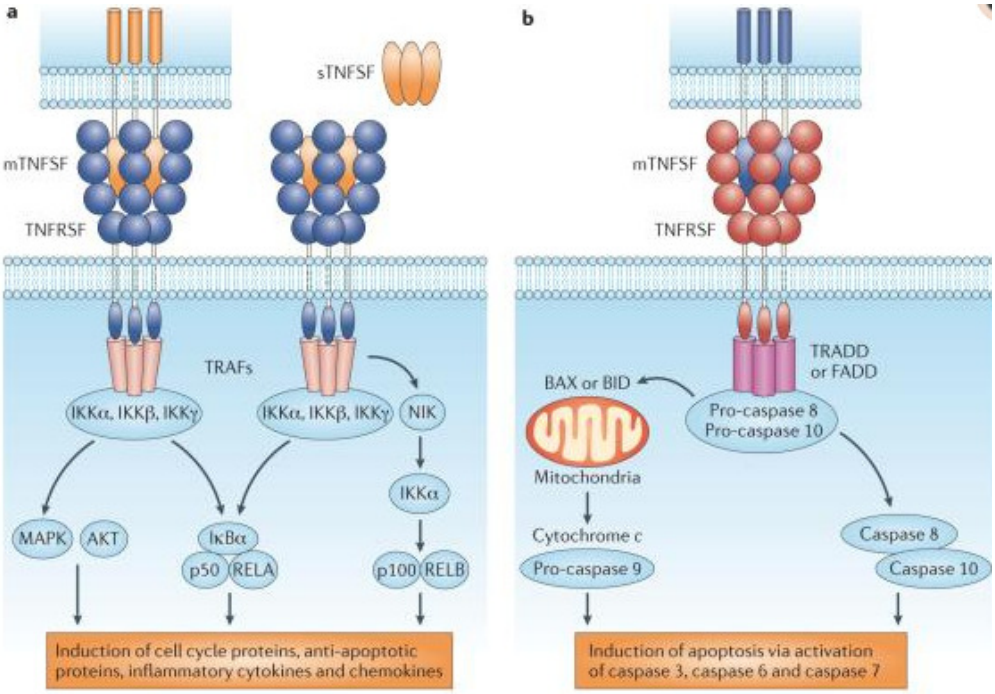

Figure 1.4: Inflammatory and death inducing activity of TNFSF. Left, pro-inflammatory activation by receptor trimerisation allowing the recruitment of TNFR-associated factors that activate serine/threonine kinase dependent pathways. Right, apoptotic activation by organising TNFRSF members containing a death domain into timeric configurations to recruit adapter molecules containing death effeector domains.[80]

factor NF-κB is thought to play a pivotal role.[76]

Predicting the cellular functional effect following the binding of a TNF superfamily member with its corresponding receptor is difficult and is further complicated by the ablility of the ligands to act as cosignals.[81] For example, TNFR2 binds its cognate ligand TNF-α and the secreted ligand lymphotoxin-α, both of which also bind to TNFR1.[82] Other members of the TNFSF and TNFRSF that are similar include glucocorticoid-induced tumour necrosis factor, Death receptor 3, TNFRSF9, OX40, CD30.[81] This is further complicated by the interactions of immediate TNF superfamily members and Herpesvirus Entry Mediator, resulting in a diversity of cellular regulation.[83]

1.3.1 The Fn14/TWEAK Receptor-Ligand System in Organ Inflammation and Repair

A novel member of the TNF superfamily of ligands called Tumour Necrosis Factor Weak Inducer of Apoptosis (TWEAK) and its cognate receptor the type 2 transmembrane protein Fn14 (Fn14) have been implicated in the regulation of hepatic inflammation and tissue remodelling as part of a broader role for Fn14/TWEAK in progenitor differentiation.[84, 85] TWEAK is mainly secreted as a soluble cytokine, having been cleaved by the furin proteases, by cells of myelomonocytic lineage including macrophages.[86, 87, 88] Fn14 is the smallest member of the TNF receptor superfamily, has only a single cysteine-rich domain and is the cognate receptor for TWEAK.[79, 88] It is expressed throughout the body and although expression is generally low in healthy tissues, it is up-regulated in diseased ones.[79, 88] CD163 has been described as a competing scavenger receptor for TWEAK that may have implications in cardiovascular mortality.[89, 90, 91] Activation of the Fn14/TWEAK receptor-ligand pathway is involved in myocyte progenitor differentiation and cardiac remodelling and has been implicated in regeneration, angiogenesis and stromal cell remodelling in response to inflammation in rheumatoid arthritis, lupus nephritis, renal tubular injury and graft versus host disease.[92, 93, 94, 95, 96, 97, 98, 99, 100] Interaction of Fn14 and TWEAK promotes cell

growth, apoptosis and autophagy through activation of intracellular signalling pathways including differential activation of the classical and non-canonical nuclear-factor kB pathways and the Activator Protein-1 (AP-1) pathway via TNF Receptor Associated Factors (TRAFs) and the MAPKs respectively (Figure 1.5).[88, 101, 102] The regulation of this incompletely characterised pathway is yet to be fully elucidated.

1.4 Mortality from Liver Disease

Mortality from chronic liver disease has increased in the United Kingdom since 1970 rising by 50% between 1990 and 2000 resulting in significant morbidity, mortality and healthcare costs (Figure 1.6).[103, 104, 105, 106] This has been despite significant reductions in the standardised UK mortality rate for circulatory, ischaemic heart, cerebrovascular, neoplasm, respiratory, endocrine diseases and diabetes throughout the same period (Figure 1.6).[106] Mortality from chronic liver disease can be clustered in to two age demographics (Figure 1.7). Those aged 45-64 years have had a higher age standardised death rate compared to those aged 25-44 years across all years since 1970.[103] The older demographic started with an age standardised mortality from liver disease of 4-6 per 100,000 population per year, increasing to 8-13 per 100,000 population in 1993 before accelerating to 14-22 per 100,000 population by 2000.[103] The younger demographic commenced with a age standardised mortality rate of 1-2 per 100,000 population in 1970, before steadily increasing to 4-6 per 100,000 population by the year 2000.[103] For both age clusters and across all years the rate of age standardised death rate for males has been at the higher end of each range.[103] Comparing mortality in the UK with Europe reveals startling differences since 1970. Whilst the age standardised mortality rate initially increased in Europe between 1970 and 1976 from 13 per 100,00 population to 15 per 100,000 population, there was subsequently a steady reduction to 9 per 100,000 population per year in 1998, the year data collection was completed (Figure 1.8).[103] In comparison, the age standarised death rate in the UK between 1970 and 1976 increased from 2 per 100,000 population per year to 3 per 100,000 population per year.[103] This gradual increase continued to

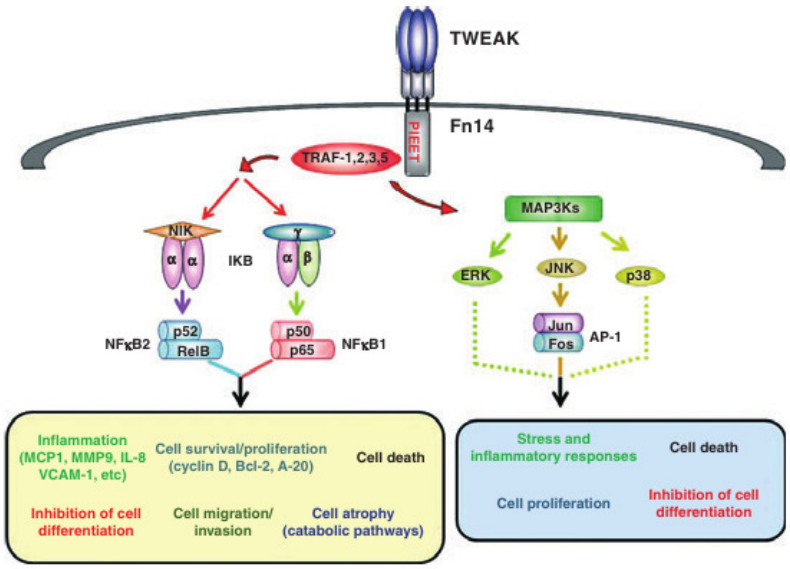

Figure 1.5: The Signalling Pathway after Fn14/TWEAK Interaction. TWEAK binds to its cognate receptor Fn14 mainly in its soluble form, although it can be cell-bound. Interaction of TWEAK and Fn14 results in the intracellular domain of Fn14 binding to various TRAFs that results in the functional activation of canonical and non-canonical NF-κB pathways, as well as the AP-1 pathway via MAPKs.[88]

just over 4 per 100,000 population per year by 1993, following which there has been a faster rate of increase. This has culminated to an age standarised death rate of 7 per 100,000 population per year for the UK in 1998.[103] Since 2000, there has been a progressive increase in liver mortality attributable to alcohol and obesity or diabetes, whilst death from viral hepatitis and autoimmune or metabolic diseases have remained relatively static, despite an increasing population (Figure 1.9).

1.5 Liver Transplantation and Meeting the Demand for Organs

1.5.1 Outcome on the Liver Transplant Waiting List

Despite scientific and medical advances, the only treatment for end-stage liver disease is transplantation. Until 2010, the number of patients on the transplant waiting list for all organs had increased to 8012 before decreasing to 6388 in 2017.[107] The number of patients on the active liver transplant waiting list demonstrated an increase from 268 in 2008 to 611 in 2015 before reducing to 530 in 2017, a decrease of 8% compared to the previous 12 months but almost doubling in 9 years.[107, 108] The outcome for patients following registration on the waiting list varies dependent on time since listing. After 6 months, 51% will have been transplated, 38% are still waiting, 3% have been removed due to their condition deteriorating and 8% have died.[108] At 2 years following addition to the waiting list 74% of patients will have been transplanted, only 5% will still be waiting whilst 8% will have been removed due deterioration and 13% will have died.[108, 109]

1.5.2 Organ Donation Rates and Changes to Donors

Overall deceased donor rates have continued to increase with an additional 4% in 2016-2017 compared to the previous year although a 3% decrease in living donor rates, a source of organs not routinely used in liver transplantation.[107] Cadaveric organ donation can be divided into

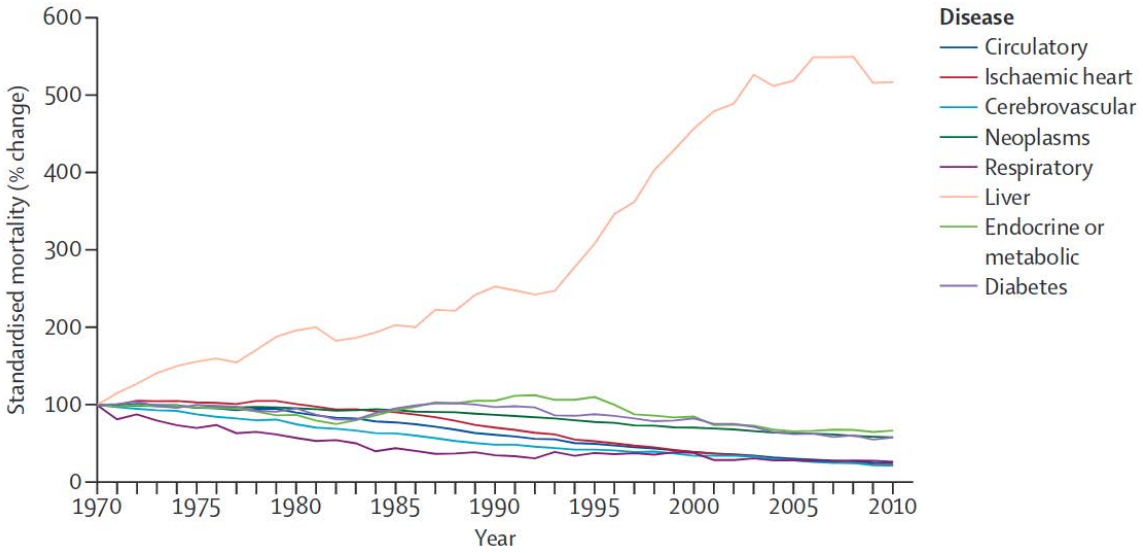

Figure 1.6: Liver mortality rates compared to other diseases in the UK since 1970 until 2010.[106]. This demonstrates a clear increase in mortality from liver disease just over doubling between 1970 to 1993, before accelerating to almost six times the standardised mortality by 2010.

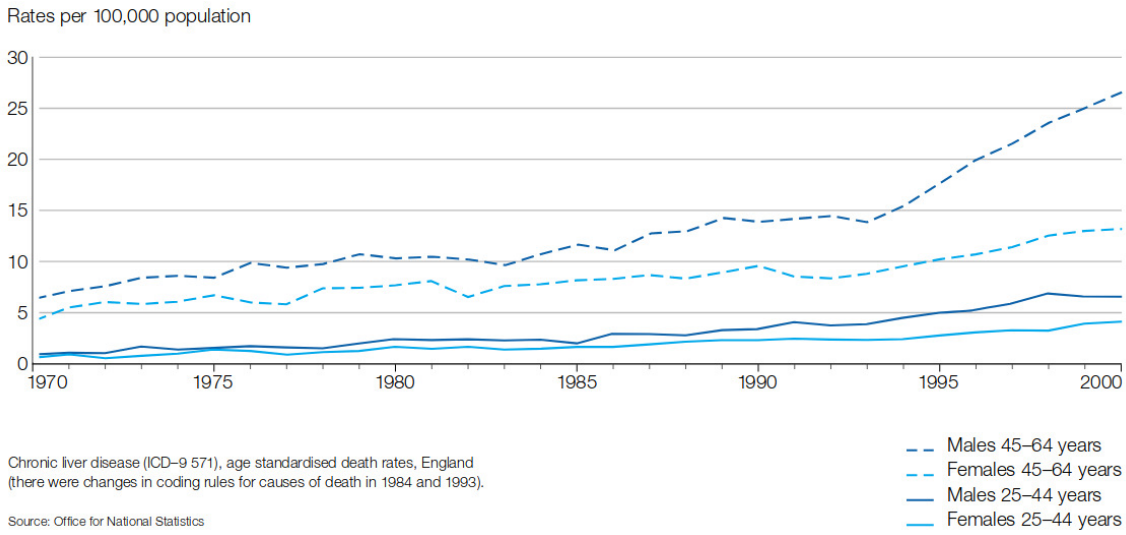

Figure 1.7: Age standardised death rates for chronic liver disease between 1970 and 2000.[103] This demonstrates two age clusters of 23-44 years and 45-64 years. Males have a higher mortality rate compared to females in both clusters across all years. There was an acceleration in mortality, particularly in males from 1993, most noticeable in the older demographic.

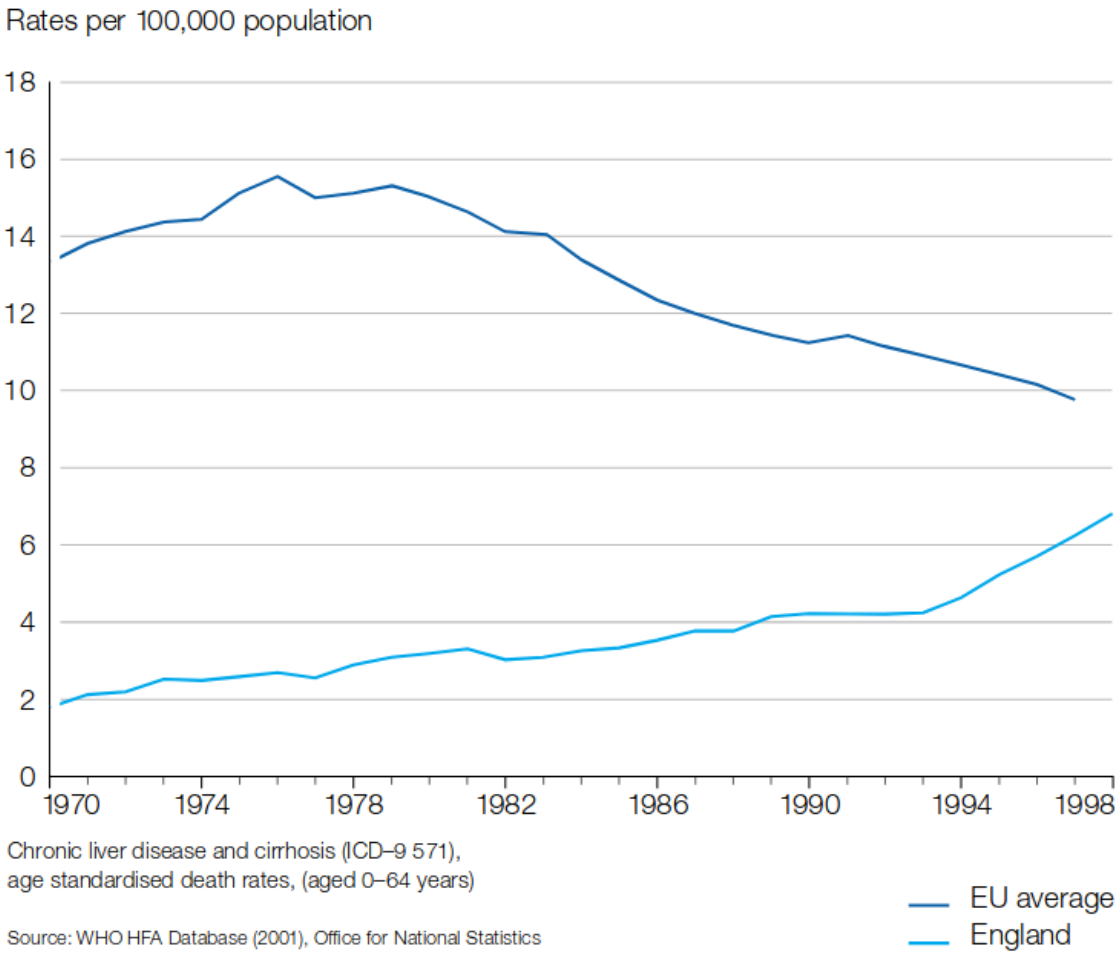

Figure 1.8: Age standarised mortality from chronic liver disease in the UK and Europe between 1970 and 1998.[103] Between 1970 and 1976 there was an increase in the age standardised mortality from liver disease in Europe from 13 to 15 per 100,000 popoulation per year, following which it has decreased to 9 per 100,000 population per year to 1998. In comparison, the UK has experienced an increase in age standardised mortality from 2 per 100,000 population per year to 7 per 100,000 per year in 1998, most notably since 1993.

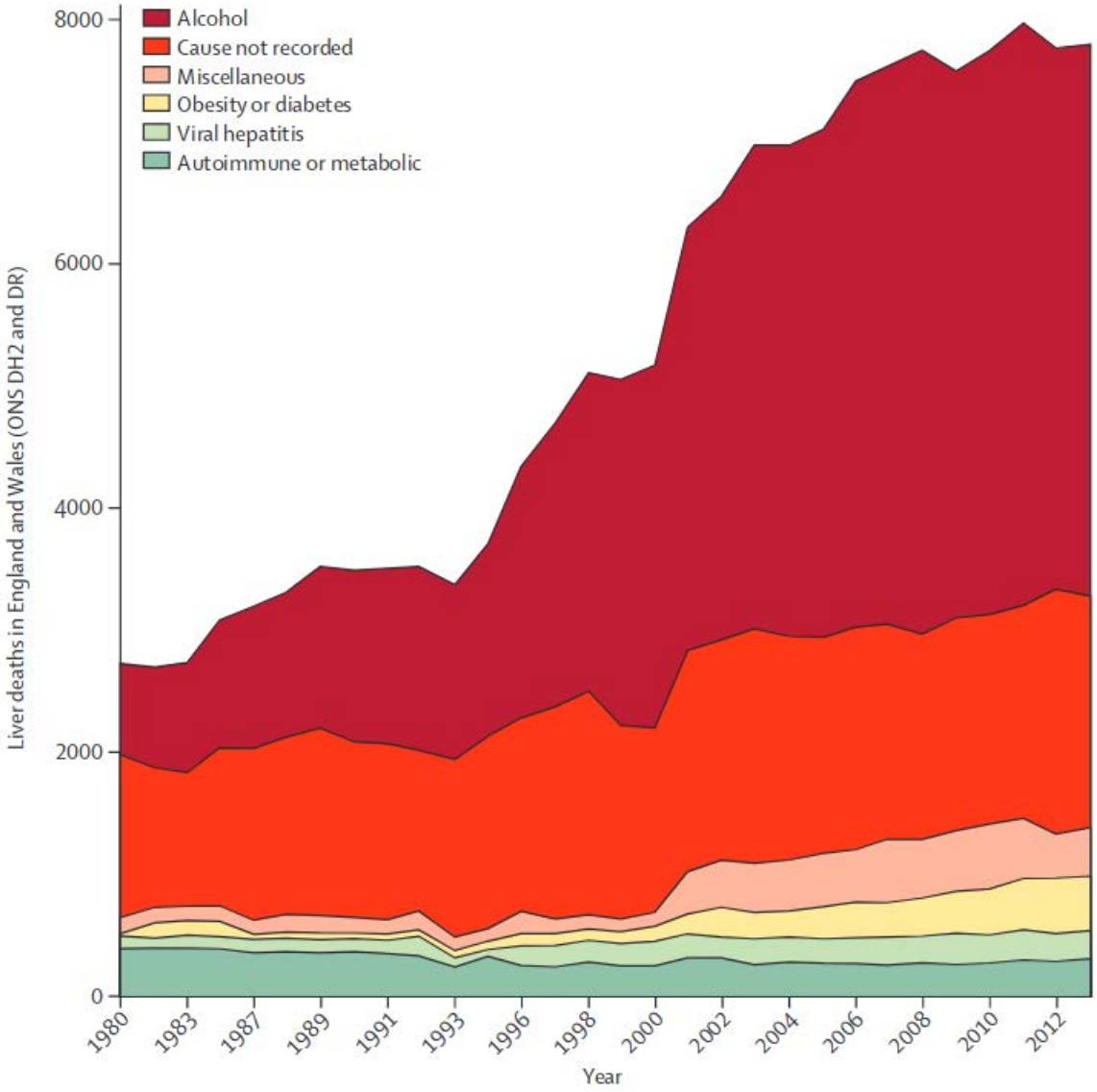

Figure 1.9: Mortality in the UK by type of liver disease between 1980 and 2013.[105]. From 1993, when there were approximately overall 3000 deaths per year attributable to liver disease, to 2013, when almost 8000 people died as a result of liver disease per year, the increase was primarily a result of alcohol or obesity or diabetes deaths. During the same period, deaths from viral hepatitis, autoimmune or cause not recorded remained static.

Donation after Brainstem Death (DBD), where the donor is neurologically tested and found to have absent brainstem function in the presence of a functioning circulatory system, and Donation after Circulatory Death (DCD) in which donation occurs after the support of life supporting treatment and the donor dies following cessation of cardiorespiratory function. The DCD donors can be further subdivided into uncontrolled and controlled DCD according to the categories defined at the first DCD worskhop held in Maastricht in 1995.[110, 111] Uncontrolled DCD donors include: donation from patients who are dead on arrival (Maastricht Category I), donation after unsuccessful ressucitation (Maastricht Category II) and donation following unexpected cardiac arrest in a critcally ill patient (Maastricht Category V).[111] Controlled DCD donors include: donation whilst awaiting cardiac arrest (Maastricht Category III) and donation following cardiac arrest in a brainstem dead donor (Maastricht Category IV).[110, 111] The number of DBD donors increased by 6% to 829 with a concomitant increase in DCD donors of 1% to 584 during the same period.[107] Specifically, the number of liver DBD donors increased by 4% (total 747) with a 10% increase in transplatation (total 738), whilst the number of DCD liver donors decreased by 1% (total 294) although there was a 1% increase in transplatantion (total 208).[107, 108] Over the ten years to March 2017, the number of donors older than 60 years increased from 20% to 36% with the largest decrease in the 18-49 year age bracket.[107] A greater proportion of DBD donors were 18-49 years (41%) compared to DCD donors (28%). Despite the reported increase in BMI for the UK population, the distribution of donor BMI has remained static with between 69-75% having a BMI between 20-29 Kg/m^2 in the 10 years to March 2017.[107] The distribution between DBD and DCD donors was almost the same. In both groups of donors, the cause of death was intracranial (DBD 86%, DCD 81%) rather than trauma (DBD and DCD 3% each).[107] Of note, the vast majority of both DBD and DCD donors were of white ethnicity (92% and 95% respectively).[107] With the expansion of the DCD liver transplant programme, it might be expected that it has contributed to any decline in the DBD however, analysis of the UK Transplant Registry does not support this.[112]

Of the 34,369 audited deaths between March 2016-2017 the proportion of potential donors who actually go on to donated could be improved. For the 1775 patients meeting the organ

donation referral crieria as potential DBD donors, 97.4% were referred formally for donation, 85.7% were tested for neurological death, of that subset the family was approached in 87.3%, consent gained in 69.0% and donation proceeded in 89.3% of those where consent gained.[113] In contrast, of the 6204 patients meeting the organ donation referral criteria as potential DCD donors where imminent death was expected, the formal referral rate for donation was 85.6%, the family approached in 29.3% and consent gained in only 58.1% of families approached with donation proceeding in 53.6% of those where consent gained.[113] Overall, whilst 81-86% of DBD livers are transplanted, only 28-36% of DCD livers are transplanted.[107, 114] The drop-off in successful donation in DBD donors is largely due to clinical unsuitability, whilst in DCD donors, livers are not retrieved or transplanted due to being clinically unsuitable, donor age, poor function that includes the degree of warm ischaemic damage secondary to a prolonged agonal phase greater than 30 minutes, rendering the organs beyond the accepted criteria for donation.[107] As a result these donors are deemed too high risk for use of their organs and those organs are subsequently discarded.

1.5.3 Selection and Outcome From Liver Transplantation

In the ten years to March 2017, there have been a total of 8042 liver transplants, increasing almost annually and most notably in the number of DCD liver transplants performed (Figure 1.10).[108]. Of these, 6831 have been deceased donor first liver only transplants, the remainder composed of re-transplants, atypical and multiorgan transplants. In first only liver transplants, 6170 have been performed in adults, 1303 DCD transplants, whilst 660 in paediatric patients, 660 DCD transplants. Both adult and paediatric liver transplants can be categorised according to whether they are elective (routine) or super-urgent (emergency), with between 10-18% performed on a super-urgently (Figure 1.11).[108] The selection criteria between elective and super-urgent liver transplantation reflects the different aetiologies and thus the markedly different short-term prognoses of these two groups.

In the UK, adult elective selection criteria is primarily based on projected 1-year mortality $>9\%$

using the predicted United Kingdom Model for End-Stage Liver Disease (UKELD) score $\geq$49 risk of death without a liver transplant and have a projected 5 year survival of greater than 50% as well as the ability to improve the quality of the recipient's life.[115] For patients with Hepatocellular Carcinoma (HCC) to be transplanted, a single tumour $\leq$5cm diameter, upto 5 tumours all $\leq$3cm or a single tumour between 5cm and upto 7cm diameter where there is no evidence of tumour progression or extraheptic spread over a 6 month period is required using both Computed Tomography (CT) and Magenetic Resonance Imaging (MRI) and in which there is no absolute contraindication, that includes ruptured tumour, Alpha-feto Protein (AFP) $>$1000iu/ml or extra-hepatic spread.[115] A list of other variant syndromes eligible for transplantation can be found at National Health Service Blood and Transplant (NHSBT).[115] In paediatric patients, chronic liver disease with a life expectancy of $<$18 months, an unacceptable quality of life, growth failure, reversible neuro-developmental impairment from liver disease or the likliehood of irreversible end organ damage are the most common indications, although rarer indications include organic acidaemia, unresectablehepatic malignancies and hepatoblastoma.[115]

The indications for super-urgent liver transplantation in adult and paediatric patients is based on the King's College Criteria that identified factors depending on whether the aetiology of fulminant hepatic failure was paracetamol or non-paracetamol induced.[116] These criteria have since been modified for paracetamol-induced liver failure (Categories 1-4), favourable (Category 5) and unfavourable (Category 6) non-paracetamol aetiologies, acute Wilson's disease or Budd-Chiari syndrome (Category 7), post liver transplant hepatic aerty thrombosis, special cases of early graft dysfunction after liver transplantation (Category 9), total absence of liver function (Category 10), a previous live liver donor developing acute liver failure postoperatively (Category 11) and acute liver failure in children under two years of age.[115]

Outcomes after liver transplantation are reported by NHSBT in terms of patient and graft survival. Overall undajusted one and five year survival for adult elective deceased donor first transplant is 93.9% and 81.2% respectively. Risk-adjusted one, five and ten year survival for the same group but between January 2005 and December 2016 is 83%, 70% and 57% respec-

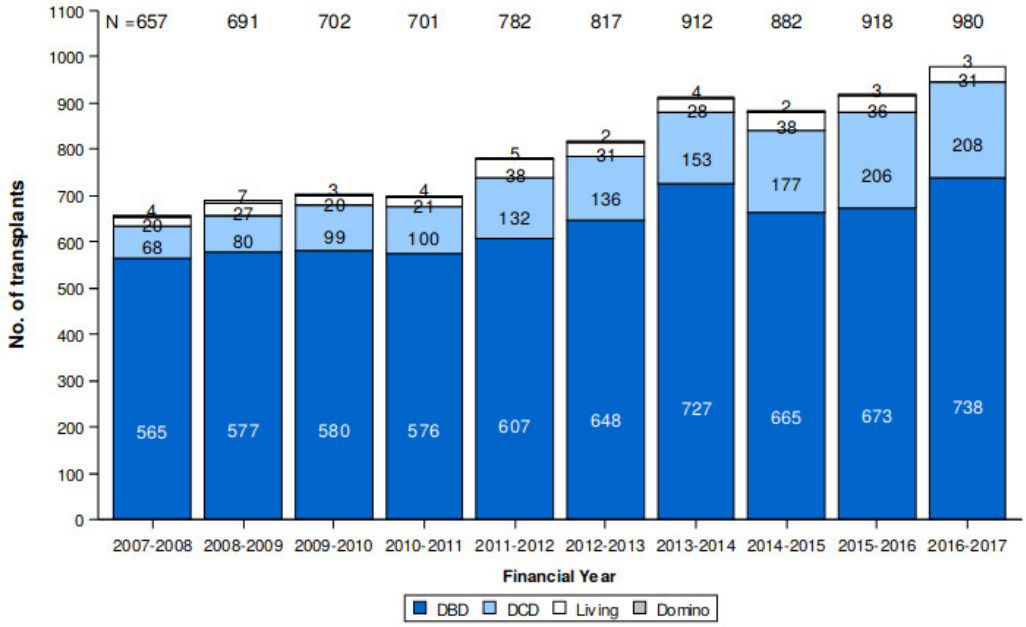

Figure 1.10: Number of liver transplants in the UK 2007-2017.[108] The numbers shown are by donor type, either DBD, DCD, living or domino transplantation.

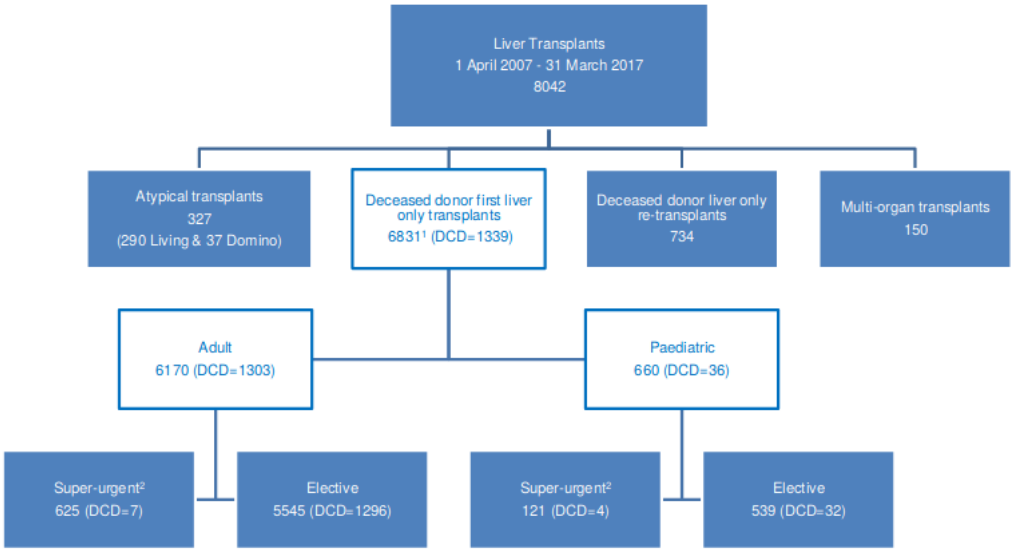

Figure 1.11: Liver tranplants 2007-2017 by urgency.[108] Adult and paediatric liver transplants can be categorised according to whther they are elective or super-urgent.

tively. Overall unadjusted one and five year survival for adult super-urgent deceased donor first transplant is 88.9% and 80.1% respectively for the period April 2012 to March 2016.[108] Paediatric elective first transplant outcomes are even better and are comparable to adults in the super-urgent group.

Differences are apparent when comparing outcome parameters between DBD and all categories of DCD liver transplantation. Studies have shown that graft survival after DCD liver transplantation is inferior compared to DBD, in particular Primary Non-Function (PNF) has been reported between 0-5.5% for DCD whislt biliary complications such as non-anastomotic strictures 13-37% compared to 1-20% of DBD liver transpants.[117, 118, 119, 120] When restricting DCD liver transplantation to Maastricht Category III with donors aged <55 years with a BMI <29 kg/m^2, a donor Warm Ischaemic Time (WIT) <30 mintes and hypotension <15 minutes, it was demonstrated in a multicentre study that 1 and 3 year patient (DCD 85% and 80%, DBD 86.3% and 80.8%) and graft (DCD 74% and 68%, DBD 80.4.3% and 74.5%) survival rates were similiar.[121] Nevertheless, the 3-year cumulative non-anastomotic biliary stricture rate was 31% in the DCD recipients whilst only 9.7% in the DBD cohort.[121] Consequently, identifying risks factors for poor outcome, especially biliary complications, in DCD liver transplantation is paramount. A meta-analysis of risk factors in 489 DCD and 4455 DBD recipients identifed that DCD recipients had a 10.8 times increased risk of ischaemic cholangiopathy (DBD 3% recipients compared to 15% DCD recipients) with a higher 1 year patient mortlaity or graft failure.[122]

Consequently, the concept of the 'Ideal' DCD donor has been proposed that provides favourable outcome after transplantation. An 'Ideal' donor is one who is: (1) <50 years old, has a WIT <30 minutes, a Cold Ischaemic Time (CIT) <10 hours and <15% steatosis.[123, 124, 119, 125, 126] A modification of this has been incorporated in to UK guidelines, in which the age is <50 years, weight <100 kg, Intensive Therapy Unit (ITU) stay < 5 days functional WIT, defined as the time between a systolic blood pressure of <50 mmHg or oxygen saturations <70% to asystole, is <20 minutes, steatosis <10% and CIT <8 hours.[111] These livers are recommended

to be used. In contrast, a 'Marginal' liver, defined as age >50 years, weight >100kg, ITU stay >5 days, a WIT 20-30 minutes, a CIT 8-12 hours and >% steatosis, should only be used selectively.[111] Furthermore, recipient factors that have been associated with graft failure inculde: age >55 years, male sex, African-American race, hepatitis C positivity, a metabolic liver disorder, transplant Model of End Stage Liver Disease (MELD) >35, hospitalisation at transplant and re-transplntation and have been recommended in UK guidelines.[111, 124, 127]

Prediction models that aim to provide an indvidual risk for the particular donor, recipient and donor recipient combination have been devised. Until recently, the most commonly utilised in liver transplantation were the MELD and UKELD scores that predict transplant recipient mortality. The MELD stratefies the severity of end stage liver disease, the model based on creatinine, bilirubin and sodium concentrations as well as Internationalised Normal Ratio (INR).[128, 129] Of more relevance to the United Kingdom is the UKELD score that uses the same parameters but a different formula to predict mortality in the potential transplant receipient.[130, 131] Models predicting risk from using a particular donor have been devised with the oringal being the Donor Risk Index (DRI), an American model that accounts for age, cause of death, race, donor type, donor height, geographical sharing and CIT.[132, 133] The Eurotransplant Donor Risk Index (ET-DRI) is more specific for donors in Europe and incorporates laboratory gamma-glutamyl transpeptidase and rescue allocation.[134] A UK specific score the Donor Liver Index (DLI) has been devised using data from all 7929 liver transplants on the UK transplant Registry that incorporates donor age, sex, height, donor type, bilirubin, smoking history and whether the donor liver was split.[135] However, this model still needs further independent validation using a prospective cohort. Models to optimise donor recipient matching include the Donor Age and Recipient Model for End stage Liver Disease (D-MELD), that is the product of donor age and MELD but does not account for older donors accurately, and Balance of Risk (BAR) score, that includes recipient MELD score, CIT, recipient age, donor age, previous liver transplant and life support dependence.[136, 137, 138] To date these scores do not provide an indication of the benefit of liver transplantation accounting for donor and recipient factors compared to remaining on the transplant waiting list. A recent liver allocation

score based on transplant benefit devised in Germany could not be validated on a UK cohort of patients, demonstrating that perhaps the future relies on national transplant benefit scores applicable to an individual country.[139] This is due to be designed for the UK in the imminent future.

1.5.4 Strategies to Reduce Demand for Liver Transplantation in the UK

In response for the demand of organs to match supply there have been different approaches by both European and UK government. These measures have included considering the introduction of Minimum Unit Price (MUP) for alcohol to reduce the burden of ALD, improved food labelling and public health awareness with repsect to Non-Alcoholic Fatty Liver Disease (NAFLD). MUP of alcohol has been proposed for a number of years with evidence indicating that patients with ALD are consuming high amounts of cheap alcohol (33p/unit) compared to low risk drinkers (£1.10/unit).[140, 141] Furthermore, it has been predicted that the impact of a minimum unit price of 50p/unit would be 200 times higher in patients with liver disease copared to low risk drinkers.[141] The Sheffield Alcohol Policy Model, that accounts for alcohol purchasing and consumption across various socioeconomic groups, has predicted that the greatest impact of a MUP of 45p/unit leads to an immediate reduction in consumption, particulary in the harmful drinkers on low incomes that conincides with substantial increases (87.1%) in quality-adjusted life-years.[142] This has been confirmed by a similar analysis of Scottish harmful drinkers as well as by systematic review.[143, 144] Although legislation is due to come in to effect in 2018 for Scotland, the rest of the UK awaits its impact before reassessing hte need for the introduction of MUP for alcohol.

In an attempt to combat the rise of obesity and the increasing impact that obesity and type 2 diabetes has on NASH related liver mortality, the introduction of a levy on sugar sweetened beverages to reduce the intake of free sugars is soon to be enacted. Qualitative thematic analysis of major UK news websites demonstrated three themes incuding the mistrust of the intention of the proposed tax, varying perceptions of the relationship between sugar, obesity and appropriate

interventions as well as the balance between responsibility and autonomy.[145] Modelling to predict the reduction in weight form a 20% sugar tax results in the reduction in obesity of 1.3% or 180,000 people and largest effect on younger adults.[146] Other modelling has predicted that the largest effect scenario would be for the reformulation of sugar sweetened beverages to reduce obesity, type 2 diabetes and dental caries.[147] the actual effect remains to elicited.

The early identification and treatment of groups at risk of being exposed to hepatitis B and C virus and the longer term implications of developing hepatocellular carcinoma currently is limited to the screening of donated blood (Hepatitis B and C) and for women during pregnancy (Hepatitis B) only.[148] Due to the natural course of hepatitis C, the safety and effectiveness of new directly acting antivirals and the cost implications fo screening, a programme for Hepatitis C appears unjustified.[149] However, the NHS vaccination schedule includes Hepatitis B vaccination to all infants as well as those at higher risk of contracting the virus, both via vertical and horizontal transmission.[150] to date, there is no vaccine for hepatitis C.

1.5.5 Strategies to Increase Supply of Donated Livers in the UK

To increase the supply of organs available for transpantation, a collaborative strategy between the Department of Health UK, The Scottish Government, the Welsh Assembly, the Department for Health, Social Services and Public Safety as well as NHSBT and various interested parties, both within the UK and internationally, has been proposed titled 'Taking Organ Transplantation to 2020 - A UK strategy'.[151, 152] This has identified four main outcomes and builds on previous recommendations for increasing the UK donor rate.

The first outcome is increasing the organ donation rate and is hoped to be achieved by changing behaviour and attitudes towards organ donation, such as education materials and increasing the opportunities for consenting to donation, for example when an individual renews their driving licence or the introduction of organ donation in to the school curriculum. Of particular importance is honouring the wishes of individual at time of donation who have already pledged to be on the organ donor register. Approximately 100 families overide the wishes of their relative

who is on the donor register and prevents them from proceeding with donation. As discssed above, the donation rate of the Black, Asian and Minority Ethnic community is significantly lower than for the white population yet they are relatively overpresented on the transplant waiting list. Increasing the donation rate in this population by increasing awareness of the need to donate and the benefits its brings to their community need to be highlighted. Another option is promoting those individuals already on the organ donor register to be of higher priority should they need a transplant themselves. Finally looking to Spain and Wales, there has been a change in legislation to an opt-out organ donation system that has been evaluated and will come into effect for England from 2020. This will change the burden of registering to be an organ donor to that of presumed consent. Whilst some in the transplant community and public are strong advocates for this system, it remains to be seen whether it actually increases the number of organs available for transplantation based on the results from Spain and Wales.[153, 154]

The second outcome is providing excellent care to donors around the time of donation which should directly impact the care provided to recipients. This can be achieved by adhering to the clinical guidelines for donation, increasing the opportunity of more DCD organs by approaching more families earlier, improving the training provided to clinical staff either employed by NHSBT or by the donor hopitals to emphasise the need to provide excellent care. This has led to the introduction of Clinical Lead for Organ Donation (CLOD)s, a clinician in every hospital in the UK who takes responsibility for and facilitates the identification of potential donors, mainly on ITU. They are supported by a network of Specialist Nurse in Organ donation (SNOD)s, specialist nurses who cover an area of the country within which there are a number of hospitals and who liaise with NHSBT to facilitate the actual organ donation process. They also provide invaluable support directly to donors and their families during a very emotive time. Specifically creating a National Referral Service to support hospitals and working with the Coroner and Procurator Fiscal to facilitate organ donation is of great importance. Additionally, the National Organ Retrieval Service (NORS) was created to provide a network of travelling surgical teams containing a surgeon, an assistant, a theatre practition and, more recently, a perfusionist. The abdominal oragan retrieval teams are provided mainly by the seven liver transplant centres, with

support from number of kidney/panreas transplant centres. The organs, once retrieved from a DBD liver donor will be placed into the national allocation system to permit equality of access to transplantation around the country for potential recipients. The DCD livers are still transplanted by the retrieving NORS teams to minimise the CIT so maintain outcomes. There is a move to commence a national allocation system for DCD livers tht will take into account such particular considerations. Another future avenue is increasing the live donor liver transplant programme, taking left lateral segments of the liver from an adult donor and transplanting it into a child or small adult. Whilst splitting of livers into these components as part of the cadaveric transplant programme, live donor transplantation is largely limited to a few of the largeer liver transpant centres due to the perceived risk of the donor. Expansion of this programme may prove fruitful and eventually become established a in the Far East, where cadaveric programmes are in their infancy.

Increasing the organ utilisation rate is the thrid outcome and can be achieved by increasing the number of DBD and DCD retrievals as well as using novel assessment and therapeutic technologies to stratify organs appropriately, which help in decision making by surgeons in conjunction with the potential recipient around suitability of organs for transplantation. Ante-mortem donor interventions in DCD donors is another area for exploration but may introduce ethical concerns regarding the intention of the intervention. However, of less dispute is the establishing the place of withdrawal for DCD donors, providing named organ recipients and investigating the length of the offering process. Analysis of data surrounding organs that are delcined for transplantation, information sharing and monitoring damage rates is imperative as is exploring novel methods of perfusion and preservation. Improving the transplant community's understanding of compatibility in organ donation and transplantation will hopefully improve organ utilisation and reduce the discard rate of organs. This might incorporate the use different immunosuppression strategies or exchange programmes to permit transplantation between previously considered incompatible donors and recipients.[152]

The final outcome is improving the process of organ donation and transplantation. This in-

corporates creating and expanding regional collaboratives to improve practice, reviewing the worksforce, IT systems and administrative processes to facilitate and maximise on donation and transplantation opportunities. Building a sustainable training and development programme has also been highlighted as has ensuring future capacity in transplant centres as the numbers increase. The creation of an expert histopathology service available 24 hours per day is also being investigated.[152]

The success of the above programme can be measured when: (1) Consent for organ donation is >80%; (2) There are 26 deceased donors per million population; (3) Organ utiliation has increased by 5%, which translated into 85% for abdominal organs; (4) The deceased donor transplantation rate is 74 per million population. The midpoint review as of May 2017 highlights that progress has been made in each of the outcome domains with more of the population joining the organ donor register, increasing rates of referral to the organ donation service, the presence of SNOD at a higher proportion of donations and an increased number of transplants as a result of this action.[155] Nevertheless further action is required to achieve the original outcomes.

1.6 Mechanisms of Ischaemia Reperfusion Injury

Liver preservation is one of the most important steps in the transplantation process as its efficacy influences organ utilisation and outcome. In DBD donors, preservation injury to the liver can occur prior to preservation, during cold preservation, during rewarming and at reperfusion. For DCD donors, an additional injury occurs between when the blood pressure drops below 50mmHg or oxygen saturations are less than 70% to the time of cold flushing a retrieval.[156] Prepreservation injury includes the effects of any underlying liver disease at the time of organ retrieval, injury associated with cardiac arrest or hypotension from either trauma or intoxication, injury during organ retrieval resulting in hypotension as well as the aforementioned warm ischaemia injury during DCD retrieval.

1.6.1 Cold Preservation Injury

Cold preservation injury affects all types of cells within the liver, but it is recognised that HSEC are particularly vunerable to this type of injury, with increasing length of CIT associated with inferior outcomes.[157] Although it is accepted that during cold preservation hepatic core temperature is approaching 0^oC, enzymatic activity is still variable, with the sodium-potassium ATPase being completely inhibited whilst lactate dehydrogenase is active at approximately 10% compared to when at 37^oC.[158]

One consequence of inhibition of the sodium-potassium ATPase is hypothermia injuced cellular swelling due to the inhibition of the Adenosine Tri-Phosphate (ATP) pump to excrete intracellular sodium and maintain a cellular membrane electrochemical gradient. Once the ATPase activity is significantly reduced during cold preservation due to enzymatic inactivity and the relative lack of ATP, osmotic equilibrium occurs between the intracelluar and extracellular space with the influx of sodium ions also bringing negatively charged proteins, resulting in intracellular hyperosmolality, water uptake, swelling and cell lysis.[156]

Although the cooling of organs the metabolic demand, some metabolic reactions are not stopped but continue despite the insufficient generation of ATP The consequence of this is the production of xanthine oxidase that ultimately results in ROS generation as well as increased glycolysis, lactate and hydrogen ion production and influx of calcium ions. With the addition of increased lipolysis, there is cellular membrane injury, receptor-channel impairment and altered cell permeability, all of which contribute to cell death by either apoptosis or necrosis.[159] It appears that HSEC are the most vulnerable hepatic cell type from cold preservation injury.[160]

1.6.2 Reperfusion Injury

There are two distinct phases to reperfusion injury, the early phase which is characterised by rapid Kupffer cell activation that releases ROS including superoxide and hydrogen peroxide.[161] This induces oxidative stress and although modest initially, it triggers a cascade of events that

results in the recruitment of activated leukocytes followed by significant liver injury. Oxidant stress induced by Ischaemia Reperfusion Injury (IRI) results in the release of complement, TLR, high-mobility group box 1 and IL-23.[162, 163] These activate Kupffer cells and induce their production of TNF-α that propagates the inflammatory response by upregulating adhesion molecules on endothelial cells. CD4 T cells are transiently recruited to the liver and, with the previous events, facilitates neutrophil recruitment into the liver parenchyma.[164] Neutrophils directly injure hepatocytes resulting in necrotic cell death, although activation of NF-κB by ROS in hepatocytes leads to the upregulation of protective cytoprotective proteins in an attempt to promote hepatocyte survival and function but concurrently releases proinflammatory TNF-α that propagates the inflammatory injury.[165]

The late phase of IRI is characterised by neutrophil recruitment and their subsequent damage to the hepatocytes via oxidants and proteases. This is dependent on the expression of CXC chemokines that are chemotactic and activating for neutrophils which interact with their receptors CXCR2.[166, 167] The capture and transmigration of neurophils across the space of Disse is dependent on the expression of adhesions molecules P-selectin on the HSEC and L-selectin expressed on neutorphils which slow the neutrophils and allow stronger biding to occur, facilitated by integrins on the neutrophils as well as ICAM-1 and VCAM-1 on the endothelial cells.[168] The release of ROS from the neutrophils causes the greatest hepatocyte damage with the production of superoxide anion that is catalysed by superoxide dismutase to hydrogen peroxide that is reduced to the highly reactive hydroxyl radical. The result is mitochondrial dysfunction, calcium accumulation and mitochondrial permeability, followed by cell death.[169] This has significant impact on organ function and disruption to whole body physiology for patients undergoing liver transplantation that can result in death from myocardial instability following the release of potassium, known as reperfusion syndrome.

1.7 Bench-to-Bedside Research and Emerging Tools for Liver Disease and Transplantation

1.7.1 Bench-to-Bedside Research in Liver Disease and Transplantation

There are a number of different research approaches to improving outcomes in liver disease and organ donation leading on to transplantation. There is a preclinical research strategy, that can be broadly divided into understanding contributors towards inflammation such as the role of VAP-1 in T-cell recruitment, the role of bile acid salts, genetic and environmental factors towards cholangiopathy.[170, 171] Other investigators are approaching T- and B-cell infiltration as their primary focus.[172, 173, 174] A further approach is investigating the effects of reactive oxygen species and their differential role in endothelial, hepatocyte and cholangiocyte damage.[175]

A second strategy is to investigate how the liver regenerates. In particular great emphasis has been placed on mesenchymal stem cells, whether they are recruited from the bone marrow or naturally resident in the liver and their potential immunomodulatory effect.[176] Other groups have approached this problem by considering a resident group of liver progenitor cells. Utilising mouse models to attempt to understand liver progenitor lineage tracking is being actively investigated.[177] Isolating the peri-biliary gland stem cells resident in the biliary tract is being studied as an alternative source of cells available following cholecystectomy.[178] Liver regeneration from a pluripotent stem cell perspective by the transformation of skin fibroblasts into a variety of different liver cells is of significant importance, potentially allowing organs to be regenerated from any other cell type.[179]

Another preclinical strategy is to try and prevent chronic rejection. This has largely been reliant on medical therapy but does also have a reliance on mouse models. New *in vitro* modelling techniques have been developed including an *ex vitro* system as well as organoids.[180, 181] Even these techniques have disadvantages, mainly surrounding the need for the correct environment for cell culture environment that does not necessarily represent the microenvironment that cells are exposed to *in vivo*.

1.7.2 Emerging Tools for Liver Disease and Transplantation

As important as the research themes are for investigating specific diseases from bench to bedside, are the cross-cutting tools that can answer the questions from a systems biology approach. Pertinent methods are metabolomics, proteomics and organ machine perfusion.

Metabolomics

The definition of the metabolome is the quantitative collection of endogenous and exogenous metabolites present in a cell or organism, whether synthesised and catabolised within the biological system or absorbed from its external environment (pharmaceuticals, food nutrients or the components of a growth medium or of symbiotic or passenger organisms).[182] Metabolomics is the study of the metabolome. Although no single technique can capture the complete metabolome, advances in sample preparation and analytical platforms based around mass-spectrometry can increase the yield. Proteomics is the large scale interrogation of biological phenomena at the protein level using mass spectrometry based techniques.[183] Advances in technology and understanding the importance of sample preparation to select the proteome of interest has led to the rapid development and integration of proteomics into pre-clinical, translational and clinical research, including biomarker discovery.[183]

The use of metabolomics in liver disease and transplantation is documented. The drug rifaximin is used to treat hepatic encephalopathy in patients with cirrhotic liver disease however, its mechanisms are not clearly understood but might involved modulation of the gut microbiota and its subsequent influence on the gut-liver-brain axis.[184] The use of serum and urinary metabolomics in conjunction with clinical cognitive testing and microbiome assessment demonstrated that rifaximin significantly improves cognition, increases in serum saturated and unsaturated fatty acids whilst having a significant reduction on gut bacterial linkage in this integrated study.[184] The use of metabolomics has expanded to the assessment of oxidative stress markers, including lipid peroxidation, and metabolic parameters in patients with NASH.[185] These were monitored at intervals during treatment to produce a timecourse of an individual's

metabolomic profile. Expansion of that pilot study involved urinary metabolomics to compare biomarkers across the spectrum of non-alcoholic fatty NAFLD, in which healthy age matched controls were compared to non-diabetic subjects with steatosis but normal liver function and sujects with NASH and abnormal liver function.[186] Not only could metabolomic analysis distinguish between controls and diseased subjects but also identified lower cholinesterase and higher indoleacetic acid in the NASH compared to the NAFLD cohort.[186] Metabolomics can help identify unique signatures assocaited with hepatorenal dyfunction and mortality in patients with cirrhosis which can potentially inform the need for transplantation more accurately than current modelling permits, whic hcould reduce the burden of demand and mortality on the liver transplant waiting list.[187]

Proteomics

To date, there has been a over 40 studies that have implemented proteomics as part of clinical trials to varying extents.[188] These studies can be broadly categorised into those that are attempting to identify stratification or diagnostic biomarkers and can be traced back to the mid 1990s.[188] Stratification of patients to identify those who are higher risk of more severe or more rapidly progressing disease is of particular importance to patient with chronic kidney disease that might necessitate haemodialysis or trasnplantation. High resolution urinary proteomics has been of value in these patients, in which a urinary proteomics-based classifer CKD276 has been quantified to predict the likelihood of a particular patient experiencing an adverse outcome and could separate patients according to their renal function.[189] Urinary proteomics has been able to identify 85 proteins that could discriminate between asymptomatic hypertensive patients with left ventricular diastolic dysfunction from healthy controls.[190] As a diagnostic tool, multiple reaction monitoring-mass spectrometry has been utilised in a prospective clinical study to identify a plasma biomarker protein panel that can differeniate between a transient ischaemic attack and non-cerebrovascular conditions in patients presenting to an accident and emergency department.[191] Nine proteins were demonstrated to be significant uniariate predictors of transient ischaemic attack which could be potentially translated to a

bedsde test.[191]

Proteomics has been translated in to clinical studies investigating potential diagnositic markers in liver disease. These have included identifying proteins that help establish the diagnosis of HCC as the aetiology of malignant ascites using a quantitative proteomics approach with iTRAQ and serum analysis of patients with HCC that has demonstrated galectin-1 as a possible biomarker for the reponse of patients to treatment with sorafenib.[192, 193] Importantly, for a disease with late presentation, difficulty in diagnosis and poor outcome, a prospective proteomic-based study of patients with cholangiocarcinoma identified 25 candidate proteins of which two were validated using other methods, albeit in only five cases compared to five healthy controls.[194] More promisingly, mass spectrometry has been used to assess the reponse of patients to gemcitabine treatment for cholangiocarcinoma and concluded that macrophage-capping protein was assocaited with overall survival.[195] Hepatitis C virus has been the target of serum proteomics that has profiled 25 infected individuals using SELDI-TOF mass spectrometry to assess their response to pegylated interferon and ribavarin.[196] This is of particular use when trying to reduce the burden of hepatitis C on the transplant waiting lists.

1.7.3 The Role of Machine Perfusion

From a translational research perspective, a number of groups have tried to increase the donor pool by understanding the DCD process and outcomes and this has extended to early work using machine perfusion.[197, 198] Here there are three main approaches. Initially hypothermic machine perfusion was approached and successfully translated by a group in America.[199] Within Europe, Clavien and Dutkowski have made substantial progress in the understanding of energy metabolism during Hypothermic oxygenated machine perfusion (HOPE).[200] Another reported approach is by normothermic machine perfusion. To date, the main proponents have been the Oxford group that have developed and translated the Organox device which is now being used as part of an International randomised control trial in which normothermic machine perfusion commences at the donor hospital soon after organ retrieval.[201] The Netherlands

have taken a slightly different approach by returning the donor organ on static cold storage to a perfusion centre for subsequent assessment.[202] There still remain open avenues of exploration to define the correct strategy, for the correct donor to maximise the chance of successful transplantation.

1.8 Aims of the Project

I will test the hypotheses that:

1. Human *ex vivo* normothermic machine liver perfusion can be developed and perfusate lactate concentration evaluated for viability testing in discarded human livers.

2. Human *ex vivo* normothermic machine liver perfusion can be used as a model of ischaemia reperfusion injury that could be translated in to early clinical applications.

3. The Fn14/TWEAK receptor-ligand systems plays a role in intra-hepatic biliary epithelial cell biology using established *in vitro* modelling. Normothermic Machine Liver Perfusion (NMLP) could be used to investigate the role of the Fn14/TWEAK receptor ligand system in an *ex vivo* human model.

CHAPTER 2

DEVELOPMENT & VALIDATION OF AN *EX VIVO* HUMAN MODEL OF THE LIVER USING NORMOTHERMIC MACHINE LIVER PERFUSION

2.1 Introduction

The demand for donor organs in Orthotopic Liver Transplantation (OLT) greatly exceeds supply. As the global incidence of end-stage liver disease continues to rise, there is disparity between the availability of livers and the pressures of increasing demand. In the UK, the number of active patients on the waiting list increased by 11%. However, approaching 20% of patients listed for OLT have either died or been removed from the transplant waiting list within one year of listing.[203] Despite the increasing utilisation of grafts from DCD and marginal DBD, together known as Extended Criteria Donors (ECD), the cadaveric liver transplant waiting list mortality has not decreased. ECD livers are associated with a higher incidence of early post-transplant complications such as PNF, Early Allograft Dysfunction (EAD) or renal failure . Utilisation of high-risk organs remains low with 168 out of 1011 livers procured in the UK during 2015-16 being discarded. Only 35% of all potential DCD livers were transplanted which can be explained by variation in interpretation of donor history, laboratory parameters, macroscopic or histological assessment, personal experience and the transplanting centre's expertise in the utilisation of marginal organs. This semi-subjective assessment impacts on the selection process, potentially compromising patient safety by acceptance of a high-risk marginal graft that does not function or discarding potentially usable organs due to a perceived fear of PNF.

The hypoxic environment of conventional Static Cold Storage (SCS) triggers a cascade of ischaemic injury. Continuing anaerobic metabolism depletes ATP leading to a loss of transcellular electrolyte gradients, influx of free calcium, activation of phospholipases and, on reperfusion, production of ROS. This results in IRI and may lead to graft PNF and Ischaemic Cholangiopathy (IC). However, ECD livers are at increased risk of graft primary non-function, dysfunction, and increased susceptibility to IRI. These remain major obstacles for the utilisation of ECD in transplantation.

One strategy to increase the number of available livers is the progressive expansion of the acceptance criteria for donated organs. There is an increasing reliance on marginal ECD livers from older donors, with higher body mass indices or longer WIT and CIT. However, not only has

mortality on the liver transplant waiting list remained stagnant, but also the potential benefits have been offset by post-transplant complications. Especially seen in recipients of DCD livers, complications include graft PNF, Delayed Graft Function (DGF) and ischaemic type biliary strictures. IRI is a fundamental cause of organ damage following static cold storage leading to complications and is exacerbated by steatosis, particularly in DCD livers. The potentially fatal consequence of PNF remains the main obstacle for the further utilisation of extremely marginal donor livers.[120, 203, 204].

Recipient and graft outcomes after transplantation of ECD livers are less predictable compared to standard criteria donors. Expert but subjective assessment at the transplanting centre of macroscopic appearance and back-table perfusion quality after several hours on ice does not guarantee graft function or recipient survival. Conversely, there may be significant wastage of donor livers that are discarded when they are in fact transplantable. During 2014 in the UK, 102 out of 932 procured livers were discarded because of prolonged WIT and CIT, inadequate perfusion or advanced steatosis.[203].

Machine perfusion is a developing technology that aims to improve preservation of organs prior to transplantation. Three machine perfusion strategies based on temperature (hypothermic, subnormothermic, normothermic) are being investigated, but in all the delivery of oxygen attenuates the detrimental effects of IRI. Several teams have pioneered NMLP using a Packed Red Cell (PRC) based perfusion fluid at 37^{o}C to achieve near physiological conditions and exposes the liver to oxygen and nutrients supporting intrinsic metabolic activity.[202, 205, 206] A randomised trial comparing the outcome of transplanted livers having been subjected to NMLP and SCS is underway as part of a European consortium. This trial utilises Standard Criteria Donor (SCD) and ECD livers.

NMLP is a novel technology developed to provide superior organ preservation compared to static cold storage. Over the last decade, NMLP has been developed to attenuate IRI and improve donor organ utilisation. Experimental data and early clinical results using livers suitable for transplantation have been encouraging.[122, 197, 202, 206, 207, 208, 209, 210, 211, **?**] The

anticipated advantages of NMLP include: (1) Attenuating IRI; (2) Assessment of liver function before transplantation; (3) Improvement of transplantation logistics and; (4) Potential to administer therapeutic interventions to repair livers currently considered unusable, to enable subsequent transplantation.

The aim of this chapter is to test the hypothesis that human *ex vivo* normothermic machine liver perfusion can be developed and evaluated using a standardised protocol for functional assessment with perfusate lactate concentration as a real-time viability test in discarded human livers that correlates with histopathological analysis.

2.2 Materials & Methods

Development of NMLP commenced in March 2013 with the delivery of the machine perfusion device. Assessment of the model commenced with the inclusion of 12 consecutively perfused human discarded donor livers offered for research to the NIHR Birmingham Liver BRU and Centre for Liver Research between May 2013 and June 2015.

2.2.1 Ethics Statement

The study was approved by University of Birmingham Local Regional Ethics Committee, University Hospitals Birmingham NHS Foundation Trust Novel Therapeutics Committee (NT001/14) and National Research Ethics Service committee in London-Surrey Borders (reference number 13/LO/1928). Consent to use donor tissues for research was obtained either directly from the donor when joining the UK Organ Donor Register (ODR) or by a SNOD from the donor's next of kin during consent for organ donation. None of the organ donors were from a vulnerable population and all donors or next of kin freely provided written informed consent.

2.2.2 NMLP Device and Consumables

Normothermic machine perfusion was performed using the CE marked Liver Assist device and the single-use set of consumables (Organ Assist, Groningen, The Netherlands) providing dual perfusion of the Hepatic Artery (HA) and Portal Vein (PV), in a semi-closed circuit, propelled by two rotatory pumps to produce pulsatile and non-pulsatile flows respectively. Arterial and portal pressures were regulated to maintain physiological flow through the HA and PV and set independently. Pressure was limited to a mean of 50 mmHg in the hepatic artery and 10 mmHg in the portal vein. Measured flow rates and calculated resistances were shown in real-time on a liquid crystal display. Oxygen was supplied to two polypropylene, rheoparin®coated, microporous hollow fibre membrane oxygenators with integrated heat exchangers, that also removed CO_2. Oxygen was supplied via a Sechrist air/oxygen blender (S3500CP-G, Inspiration Healthcare Ltd., Leicester, UK). A novel human-based oxygen carrying solution was developed to permit perfusion of livers on the normothermic device that would be physiologically representative. The development of the perfusion fluid is detailed in the section 2.3.

2.2.3 Procurement of Human Discarded Cadaveric Donor Livers

All organs were initially procured by the UK NORS using a standardised surgical protocol, according to NHSBT and British Transplant Society (BTS) guidelines, with the intention of clinical transplantation. Upon inspection by the retrieval or accepting transplant surgeon, livers were subsequently declined for transplantation by all UK transplant centres and were offered for research by the NHSBT co-ordinating office. The decision not to transplant was based on either suboptimal *ex vivo* appearance established by the transplanting surgeon, histological findings or the presence of extra-hepatic donor malignancy. All livers were preserved by University of Wisconsin preservation fluid and exposed to a period of static cold storage at 4^oC.

2.2.4 Preparation and Initiation of NMLP in Human Discarded Cadaveric Donor Livers

Preparation of the liver for NMLP was analogous to clinical transplantation. Redundant tissue was removed whilst the liver was bathed in cold Ringer's solution at 4^oC with slushed ice. The inferior vena cava was dissected and the ends left open. The portal vein was cleaned to its bifurcation and hepatic artery dissected to the gastroduodenal artery. If present, accessory right hepatic artery was anastomosed to gastroduodenal artery stump. The weight of each liver was recorded.

Straight and curved 20 French cannulae (Medos) were inserted into the coeliac trunk and portal vein respectively and secured with ligatures. If the coeliac trunk diameter did not allow direct insertion of the cannula provided with the perfusion set, an iliac artery interposition graft was anastomosed to the aortic patch to permit cannulation (Figure 2.1). The cystic duct was ligated and bile duct cannulated with a transparent plastic tube. Immediately prior to commencing perfusion, the livers were flushed with 2 litres of 10% dextrose solution at 37^oC as per the unit's clinical protocol for transplantation. The liver was then placed into the machine reservoir, the cannulae primed with the perfusion fluid (Results section, Tables 2.4 & 2.5) and connected to the perfusion circuits.

The perfusion was controlled by setting the perfusion temperature and individual pressures in the HA and PV circuits, with the device calculating and displaying real-time resistances and flow rates. Temperature was initially set to 25^oC and increased incrementally to 37^oC within 30 minutes of starting NMLP. The initial pressure setting of 30 mmHg and 8 mmHg in the arterial and portal circuits respectively was increased to 50 mmHg and 10 mmHg within 30 minutes of commencing NMLP. The Fraction of Inspired Oxygen (FiO_2) was set at 0.21 with 2L of flow per minute.

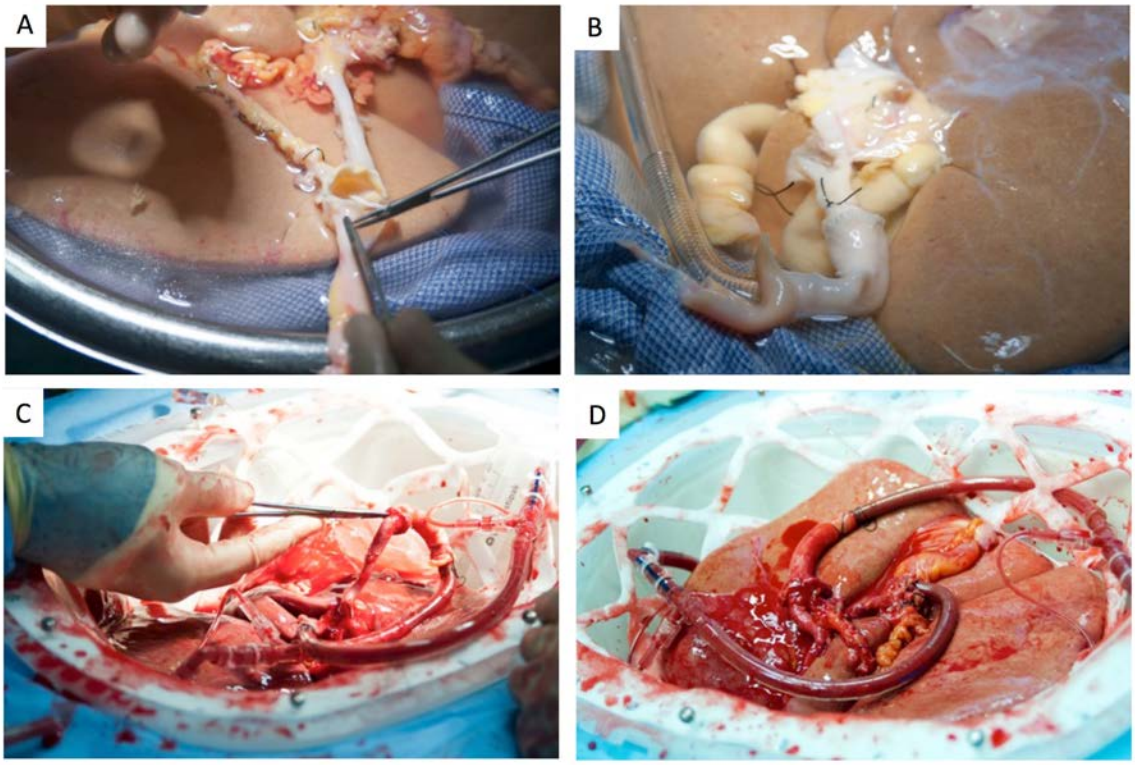

Figure 2.1: Back-table preparation of donor liver for NMLP. (A) If the vessels of the liver were unable to accommodate the cannulae provided, resconstruction using an iliac interposition graft; (B) Flushing the liver with 2L 10%dextrose; (C) Positioning of the vessels at the start of perfusion to ensure uninterrupted flow; (D) Completion of donor preparation and commencement of NMLP.

2.2.5 Sample and Data Collection Protocol

Pressure, resistance, flow and temperature were recorded every 30 minutes. A blood gas sample was collected from the post-oxygenator hepatic arterial circuit and pre-oxygenator hepatic venous circuit at the start and after every 30 minutes of perfusion. Perfusate samples for the clinical biochemistry laboratory, a 4.5ml pre-oxygenator hepatic venous circuit sample transferred in a serum separating tube containing silica particles to activate clotting and serum separator consisting of an inert polymer gel aiding centrifugation, were collected at the same time as the blood gas samples. A further two 10ml samples from the pre-oxygenator hepatic venous circuit were collected at the same time as the blood gas samples and immediately snap frozen in liquid nitrogen for future proteomic and metabolomic analysis. If produced, bile was collected every 30 minutes once perfusion had commenced and subsequently weighed. Both 16G and 3cm cubed wedge parenchymal biopsies snap frozen in liquid nitrogen and formalin fixed for paraffin embedding were collected immediately before perfusion and every 3 hours following commencement of NMLP. Bile duct samples were taken immediately prior to perfusion snap frozen in liquid nitrogen and formalin fixated for paraffin embedding as well as 2.5% glutaraldehyde followed by embedding in a resin block for electron microscopy. A summary of the sample collection protocol is demonstrated in Figure 2.2.

2.2.6 Assessment of Physiology for Livers Subjected to NMLP

Arterial and hepatic venous perfusion fluid was samples were assessed immediately using a Cobas b 221 point of care system (Roche Diagnostics, USA) blood gas analyser measuring partial pressures of O_2, and CO_2, pH, base excess, bicarbonate, O_2 saturation, haemoglobin, haematocrit, sodium, potassium, chloride, calcium, glucose and lactate concentrations. Oxygen consumption per gramme of liver tissue (ml/min/g) and oxygen extraction ratio ($O_{2_{ER}}$) were calculated based on perfusate oxygen content, delivery and extraction from the arterial and hepatic venous elements of the NMLP circuit respectively. Content of oxygen (ml/L) in the arterial, Ca_{O_2}, and hepatic venous, Cv_{O_2}, circuits is defined as:

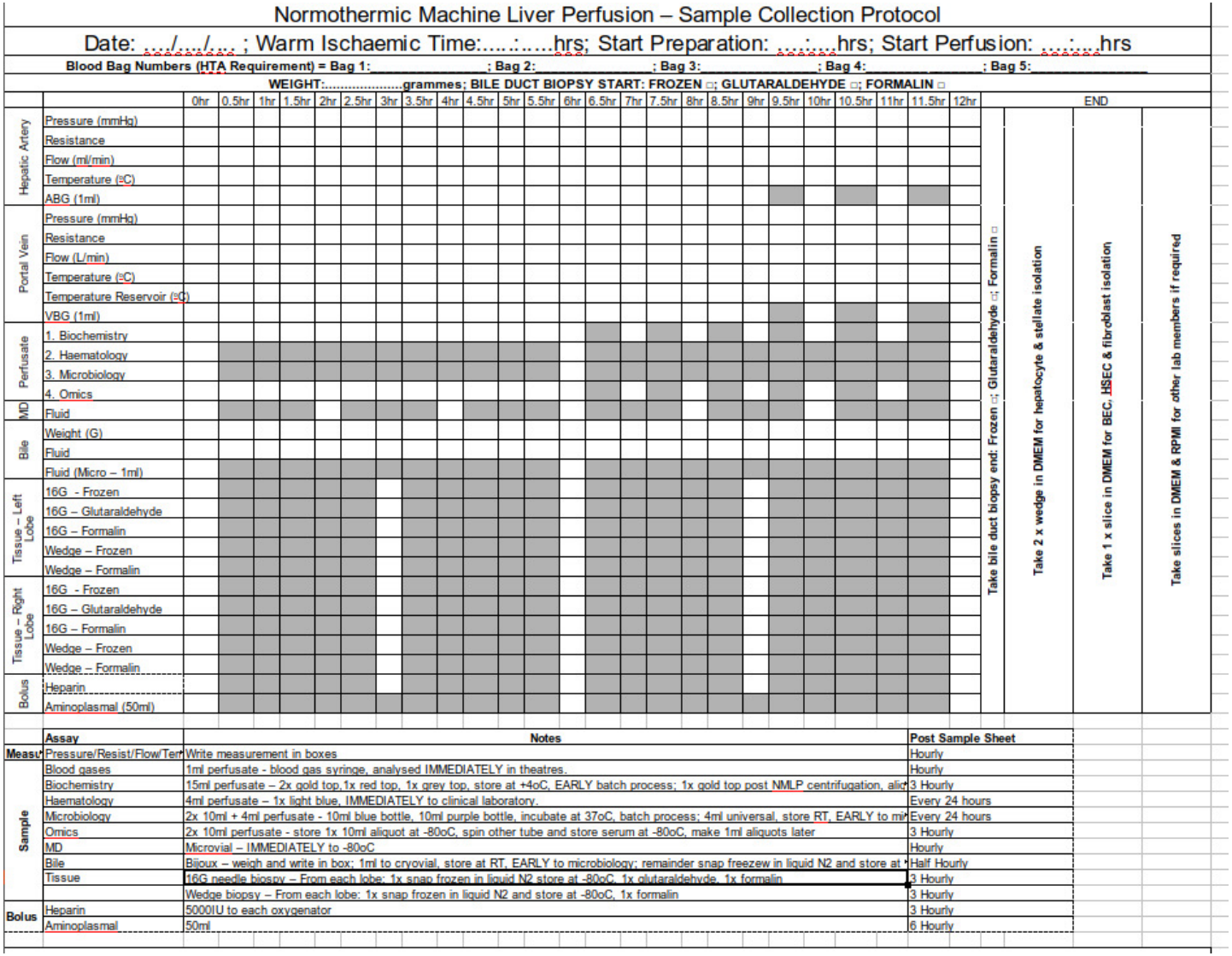

Normothermic Machine Liver Perfusion – Sample Collection Protocol

Date: …/…/… ; Warm Ischaemic Time:…..:…..hrs; Start Preparation: …:…hrs; Start Perfusion: …:…hrs

Blood Bag Numbers (HTA Requirement) = Bag 1:_____; Bag 2:_____; Bag 3:_____; Bag 4:_____; Bag 5:_____

WEIGHT:……grammes; BILE DUCT BIOPSY START: FROZEN □; GLUTARALDEHYDE □; FORMALIN □

		0hr	0.5hr	1hr	1.5hr	2hr	2.5hr	3hr	3.5hr	4hr	4.5hr	5hr	5.5hr	6hr	6.5hr	7hr	7.5hr	8hr	8.5hr	9hr	9.5hr	10hr	10.5hr	11hr	11.5hr	12hr	END
Hepatic Artery	Pressure (mmHg)																										
	Resistance																										
	Flow (ml/min)																										
	Temperature (¤C)																										
	ABG (1ml)																										
Portal Vein	Pressure (mmHg)																										
	Resistance																										
	Flow (L/min)																										
	Temperature (¤C)																										
	Temperature Reservoir (¤C)																										
	VBG (1ml)																										
Perfusate	1. Biochemistry																										
	2. Haematology																										
	3. Microbiology																										
	4. Omics																										
MD	Fluid																										
Bile	Weight (G)																										
	Fluid																										
	Fluid (Micro – 1ml)																										
Tissue – Left Lobe	16G - Frozen																										
	16G – Glutaraldehyde																										
	16G – Formalin																										
	Wedge – Frozen																										
	Wedge – Formalin																										
Tissue – Right Lobe	16G - Frozen																										
	16G – Glutaraldehyde																										
	16G – Formalin																										
	Wedge – Frozen																										
	Wedge – Formalin																										
Bolus	Heparin																										
	Aminoplasmal (50ml)																										

Take bile duct biopsy end: Frozen □; Glutaraldehyde □; Formalin □

Take 2 x wedge in DMEM for hepatocyte & stellate isolation

Take 1 x slice in DMEM for BEC, HSEC & fibroblast isolation

Take slices in DMEM & RPMI for other lab members if required

	Assay	Notes	Post Sample Sheet
Measu	Pressure/Resist/Flow/Ten	Write measurement in boxes	Hourly
Sample	Blood gases	1ml perfusate - blood gas syringe, analysed IMMEDIATELY in theatres.	Hourly
	Biochemistry	15ml perfusate – 2x gold top,1x red top, 1x grey top, store at +4oC, EARLY batch process; 1x gold top post NMLP centrifugation, alic	3 Hourly
	Haematology	4ml perfusate – 1x light blue, IMMEDIATELY to clinical laboratory.	Every 24 hours
	Microbiology	2x 10ml + 4ml perfusate - 10ml blue bottle, 10ml purple bottle, incubate at 37oC, batch process; 4ml universal, store RT, EARLY to mi	Every 24 hours
	Omics	2x 10ml perfusate - store 1x 10ml aliquot at -80oC, spin other tube and store serum at -80oC, make 1ml aliquots later	3 Hourly
	MD	Microvial – IMMEDIATELY to -80oC	Hourly
	Bile	Bijoux – weigh and write in box; 1ml to cryovial, store at RT, EARLY to microbiology; remainder snap freezew in liquid N2 and store at -	Half Hourly
	Tissue	16G needle biopsy – From each lobe: 1x snap frozen in liquid N2 store at -80oC, 1x glutaraldehyde, 1x formalin	3 Hourly
		Wedge biopsy – From each lobe: 1x snap frozen in liquid N2 and store at -80oC, 1x formalin	3 Hourly
Bolus	Heparin	5000IU to each oxygenator	3 Hourly
	Aminoplasmal	50ml	6 Hourly

Figure 2.2: Sample collection protocol for NMLP. See text for details. At the end of perfusion, samples were also collected for epithelial, endothelial and immulogical cell isolation and experimentation.

$$Ca_{O_2} = (1.34 \times Hb \times \frac{Sa_{O_2}}{100}) + (0.23 \times Pa_{O_2}) \tag{2.1}$$

$$Cv_{O_2} = (1.34 \times Hb \times \frac{Sv_{O_2}}{100}) + (0.23 \times Pv_{O_2}) \tag{2.2}$$

Where:

1. Hb is haemoglobin (g/L).
2. Sa_{O_2} and Sv_{O_2} are arterial and hepatic venous oxygen saturations (%) repsectively.
3. Pa_{O_2} and Pv_{O_2} are partial pressures (kPa) of arterial and hepatic venous oxygen repsectively.
4. 1.34 is the direct measurement of the maximum oxygen carrying capacity, known as Hüfner's constant.

Oxygen delivery, $\dot{D}O_2$, (L/min) is defined as:

$$\dot{D}O_2 = CO \times Ca_{O_2} \tag{2.3}$$

Where CO (L/min) is the combined inflow rate in the arterial and portal venous circuits.

Oxygen consumption, $\dot{V}O_2$, (L/min) is defined as:

$$\dot{V}O_2 = CO \times (Ca_{O_2} - Cv_{O_2}) \tag{2.4}$$

This can then be expressed in millilitres per gramme of liver tissue (ml/min/g)

Oxygen extraction ratio ($O_{2_{ER}}$) is defined as:

$$O_{2_{ER}} = \frac{\dot{V}O_2}{\dot{D}O_2} \tag{2.5}$$

2.2.7 Structural and Functional Histological Assessment

Biopsies taken at the timepoints above were formalin fixed and embedded in paraffin blocks for histological evaluation. Slide mounted sections were obtained by cutting the blocks in to sections of 10μm thickness using a microtome then floating the sections on to a pencil labelled slide using a water bath. These were then prepared for Haematoxylin & Eosin (H&E) staining and assessed semi-quantitatively for large and small droplet macrovesicular steatosis (ldMS and sdMS respectively), coagulative necrosis and intrahepatic bile duct injury (apoptosis, vacuolation and lifting of epithelium from basement membrane), that were recorded as percentages of cells affected. Additional sections were assessed for polysaccharide (glycogen) content using Periodic Acid-Schiff (PAS) staining and the mitochondrial Uncoupling Protein 2 (UCP2) staining. Histological assessment of slides stained with H&E was performed by a qualified pathologist who was blinded to 5 random fields from each section from the samples.

Period-acid Schiff Staining

Periodic-acid Schiff staining was performed by initially dewaxing batches of sections in Xylene for 3 minutes, then repeated twice. After dehydration in 99% Industrial Denatured Alcohol (IDA) for 3 minutes, repeated twice, the sections were rehydrated in tap water for 3 minutes, repeated once. Subsequently, sections were bathed in periodic acid 1% with aqueous (Sigma-

Aldrich 395132-1L) for 10 minutes then the excess drained, following which they were placed under running water for 5 minutes. Schiff reagent (Feulgen stain for microscopy, VWR Chemicals 351204L) was added for 30 minutes, after which the sections were placed under running tap water for 10 minutes. Sections were covered with filtered haematoxylin using a pipette for 30 seconds whilst placed on a horizontal rack. Following rinsing in warm tap water, sections were bathed in Scott's tap water for 30 seconds then, after rinsing, were bathed in tap water for 3 minutes, repeated once, to rehydrate them. Sections were bathed in 99% IDA for 3 minutes, repeated twice, then xylene for 3 minutes, repeated twice, before mounting in Distyrene Polystyrene Xylene (DPX) CellPath, UK) using a glass coverslip.

Assessment of Adenosine Triphosphate

Confirmation of maintaining or increasing ATP during NMLP was important to establish thus demonstrating the amelioration of IRI. Measurement of ATP was performed by immediately homogenising snap frozen liver tissue in SONOP Buffer using the GentleMacs system. Protein concentration was determined using a Pierce BCA Protein Assay kit. ATP concentration determined was performed using the ATP Bioluminescent Kit (Sigma FL-AA). Concentrations were determined from a calibration curve on the same plate, corrected for amount of protein and expressed as nmol/g protein.

Staining for Mitochondrial Uncoupling Protein 2

As pertained in the Introduction, it has been demonstrated that UCP2 induces mitochondrial uncoupling which can be initially protective against IRI but reduces the liver's capacity to tolerate further IRI in human and rat models of NASH.[212] It does this by being a negative regulator of superoxide by increasing respiration.[213] As NMLP can help ameliorate IRI and maintain ATP content, establishing a relationship between UCP2 and ATP is important. To summarise, staining for UCP2 was performed by dewaxing, dehydrating and rehydrating batches of slides as described above. During the second bathing in 99% IDA ethanol, a high pH buffer was made by adding 10ml of high pH buffer solution in to 1L of distilled water in a large plastic

tub. After initial rehydration, the slides were transferred to a plastic microwave rack and then to the tub containing high pH buffer solution. After microwaving for 30 minutes at high power (800W) followed by cooling for 10 minutes, the plastic rack and slides were extracted from the microwave, the lid of the tub removed and the slides rinsed in cold tap water. Once cooled, the slides were transferred to a glass jar and then assembled as part of the Sequenza®rack and Coverplate^{TM}system (Thermo Scientific, Runcorn, UK), to ensure reproduction staining consistency and reduce error. Each reservoir was filled with Phosphate Buffered Saline (PBS) to check that even flow rates between the chambers. To each chamber, 100μL (2 drops) of BLOX-ALL blocking solution (SP-6000, Vector Laboratories, Ltd., Peterborough, UK) was added for 10 minutes, followed by PBS wash buffer for 5 minutes. Whilst 100μL of 2% Casein (SP-5020, Vector Laboratories, Ltd., Peterborough, UK; 1ml 10x Casein + 4ml distilled water) was added for 10 minutes, the primary rabbit anti-human polyclonal UCP2 antibody was prepared 1:400 in 2% Caesin. Once completed, 100μL of UCP2 primary antibody (ab203244, Abcam, Cambridge, UK) was pipetted to each chamber and incubated for 1 hour. This was followed by a 5 minute wash buffer step then the addition of 2 drops goat anti-rabbit IgG Amplifier^{TM}Antibody (MP-7602, Vector Laboratories, Ltd., Peterborough, UK), before incubation for 15 minutes. After another wash in PBS buffer for 5 minutes, 2 drops of ImmPRESS^{TM}Excel Amplified Horse Radish Peroxidase (HRP) Polymer Reagent (anti-goat IgG, MP-7602, Vector Laboratories, Ltd., Peterborough, UK) was added and incubated for 30 minutes. This was followed by 2 washes in PBS buffer, during which equal volumes of ImmPACT DAB EqV Reagent 1 with Reagent 2 (SK-4103, MP-7602, Vector Laboratories, Ltd., Peterborough, UK) were combined and mixed well. Subsequent to the last incubation, incubated with ImmPACT DAB EqV working solution for 5 minutes, before another incubation with wash buffer over 5 minutes. Two drops of filtered Mayers haemotoxylin was pipetted to each slide for 30 seconds, before the reaction stopped by adding warm tap water. The sections were then brought to Xylene and finally mounted to DPX using a glass coverslip as described above.

Spectral Image Analysis of Stained Sections

For PAS and UCP2, photomicrographs of complete sections were obtained using a slide scanner (Axio Scan Z1, Zeiss, GmBH) at 5x objective, with the raw .ZVI images processed using Zen Blue software (Zeiss, GmBH) and exported as lossless Tagged Image Format (.TIF). Subsequently, spectral image analysis was performed using Fiji.[214] Each image was opened and colour deconvolution was performed, splitting each image into its Red Green Blue (RGB) channels, using vectors based upon the histological staining technique incorporated.[215] Using the 'Colour_2' image, the default threshold was applied, that uses an iterative procedure based upon the *isodata* algorithm.[216] Once the measurements had been set to include the median intensity density, the image was processed and the data exported as a comma separated file (.CSV).

For ultrastructural examination by Transmission Electron Microscopy (TEM), 2mm segments of the pre-fixed biopsies, pre-fixed in 2.5% glutaraldehyde and processed to a resin block, were cut and mounted. Photomicrographs were taken at 13000x magnification of mitochondria within random hepatocytes and examined for signs of injury.[217]

2.2.8 Statistical Analysis

Calculation of Missing Liver Masses

The first three perfused livers were not weighed for logistical reasons. A derived mass for the missing values was determined by initially calculating the body surface area (BSA) for each perfused liver using the Mostellar formula:

$$BSA(m^2) = \sqrt{\frac{Height(cm) \times DonorMass(kg)}{3600}} \tag{2.6}$$

The Calculated Liver Mass (CLM) for each perfused livers was determined using the published method:[218]

$$CLM(g) = 772 \times BSA \tag{2.7}$$

A linear regression model was determined, through the origin, for all perfused livers where an Actual Liver Mass (ALM) was available (Figure 2.3):

$$ALM(g) = 1.281 \times (CLM); R^2 = 0.981 \tag{2.8}$$

From this, the derived liver masses for the missing values were obtained. The outliers at each extreme of liver mass in Figure 2.3 were acknowledged as was the need for any regression model to intercept at the origin. Whilst the linear regression model could be affected by bias, particularly with small numbers used to generate the model, the high coefficient of determination of 0.981 was encouraging as well as the fact that such weights are seen in clinical practice. A more accurate model, that would minimise any residuals, could be obtained potentially using the Liver Unit Transplant Database at Queen Elizabeth Hospital. However, although the mass of 720 grafts were available from the database, corresponding donor mass and height were incomplete hence could not be added to the linear regression model. Nevertheless, with mean mass of 1535g, standard deviation of 466g and being normally distributed, all the liver masses in Figure 2.3 were within the 95% confidence interval [620g, 2449g] of the database, thus not regarded as outliers. For these reasons, the linear regression model presented was used for further statistical analysis.

Initial Analysis of Perfusion Data

All data was analysed using R 3.3.0 within the RStudio 0.99.896 (RStudio Inc., Boston, MA, USA) Integrated Development Environment.[219] Individual plots of perfusion parameters were generated using the Stata software programme.

The perfusion parameters were limited to either 6 hours NMLP duration or the end of perfu-

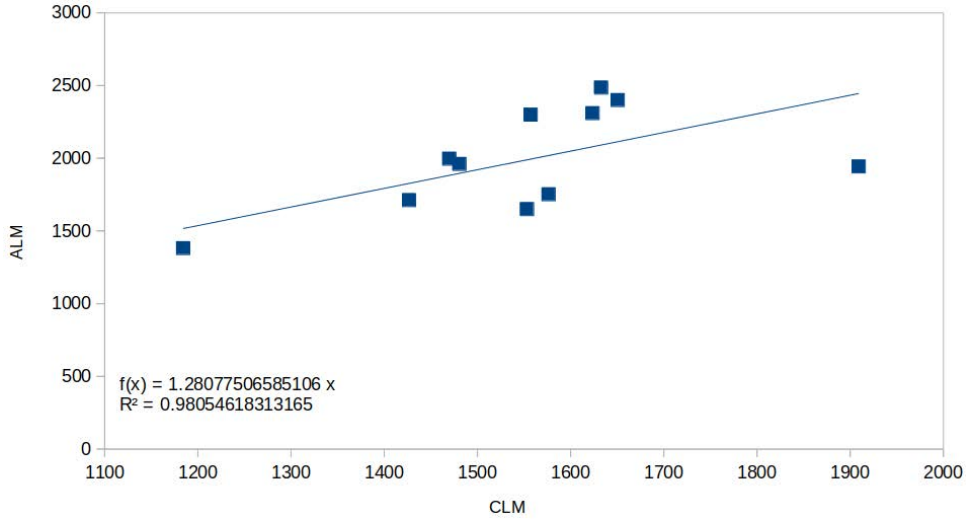

Figure 2.3: Linear regression model for liver masses. The actual liver mass (ALM) for each perfused liver, if available, was plotted against its corresponding calculated liver mass (CLM). From this, a linear regression model with its intercept through the origin was obtained in order to calculate the derived liver mass of the missing values.

sion, whichever was shorter. Assessment of which perfusion parameter produced the best two separate groups for viability testing was determined by cluster analysis using the unsupervised machine learning Partitioning Around Medoids (PAM) algorithm based on K-Medoids. This method is robust to outliers compared to K-means clustering.[220]

For grouped graphs, dots represent the individual data points, whilst the blue lines are smoothed, parabolic, weighted regression curve for the data using the Locally Estimated Scatterplot Smoothing (LOESS) method and shaded areas are the 95% confidence interval for the regression curve. This provides a graphical representation of local regression to model non-parametric data. Plots were created using the 'ggplot2' and 'cowplot' packages for R.

Statistical analysis was performed using the 'psych' and 'exactRankTests' R packages.Categorical data is presented as rounded whole numbers and frequencies. Tests of association were performed using Fisher's exact test. Numerical data are presented as median and range. Data out of range were assigned the appropriate upper or lower limit value for statistical analysis. One and two-tailed Mann-Whitney U allowing for ties were performed as appropriate. Two-way repeated measures factorial Analysis of Variance (ANOVA) was conducted to determine the influence of two independent variables (viabililty and perfusion time) using the 'nlme' package.[221] Viability included two levels (Non-viable, viable) and time consisted of three levels (Start, 2 or 3 hours of NMLP, end of NMLP) with post-hoc Friedman's tests performed if factors or interactions were significant. A p-value of < 0.05 was deemed significant and presented to three decimal places.

Secondary Analysis of Perfusion Data

Twenty-seven perfusion parameters were measured and recorded over a maximum 6-hour period at 30 minute intervals, giving the data a repeated measures structure (Table 2.1). Each perfusion parameter was evaluated using connected scatter plots. Perfusion measurements were plotted against time, combining all study livers' measurements on the same axes for comparative purposes. By giving each liver its own observable trajectory, this enabled any specific,

Function	Parameter	Unit	Type
Fluid Dynamics	Hepatic arterial flow rate	ml/min/100g	Actual
	Hepatic arterial pressure	mmHg	Actual
	Hepatic arterial resistance	mmHg/(ml/min)	Derived
	Portal flow rate	ml/min/100g	Actual
	Portal pressure	mmHg	Actual
	Portal resistance	mmHg/(ml/min)	Derived
Acid-Base	pH	-log10[H+]	Actual
	pCO_2	kPa	Actual
	pO_2	kPa	Actual
	HCO_3	mmol/L	Actual
	BE	mmol/L	Actual
Electrolytes	Na^+	mmol/L	Actual
	K^+	mmol/L	Actual
	Cl^-	mmol/L	Actual
	Ca^{2+}	mmol/L	Actual
Oxygenation	tHb	g/L	Actual
	O_2Hb	%	Actual
	COHb	%	Actual
	MetHb	%	Actual
	HHb	%	Actual
	SO_2	%	Actual
	Hct	%	Actual
Metabolism	Lactate	mmol/L	Actual
	Glucose	mmol/L	Actual
	Oxygen consumption mass	ml/min/100g	Derived
	Oxygen extraction ratio		Derived
	Bile production	g	Actual

Table 2.1: Collected NMLP Parameters. All parameters either directly collected or calculated every 30 minutes for the duration of the NMLP. pCO_2, partial pressure CO_2; pO_2, partial pressure of O_2; HCO_3, bicarbonate; BE, base excess; Na^+, sodium; K^+, potassium; Cl^-, chloride; Ca^{2+}, calcium; O_2Hb, concentration of oxygenated haemoglobin; COHb, concentration of carboxyhaemoglobin ; MetHb, concentration of methemoglobin; HHb, concentration of deoxygenated haemoglobin; SO_2, oxygenation saturation; Hct, haematocrit

common trends to be identified.

Descriptive statistics were obtained for all variables. The median, minimum and maximum values are presented for continuous variables due to the small sample size and accounts for any skewed observations in the data. Numbers are reported at initiation of NMLP (T0) and then after two, four and six hours of NMLP to illustrate performance over time.

Multilevel repeated measures models were employed by a statisitcian (Amanda Kirkham), in view of the complexity of the method, to investigate response variables over time between two groups using a limited sample size. To model the data faithfully, the time variable used for modelling consisted of the actual minute at which each perfusion time point was measured. Random intercept models were constructed with response repeated measures over time and clustered within each liver. Where linear relationships were not observed, data were transformed as appropriate. Explanatory variables and interactions were tested where applicable and included if found to be significant at the 5% level. Models were estimated using the method of maximum likelihood estimation.

2.3 Results

2.3.1 Compilation of Human-Based Oxygen Carrying Solutions for NMLP

The initial fluid was based on PRC and Fresh Frozen Plasma (FFP) described by the Groningen group.[202] As the volume of fluid within the circuit of the Liver Assist device is 2L, dosage calculations were based on 40% adult blood volume. Arterial Blood Gases (ABG) and perfusate samples were taken every 30 minutes during NMLP and informed subsequent interventions.

Oxygen Carrier

For ethical, financial and logistical reasons, initial perfusions were performed with 3 units of either group specific or O-negative PRC aged between 35-45 days, the maximum for clinical usage in the UK and US respectively. The PRC were provided by Blood Bank at Queen Elizabeth Hospital Birmingham. Progressive erythrocyte haemolysis was noted and declining oxygen transport capacity beyond four hours of NMLP was observed. Erythrocyte fragility was associated with the age of PRC and compounded by sheer stress from the centrifugal pumps, circuit tubing and the large surface area of the fluid-air interface in the device's reservoir. After four NMLPs and with ethical approval, transfer to non-clinical grade group specific or O-negative PRC of less than 35 days age, where the volume in each bag was in excess of the 15% tolerance permitted for human transfusion, was instigated. This decreased haemolysis and allowed more stable NMLP lasting 6-10 hours.

Oncotic Pressure

Three bags of FFP were used for the initial pre-study NMLP, performed with a porcine liver (data not shown). During the second pre-study NMLP, using a human discarded liver, defrosting FFP delayed commencement of perfusion, precipitation was observed in the circuit at priming and overall was associated with very poor oxygenator performance. As FFP exposes the liver to complement and inflammatory mediators that may intensify IRI and adding clotting factors may interfere with functional assessment, FFP was replaced with Human Albumin Solution (HAS) 5% (Alburex 5, CSL Behring GmbH, Germany; Na^+ 144-160 mmol/L). The first two study livers were beyond resuscitation and pH was not maintained above 7.20 despite intervention. The significant sodium rise in these perfusions was a result of additional sodium bicarbonate administered. To counteract hypernatraemia, the initial fluid was amended to reduce starting sodium concentration. This was achieved using 250ml HAS 20% (Alburex 20, CSL Behring GmbH, Germany; Na^+ 144-160 mmol/L) and 750ml water for injections (Fresenius Kabi, UK), supplemented with 12ml 30% sodium chloride (approximately 60 mmol Na^+), to achieve the same oncotic pressure with a lower initial sodium concentration of 110-120 mmol/L. As NMLP

development progressed, one refrained from perfusing severely steatotic livers, with their associated lower initial pH value. Therefore, the need for a low starting sodium was negated and so reverted to using 5% HAS. This also had the advantage of reducing the pre-NMLP preparation time.

Concurrently, a perfusion fluid using Gelofusine (B. Braun Medical Limited, UK) as an alternative to HAS was developed. The sodium content, cost and preparation time were favourable however, after observing precipitation in the circuit tubing close to the antibiotic administration port, Gelofusine was concluded to be incompatible with vancomycin. Reduced oxygenation during NMLP beyond 8 hours perfusion was also noted with Gelofusine but not HAS 5%.

Maintaining Adequate Flow During NMLP

Heparin

In accordance with national guidance, intravenous heparin was administered to DBD donors prior to commencing aortic perfusion. In DCD donors, as intravenous heparin administration prior to life support withdrawal is prohibited, the drug was added to the perfusion fluid bags.

Heparin is essential to prevent microthrombi formation in the NMLP circuit, particularly within the oxygenators. As suboptimal *in-situ* organ perfusion is a major reason for declining livers for transplantation, an initial bolus of 10,000 International Units (IU) of heparin sodium (Wockhardt, UK) was added, followed by an additional 10,000 IU bolus every 3 hours.

Vasodilators

Adequate arterial flow is essential for liver function. No vasoactive drugs were used by the Groningen group, whilst the team using the OrganOx®*metra*™device considered a vasodilator to be essential.[202, 222] During the second pre-study perfusion arterial flow reached 200-250 ml/min but decreased to 100-120 ml/min after an hour and was associated with a deterioration in ABG readings. Increasing arterial pressure alone achieved only a transient improvement.

A continuous infusion of Glyceryl Trinitrate (GTN) with additional boluses was administrated after 2.5 hours of NMLP. With this intervention, over 5 hours of NMLP with adequate arterial flow was achieved.

Increased sodium concentrations of up to 200 mmol/L within 6 hours of NMLP were observed when administering a GTN infusion in severely steatotic livers. One hypothesised that supra-physiological perfusate sodium concentrations would interfere with the function of cellular sodium-potassium ATP transporters and be detrimental to liver physiology. From the first study perfusion onwards a switch to epoprostenol (Flolan, GlaxoSmithKline, UK) infusion was made, commencing at 8 μg/hr and increased if HA flow rates sequentially decreased. Except for technical difficulties in cannulation, HA flow rates of greater than 200 ml/min were achieved. The half-lives of these vasoactive drugs are short; 1-4 minutes for GTN and approximately 6 minutes for epoprostenol, hence the need for continuous infusion.

Maintaining Physiological pH

An ABG of the fluid following priming the circuit but prior to connecting the liver was performed. Physiological pH was maintained by administering 30 ml boluses of 8.4% sodium bicarbonate (B. Braun Medical Limited, UK), containing a sodium ion content of 23 mg/ml, to achieve a pH of greater than 7.20. Whilst bicarbonate, phosphate, protein or carbonic acid buffers are contros of physiologcal pH *in vivo*, bicarbonate was the most straightforward to manipulate and quantitate, as well as being used clinically hence permitting ease of translation to practice. Hence it was used for the model. Prior to using non-clinical grade PRC of less than 35 days age as the main oxygen carrier, pH always dropped to less than 7.00 following the start of NMLP. Severely steatotic livers and those with CIT longer than 10 hours required frequent 30 ml boluses of 8.4% sodium bicarbonate, leading to hypernatremia in 6 NMLPs and resulted in alterations to the fluid constituents. The alkalinity of epoprostenol (pH approximately 10.5), increased the overall pH of the fluid and may have reduced the need for further boluses of 8.4% sodium bicarbonate, therefore attenuating hypernatraemia.

Promoting Bile Production

Taurocholic acid, a water-soluble bile acid, has been demonstrated to increase bile production in porcine livers subjected to prolonged NMLP over almost 30 hours.[206] Taurocholic acid (Sigma-Aldrich, UK) was infused during our NMLP in a 2% solution at a rate of 7 ml/hr, equivalent to that previously published.[206] As there was no access to clinical grade taurocholic acid, it was omitted as livers were targeted for subsequent transplantation. Bile was produced without a taurocholic acid infusion when perfusion was limited to 6 hours.

Nutrition and Trace Elements

Insulin and Glucose

A continuous insulin (Actrapid, Novo Nordisk, Denmark) infusion (10 IU/ml) was initially administered at 5 IU/hour to facilitate glucose uptake and utilisation by hepatocytes, similar to the Oxford group. As one did not observe a relationship between glucose decrease and insulin dosage, insulin was removed from the perfusion protocol. If glucose concentration was less than 10 mmol/L then a 50ml bolus of 10% glucose (Macopharma, UK) was administered to the circuit.

Amino Acids

Calculating the liver's energy requirements based on its mass as a proportion of the total energy requirements of the body is inadequate and it is likely to underestimate the amino acid demands. The liver utilises 25% of total amino acid requirement.[223] Based on a typical adult's parenteral nutritional need for 12g nitrogen over 24 hours, an estimate of 25% of this amount was administered as 50ml (0.8g nitrogen) boluses of Aminoplasmal 10% (B. Braun Medical Limited, UK; nitrogen content 16g/L) every 6 hours.

Vitamins

Multivitamins for infusion, containing vitamins A (retinol), D3, E (α tocopherol), C, B1 (thiamine), B2 (riboflavin), B6 (pyridoxine), B12, folic acid, pantothenic acid, biotin and vitamin PP (niacin), were administered with Aminoplasmal every 6 hours as 2ml of Cernevit (Baxter Healthcare Ltd., UK) reconstituted with 5ml water for injections. Additionally, 1mg phytomenadione as Konakion Paediatric MM (Roche Products Limited, UK), was administered to provide the substrate for potential factor V assays during NMLP. Although typically used in parenteral nutrition, lipid was not added to the circuit, in an attempt to reduce the metabolic load on steatotic and severely ischaemic livers.

Antibiotics

Antibiotics were added to minimise bacterial contamination. The Groningen protocol included cefazolin, a first generation cephalosporin that is not readily available in the UK.[202] For this perfusion protocol antibiotics would be: (1) Compatible with other constituents of the fluid; (2) provide adequate broad-spectrum cover without undergoing hepatic metabolism; (3) have assays available to measure concentration within the fluid; (4) administered to livers that could be transplanted in to recipients irrespective of penicillin allergy. Dosages were calculated based on perfusion fluid volume in relation to the circulating volume of an adult human (40-50%). Compatibility studies to identify precipitation with the non-PRC components were conducted (Table 2.2).

2.3.2 Compatibility Testing of Perfusion Fluid Components

Compatibility testing of various components of the perfusion fluid demonstrated that either a combination of vancomycin and meropenem or vancomycin and gentamicin would provide the most appropriate antimicrobial cover, whilst minimising precipitation when albumin was used to provide oncotic pressure to the solution. If gelofusine was used to provide oncotic pressure, then precipiation, particularly with vancomycin and gentamicin combined, was exacerbated and

ANTIBIOTIC	NMLP DOSE (HALF HUMAN DOSE)	VOLUME	In 0.5ml
Amoxicillin	250mg	5ml	25mg
Ceftazidime	1g	10ml	50mg
Cefuroxime	750mg	6ml	62.5mg
Ciprofloxacin	200mg	100ml	1mg
Clarithromycin	250mg	5ml	25mg
Clindamycin	300mg	2ml	75mg
Co-amoxiclav	600mg	10ml	30mg
Gentamicin	60mg	1.5ml	20mg
Meropenem	500mg	10ml	25mg
Metronidazole	250mg	50ml	2.5mg
Tazocin	2.25g	10ml	112.5mg
Vancomycin	500mg	10ml	25mg
Vancomycin + Gentamicin			
Vanocmycin + Meropenem			

Table 2.2: List of antibiotics used for compatibility testing with perfusion fluid. The list contains antibiotics that provide a wide spectrum of antimicrobial cover and provide alternatives for patients with a potential penicillin allergy. All doses tested at half the normal adult dose due to the isolated organ, before being reduced proportionally for testing.

				5% ALBUMIN			20% ALBUMIN			GELOFUSINE		
ANTIBIOTIC	NMLP DOSE (HALF HUMAN DOSE)	VOLUME	In 0.5ml	BASE	BASE + INFUSIONS	FLUCONAZOLE	BASE	BASE + INFUSIONS	FLUCONAZOLE	BASE	BASE + INFUSIONS	FLUCONAZOLE
Amoxicillin	250mg	5ml	25mg	0	0	0	0	0	0	0	0	0
Ceftazidime	1g	10ml	50mg	0	0	0	0	0	0	0	0	0
Cefuroxime	750mg	6ml	62.5mg	0	0	0	0	0	0	0	0	0
Ciprofloxacin	200mg	100ml	1mg	0	0	0	0	0	0	0	0	0
Clarithromycin	250mg	5ml	25mg	1	1	0	1	1	0	1	1	0
Clindamycin	300mg	2ml	75mg	0	0	0	0	0	0	0	0	0
Co-amoxiclav	600mg	10ml	30mg	0	0	0	0	0	0	0	0	0
Gentamicin	60mg	1.5ml	20mg	0.5	0.5	0.5	0.5	0.5	0.5	0.5	0.5	0.5
Meropenem	500mg	10ml	25mg	0	0	0	0	0	0	0	0	0
Metronidazole	250mg	50ml	2.5mg	0	0	0	0	0	0	0	0	0
Tazocin	2.25g	10ml	112.5mg	0	0	0	0	0	0	0	0	0
Vancomycin	500mg	10ml	25mg	0.5	0.5	0.5	0.5	0.5	0.5	1	1	1
Vancomycin + Gentamicin				0.5	0.5	0.5	0.5	0.5	0.5	1	1	1
Vanocmycin + Meropenem				0	0	0	0	0	0	0.5	0.5	0

Table 2.3: Results of compatibility testing components of perfusion fluid with various antibiotics. The scale incorporated denotes: ‘0’ does not result in any precipitation, ‘0.5’= some precipitation but held in suspension after centrifugation, ‘1’ = precipitation in bottom of universal container after centrifugation.

would be deleterious to the perfusion circuit and the perfused liver (Table 2.3)

2.3.3 Final Regimens

Vancomycin (Wockhardt, UK) 500mg and gentamicin (Cidomycin, Sanofi, UK) 60mg were identified as the appropriate antibiotics for administration with the HAS based fluid. Cefuroxime 750mg was used for the Gelofusine based fluid.

Two perfusion fluids were developed providing the components for successful resuscitation and subsequent transplantation. The first was demonstrated to be suitable in NMLP directed at preclinical research and potential clinical transplantation in to patients without penicillin allergy that required NMLP for longer than 6 hours (Table 2.4). The second was shown to be appropriate for perfusions resulting in potential clinical transplantation in patients with a known penicillin allergy and where NMLP is required for less than 6 hours (Table 2.5).

These perfusion fluids achieve oxygenation and adequate flow by using either group specific or O-negative PRC and the dynamic adminstration of epoprostenol respectively. A range of other pharmacological interventions provide a near physiological environment that facilitates assessment of viability. The fluids are versatile as they can be applied in both preclinical research environments and in translational studies, as demonstrated by the successful transplantation of two livers after NMLP, each using a different fluid. Additionally, the fluids can be stratified according to the penicillin allergy status of the potential recipient whose donor liver has been subjected to NMLP. These regimens permit the rapid establishment of NMLP, as PRC and either HAS or Gelofusine, supplemented by epoprostenol, are essential for initiating perfusion, with the remaining drugs being infused after commencement. However, composition of the fluids are reliant on the donation and processing of whole blood to provide PRC, an increasingly scarce resource associated with potential incompatibility with the donated liver and recipient as well transfusion-related infection. Although these fluids have accounted for available evidence, the majority of design has been based on expert rationale.

Prior to commencing NMLP:		
Drug	**Amount/rate**	**Comments**
Human albumin solution 5%	1 litre	
Packed red cells	3 units	
Heparin 5,000iu/5ml	10,000iu (10ml)	Single bolus
Sodium bicarbonate 8.4%	30ml	
Calcium gluconate 10%	10ml	
Epoprostenol	2mcg/ml in 50ml syringe	Continuous infusion at 4ml/hour
After commencing NMLP:		
Drug	**Amount/rate**	**Comments**
Vancomycin	500mg	Single bolus
Gentamicin	60mg	
Taurocholic acid 2%	2%, 50ml syringe	Continuous infusion at 7ml/hr
Aminoplasmal 10%	50ml	Single bolus every 6 hours
Sodium bicarbonate 8.4%	30ml	Single bolus if pH $<$7.20
Glucose 10%	50ml bag	Single bolus if perfusate glucose $<$10 mmol/L
Heparin 5,000iu/5ml	10,000iu (10ml)	Single bolus every 3 hours

Table 2.4: Final perfusion fluid regimen. Epoprostenol, in 50ml syringe, according to manufacturers instructions. Aminoplasmal, add 5ml water to a vial of Cernevit and add 2ml & phytomenadione 1mg (0.1ml) to Aminoplasmal 500 ml bottle. Taurocholic acid for research livers only.

Prior to commencing NMLP:		
Drug	**Amount/rate**	**Comments**
Gelofusine	1 litre	
Packed red cells	3 units	
Heparin 5,000iu/5ml	10,000iu (10ml)	Single bolus
Sodium bicarbonate 8.4%	30ml	
Calcium gluconate 10%	10ml	
Epoprostenol	2mcg/ml in 50ml syringe	Continuous infusion at 4ml/hour
After commencing NMLP:		
Drug	**Amount/rate**	**Comments**
Cefuroxime	750mg	Single bolus
Taurocholic acid 2%	2%, 50ml syringe	Continuous infusion at 7ml/hr; research only
Aminoplasmal 10%	50ml	Single bolus every 6 hours
Sodium bicarbonate 8.4%	30ml	Single bolus if pH $<$7.20
Glucose 10%	50ml bag	Single bolus if perfusate glucose $<$10 mmol/L
Heparin 5,000iu/5ml	10,000iu (10ml)	Single bolus every 3 hours

Table 2.5: Final perfusion fluid regimen for those with a penicillin allergy. Epoprostenool, in 50ml syringe, according to manufacturers instructions. Aminoplasmal, add 5ml water to a vial of Cernevit and add 2ml & phytomenadione 1mg (0.1ml) to Aminoplasmal 500 ml bottle. Taurocholic acid for research livers only.

2.3.4 Demographics of Human Livers

A total of twelve livers, eight of which where DCD, were included in the study. The median donor age was 56 (range 30 - 76) years and the body mass index 30 (23-47) kg/m^2. The median CIT was 483 (range 380 - 797) minutes. Three livers were discarded due to steatosis, two livers for extrahepatic primary donor malignancy, 2 for excessive CIT and 2 for excessive donor WIT. Liver fibrosis, prolonged stay on ITU and poor perfusion in the remaining 3 livers precluded use for OLT (Table 2.6).

There was a significant discrepancy between the subjective assessment of liver quality performed by the organ retrieval or transplant surgeon and the subsequent histological findings. Microscopic evaluation confirmed only a mild large droplet macrovesicular steatosis in livers declined for steatosis. Histology did not reveal any fibrosis in the liver declined for this presumed diagnosis. Two livers (Table 2.6, donors 8 and 9), were declined for unexpected remote donor malignancy and otherwise had favourable macroscopic appearances and stable perfusion characteristics during NMLP (Figure 2.4 A). Similar characteristics were observed in another four livers. The remaining six livers had unsatisfactory macroscopic appearances, including steatosis and fibrosis, or unsatisfactory perfusion parameters during NMLP (Figure 2.4 B).

2.3.5 Identification and Confirmation of Differentiating Perfusion Parameters for Viability Testing of Discarded Human Cadaveric Donor Livers Subjected to NMLP

Lactate Metabolism Clusters Perfused Livers into Two Distinct Groups

Only the lactate plot for individual NMLPs visually demonstrated clustering in to two distinct groups (Figure 2.5). Plots for flow parameters (Hepatic artery flow per gramme of liver tissue, hepatic artery pressure, hepatic artery resistance and congruent portal vein flow parameters), acid-base balance (pH, bicarbonate and base excess), oxygen carrying capacity (total haemoglobin, haematocrit, oxygen consumption per gramme of liver and oxygen extraction ratio) and glucose metabolism did not show any clustering (Figures 2.6-2.17). Although total

Perfusion number	**1**	**2**	**3**	**4**	**5**	**6**	**7**	**8**	**9**	**10**	**11**	**12**
Donor age (years)	55	55	76	60	46	30	69	55	57	71	70	50
Donor gender	Female	Male	Female	Female	Male	Male	Male	Male	Male	Male	Female	Female
BMI (kg/m^2)	47	33	28	36	23	25	31	24	25	30	34	45
Blood group	B+	A+	O+	A+	O+	A+	O+	O+	A+	O-	O+	O+
Cause of death	Meningitis	ICH	ICH	HBI	ICH	HBI	HBI	Meningitis	ICH	HBI	HBI	HBI
Donor type	DBD	DCD	DCD	DCD	DBD	DCD	DBD	DBD	DCD	DCD	DCD	DCD
Agonal period (mins)	NA	14	8	17	NA	100	NA	NA	14	31	16	29
Primary WIT (mins)	NA	12	17	15	NA	12	NA	NA	14	12	18	11
Liver weight (grammes)[1]	2420	2129	1775	1712	1961	1997	2400	2300	1752	2310	1650	1943
Steatosis assessment	Moderate	Moderate	Nil	Moderate	Mild	Nil	Mild	Nil	Mild	Moderate	Mild	Nil
Cold ischaemic time (mins)	792	797	554	491	380	445	496	454	532	467	583	408
Donor risk index	1.846	2.643	3.228	2.77	1.411	1.766	1.782	1.612	2.361	3.216	3.053	2.385
Reason for discard	Steatosis	Steatosis	CIT	Steatosis	ITU	WIT	Fibrosis	Cancer	Cancer	Perfusion	CIT	WIT
Designated viability	Non-viable	Non-viable	Non-viable	Non-viable	Non-viable	Viable	Viable	Viable	Viable	Non-viable	Viable	Viable

Table 2.6: Donor demographics and chronology. NA, not applicable; ICH, intracranial haemorrhage; HBI, hypoxic brain injury
Note: Agonal period in DCD procurement was defined as period between withdrawal of treatment to circulatory arrest. Primary warm ischaemic time in DCD procurement defined as time from circulatory arrest to in-situ organs perfusion.

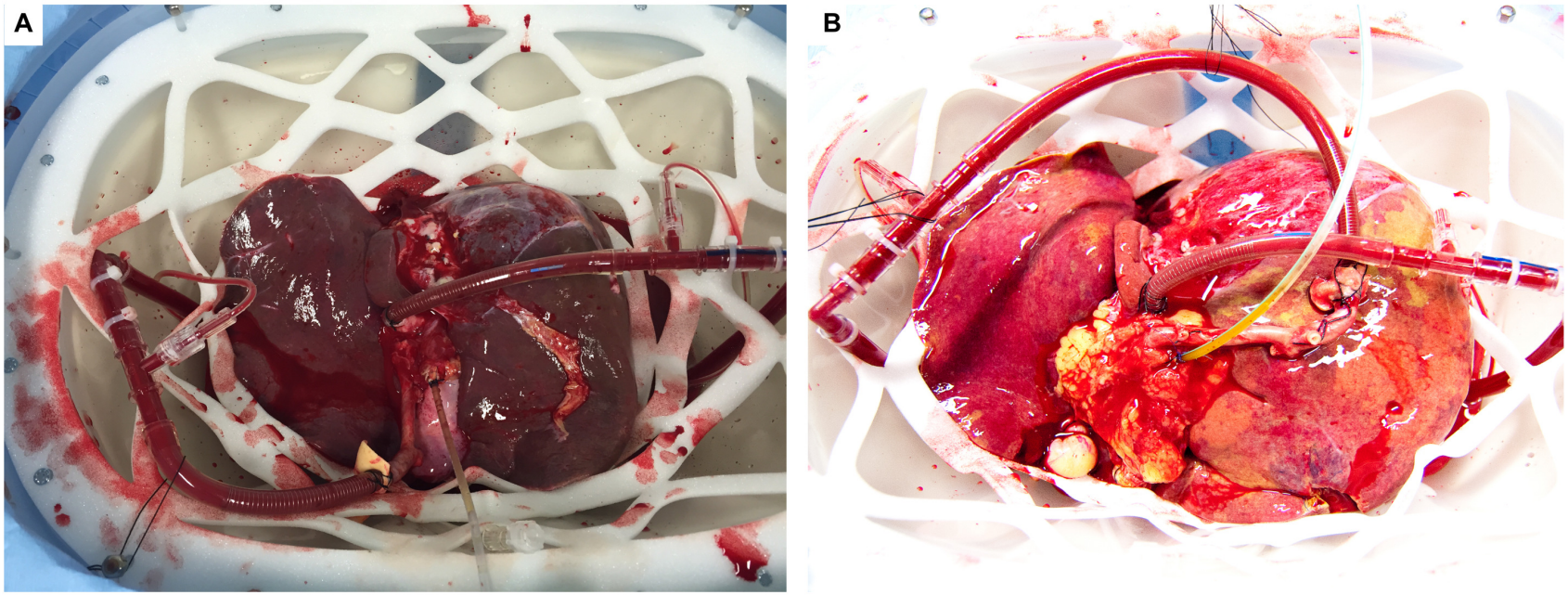

Figure 2.4: Macroscopic appearance of steatotic and non-steatotic livers. Well-perfused liver with optimal macroscopic appearance (A). The organ was rejected for transplantation due to the incidental discovery after cross-clamping of a malignant melanoma. The liver appeared to function shortly after commencing the perfusion with vascular flows and blood gas profile patterns used to help define criteria for liver graft viability (perfusion number 8). Steatotic liver with suboptimal macroscopic appearance (B). Photographs provided by the Normothermic Machine Liver Perfusion Study Group.

haemoglobin graphically appeared to form two clusters, this could not be justified as NMLP 3 terminated after 3 hours of perfusion. Furthermore, PAM cluster analysis confirmed that lactate concentration in the perfusate could group the data in to two distinct clusters, confirming the visual representation.

Parameters were then categorised in to two groups based on lactate group, named 'viable' and 'non-viable', interchangeable with 'lactate clearing' and 'non lactate clearing' respectively. There was no difference in the median starting lactate concentration between the viable and non-viable groups (13.1 mmol/L vs. 13.4 mmol/L, p = 0.411). During NMLP, viable livers showed significantly higher lactate clearance (Figure 2.18). After 2 hours, the median lactate concentration in the viable group was 3.1 mmol/L vs. 15.8 mmol/L in the non-viable group (p = 0.004). By the end of NMLP, the median lactate in the viable group was lower compared to the non-viable group (2.3 mmol/L vs. 15.2 mmol/L, p = 0.001). These were reinforced by greater reductions in lactate concentrations compared to initial concentration, known as the delta lactate, in the viable group at both 2 hours of NMLP (-9.6mmol/L vs. -0.5mmol/L, p = 0.002) and at the end (-10.4mmol/L vs. -0.1mmol/L, p = 0.013). Detailed information concerning lactate clearance is provided in Figures 2.18 and 2.19 as well as in Tables 2.7 and 2.8.

Bile Production

In the non-viable group, only one liver produced bile by the end of the NMLP (2.6g at 6 hours). A binomial test indicated that the proportion of non-viable livers producing bile during the perfusion 0.0139 was lower than the expected 0.5, $p < 0.001$. There was more sustained bile production in the viable group, although this only occurred in 4 livers. A binomial test indicated that the proportion of viable livers producing bile during the perfusion 0.486 was similar to the expected 0.5, p = 0.906. After 2 hours, the median production was similar (viable 0.0g vs. non-viable 0.0g, p = 0.227), but was significantly higher in the viable group at the end of NMLP (6.5g vs. 0.0g, p = 0.030)(Figure 2.20).

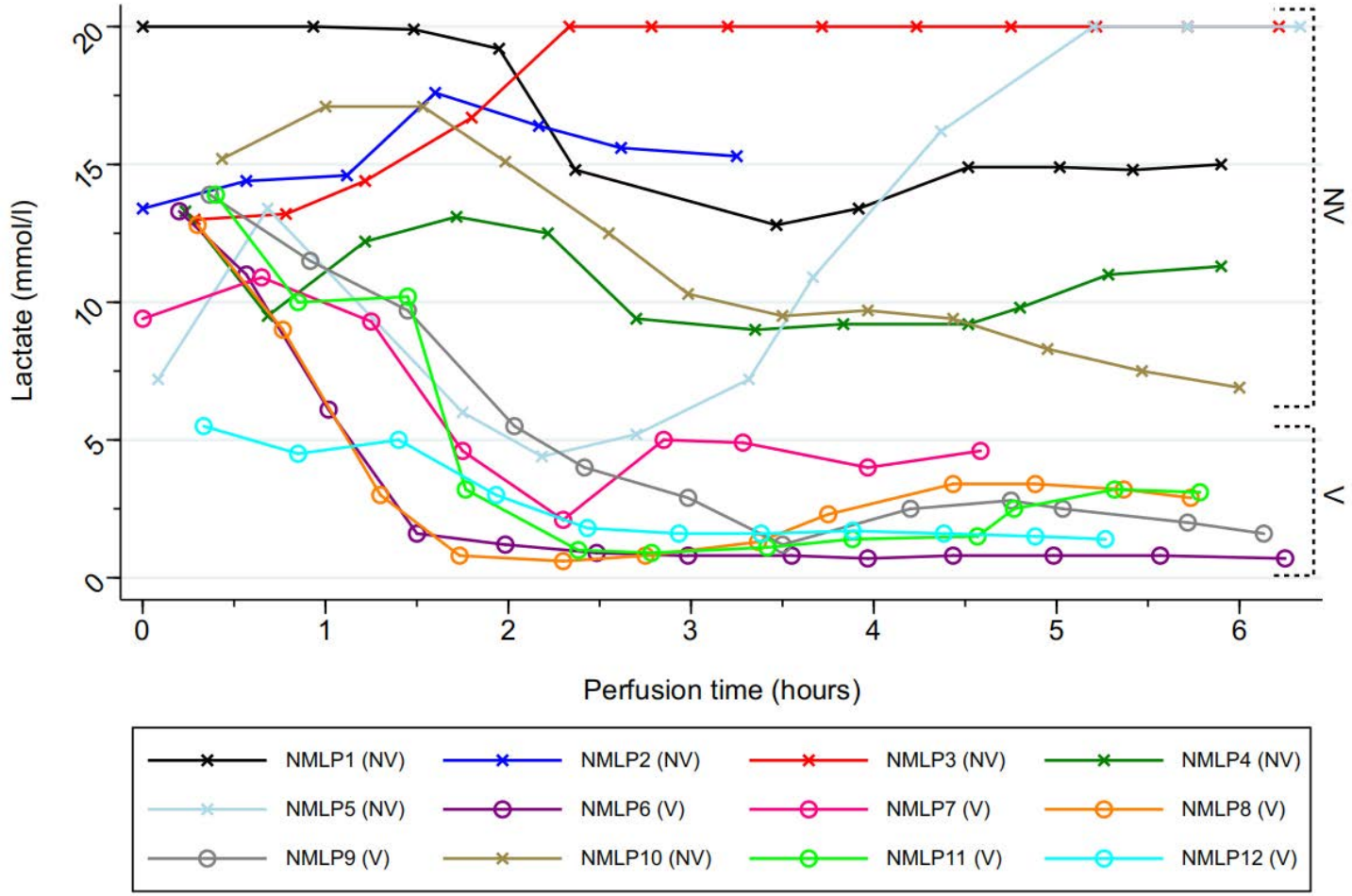

Figure 2.5: Lactate concentration over time by individual NMLP. This visually demonstrates clustering in to two distinct groups, viable (V) and non-viable (NV) denoted by the dotted lines, with the non-viable group (NMLP 1-5,10) being at higher lactate concentrations for most time points compared to the viable group (NMLP 6-9,11,12).

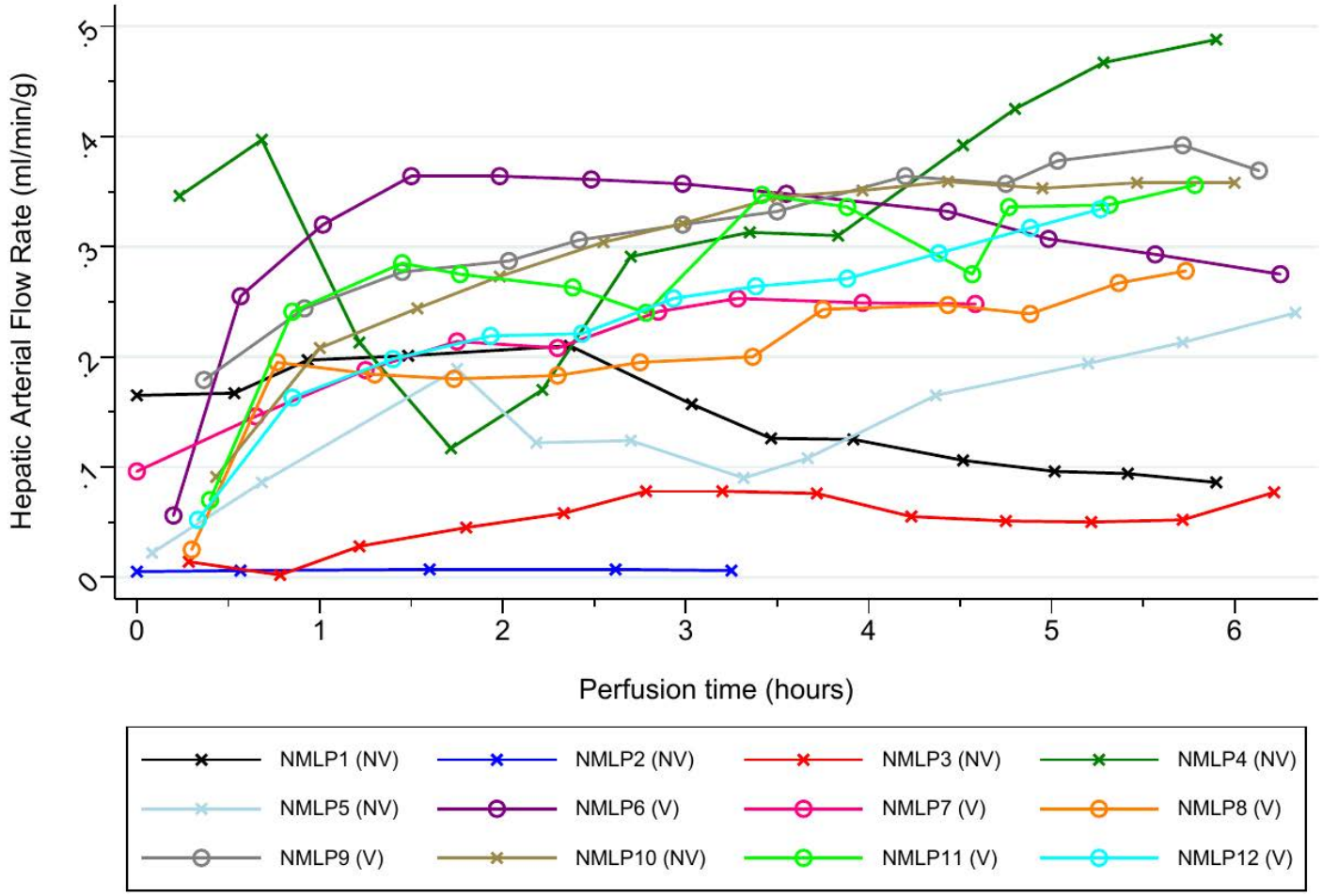

Figure 2.6: Hepatic artery flow rate per gramme of liver over time by individual NMLP. This visually does not demonstrate clustering in to two distinct groups. Cross-referencing to viable (V) or non-viable (NV) groups based on lactate concentration.

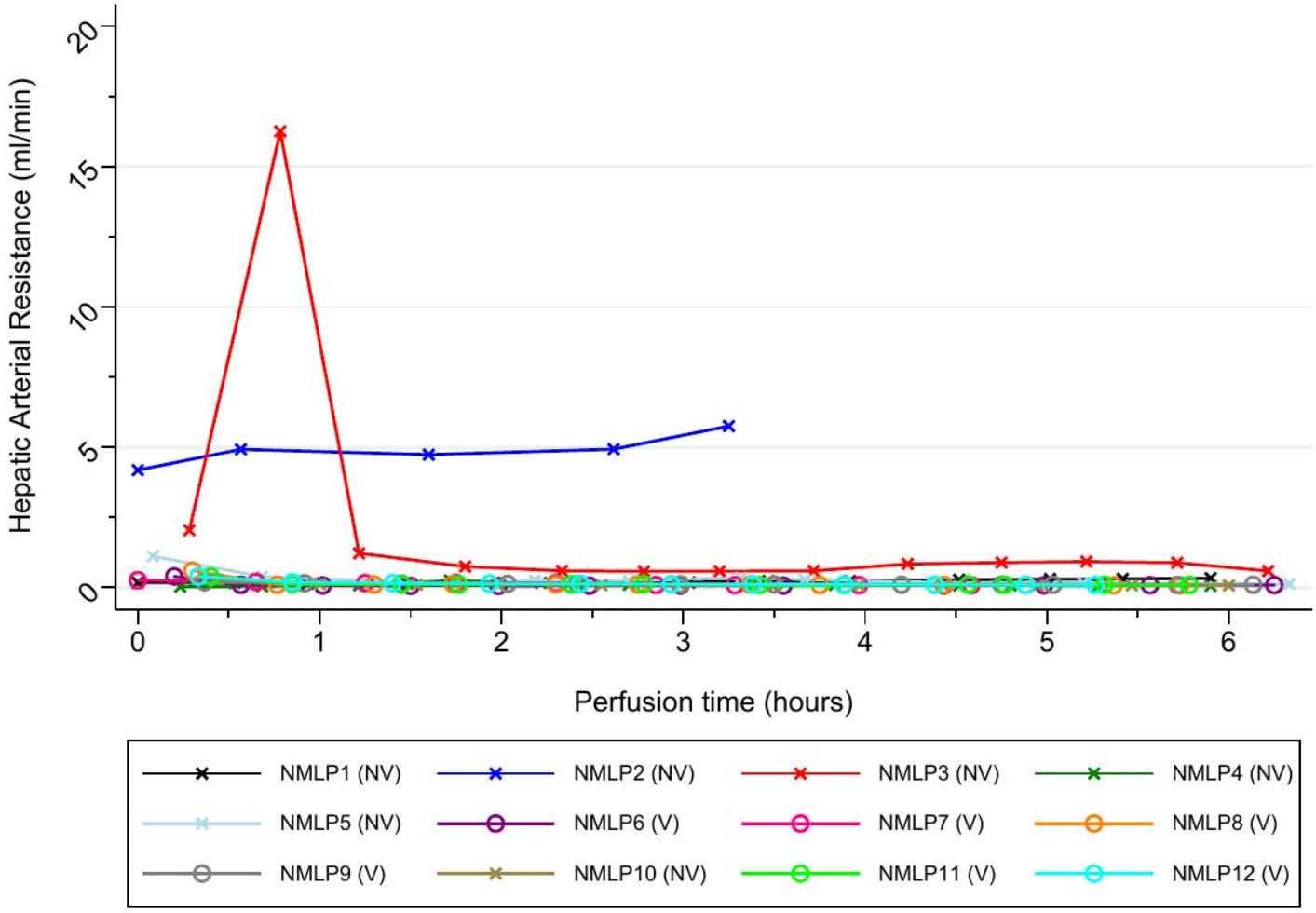

Figure 2.7: Hepatic artery resistance over time by individual NMLP. This visually does not demonstrate clustering in to two distinct groups. Cross-referencing to viable (V) or non-viable (NV) groups based on lactate concentration.

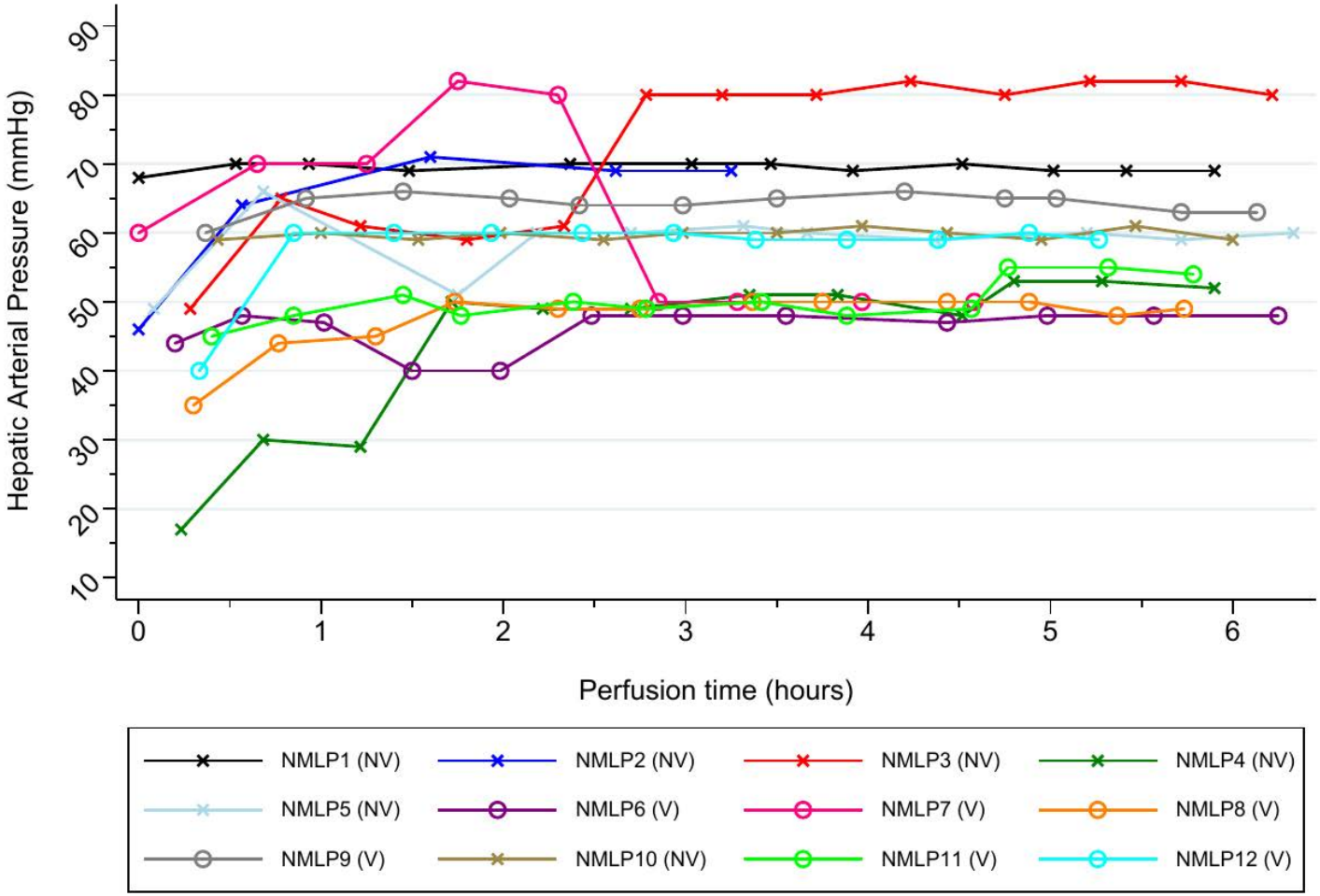

Figure 2.8: Hepatic artery pressure over time by individual NMLP. This visually does not demonstrate clustering in to two distinct groups. Cross-referencing to viable (V) or non-viable (NV) groups based on lactate concentration.

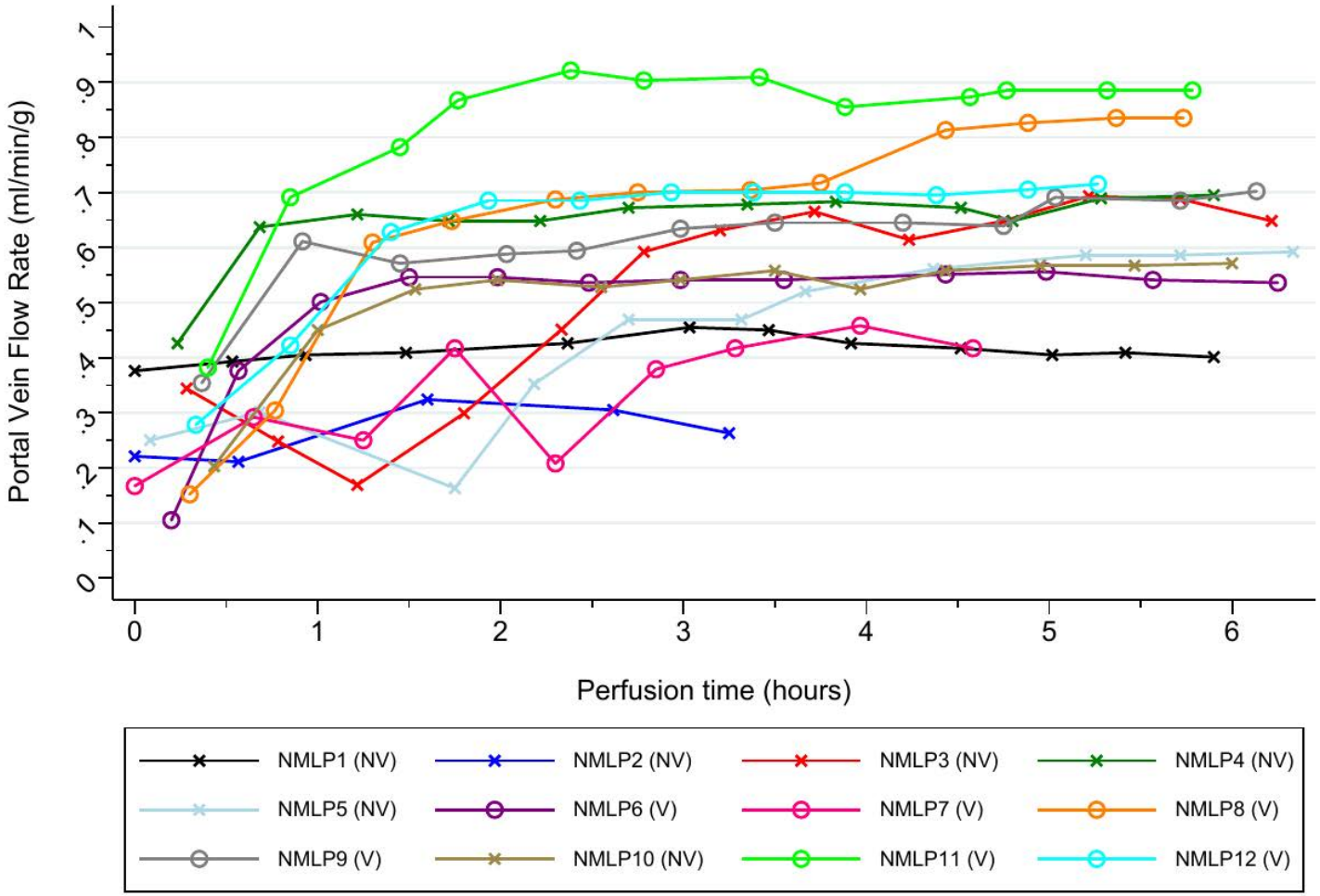

Figure 2.9: Portal vein flow rate per gramme of liver over time by individual NMLP. This visually does not demonstrate clustering in to two distinct groups. Cross-referencing of NMLP to viable (V) or non-viable (NV) based on lactate concentration.

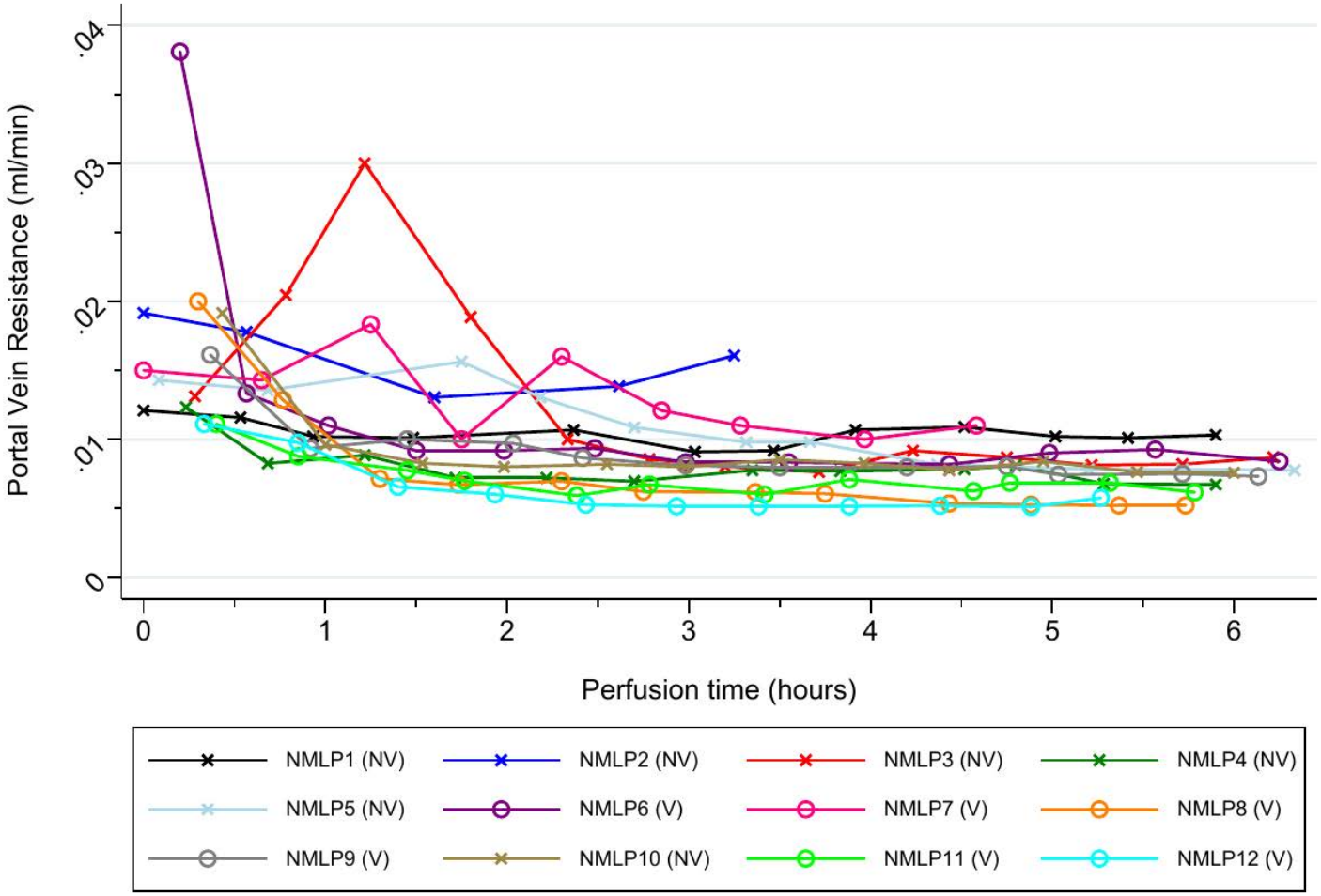

Figure 2.10: Portal vein resistance over time by individual NMLP. This visually does not demonstrate clustering in to two distinct groups. Cross-referencing of NMLP to viable (V) or non-viable (NV) based on lactate concentration.

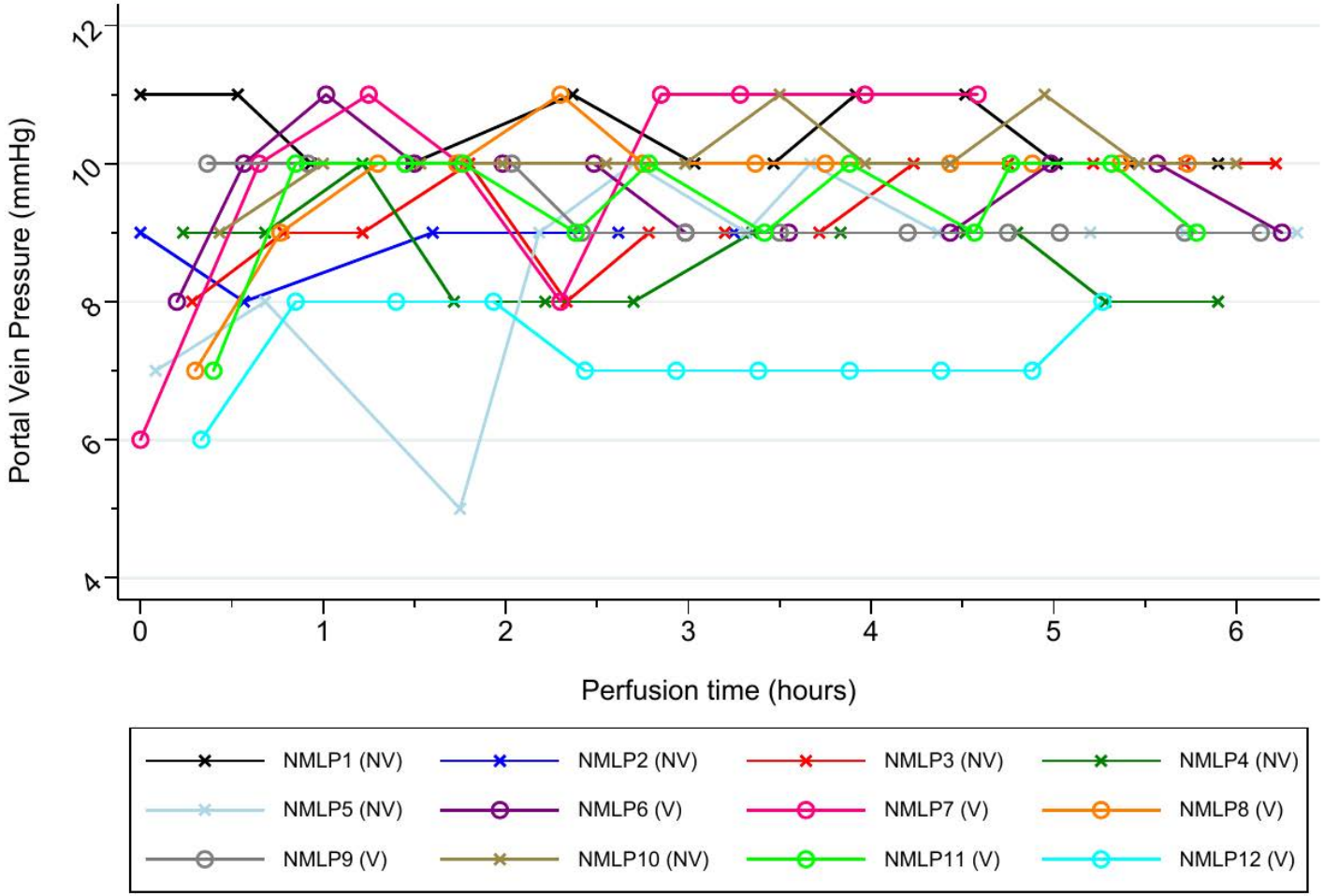

Figure 2.11: Portal vein pressure over time by individual NMLP. This visually does not demonstrate clustering in to two distinct groups. Cross-referencing of NMLP to viable (V) or non-viable (NV) based on lactate concentration.

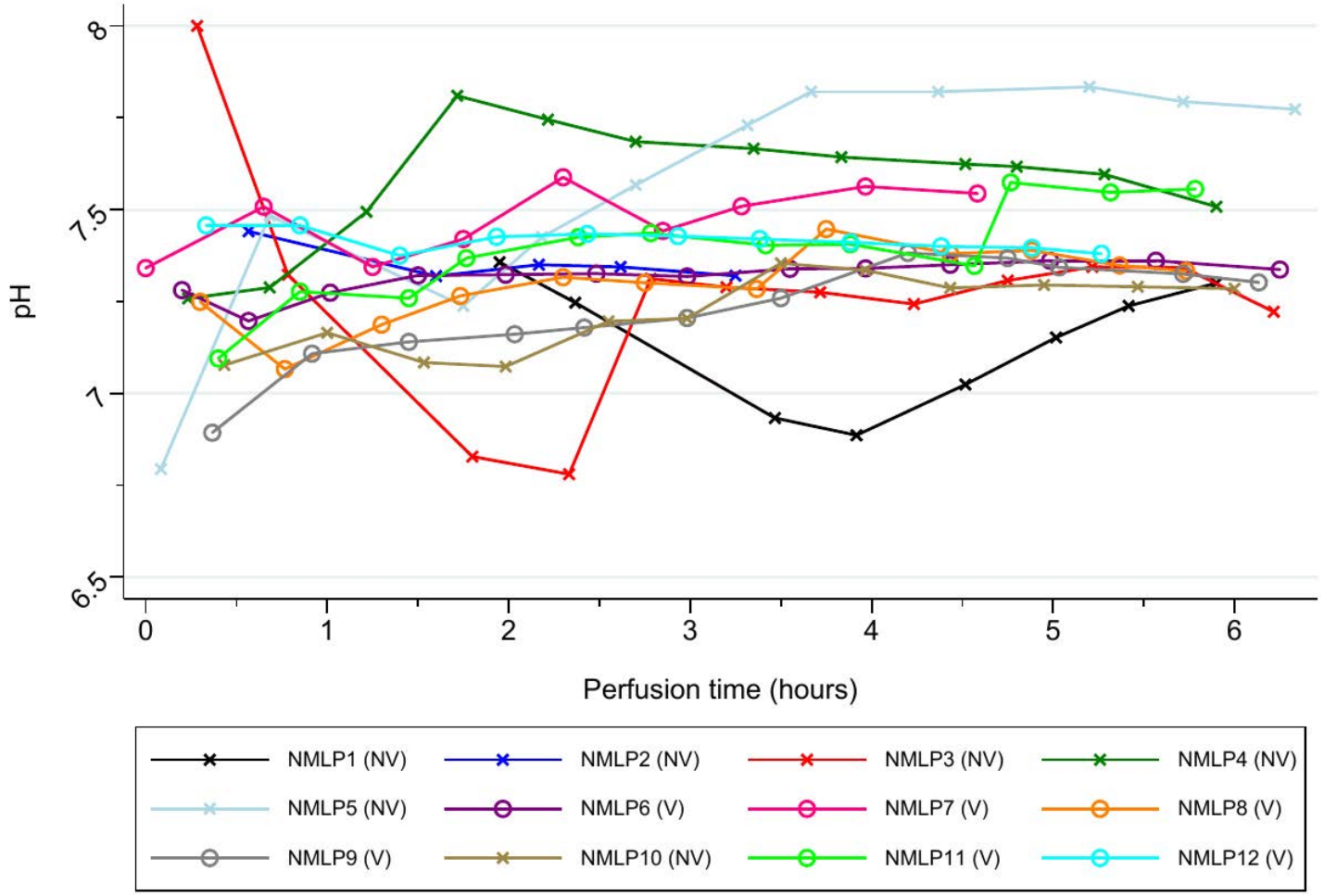

Figure 2.12: pH over time by individual NMLP. This visually does not demonstrate clustering in to two distinct groups. Cross-referencing of NMLP to viable (V) or non-viable (NV) based on lactate concentration.

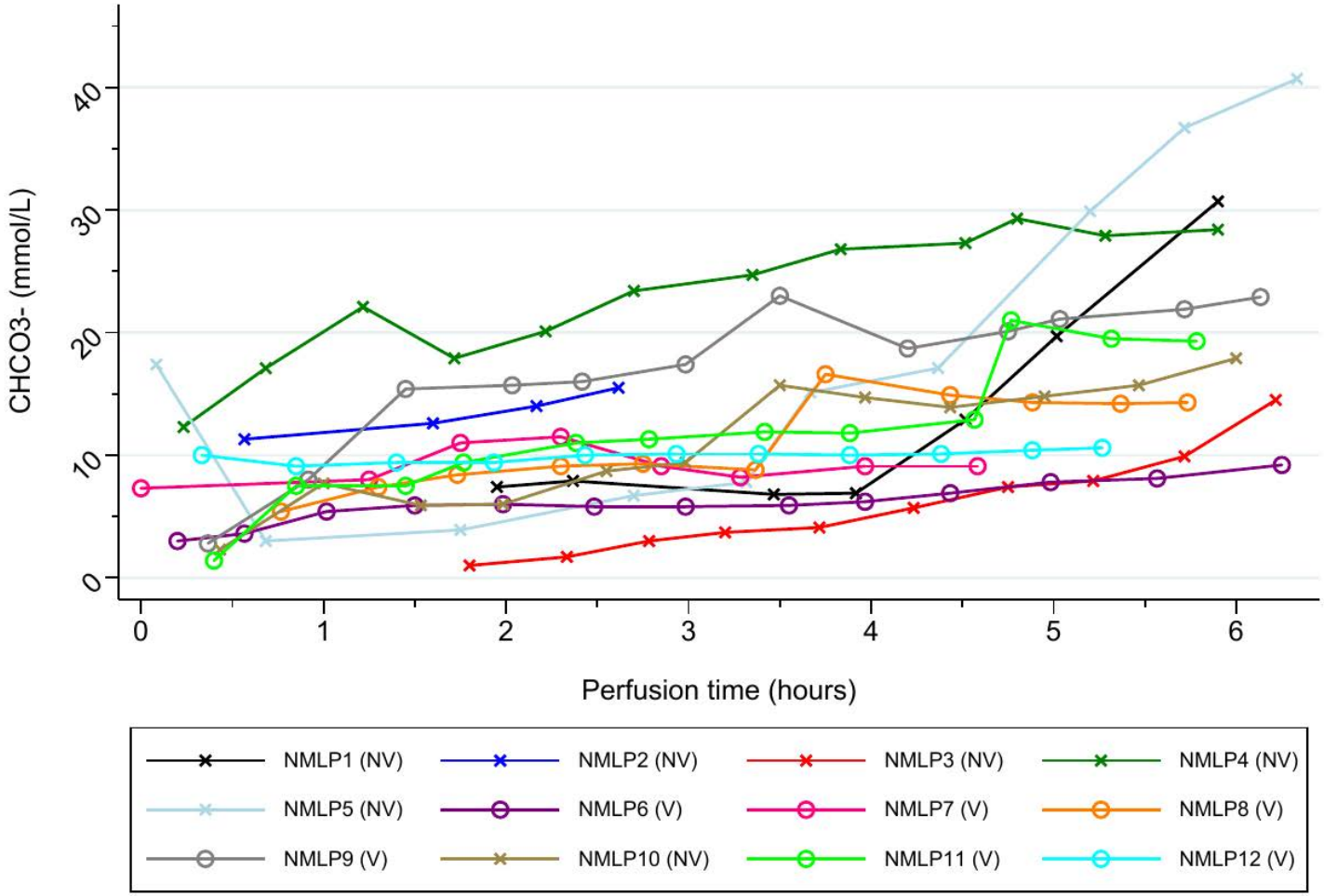

Figure 2.13: Bicarbonate over time by individual NMLP. This visually does not demonstrate clustering in to two distinct groups. Cross-referencing of NMLP to viable (V) or non-viable (NV) based on lactate concentration.

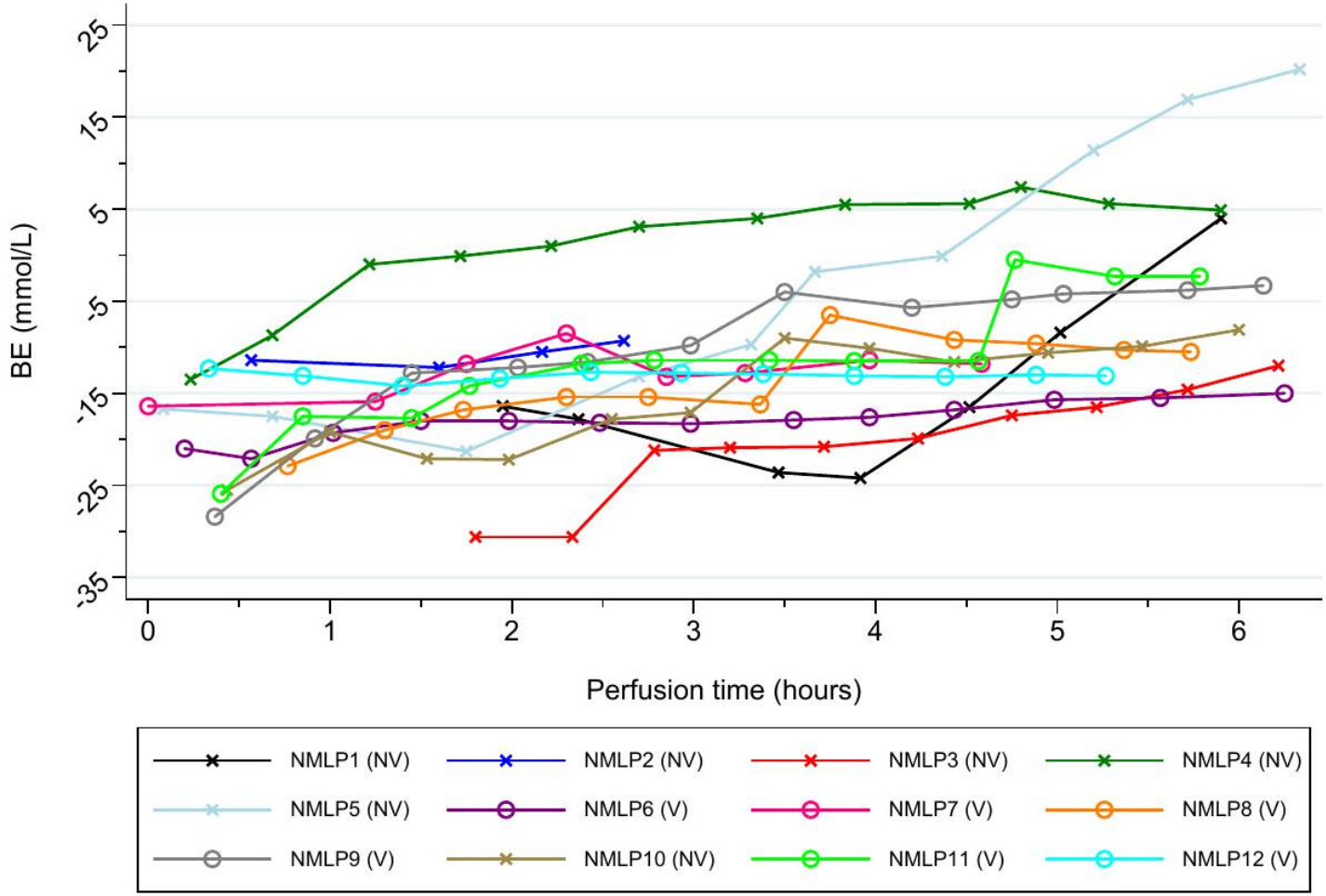

Figure 2.14: Base excess over time by individual NMLP. This visually does not demonstrate clustering in to two distinct groups. Cross-referencing of NMLP to viable (V) or non-viable (NV) based on lactate concentration.

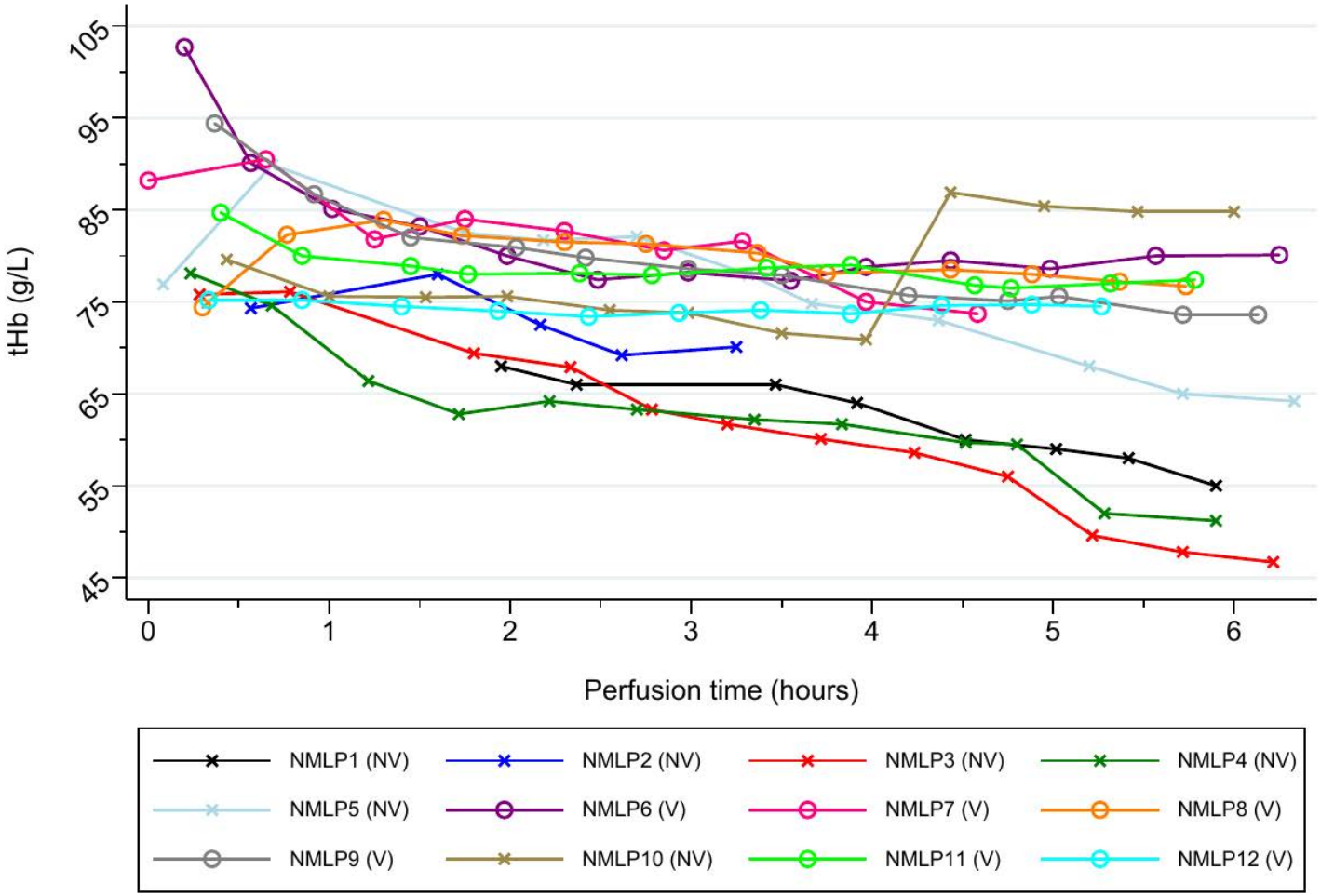

Figure 2.15: Haemoglobin over time by individual NMLP. This visually does not demonstrate clustering in to two distinct groups. Cross-referencing of NMLP to viable (V) or non-viable (NV) based on lactate concentration.

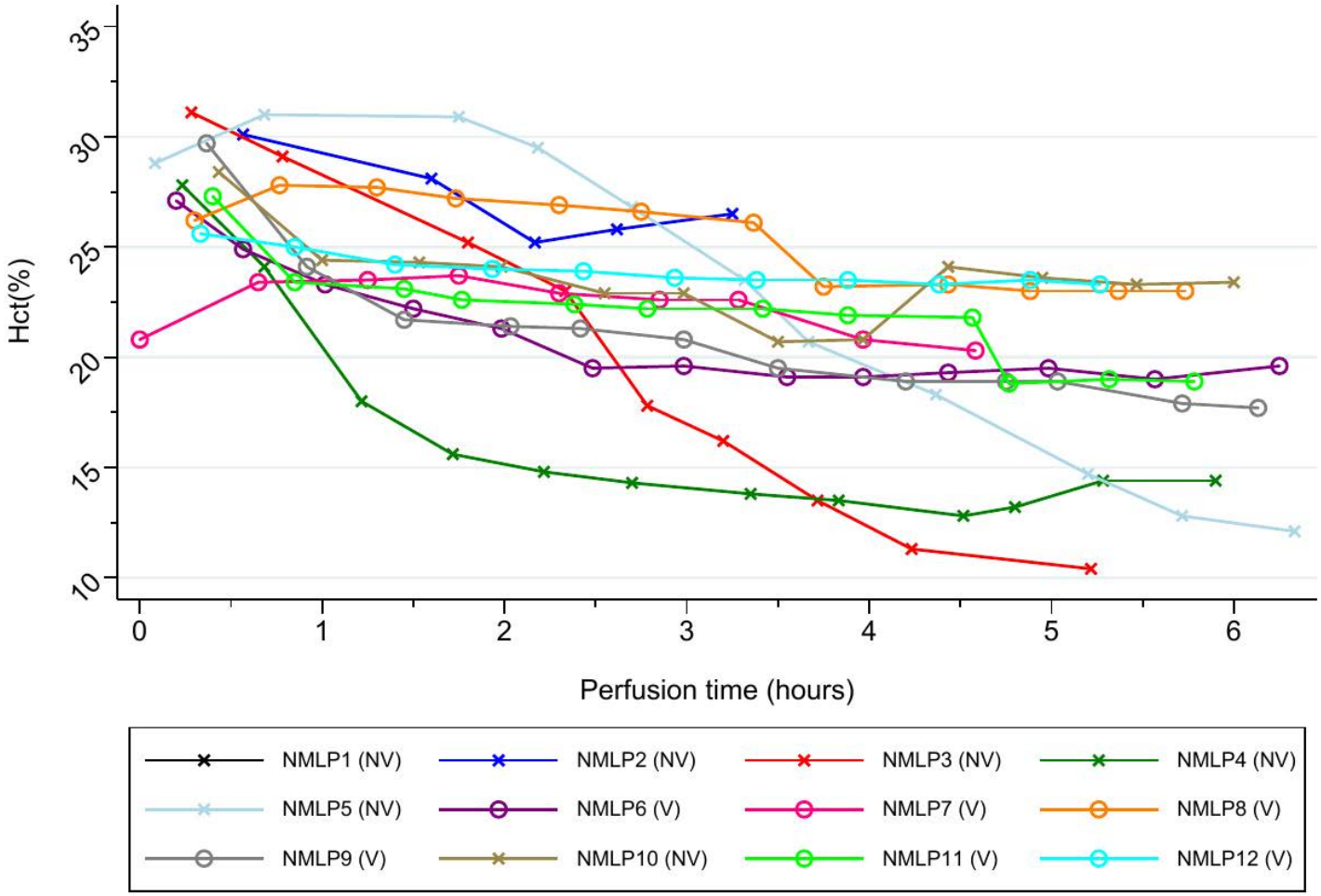

Figure 2.16: Haematocrit over time by individual NMLP. This visually does not demonstrate clustering in to two distinct groups. Cross-referencing of NMLP to viable (V) or non-viable (NV) based on lactate concentration.

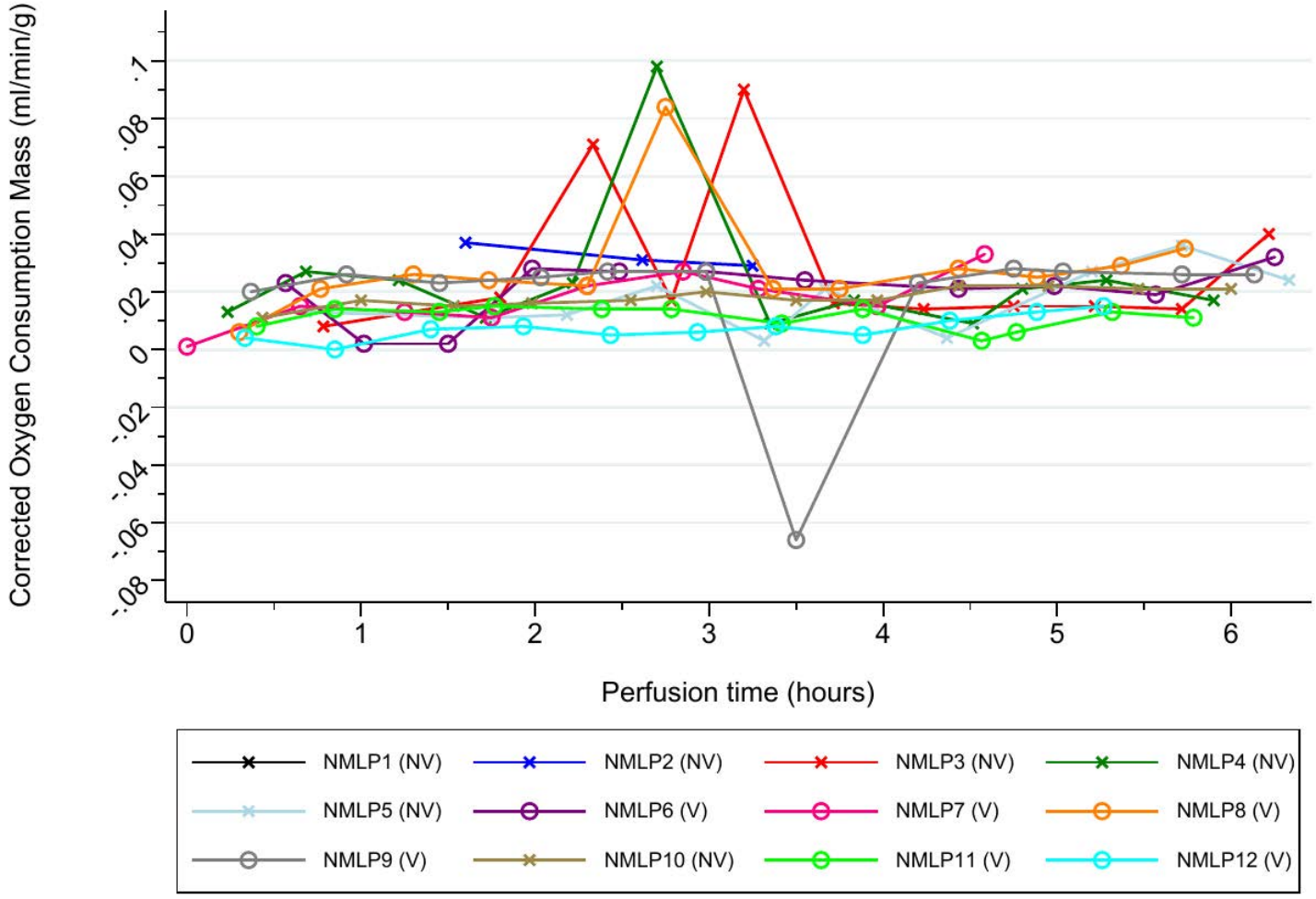

Figure 2.17: Oxygen consumption per gramme of liver over time by individual NMLP. This visually does not demonstrate clustering in to two distinct groups. Cross-referencing of NMLP to viable (V) or non-viable (NV) based on lactate concentration.

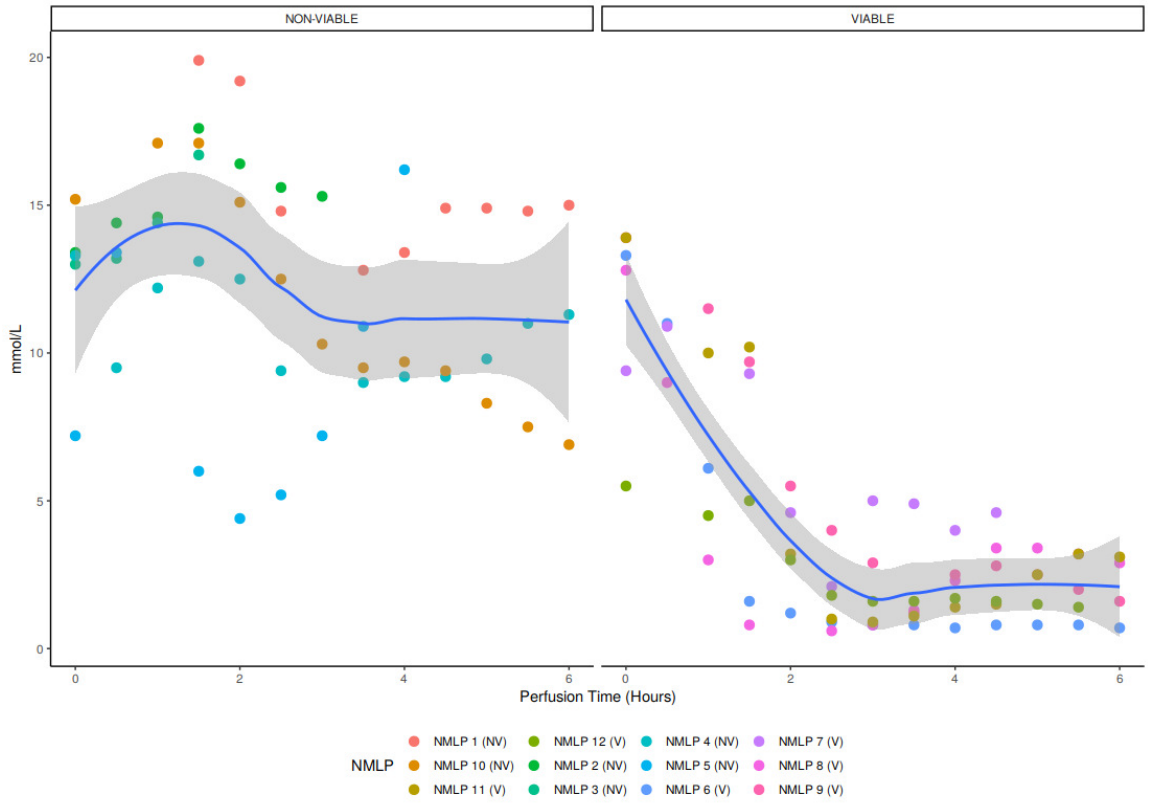

Figure 2.18: Lactate concentration (mmol/L) during NMLP based on viability criteria. There was no difference in the median lactate at the start of perfusion. At 2 hours, viable livers had lower lactate concentrations than non-viable livers (median viable 3.1 mmol/L vs. non-viable 15.8 mmol/L, p = 0.004) This was maintained at the end of perfusion (median viable 2.3 mmol/L vs. non-viable 15.2 mmol/L, p = 0.001). Line is the LOESS regression curve, shaded area is the 95% confidence interval for the regression curve. Non-viable, NMLP 1-5,10; Viable, NMLP 6-9,11,12.

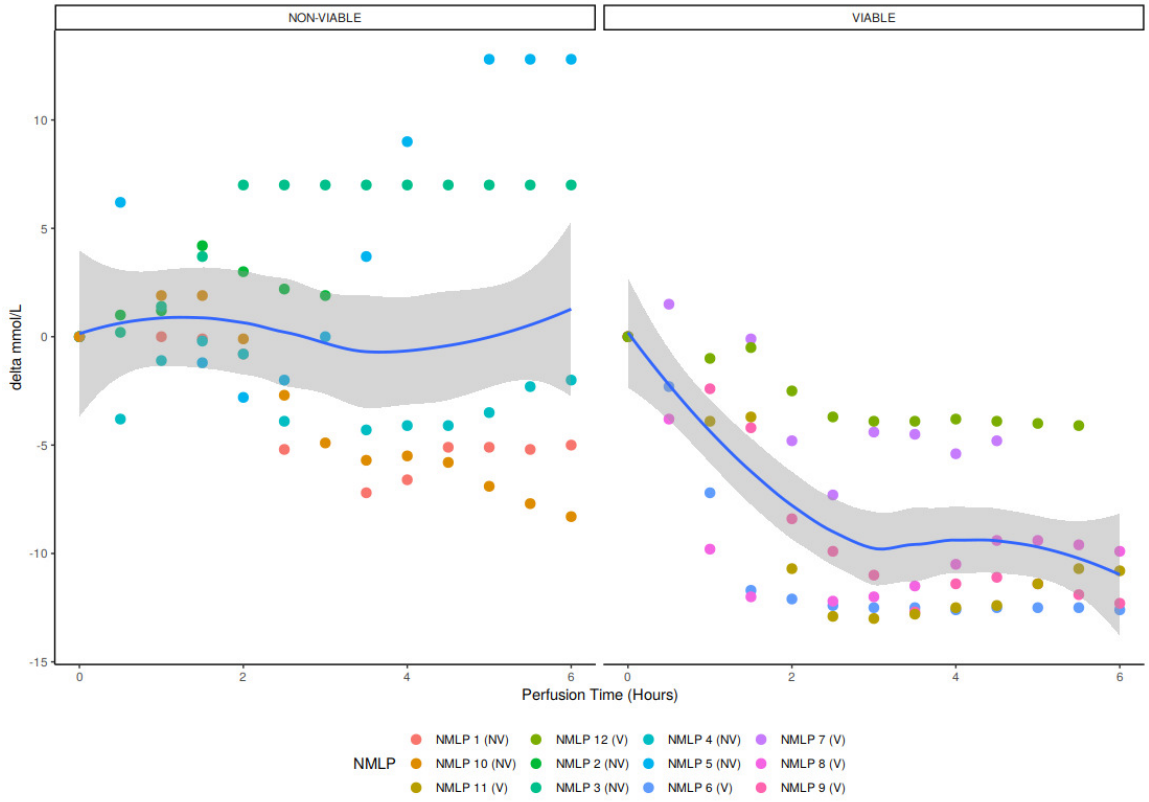

Figure 2.19: Delta lactate concentration during NMLP based on designated viability.The difference in delta lactate after 2 hours of NMLP between viable and non-viable livers (-9.6mmol/L vs. -0.5mmol/L respectively, p = 0.002) reinforces the differences seen in absolute lactate concentrations despite relatively low n numbers. Line is the LOESS regression curve, shaded area is the 95% confidence interval for the regression curve. Non-viable, NMLP 1-5,10; Viable, NMLP 6-9,11,12.

Perfusion number	1	2	3	4	5	6	7	8	9	10	11	12
Designated viability	Non-viable	Non-viable	Non-viable	Non-viable	Non-viable	Viable	Viable	Viable	Viable	Non-viable	Viable	Viable
Lactate level (mmol/L)[1]	19.2	16.4	20	12.5	4.4	1.2	4.6	0.6	5.5	15.1	3.2	3
Trough lactate (mmol/L)	12.8	13.4	13	8.8	4.4	0.7	2.1	0.6	1.2	6.9	0.8	1.4
Bile production (grammes)[2]	0	0	0	0	2.6	23	6.1	10.4	0	0	6.9	0
pH (-log10[H+])[1]	7.357	7.35	6.78	7.745	7.425	7.323	7.42	7.316	7.161	7.073	7.368	7.426
Arterial flow (ml/min)[1]	508	14	103	291	240	727	513	420	502	631	453	426
Change in arterial flow (ml/min)[3]	108	3	79	-302	196	616	283	362	189	420	337	324
Portal flow (ml/min)[1]	1030	650	800	1110	690	1090	1000	1580	1030	1250	1430	1330
Change in portal flow (ml/min)[3]	120	180	190	380	200	880	600	1230	410	780	800	790
Perfusion time (hrs:mins)	09:01:00	03:12:00	08:21:00	18:22:00	12:18:00	06:33:00	04:37:00	06:18:00	06:43:00	06:34:00	06:28:00	05:16:00

Note:*1: parameter measured after 2 hours of perfusion; *3: Cumulative bile production at the end of perfusion; *3: parameter measured at the end of perfusion.

Table 2.7: Machine perfusion parameters by NMLP.

	Overall	Non-Viable	Viable	p-value
Age (years)	56 (30-76)	58 (46-76)	56 (30-70)	0.485
BMI (kg/m^2)	30.2 (23.1 – 47.2)	31.3 (23.1 – 47.2)	27.7 (23.9-44.8)	0.699
Cold ischaemic time (mins)	493 (380 - 797)	523 (380 - 797)	475 (408 - 583)	0.485
Donor risk index	2.373 (1.411 - 3.228)	2.707 (1.411 -3.228)	2.072 (1.612 -3.053)	0.31
Lactate (mmol/L)[1]	5.1 (0.6 - 20.0)	15.8 (4.4 - 20.0)	3.1 (0.6 - 5.5)	**0.004**
Change in lactate (mmol/L)[1]	-.27 (-12.2-7.0)	-0.5 (-2.8-7.0)	-9.6 (-12.2 - -2.5)	**0.002**
Lactate (mmol/L)[2]	5.8 (0.7-20.0)	15.2 (6.9-20.0)	2.3 (0.7-4.6)	**0.001**
Change in lactate (mmol/L)[2]	-4.9 (-12.6-12.8)	-0.1 (-8.3-12.8)	-10.4 (-12.6 - -4.1)	**0.013**
Trough lactate (mmol/L)	3.3 (0.6 – 13.4)	10.8 (4.4 – 13.4)	1.0 (0.6 – 2.1)	**0.001**
Bile production (grammes)[1]	0.0 (0.0 - 10.9)	0.0 (0.0 - 0.0)	0.0 (0.0 - 10.9)	0.227
Cumulative bile production (grammes)[2]	0.0 (0.0 - 23.0)	0.0 (0.0 - 2.6)	6.5 (0.0 - 23.0)	**0.03**
Arterial flow (ml/min)[1]	440 (14 - 727)	266 (14 - 631)	478 (420 - 727)	0.09
Change in arterial flow (ml/min)[1]	+240 (-302 to +616)	+94 (-302 to +420)	+331 (+189 to +616)	**0.032**
Arterial resistance[1]		0,209 (0.095-4.929)	0.123 (0.055-0.160)	**0.047**
Portal flow (ml/min.)[1]	1060 (650 - 1580)	915 (650 - 1250)	1210 (1000 - 1580)	0.051
Change in portal flow (ml/min)[1]	+505 (+120 to +1230)	+195 (+120 to +780)	+795 (+410 to +1230)	**0.004**
Change in portal flow (ml/min)[2]	+640 (60-1570)	+500 (60-850)	840 (600-1570)	0.023
Portal resistance[1]	0.010 (0.006-0.014)	0.010 (0.007-0.014)	0.008 (0.006-0.010)	0.036
Glucose (mmol/L)[1]	43.1 (23.3-64.5)	50.0 (39.5-64.5)	40.0 (23.3-59.3)	0.083
Glucose (mmol/L)[2]	32.1 (8.0-56.2)	32.1 (15.1-56.2)	29.1 (8.0-52.4)	0.393
HCO3 (mmol/L)[2]	17.9 (9.1-40.7)	28.4 (14.5-40.7)	12.5 (9.1-22.9)	**0.026**
Haemoglobin (g/L)[1]	76.8 (64.2-84.0)	70.3 (64.2-81.7)	80.5 (74.0-84.0)	**0.032**
Haemoglobin (g/L)[2]	73.7 (46.7-84.8)	59.6 (46.7-84.8)	75.6 (73.6-80.1)	**0.032**
Sodium (mmol/L)[2]	139.8 (126.8-196.5)	145.8 (136.6-196.5)	131.9 (126.8-149.5)	**0.013**
Change in sodium (mmol/L)[2]	22.6 (-19.4-66.2)	38.0 (26.5-66.2)	13.2 (-19.4-26.5)	**0.01**
Oxygen Extraction Ratio[1]	0.270 (0.085-0.831	0.266 (0.181-0.831)	0.245 (0.085-0.460)	0.284
Oxygen Extraction Ratio[2]	0.280 (0.124-0.645)	0.259 (0.202-0.645)	0.288 (0.124-0.490)	0.457

Note:Values are presented as median with range; *1 parameter measured after 2 hours of perfusion; *2 parameter measured at end of perfusion

Table 2.8: Donor and perfusion parameters comparison between viable vs. non-viable groups.

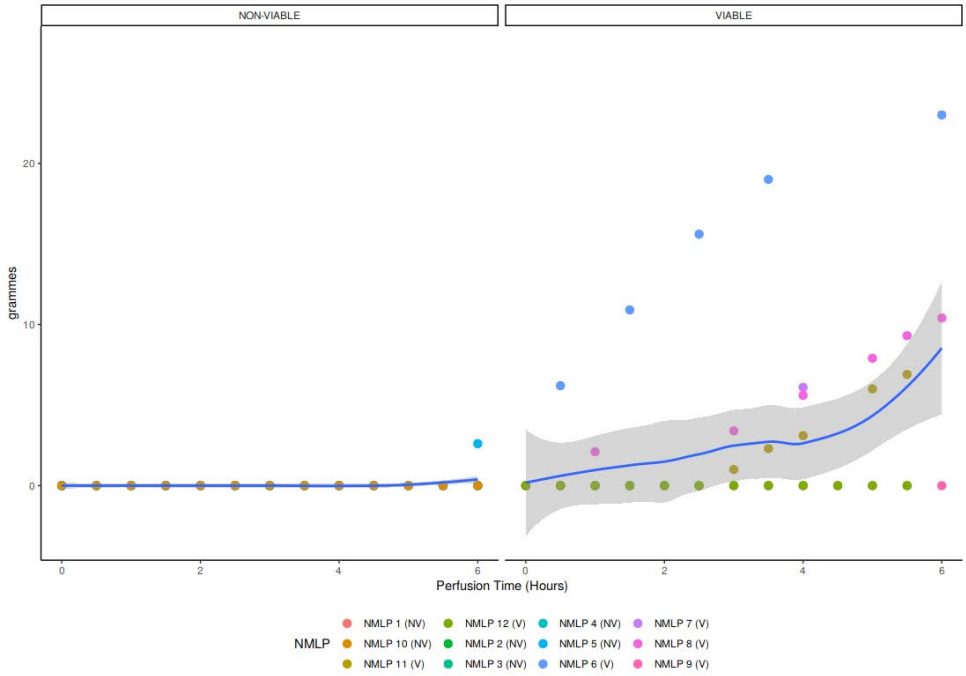

Figure 2.20: Bile production by viability group. Bile production was sporadic in both groups however, cumulative bile production in the viable group was higher than the non-viable group by the end of NMLP. There was no difference after 2 hours of NMLP when the viability assessment was made. Line is the LOESS regression curve, shaded area is the 95% confidence interval for the regression curve. Non-viable, NMLP 1-5,10; Viable, NMLP 6-9,11,12.

Flow Parameters

There was no difference in the initial hepatic artery flow rates between the groups (Figure 2.21 A; median non-viable 128ml/min vs. viable 114ml/min, p = 0.818). After 2 hours of NMLP, hepatic artery flow rates had increased more in the viable group (478ml/min, change +331ml/min vs. 266ml/min, change +94ml/min, p = 0.032). There was no difference in the arterial flows at the end of NMLP (viable 617ml/min vs. non-viable 376ml/min, p = 0.197). These differences were maintained when accounting for the mass of liver perfused. Similarly, there were no differences in initial hepatic artery flow rates per 100 grammes of liver between the groups (2.22 A; median non-viable 5.689ml/min/100g vs. viable 6.294ml/min/100g, p = 0.699). After 2 hours of NMLP, not only had there been an increase in hepatic arterial flow rates per 100 grammes of liver between the groups (non-viable +4.458ml/min/100g vs. viable 16.207ml/min/100g, p = 0.026) but also the absolute flow rates was higher in the viable group (non-viable 14.619ml/min/100g vs. viable 24.690ml/min/100g, p = 0.013). However, absolute and changes in hepatic arterial flow rates were similar by the end of NMLP.

Portal vein flow rates were similar in both groups at the start of NMLP (Figure 2.21 B; median viable 470ml/min vs. non-viable 550ml/min, p = 0.288). After 2 hours of NMLP, portal vein flow rates in the viable group had increased more compared to the non-viable group (viable 1210ml/min, change +795ml/min vs. non-viable 915ml/min, change +195ml/min, p = 0.004). Portal vein flow rates were higher in the viable group at the end of NMLP (viable 1320ml/min vs. non-viable 1060ml/min, p = 0.047). Accounting for mass of liver perfused, there were no differences in portal vein flow per 100 grammes of liver between the two groups at the start of NMLP (2.22 B; non-viable 29.687ml/min/100g vs. viable 22.230 ml/min/100g, p = 0.394). Again, not only was there an increase in the portal vein flow rates per 100 grammes of liver between the groups after 2 hours of NMLP (non-viable +10.455ml/min/100g vs. viable 42.362ml/min/100g, p = 0.008), but also the absolute flow rate per 100 grammes of liver in the portal vein was higher in the viable group (non-viable 43.829ml/min/100g vs. viable 63.621 ml/min/100g, p = 0.032). In comparison to the hepatic arterial flow rates at the end of NMLP,

absolute and changes to portal vein flow rates per 100 grammes of liver were higher in the viable group (absolute non-viable 57.932ml/min/100g vs. viable 71.387ml/min/100g, p = 0.004; change non-viable +28.654ml/min/100g vs. viable 43.920ml/min/100g, p = 0.008).

Hepatic artery and portal vein resistances were similar between the two groups at the start of NMLP (Figure 2.23). After 2 hours of NMLP, hepatic artery resistance was higher in the non-viable group (Figure 2.23 B); viable 0.123 vs. non-viable 0.209, p = 0.047) but returned to similar values by the end of NMLP. These differences were reflected in portal vein resistance after 2 hours of NMLP (Figure 2.23 D); viable 0.008 vs. non-viable 0.010, p = 0.036), but returned to similar values by the end of perfusion.

Blood Gas Parameters and Glucose Utilisation

Oxygen consumption per 100 grammes of liver was similar in both groups at the start of NMLP (Figure 2.24, non-viable 1.188ml/mn/100g vs. viable 1.182ml/min/100g, p = 0.914). Subsequently, after both 2 hours and the end of NMLP, there were no differences in oxygen consumption between the groups across the timepoints (2 hours non-viable 2.238ml/min/100g vs. 2.211ml/min/100g, p = 0.331; end NMLP non-viable 2.415ml/min/100g vs. 2.926ml/min/100g, p = 0.535). The curvature seen in the non-viable group is most likely due to outlying values. The Oxygen Extraction Ratio (O2ER) was similar for both groups at the start of NMLP (Figure 2.25; viable 0.285 vs. non-viable 0.223, p = 0.962). There was a trend for O2ER to be higher in the non-viable group after 2 hours of NMLP, but this did not reach statistical significance. There was no difference between the groups at the end of perfusion.

The pH of the perfusion fluid was similar for both groups at the start of NMLP (Figure 2.26 A; viable 7.265 vs. non-viable 7.168, p = 0.762). There was a trend for the non-viable group to become more acidotic at the end of NMLP, this did not reach significance. Perfusion fluid acidosis with pH less than 7.20 was corrected throughout NMLP using 20ml boluses of sodium bicarbonate 8.4% however, both groups received a similar number of boluses.

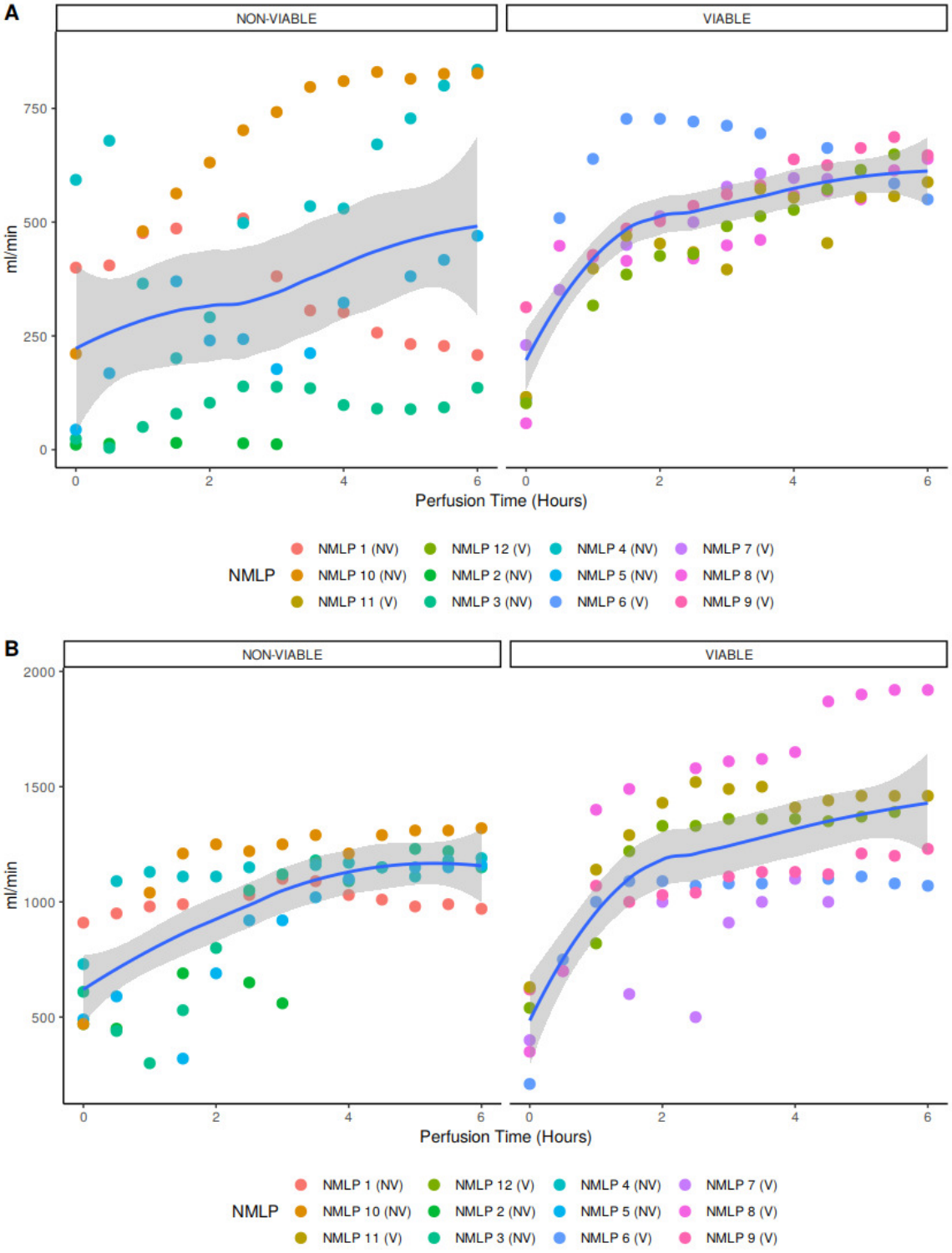

Figure 2.21: Arterial and portal flow rates during NMLP based on viability. Flow rates in hepatic artery (ml/min; A) and portal vein (ml/min; B). Line is the LOESS regression curve, shaded area is the 95% confidence interval for the regression curve. Non-viable, NMLP 1-5,10; Viable, NMLP 6-9,11,12.

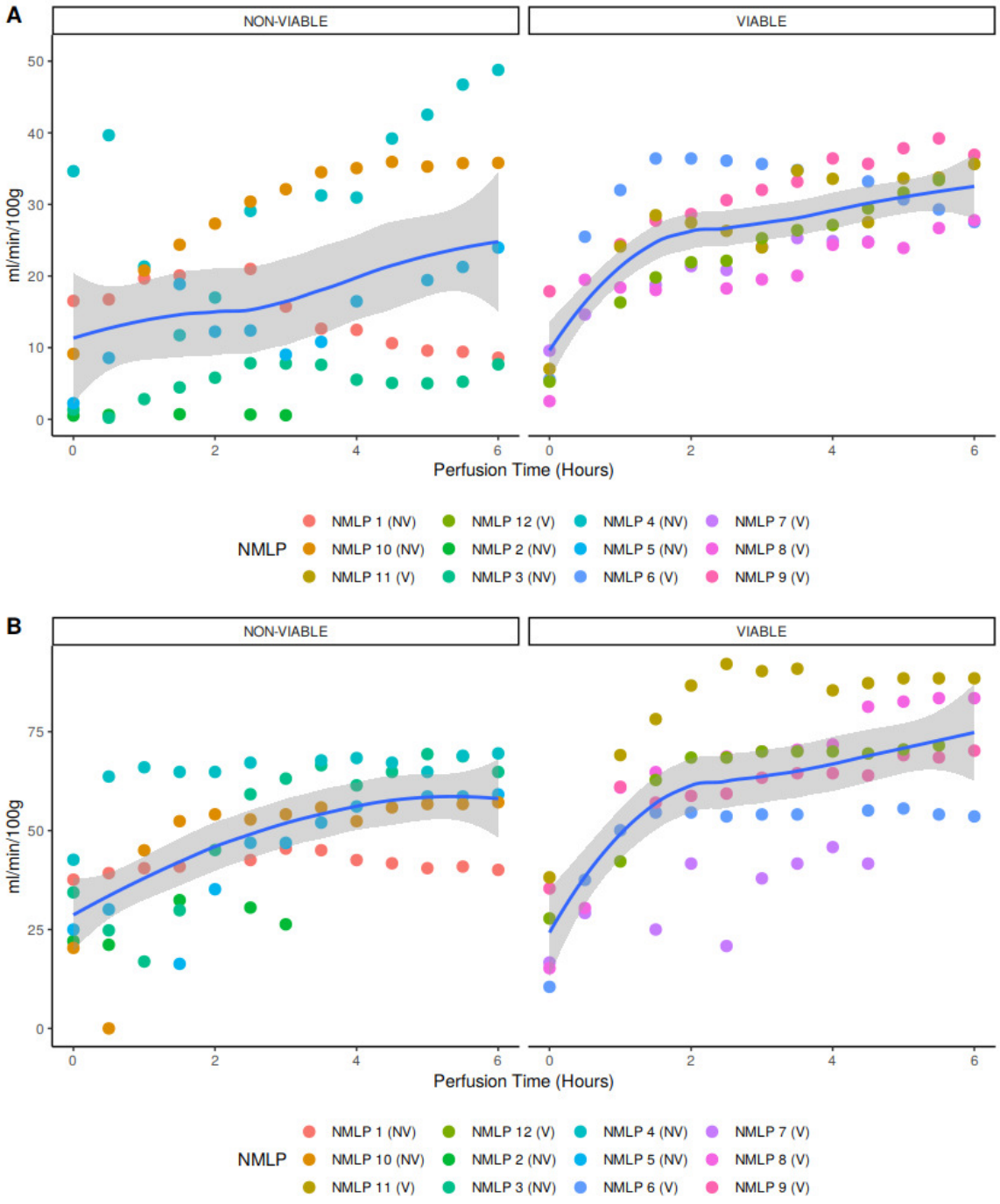

Figure 2.22: Arterial and portal flow rates by mass of liver during NMLP based on viability.Flow rates in hepatic artery (ml/min/100g; A) and portal vein (ml/min/100g; B). Line is the LOESS regression curve, shaded area is the 95% confidence interval for the regression curve. Non-viable, NMLP 1-5,10; Viable, NMLP 6-9,11,12.

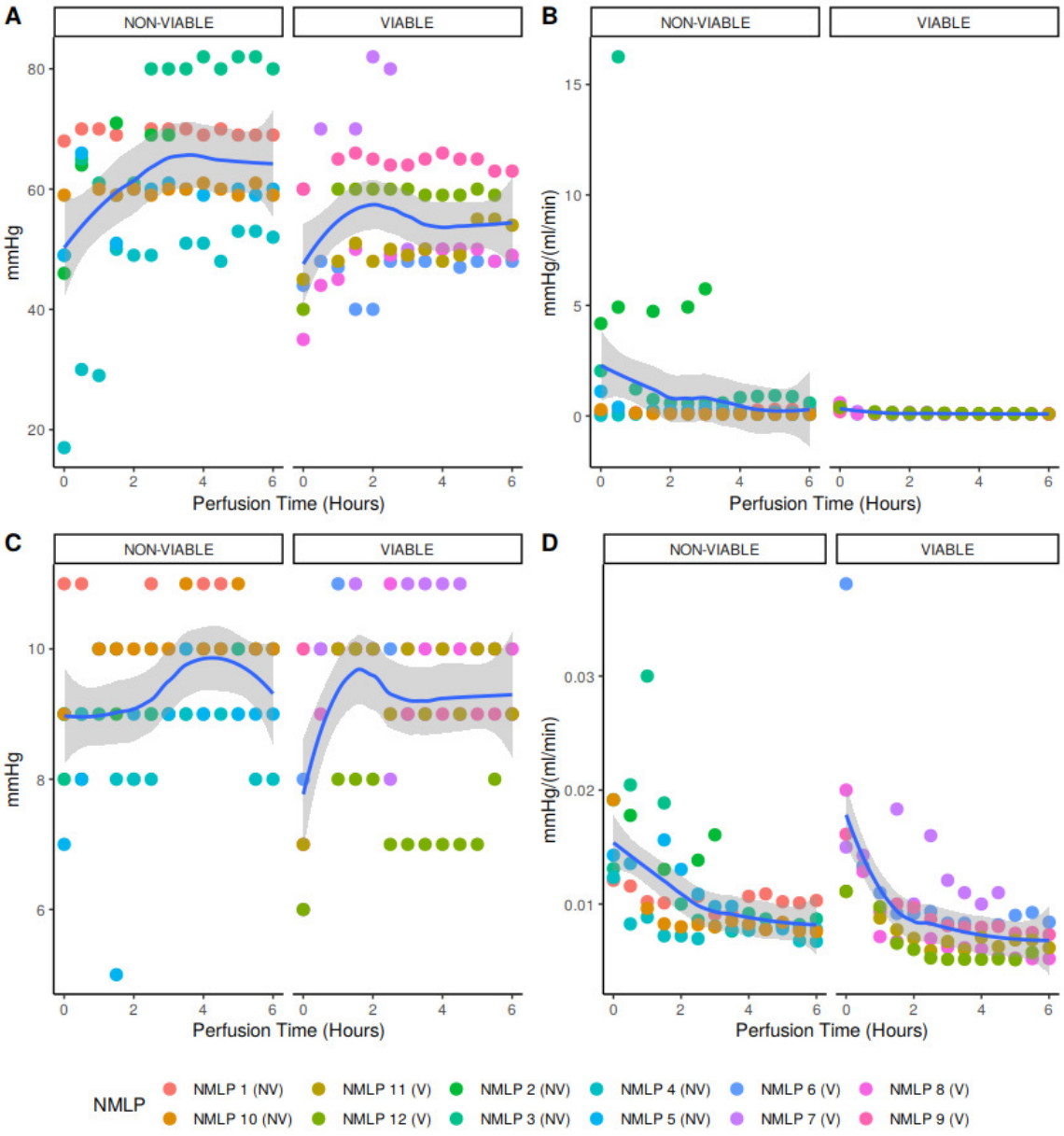

Figure 2.23: Arterial and portal pressures and resistances during NMLP based on viability. Pressures (mmHg; A, C) and resistances (mmHg/(ml/min); B, D) in the hepatic artery (A, B) and portal vein (C, D) during NMLP based on designated viability. Line is the LOESS regression curve, shaded area is the 95% confidence interval for the regression curve. Non-viable, NMLP 1-5,10; Viable, NMLP 6-9,11,12.

Glucose concentrations were similar in both groups at the start of NMLP (viable 43.4mmol/L vs. non-viable 50.8mmol/L, p = 0.258). Glucose utilisation in the viable livers tended to be higher after 2 hours of NMLP however, this did not reach significance (Table 2.8, viable 40.0mmol/L, vs. non-viable 50.0mmol/L, p = 0.083). There was no difference in glucose concentration at the end of NMLP (Figure 2.27).

Histological Findings

Ischaemic type coagulative necrosis was minimal across both groups. Lost cohesion of hepatocytes predominantly in zone 3 was observed in the non-viable group (Figure 2.28 B) with all post-NMLP livers showing variable amounts of hepatocyte detachment (non-viable 15%, 1-40% v viable 1.5%, 0-10%) (Table 2.9 and Figure 2.28).

By pathologist assessment, there was no difference in amount of glycogen depletion pre-NMLP between the groups (viable 80% depletion, 5-95% vs. non-viable 75% depletion, 5-99%). At the end of the perfusion, livers in the viable group displaying increased PAS staining (viable 22.5% glycogen depletion, 5-80% vs. non-viable 80% depletion, 10-90%) in the viable group, indicating that viable livers were able to uptake glucose and store this as glycogen (Figure 2.29).

None of the livers displayed significant large droplet steatosis and at most reached a mild degree (maximum of 15%). Small droplet macrovesicular steatosis was greater in the non-viable livers (Figure 2.30 and Table 2.9). Liver 5, declined for transplantation based on its macroscopic appearance, had a portal hepatitis (Figure 2.30 A) and severe zone 3 cholestasis (Figure 2.30 B). PAS stained section of liver 4 (Figure 2.30 C) which had the most severe large droplet macrovesicular steatosis (oval), the type of fat considered in evaluating suitability for transplantation. It is mild involving up to 15% of hepatocytes. This liver was turned down on macroscopic assessment of steatosis. PAS stained section of liver 1 (Figure 2.30 D) pre-NMLP showed extensive small droplet microvesicular steatosis, where hepatocyte cytoplasm often contains numerous small droplets of fat which do not displace the hepatocyte nuclei. Several large droplet fat droplets are also present. This liver was turned down due to the macroscopic appear-

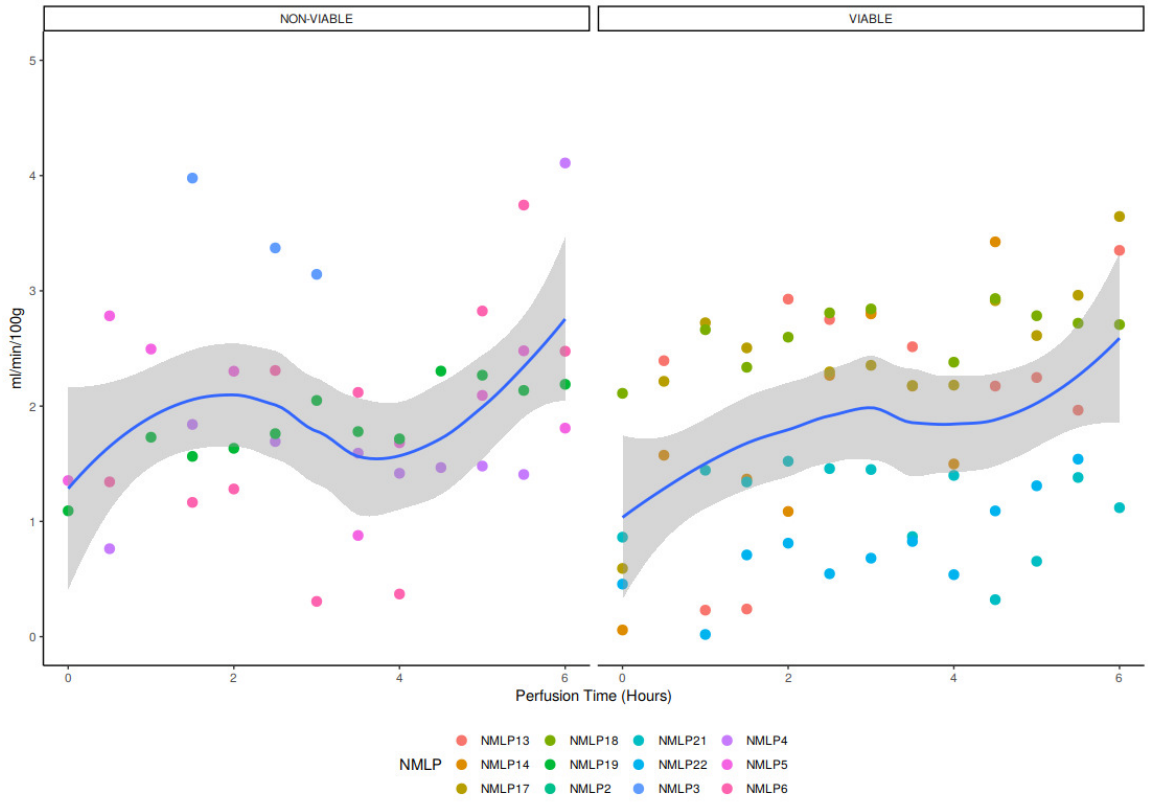

Figure 2.24: Oxygen consumption by mass during NMLP based on viability. No differences were observed in oxygen consumption per 100 grammes of liver throughout NMLP between both groups. Line is the LOESS regression curve, shaded area is the 95% confidence interval for the regression curve. Non-viable, NMLP 1-5,10; Viable, NMLP 6-9,11,12.

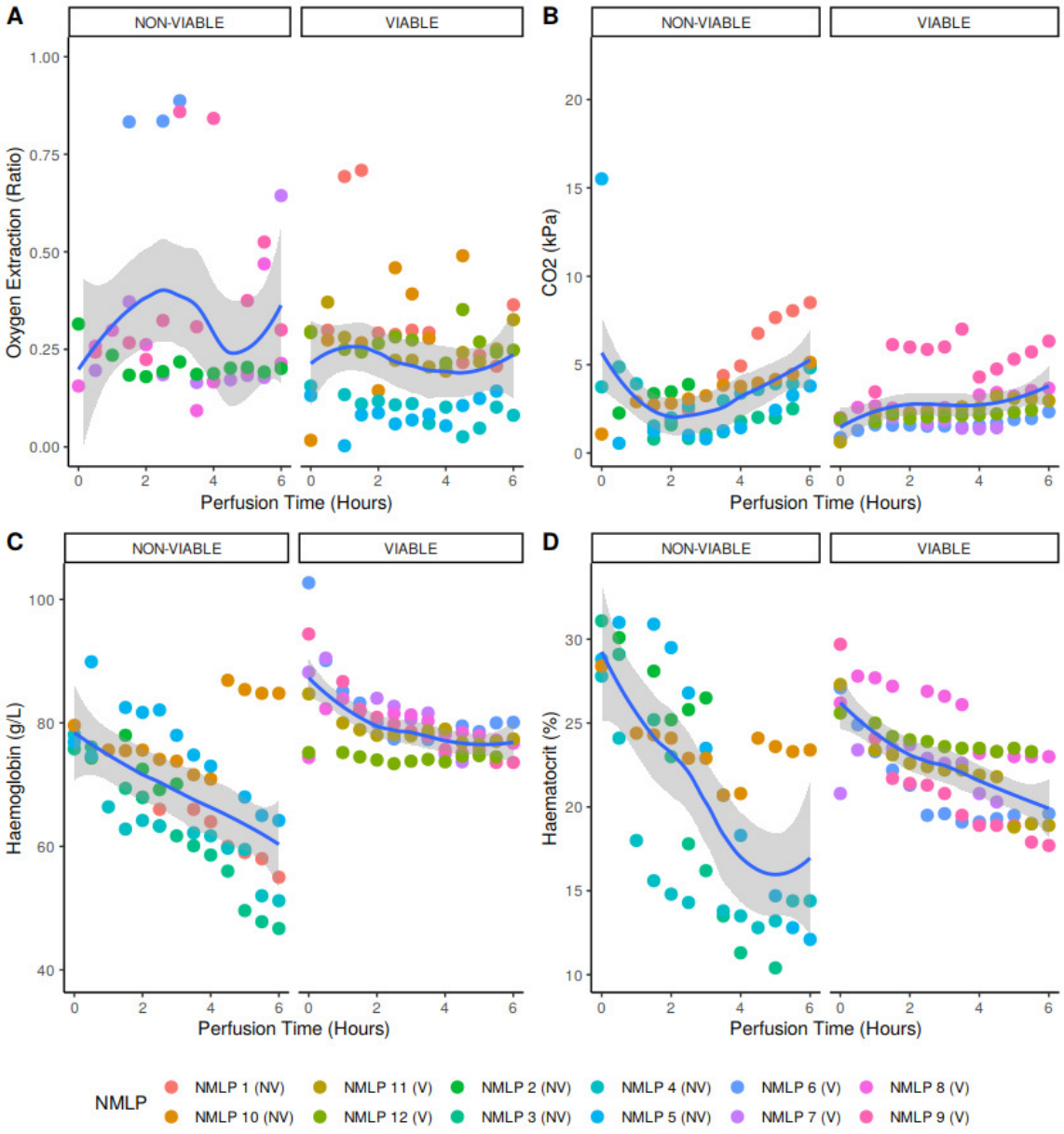

Figure 2.25: Blood gas parameters during NMLP based on viability criteria. Oxygen extraction ratio (A), pCO2 (kPa; B), haemoglobin concentration (g/L; C) and haematocrit (%; D) during NMLP based on designated viability. Line is the LOESS regression curve, shaded area is the 95% confidence interval for the regression curve. Non-viable, NMLP 1-5,10; Viable, NMLP 6-9,11,12.

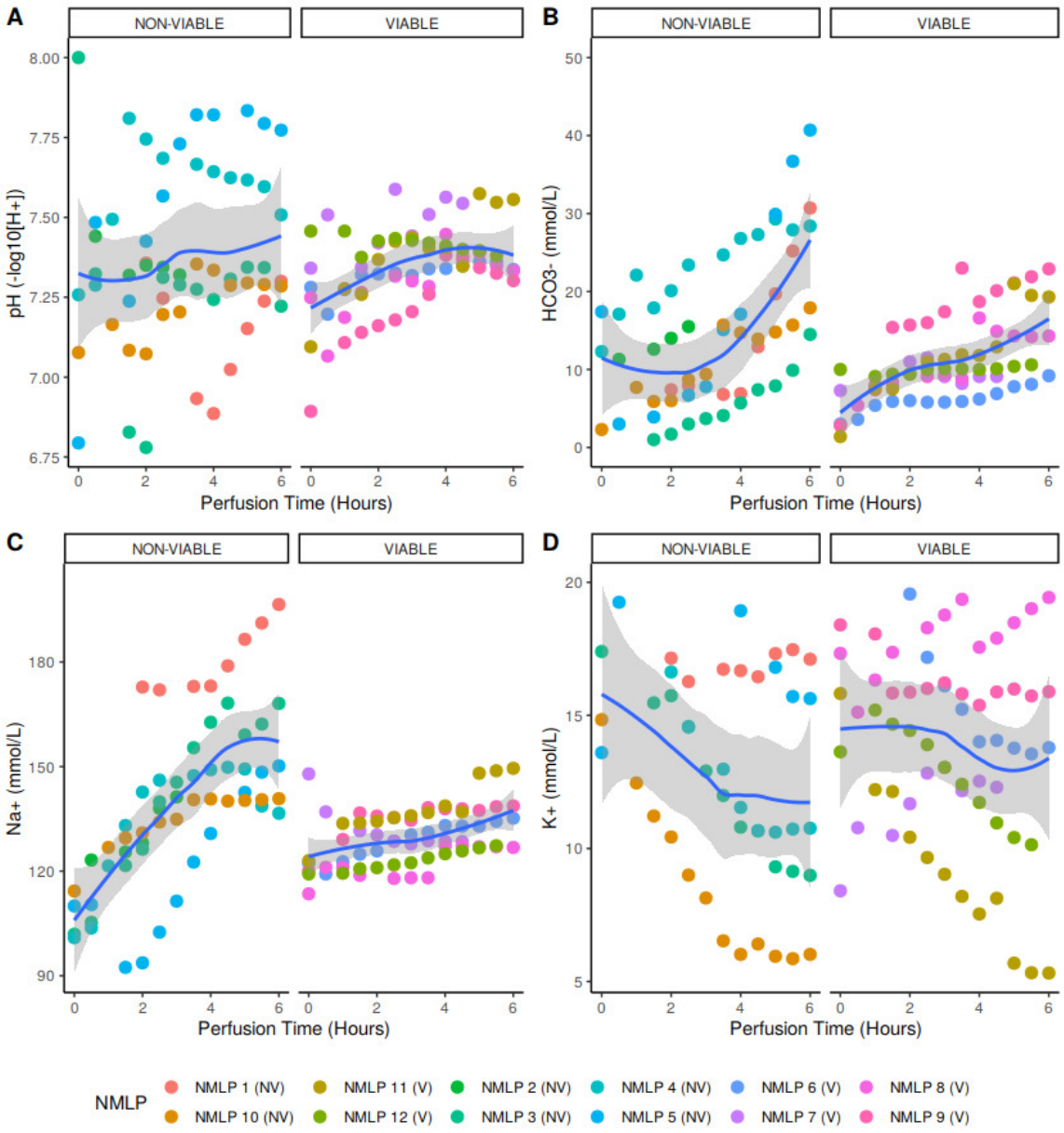

Figure 2.26: Acid/base and electrolytes during NMLP based on viability criteria. pH (-log10[H+]; A), bicarbonate (mmol/L; B), sodium (mmol/L; C) and potassium (mmol/L; D) concentrations during NMLP based on designated viability. There was a trend towards more stable maintenance of pH and sodium concentration and a more consistent bicarbonate concentration in the group deemed viable. Line is the LOESS regression curve, shaded area is the 95% confidence interval for the regression curve. Non-viable, NMLP 1-5,10; Viable, NMLP 6-9,11,12.

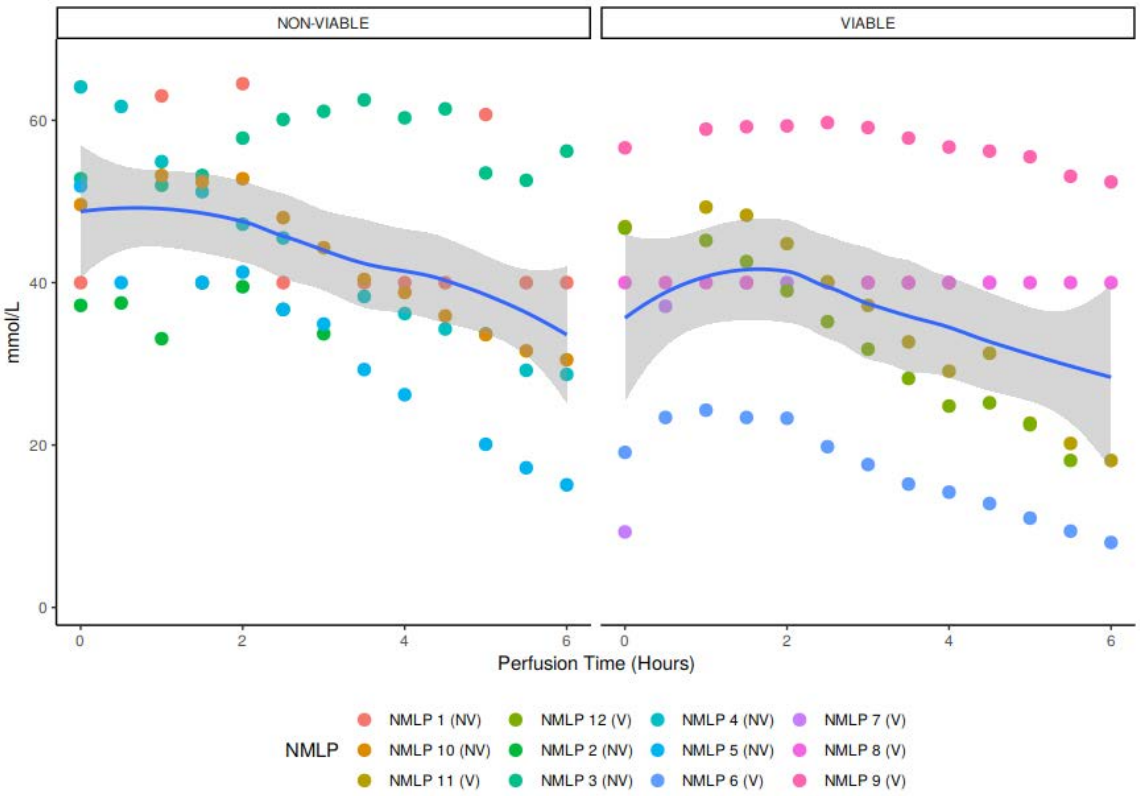

Figure 2.27: Glucose concentration during NMLP by viability group. Line is the LOESS regression curve, shaded area is the 95% confidence interval for the regression curve. Non-viable, NMLP 1-5,10; Viable, NMLP 6-9,11,12.

ance of steatosis, but large droplet steatosis was mild involving only 5% of hepatocytes in the whole biopsy. It is likely that the small droplet steatosis was also seen macroscopically. This is not traditionally considered in assessing a liver for transplantation and indicates the requirement of a liver biopsy to accurately assess the type and amount of both types of fat droplets. H&E stained section of liver 7 (Figure 2.30 E) turned down because macroscopically thought to have fibrosis. There is no fibrosis present. There is a normal portal tract (PT) showing no fibrous expansion. The abnormality present is centred around hepatic veins (HV) consisting of confluent areas of hepatocyte loss in which there is variable haemorrhage/congestion (red colour of red blood cells seen) and pigment laden macrophages. Detailed histological findings are shown in Table 2.9 and Figures 2.28,2.29,2.30.

Graphically, quantitative histological assessment using the described slide scanning technique suggested that viable livers at the start of NMLP had a higher polysaccharide content compared to those in the non-viable group and behaves in a hyperbolic manner compared to the parabolic curve in the non-viable group (Figure 2.31). However statistical analysis revealed no difference in the starting polysaccharide content (median viable $4.55\text{x}10^7$ v non-viable $3.95\text{x}10^5$, p = 1.00). Repeated measures ANOVA demonstrated the main effect for viability yielded a F value of F = 0.597, $p > 0.05$, indicating that the effect for viability was not significant. The main effect for perfusion time yielded a F value of F = 1.089, $p > 0.05$, indicating that the effect for NMLP time was not significant. The interaction effect was insignificant, F = 1.369, $p > 0.05$. Overall, neither viability nor perfusion time influenced polysaccharide content, in contrast to the semi-quantitiative scoring assessment by a trained clinical pathologist.

Mitochondrial Responses During NMLP With Respect to Viability

The mitochondrial response to NMLP was determined by ATP content and UCP2. Graphically, there was a trend towards an increased ATP content in viable livers at the end of NMLP (Figure 2.32). However on ANOVA, both the main effect of viability with F = 2.565, $p > 0.05$, and perfusion time with F = 2.069, $p > 0.05$, were not significant. Similarly, the interaction effect

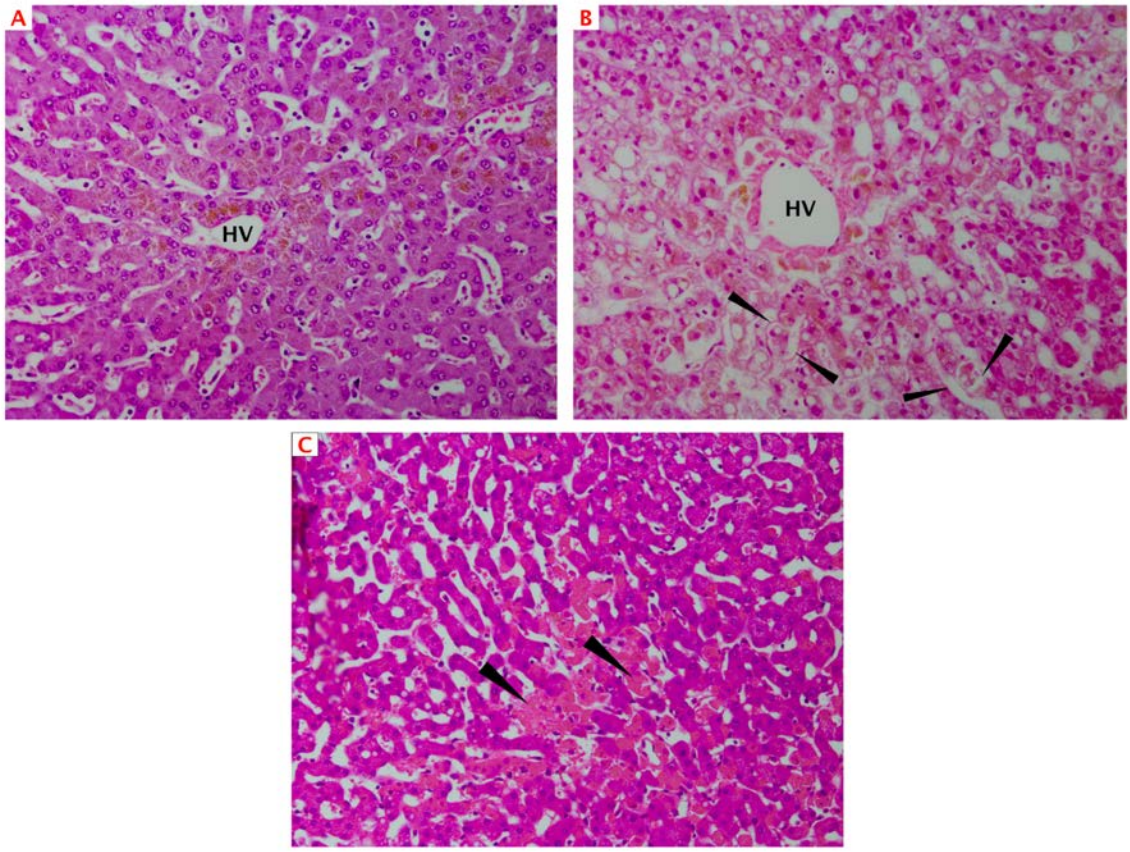

Figure 2.28: Histological findings pre- and post-NMLP in viable and non-viable livers: H&E stain. H&E stained sections (A) viable liver number 8 after 6 hours of NMLP showing normal hepatocyte plate morphology and attachment of hepatocyte plates to the hepatic vein (HV). (B) non-viable liver number 3, 6 hours after NMLP showing loss of cohesion of hepatocytes from each other and from the sinusoidal lining (arrows) and from the hepatic vein (HV). (C) Viable liver number 12, 6 hours post NMLP showing a small area of coagulative necrosis where the cells become hypereosinophilic (arrows). This was seen to an equal extent in both viable and non-viable livers pre and post NMLP and was very mild in this series of livers [original objective x20]. Acknowledgement to Dr. Desley Neil for interpretation.

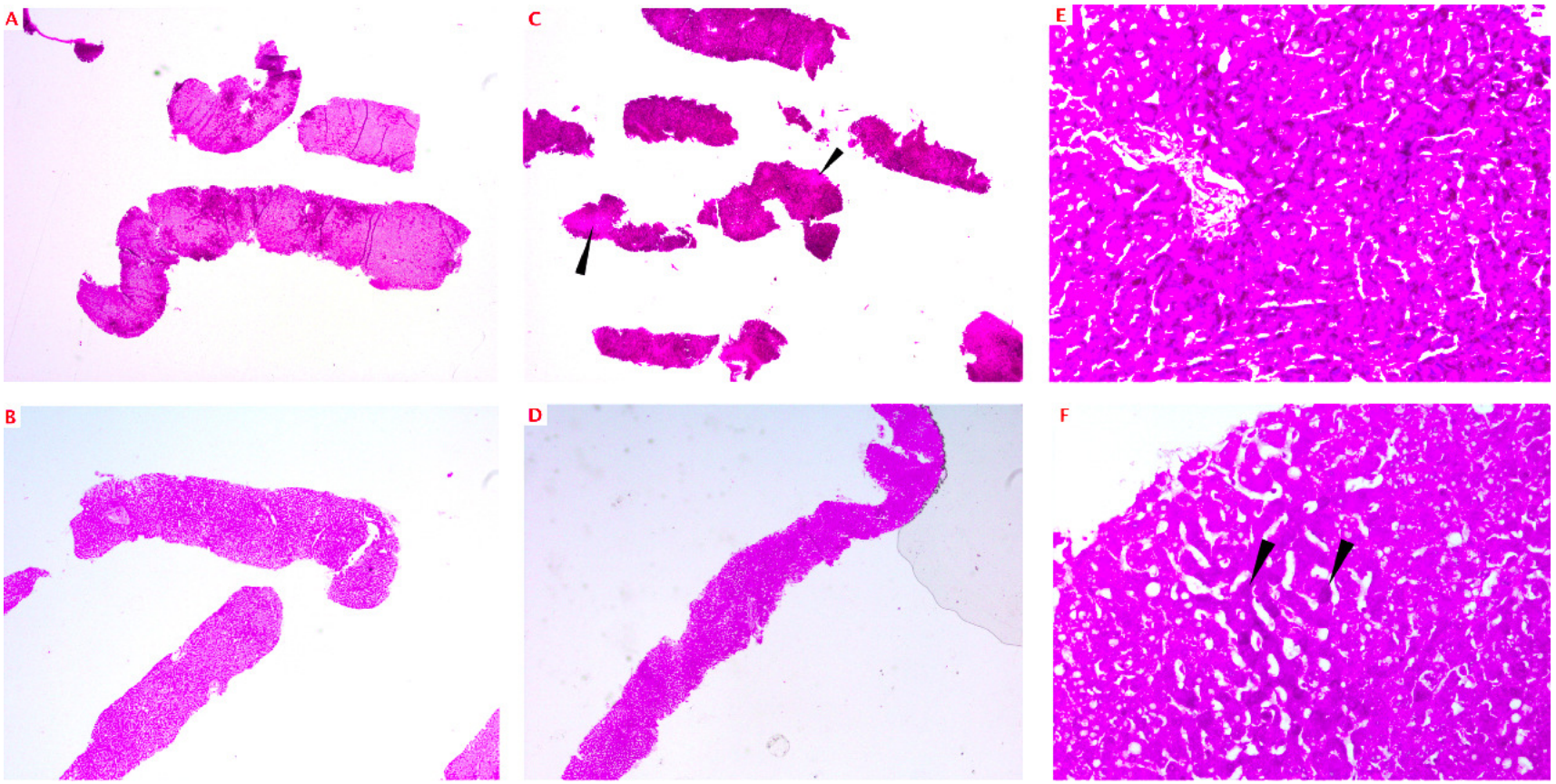

Figure 2.29: Histological findings pre- and post NMLP in viable and non-viable livers: PAS stain. PAS stained sections of viable liver 6 (A, C, E) and non-viable liver 4 (B, D, F). Both have marked glycogen depletion pre-NMP (A and B), whilst post-NMLP the viable liver has restored its glycogen stores (C and E) whilst the non-viable liver (D and F) still remains significantly glycogen depleted. Bright magenta staining of the cytoplasm indicates glycogen, whilst pale pink staining indicates no glycogen. (C) pale pink areas lacking glycogen arrowed. (F) The few darker staining hepatocytes containing some glycogen are arrowed. [A-D original objective x2; E, F original objective x20]. Acknowledgement to Dr. Desley Neil for interpretation.

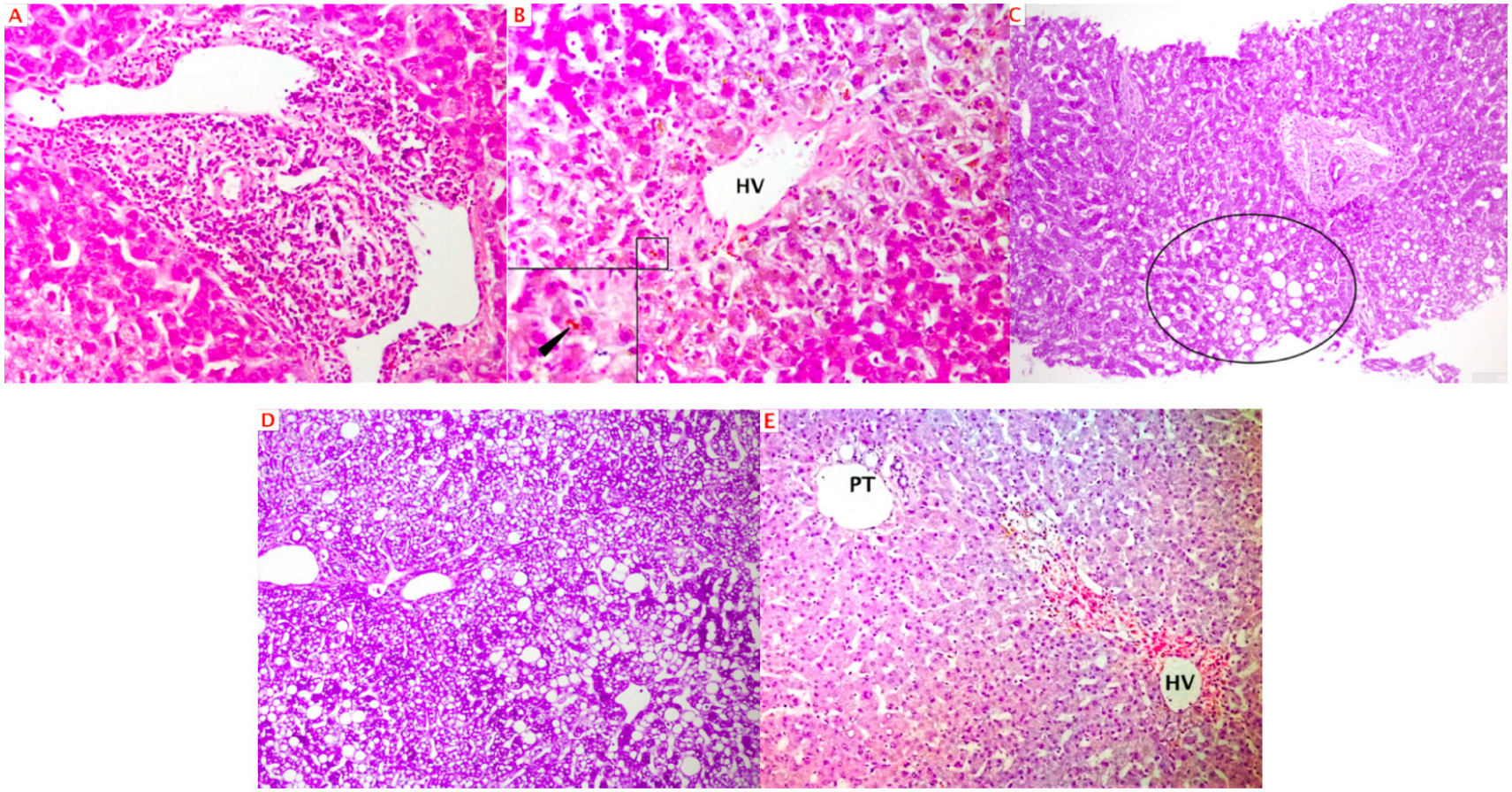

Figure 2.30: Histological observations in the perfused viable and non-viable livers. A & B, H&E stained sections of liver 5 which was turned down for transplantation based on its macroscopic appearance (objective x20 for both). It had a portal hepatitis (A) and severe zone 3 cholestasis (B) (inset – high power of bile plug, arrow); C, PAS stained section of liver 4 (objective x10); D, PAS stained section of liver 1 pre-NMLP (objective x20); E, H&E stained section of liver 7 turned down because macroscopically thought to have fibrosis. There is no fibrosis present (original objective x10). Acknowledgement to Dr. Desley Neil for interpretation.

Perfusion number	1	2	3	4	5	6	7	8	9	10	11	12
Designated viability	Non-Viable	Non-Viable	Non-Viable	Non-Viable	Non-Viable	Viable	Viable	Viable	Viable	Non-Viable	Viable	Viable
Large droplet steatosis[1] (%)	5	5	<5	15	0	0	0	0	0	0	0	<1
Small droplet steatosis[2] (%)	90	30	<5	40	0	5	10	0	0	0	0	10
Glycogen depletion[3] (%) (pre / post NMP)	30/90	75/90	99/80	90/80	-	80/15	-	5/5	85/75	5/10	40/30	95/10
Detached hepatocytes[4] (%) (pre-NMP / post-NMP)	0/1	4/30	0/40	20/15	-	0/1	- /0	0/0	10/10	0/5	0/5	1/2
Bile duct injury[5] (pre-NMP / post-NMP)	0/2	0/2	0/1	0/0	-	0/1	- /0	0/0	0/1	0/1	0/0	0/0
Coagulative Necrosis[6] (%) (pre-NMP / post-NMP)	0/1	0/0	0/0	0/5	-	0/0	- /0	0/0	0/2	0/10	0/10	0/5
Other findings	Microthrombi	Mild portal hepatitis		Patchy congestion	Hepatitis with severe cholestasis		l-2 week old lytic zone 3 necrosis			Mild portal oedema with eosinophils		
Time of 2nd Biopsy (hrs)	6	3.2	6	6	6	6.5	4.5	6	6	6	6	5

Table 2.9: Histological features on liver biopsies. Values designated with "–" are missing. *1: Large droplet macrovesicular steatosis is defined as a single large fat droplet within the hepatocyte cytoplasm displacing the nucleus; values are % of hepatocytes containing fat. *2: Small droplet macrovesicular steatosis is defined as fat droplets, usually multiple within the cytoplasm of the hepatocyte which do not displace the nucleus; values are % of hepatocytes containing fat. *3: Glycogen depletion is graded as % of hepatocytes which do not contain glycogen. *4: Detached hepatocytes is the % of hepatocytes which have lost cohesion from each other and from the sinusoidal lining. *5: Bile duct injury is defined as apoptotic debris within the wall or lumen or loss of cohesion between the epithelium and basement membrane; it is graded as 0 (nil), 1 (minimal) and 2 (mild). *6: Necrosis is depicted as the percent of total hepatocytes in the biopsy which show classical ischaemic type coagulative necrosis. Shaded columns highlight non-viable livers.

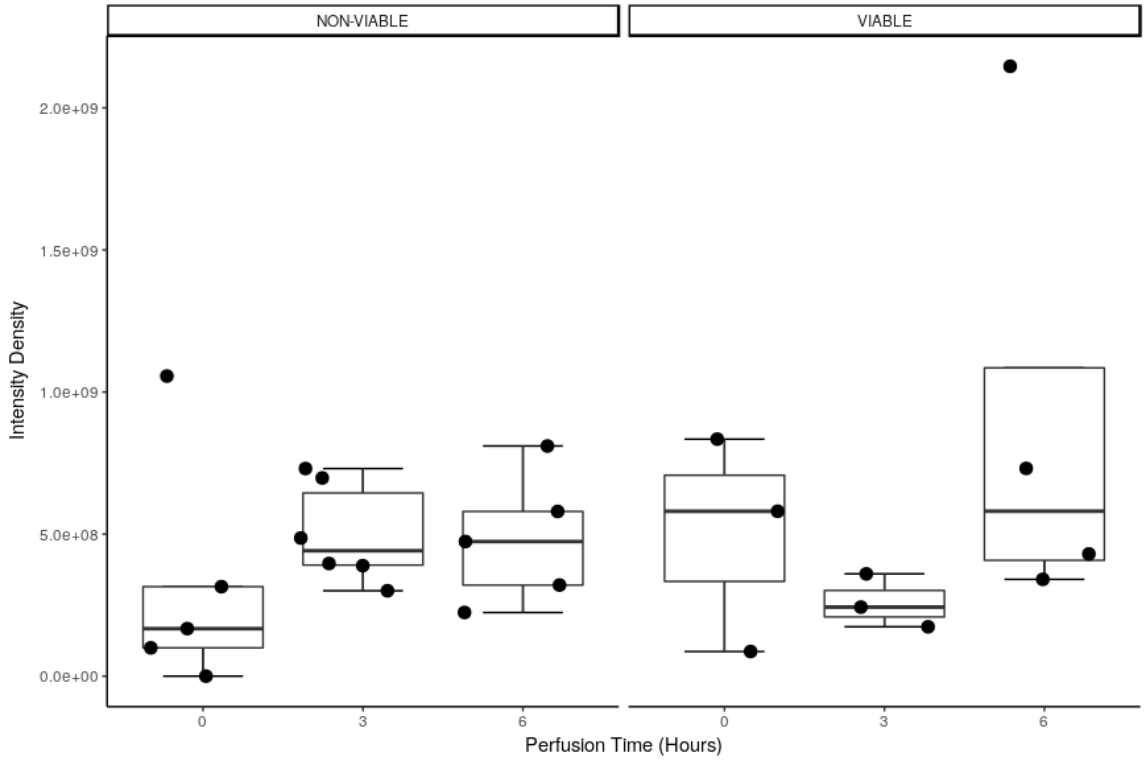

Figure 2.31: Quantitiative assessment of PAS staining over NMLP time by viability. Repeated measures ANOVA main effect for viability F = 0.597, $p > 0.05$. Main effect for perfusion time F = 1.089, $p > 0.05$. The interaction effect was insignificant, F = 1.369, $p > 0.05$. Overall, neither viability nor perfusion time influenced polysaccharide content.

was insignificant, F = 1.244, $p > 0.05$.

In both viable and non-viable liver, there appeared to be reductions in UCP2 after 3 hours of NMLP followed by an increase by the end of perfusion. The latter increase appeared to be more pronounced in the viable group. However, on repeated measures ANOVA, both the main effect of viability with F = 0.110, $p > 0.05$, and perfusion time with F = 2.677, $p > 0.05$, were not significant (Figure 2.33). Similarly, the interaction effect was insignificant, F = 1.146, $p > 0.05$. There was no correlation between ATP content and UCP2 staining (Data not shown).

Secondary Analysis of Perfusion Data Using Multilevel Random Intercept and Slope Models

Due to the complexity of mutliple variables measured repeatedly over time and compared between two groups using a realtively small sample size, separate models were created for each response variable as detailed in section 2.2.8: lactate and glucose metabolism, pH, arterial and portal flow rates, oxygen extraction ratio, oxygen consumption, oxygen consumption per gramme of liver and haematocrit. Explanatory variables included a dummy variable based on lactate clearing trajectories, denoted as Lactate Clearing (LC) and Non-Lactate Clearing (Non-LC), and perfusion time (in hours). To quantify any changes in response variables over time, multilevel models were created. It was found that the better fitting models with lowest Akaike Information Criterion (AIC) values, an estimator of the relative quality of statistical models, included a random intercept and slope, perfusion time duration and lactate clearing dummy variable.

Model results showed that lactate levels were 10.225 mmol/L (95% CI: 12.745, 7.705) lower on average for the LC dummy variable in comparison to the Non-LC group, with the LC dummy variable effect being strongly significant ($p<0.0001$), holding other model parameters constant (Figure 2.34). There was on average 2.341 mmol/L (95% CI: 0.806, 3.876) difference in lactate levels associated with a mmol/L difference in the inverse of time, with the time parameter requiring transformation, and the time effect being very significant (p = 0.003), holding other

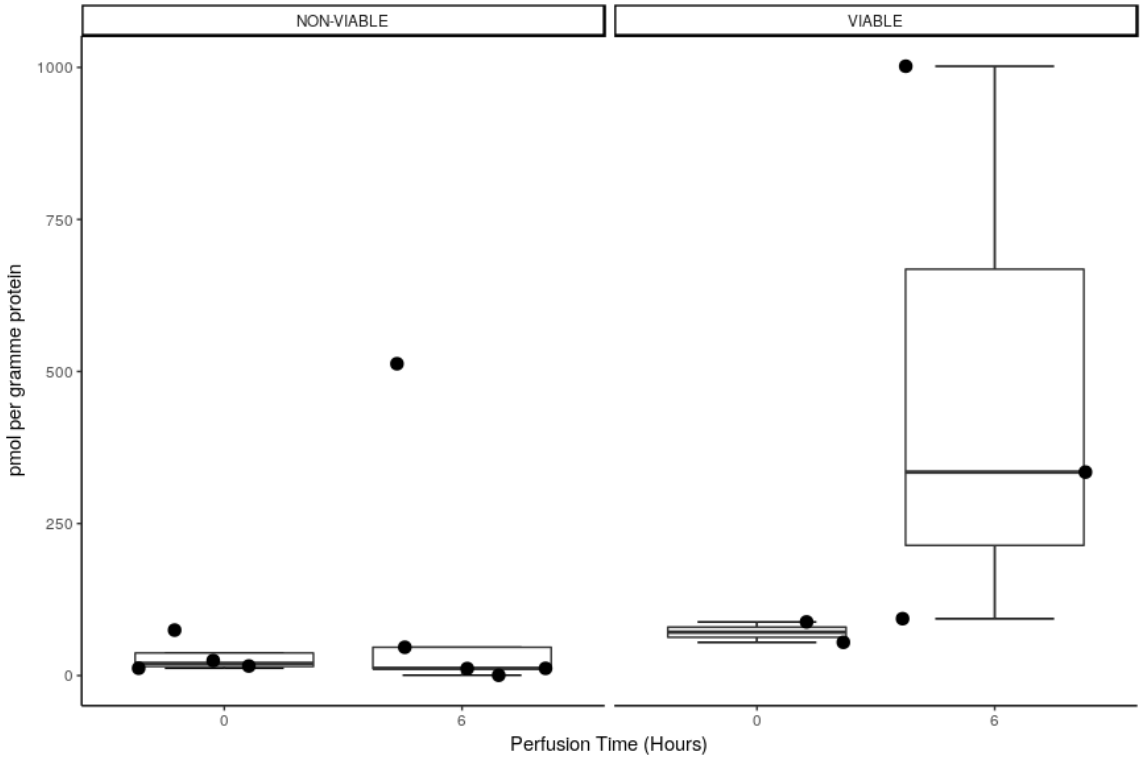

Figure 2.32: ATP content per gramme of protein in liver during NMLP by viability. The trend for increased ATP content at the end of NMLP in the viable group was not statistically significant on repeated measures ANOVA (see main text).

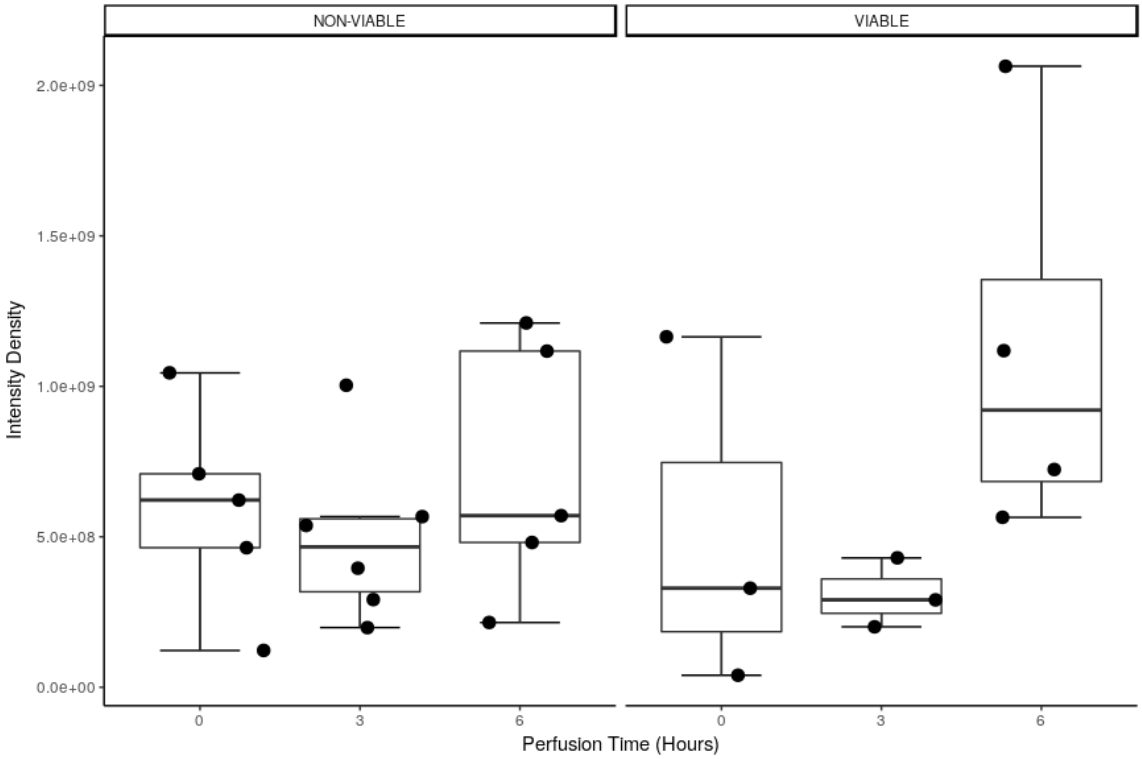

Figure 2.33: UCP2 immunohistochemical staining during NMLP based on viability.The trends in an initial reduction then increase in UCP2 staining, particularly in the viable group, were not statistically significant on repeated measures ANOVA (see main text).

model parameters constant. This demonstrates that lactate not only decreases over time but also can be described as two distinct groups for the purposes of viability assessment.

The model created for glucose as the response parameter found that change in glucose concentrations over time had a linear relationship (Figure 2.35). Results indicated that glucose levels decreased by 2.469 mmol/L (95% CI: 4.246, 0.694) on average per unit change in time, where the time effect was very significant (p = 0.006). However, the LC dummy variable effect was found non-significant in this model (p = 0.148). This demonstrates that using this mathematical technique, whilst glucose concentration decreases over time, it is not a function of lactate clearance for the purposes of viability assessment.

Individual models for arterial and portal flow rate responses were constructed, with better fitting models having the lowest AIC values containing time, LC dummy variable, pressure and resistance explanatory variables. Time was log (natural) transformed for the arterial flow rate model and log (base 10) transformed for the portal flow rate model. The arterial flow rate model showed that pressure and resistance were necessary for the model and had an important interaction, with their effects being strongly significant ($p<0.0001$). Results indicated that for a unit increase in pressure, arterial flow rate decreased by 0.003 ml/min/g (95%CI: 0.004, 0.001); and for a unit increase in resistance, arterial flow rate decreased by 0.391 (95%CI: 0.569, 0.212); the interaction term indicated that for a unit increase in both pressure and resistance, the arterial flow rate changed by 0.006 ml/min/g (95%CI: 0.003, 0.009), holding other variables in the model constant. There was on average 0.034 units (95% CI: 0.0003, 0.067) difference in arterial flow rate associated with a unit difference in the natural log of time, with the time effect being significant (p = 0.048), holding other model parameters constant. The LC dummy variable effect was found non-significant in this model (p = 0.824) (Figure 2.36). This demonstrates that arterial flow rate is dependent on pressure and resistance but that although it increases with time, arterial flow rate does not vary as a function of lactate clearance.

The portal flow rate model differed to the arterial flow rate model by showing that the resistance parameter alone did not have a significant effect on the model (p = 0.121), however its

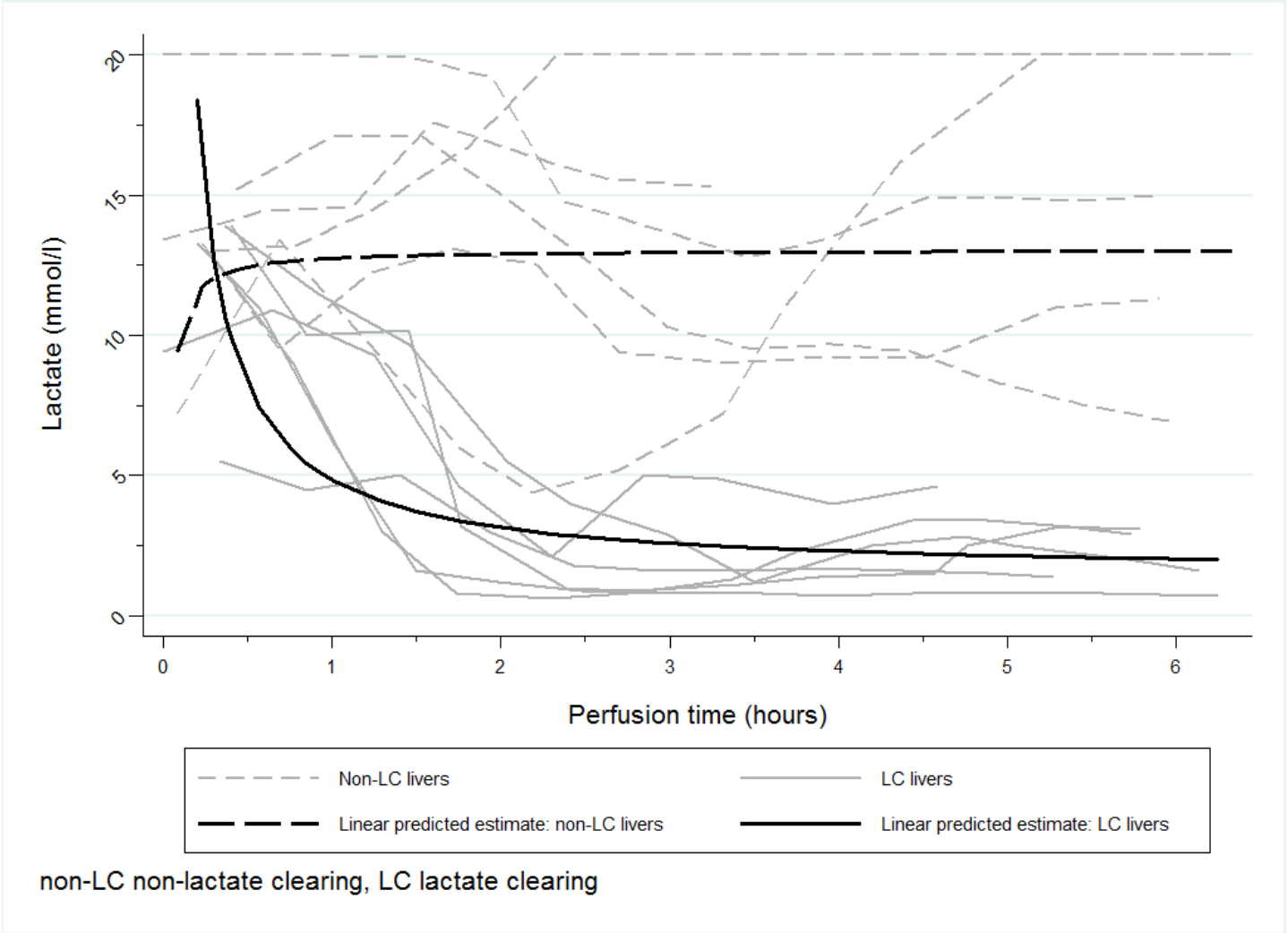

Figure 2.34: Lactate concentration during NMLP using multilevel random intercept and slope model. This demonstrates that lactate concentration divides the perfused livers in to 2 distinct groups as described earlier.

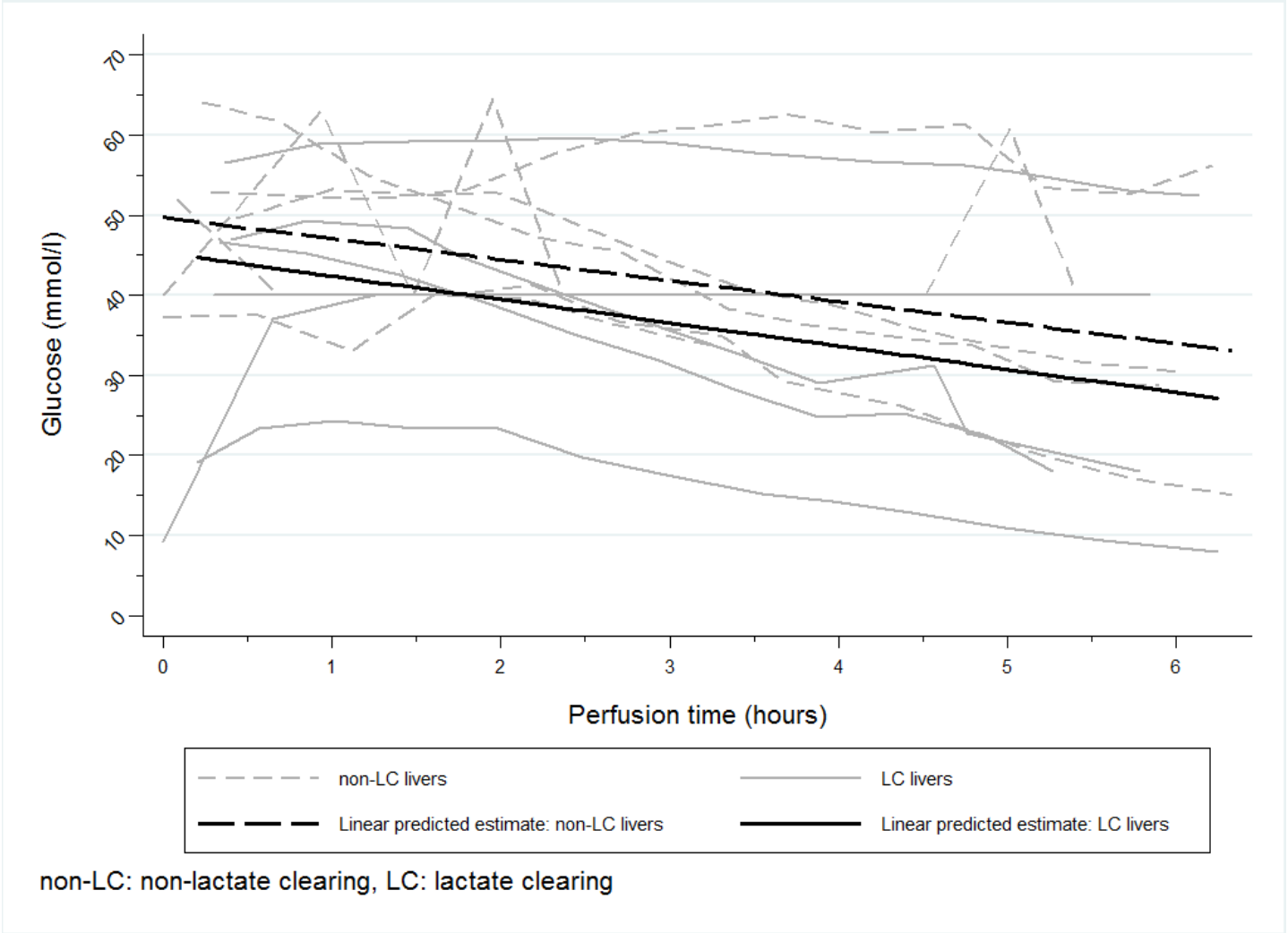

Figure 2.35: Glucose concentration during NMLP using multilevel random intercept and slope model. Although glucose concentration changed with time, there was no effect of lactate clearance

interaction with pressure was found to be strongly significant ($p<0.0001$) as was the pressure parameter. For a one-unit increase in pressure, portal flow rate increased by 0.074 ml/min/g (95%CI: 0.047, 0.100), whereas for a one-unit increase in both pressure and resistance, the portal flow rate decreased on average by 3.751 ml/min/g (95%CI: 5.762, 1.742), holding all other model parameters constant. Time was log (base 10) transformed and found to be strongly significant ($p<0.0001$). For a one-unit increase in log (base 10) of time, the portal flow rate changed on average by 0.116 ml/min/g (95%CI: 0.053, 0.179), holding other model parameters constant. The LC dummy variable effect was found non-significant in this model ($p = 0.500$)(Figure 2.37). This demonstrates that portal flow rate was dependent on pressure and resistance over time but was not a function of lactate clearance.

Oxygen extraction ratio response was modelled including time and LC dummy variable only (Figure 2.38). Neither explanatory variable was found to be significant in the model: time $p = 0.985$; LC dummy variable $p = 0.07$. Similar models were constructed for oxygen consumption and oxygen consumption per gramme of liver responses (Figure 2.39). On modelling, oxygen consumption per gramme of liver was found to have a significant ($p<0.0001$) linear relationship with time; for a one-unit increase in time, oxygen consumption per gramme increased by 0.002 (95%CI: 0.0008, 0.003). The LC dummy variable was found not to be significant ($p = 0.579$). Again, whilst the oxygen extraction per gramme of tissue increased during NMLP, this was not as a function of lactate clearance so has limited value in viability assessment.

The pH response model contained three additional explanatory variables (HCO3, Partial Pressure of CO_2 (pCO_2) and Base Excess (BE)) together with time (natural log transformation) and LC dummy variable (Figure 2.40). Findings showed for a one-unit increase in HCO3, pH significantly ($p<0.0001$) decreased on average by 0.055 units (95%CI: 0.056, 0.053); a one-unit increase in pCO2, pH significantly ($p<0.0001$) decreased on average by 0.005 units (95%CI: 0.007, 0.004); and a one-mmol/L increase in BE, significantly ($p<0.0001$) increased pH on average by 0.061 units (95%CI: 0.060, 0.062), holding all other model parameters constant. Also, the LC dummy variable was found to be strongly significant ($p<0.0001$), with pH being 0.013

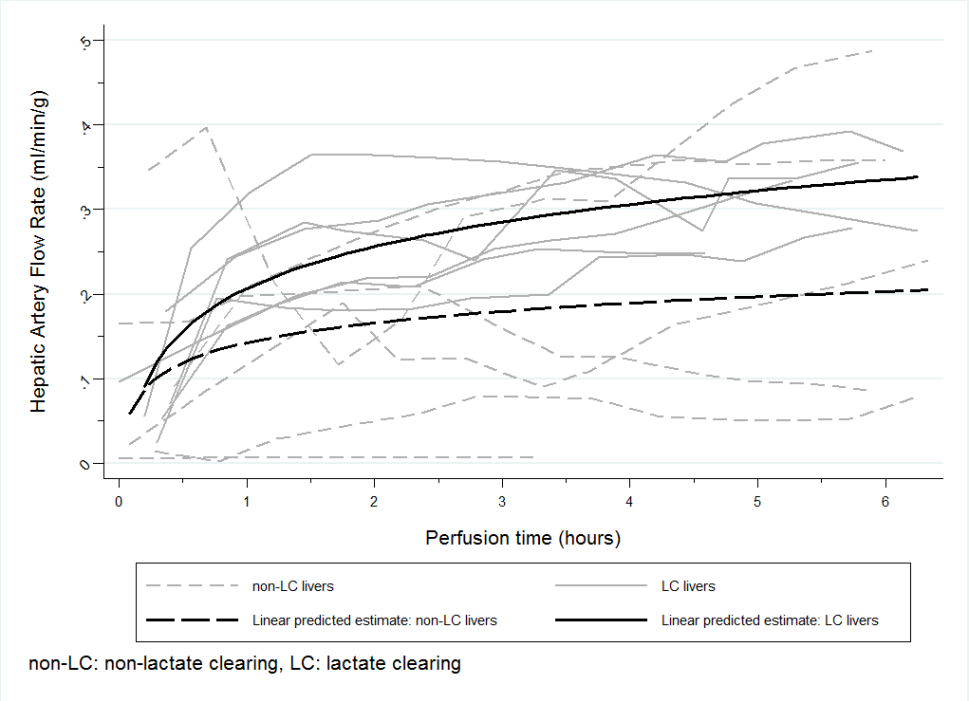

Figure 2.36: Arterial flow rates per gramme of liver during NMLP using multilevel random intercept and slope model. Arterial flow rate interacted with pressure and resistance as well as changing over time, but there was no effect of lactate clearance.

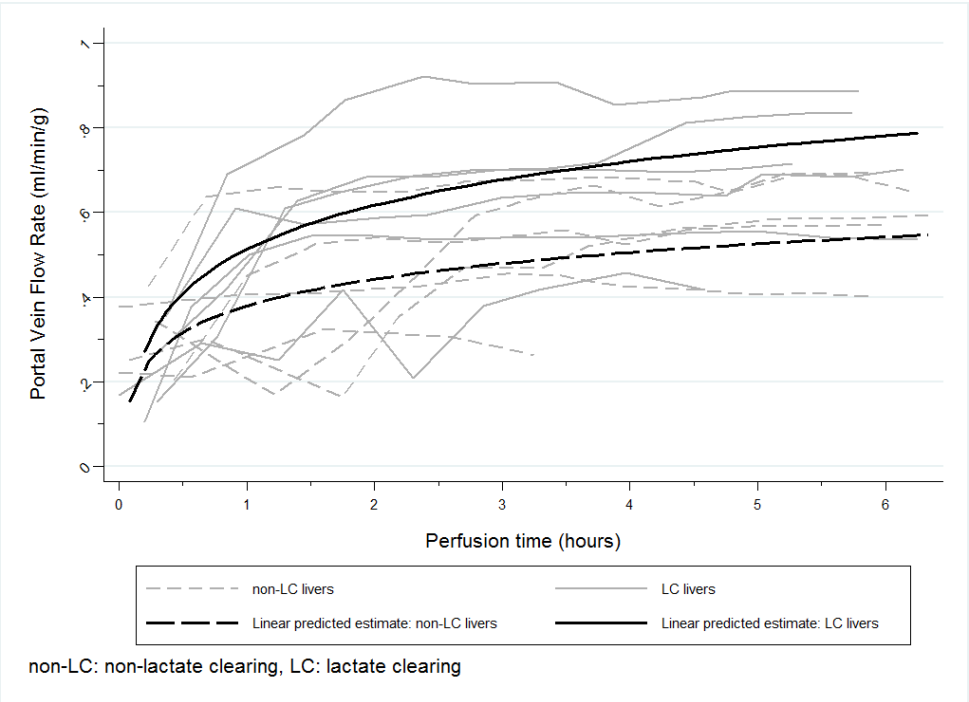

Figure 2.37: Portal flow rates per gramme of liver during NMLP using multilevel random intercept and slope model. Pressure and resistance together interacted with portal vein flow rates, with there being increases in portal flow rates over time. However, in this model the effect of lactate clearance was not significant.

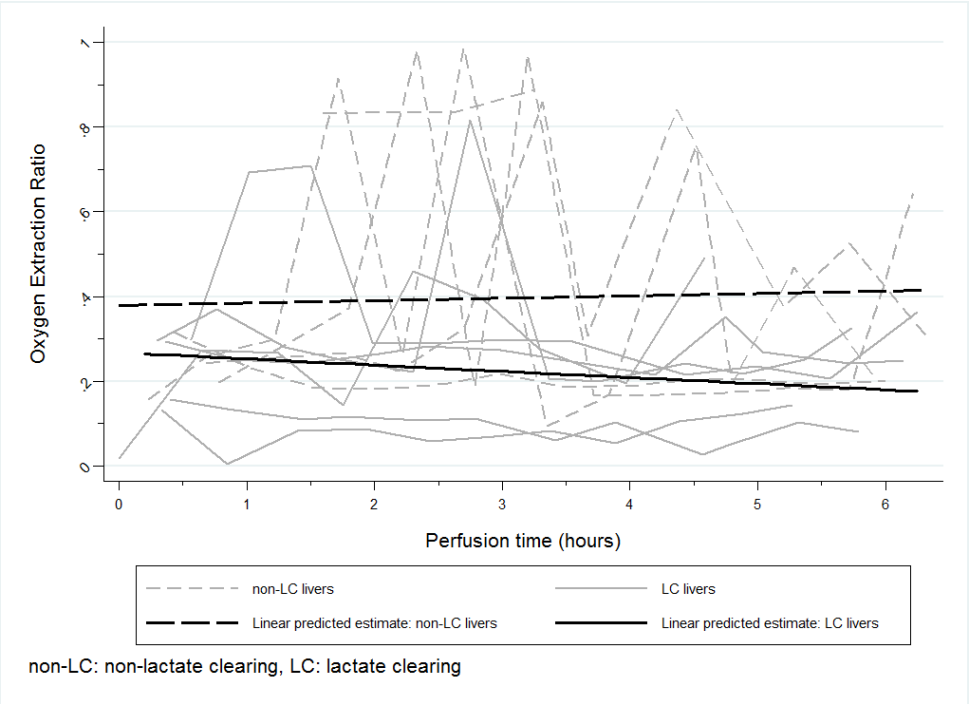

Figure 2.38: Oxygen extraction ratios during NMLP using multilevel random intercept and slope model. Neither perfusion time nor lactate clearance were found to have a significant effect.

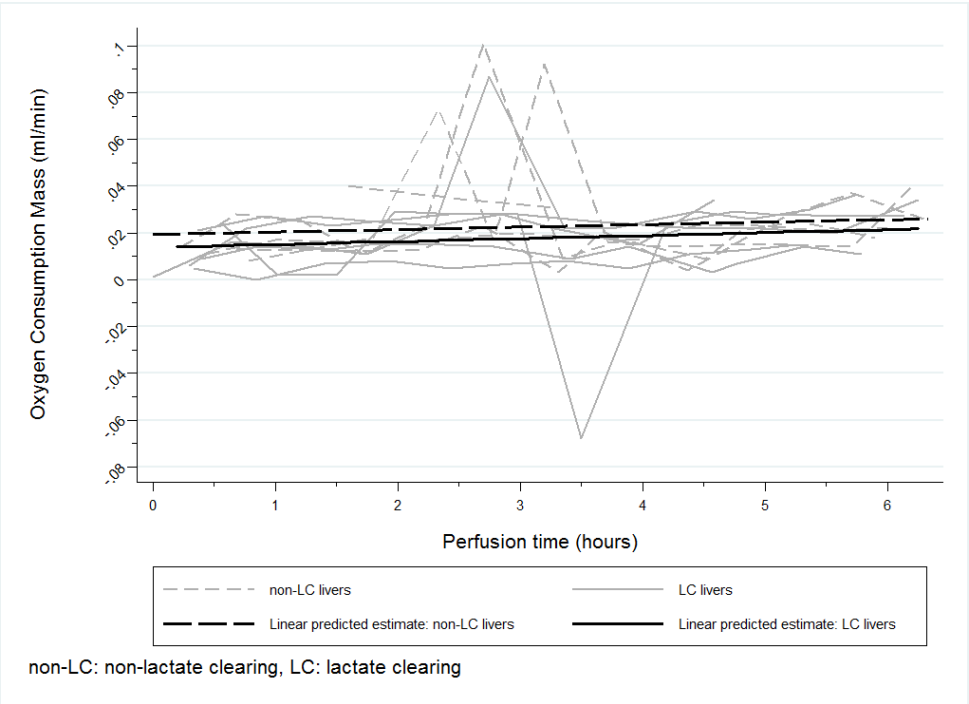

Figure 2.39: Oxygen consumption per gramme of liver during NMLP using multilevel random intercept and slope model.There was a significant effect of time on oxygen consumption per gramme of liver perfused. However, lactate clearance did not have an effect.

units (95% CI: 0.019, 0.006) lower on average for the LC group in comparison to the non-LC group. There was on average 0.005 units (95% CI: 0.0004, 0.009) increase in pH associated with a unit difference in the natural log of time, with the time effect being significant (p = 0.031), holding all other model parameters constant. These results are in keeping with Henderson–Hasselbalch equation in relation to the physiological Carbon Dioxide (CO_2) bicarbonate buffering system.

Results for haematocrit modelled with the LC dummy variable found a decreasing linear relationship between haematocrit and time (Figure 2.41). For a one-unit increase in time, haematocrit decreased on average by 1.612 units (95%CI: 2.374, 0.0850; p<0.0001). The LC dummy variable was found not significant (p = 0.818). That haematocrit decresaes over time might be expected using mechanical rotorary pumps in the perfusion device and packed red cells that are beyond acceptable thresholds for clinical transfusion. However, haematocrit was not a function of lactate clearance.

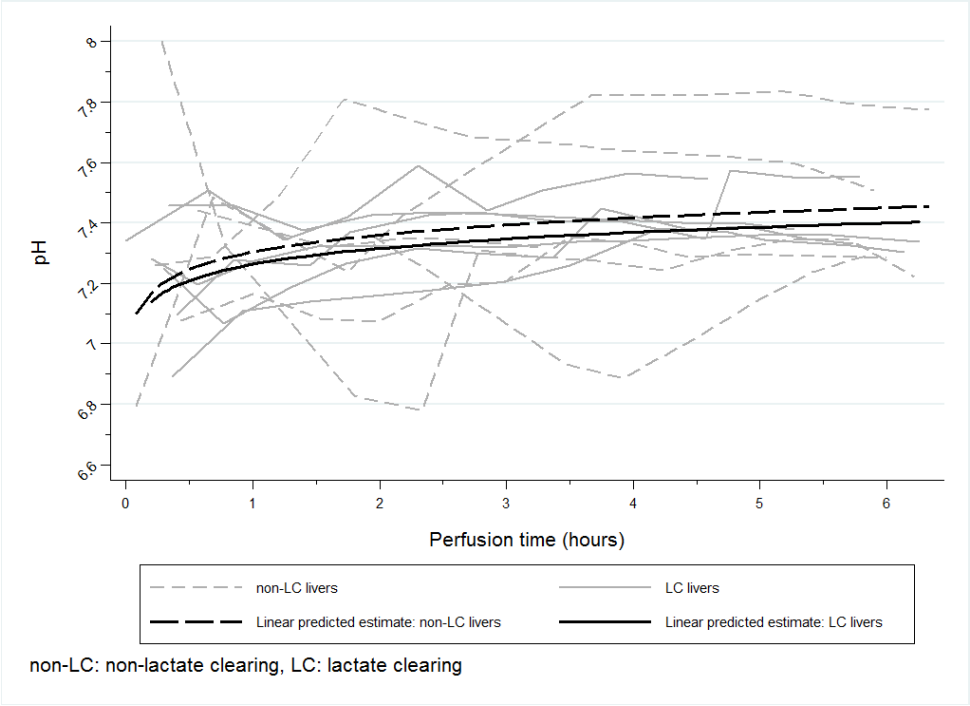

Figure 2.40: pH during NMLP using multilevel random intercept and slope model. Bicarbonate, pCO_2 and base excess all interacted with pH. Not only did pH increase over time, but also was higher in the non-lactate clearing group.

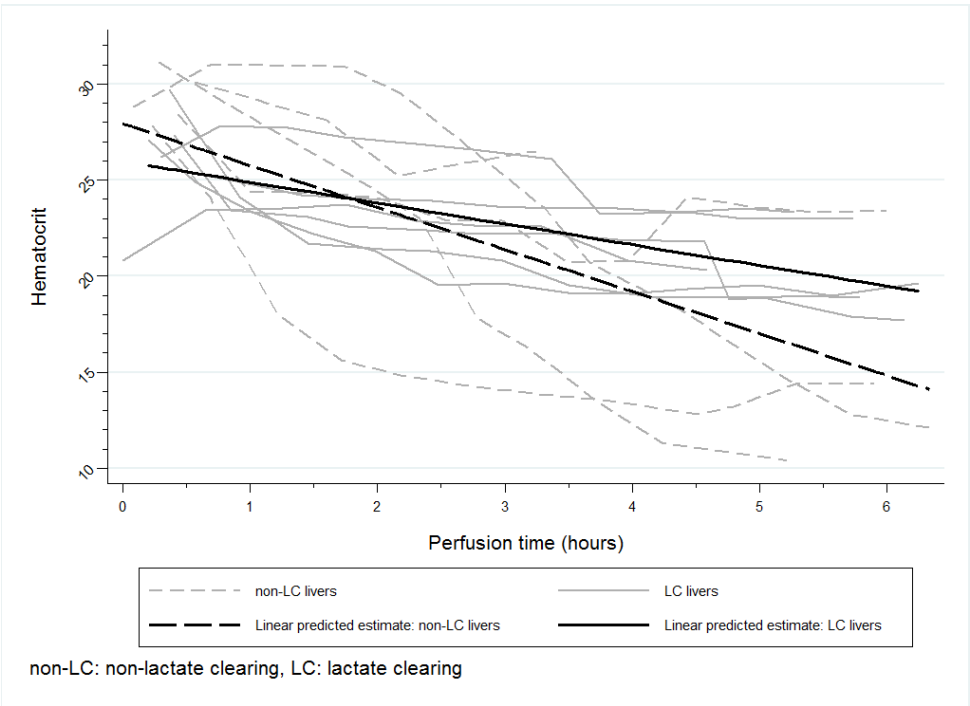

Figure 2.41: Hct during NMLP using multilevel random intercept and slope model. Hct decreased during NMLP but there was no effect of lactate clearance in the model.

Defining Viability Assessment Criteria

Based upon the results presented above, criteria defining viability to permit transplantation of livers being subjected to NMLP are proposed. Timing of this assessment has been defined as after two hours of NMLP which allows for stabilisation in the performance of each perfused liver to be established. With the normothermic machine used and accounting for the specifications of the oxygenators which maintain their licenced performance for 6 hours, an assessment after 2 hours of NMLP permitted 4 hours for the sending and arrival of the patient to the operating theatre department, completion of anaesthesia and recipient hepatectomy. The proposed criteria are as follows:

1. Absolute Criteria (after 2 hours of NMLP)
    (a) Perfusate lactate concentration $<$2.5 mmol/L
    (b) Evidence of bile production
2. Other Considerations (after 2 hours of NMLP)
    (a) Arterial flow rate $>$500 ml/min or $>$30 ml/min/100g and portal vein flow rate $>$1250 ml/min or $>$70 ml/min/100g
    (b) Perfusate pH $>$7.30
    (c) Evidence of homogenous perfusion and soft consistency of the liver.

To ensure patient safety during the early stages of the development of NMLP in discarded human livers, both of the absolute criteria had to be present whilst the other considerations were highly desirable and would provide reassurance to the perfusion and transplanting team in the context of meeting the absolute criteria. As devlopment continues, these criteria could be refined. Validation of the criteria is presented below in the first human allotransplantation of a human discarded cadaveric donor liver subjected to NMLP.

2.3.6 Validation of the Model by the First Allotransplantation of a Human Discarded Cadaveric Donor Liver Subjected to NMLP

The Patient and the Donor

The patient was a 47-year-old man diagnosed with end-stage liver disease secondary to alcoholic cirrhosis complicated by hepatic encephalopathy. He was placed on the UK liver transplant waiting list in June 2014 with a Model for End-stage Liver Disease score of 17. NMLP was discussed with the patient during transplant assessment, where he was seen by a surgeon, anaesthetist, physician and clinical psychologist. NMLP was approved by the Novel Therapeutics Committee at the Queen Elizabeth Hospital and the patient provided written informed consent for the procedure.

A DCD liver from a 29-year-old male donor with Type I diabetes, who sustained an irrecoverable hypoxic brain injury following a cardiac arrest and had been admitted to the ITU for 7 days, was initially accepted for transplantation. Withdrawal of life sustaining treatment was conducted in ITU according to UK standard practice. Donor oxygen saturation was unrecordable 3 minutes after withdrawal of treatment. Systolic blood pressure fell to below 50mmHg after 98 minutes. Asystole ensued 2 minutes later. Dual liver perfusion with University of Wisconsin (UW) perfusion fluid at 4^oC commenced 12 minutes after asystole using the established super-rapid technique.[120] On back-table inspection, the retrieval surgeon described the liver as non-steatotic, with soft consistency and normal vascular anatomy but with several areas of suboptimal perfusion.

The shortest expected CIT on arrival at the Queen Elizabeth Hospital was 7 hours. The liver was declined for transplantation following static cold storage however, after consideration it was decided to subject the liver to NMLP for viability assessment.

Normothermic Machine Liver Perfusion

On arrival at Liver Theatres within Queen Elizabeth Hospital Birmingham, good macroscopic appearance was confirmed with a frozen histological needle biopsy. The liver was prepared for transplantation in our usual manner. After a CIT of 426 minutes, NMLP commenced with the packed red cell based fluid, supplemented with antibiotics and a prostacyclin infusion, at 37^{o}C using the Liver Assist device (Organ Assist®, The Netherlands) as described above. Oxygenated pulsatile flow at 48 mmHg and non-pulsatile flow at 9 mmHg perfused the liver via the hepatic artery and portal vein respectively, before recirculating from the hepatic veins via the open circuit reservoir. During NMLP, flow parameters, perfusate blood gases and bile production were assessed every 30 minutes as described previously. After 2 hours, organ function was assessed by two transplant surgeons and an anaesthetist independent of the clinical and perfusion teams. Another histological biopsy was taken at the end of NMLP.

The duration of NMLP was 393 minutes. Within one minute of commencing, heterogenous macroscopic perfusion was noted on the surface of the liver. Homogenous perfusion was recorded after 3 minutes of NMLP which was maintained until implantation.

At the start of NMLP, arterial and portal venous flow rates were 110 ml/min and 210 ml/min respectively. Flow rates increased rapidly, reaching zeniths of 727 ml/min (artery) and 1090 ml/min (portal vein) after 90 minutes of NMLP (Figure 2.42 A). Flow rates at the end of NMLP were 531 ml/min for the artery and 1070 ml/min for the portal vein. Arterial and portal venous pressures were maintained within physiological thresholds (Figure 2.42 B). After an initial decrease, resistances in the artery and portal vein remained low. The initial reservoir temperature was 20^{o}C, reaching 35^{o}C after 34 minutes of NMLP.

The initial lactate of 13.3 mmol/L decreased rapidly (Figure 2.42 C). After 2 hours of NMLP, when the suitability for transplantation was assessed, the lactate was 1.2 mmol/L. It continued to decrease, although more slowly, being 0.4mmol/L at the end of NMLP. Bile production commenced 30 minutes after starting perfusion (Figure 2.42 D). In total, 27 grammes were

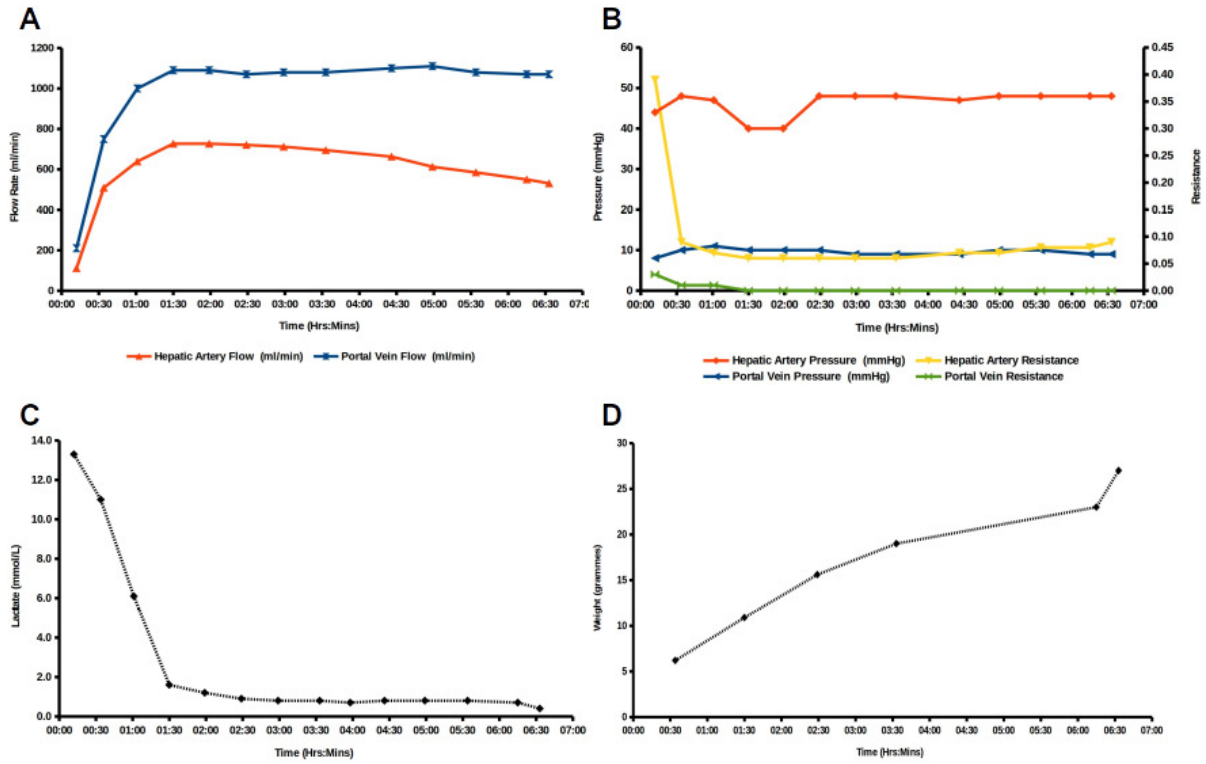

Figure 2.42: A: Flow parameters. Hepatic artery flow (red) and portal vein flow (blue). B: Pressure and resistances. Hepatic artery pressure (red), hepatic artery resistance (yellow), portal vein pressure (blue), portal vein resistance (green). C: Lactate concentration. D: Cumulative bile production.

excreted.

Histological assessment demonstrated maintenance of architectural structure on H&E staining (Figure 2.43 A-D). Sinusoidal vasodilatation was noted at the end of NMLP (Figure 2.43 B&D). PAS staining highlighted considerable replenishment of hepatocyte glycogen stores (Figure 2.43 E-H). This was accompanied by a reduction in perfusate glucose concentration from a maximum of 24.3 mmol/L to 11.4 mmol/L without the adminstration of exogenous insulin (Data not shown).

Surgical Procedure

Implantation was performed using an inferior vena cava preserving, modified piggyback technique with the creation of a temporary porto-caval shunt. Once the transplanting surgeon was ready for implantation, NMLP was stopped, the donor liver disconnected and flushed with 2 litres of Histidine-Tryptophan-Ketoglutarate (HTK) solution (Custodiol, Koehler Chemie, Germany). The liver was reperfused using an artery-first anastomosis technique. There was an attenuated reperfusion syndrome. The operation was uneventful, with 5 units of packed red cells and 6 units of fresh frozen plasma being transfused. The operation time was 5 hours and 3 minutes.

Postoperative Function and Course

The patient's post-operative recovery was uneventful. The patient was transferred to ITU and commenced on the standard immunosuppression regimen utilised at Queen Elizabeth Hospital Birmingham, including oral tacrolimus, maintaining levels between 4 and 8 ng/mL, azathioprine and steroids. These continued on transfer to the ward. Liver and renal function tests were checked daily. A peak Alanine Aminotransferase (ALT) of 1215 IU/L immediately post-transplant halved by the 2nd post-operative day and was within the normal range (<41 IU/L) 4 weeks after transplantation (Figure 2.44 A). Aspartate Aminotransferase (AST) returned to and was maintained within the normal range (<43 IU/L) after 7 days. The initial bilirubin of

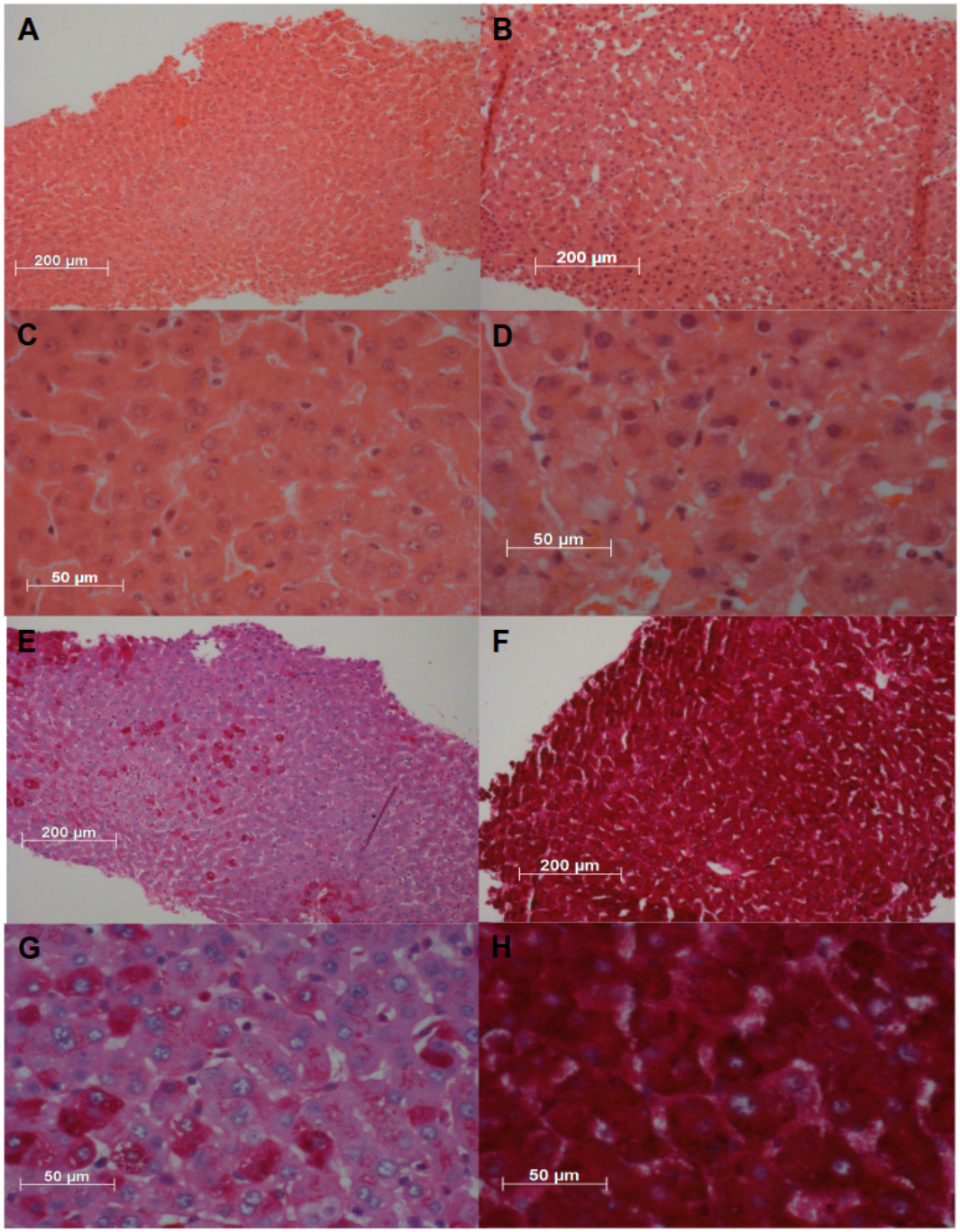

Figure 2.43: A,C,E,G prior to NMLP. B,D,F,H after NMLP prior to implantation. A-D haematoxylin and eosin staining to demonstrate tissue architecture. E-H PAS staining to detect glycogen content. A,B,E,F at 10x magnification. C,D,G,H at 40x magnification.

45 μmol/L increased to a peak of 110 μmol/L on the 5th post-operative day, but returned to and continued within the normal range (<22 μmol/L) after 34 days. Renal function remained stable and within physiological threasholds (Figure 2.44 B). The patient was discharged home on the 10th post-operative day. At discharge, the patient was reviewed in the out-patient clinic weekly for 1 month, fortnightly for 2 months and subsequently monthly. Liver function tests were checked at each visit. There has been no graft rejection since discharge. A Magnetic Resonance Cholangio-Pancreatogram (MRCP) conducted 6 months after transplantation, performed to assess the biliary tree, revealed normal intrahepatic bile ducts with neither anastomotic nor non-anastomotic strcturing (Figure 2.45).

2.4 Discussion

This study presents the initial experience of NMLP with a cohort of discarded human livers. These organs gave the opportunity to assess the full spectrum of liver function on NMLP and propose criteria to discriminate between viable and non-viable livers.

The present study reveals unique data and novel observations. These are the first criteria to be successfully tested in clinical practice and subsequently adopted within a clinical study of viability testing and transplantation of discarded human livers.[224] The criteria are easy to measure and consist of familiar parameters. Lactate concentration is an important indicator of graft function in the peritransplantation period, and as such, its inclusion facilitated clinical adoption of the protocol.[225] This is the first report that includes marginal organs that were so severely damaged that we were unable to maintain the perfusion for 6 hours, which has enabled the assessment of the full spectrum of liver function. The proposed criteria appear to correlate closely with the current gold standard assessment of liver transplantability: histopathological assessment. It has demonstrated the quite marked variability in the assessment of steatosis by the retrieving or transplanting surgeon and the histology of the liver. In this era of progressive organ shortage, such inconsistency may contribute to the waste of potentially usable livers, further highlighting the urgent need to develop objective assessment methods to improve the

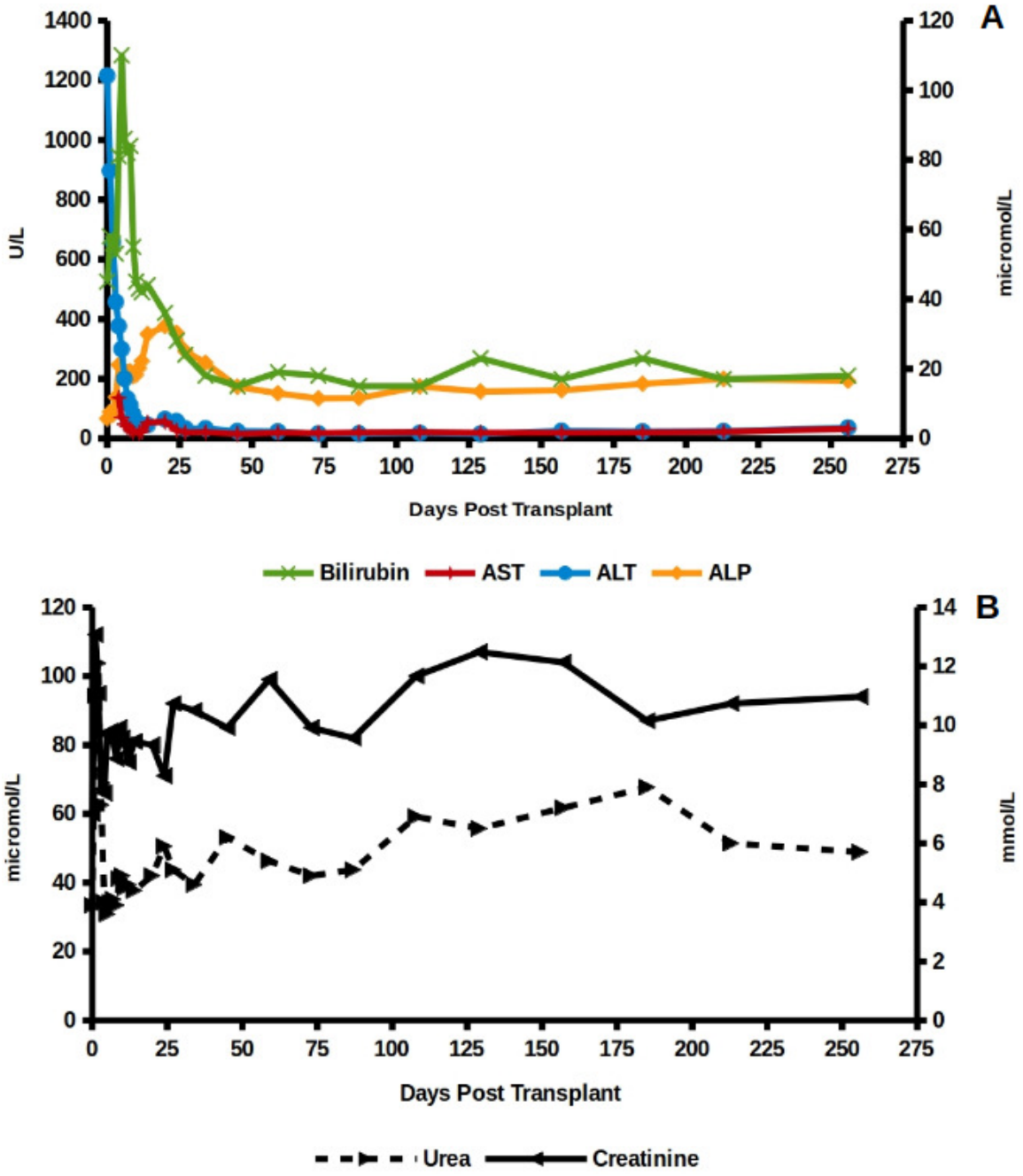

Figure 2.44: Post transplant results in the recipient. A: Liver function tests. Alanine transaminase (ALT), aspartate aminotransferase (AST), alkaline phosphate (ALP) in IU/L. Bilirubin measured in μmol/L. B: Urea measured in mmol/L and creatinine in μmol/L.

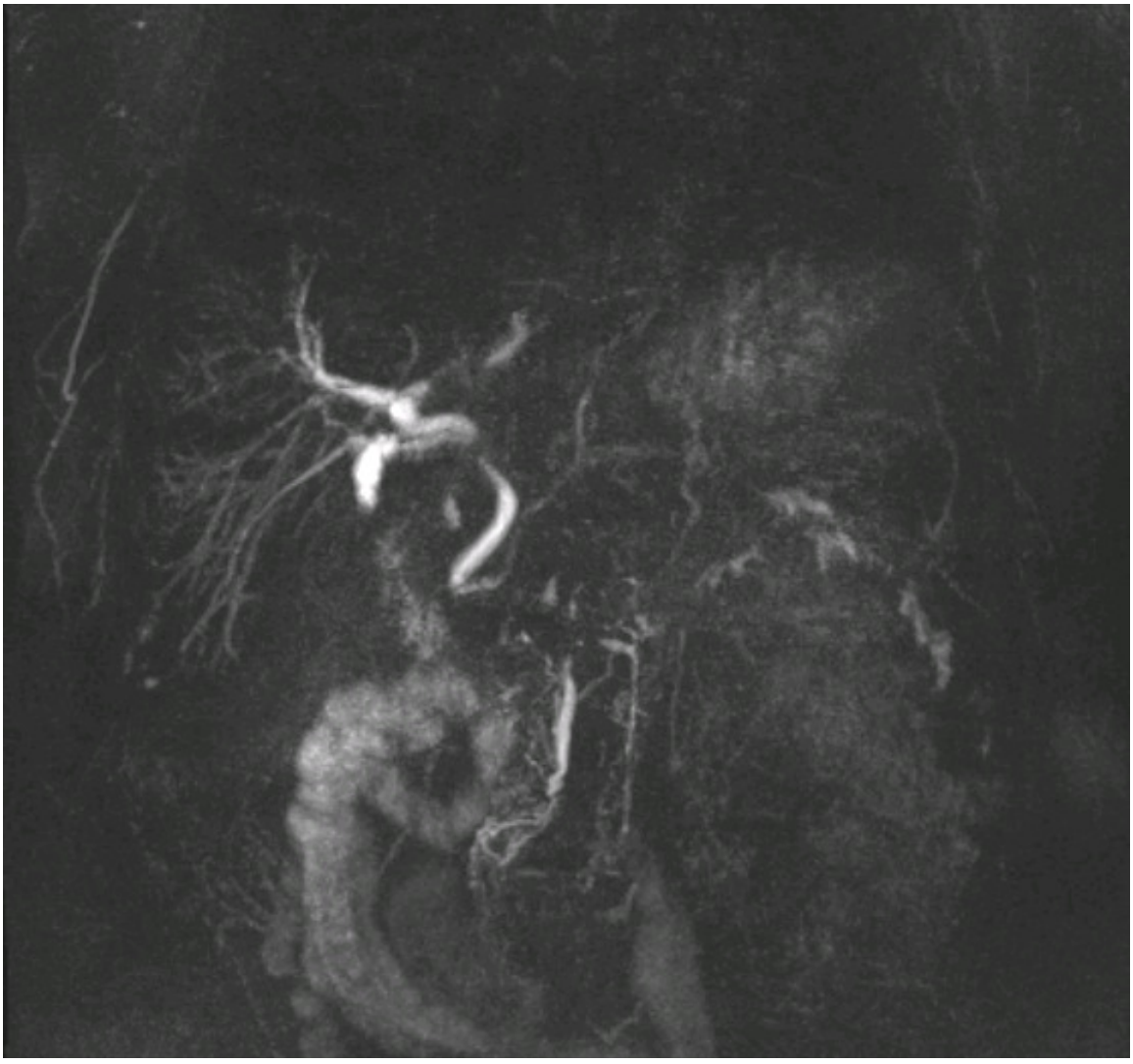

Figure 2.45: MRCP at 6 months post NMLP assisted transplant.

relatively low utilization of high risk organs.

The Groningen group was the first to demonstrate the feasibility of NMLP on 4 discarded human livers.[202] The livers were subjected to 6 hours of NMLP following a median CIT of 6:55 hours with all organs showing recovery of function and being deemed viable.[202] The inferior outcomes of some livers from this series may be explained in part by CIT being an average of 2 hours longer. A subsequent study from the Groningen group reported a NMLP series on 12 discarded livers, proposing six hours of cumulative bile production greater than 20 grammes as a marker of a good liver function.[226] A cut-off volume for bile volumes could not be determined because some viable organs in the series did not produce bile.

The Cambridge group advocated assessment based on perfusate transaminases and bile pH.[227] The authors observed a significant correlation between the ALT in the perfusate measured after 2 hours' perfusion and the peak ALT post-transplant levels within the first week.[227] They also hypothesized that the liver's capacity to produce an alkaline bile (pH $>$7.4) might be a good marker of cholangiocyte function, possibly identifying a selection of organs with a low risk of developing Ischaemic Type Biliary Lesions (ITBL). If validated, this observation might revolutionize DCD liver utilization. However, issues with bile collection, such as technical problems with bile duct cannulation, could lead to discarding usable livers. In concordance with the Cleveland group, the importance of bile production in the context of NMLP is possibly overestimated.[228]

Lactate is the intermediate metabolite of pyruvate within the glycolysis metabolic pathway. Under anaerobic conditions, pyruvate is converted to lactate by lactate-dehydrogenase. In well-functioning livers, the periportal hepatocytes use lactate as a primary substrate for gluconeogenesis as one part of the Cori Cycle. In NMLP, hyperlactaemia is predominantly due to tissue hypoxia resulting from impaired liver blood flow and decreased gluconeogenesis. In this setting lactate production may exceed its clearance and may therefore be an indicator for real-time liver function monitoring. A method to further elucidate the role of lactate and glucose metabolism in

NMLP could be achieved via (13)C glucose labelling studies using 2D NMR, that has demonstrated whole organ glucose metabolism within an hypoxic environment using a porcine model of hypothermic machine perufsion.[229] If successfully applied to NMLP, a more detailed and accurate mathematical model of lactate and glucose metabolism within the liver might be generated, rather than relying on perfusate samples that are more prone to sample and other errors. Additionally, bile production has generally been accepted to be a simple, yet sensitive, marker of graft function in liver transplantation. However, as bile production may be frequently absent at the end of OLT and does not necessarily indicate PNF, lactate concentration maybe a better primary parameter for assessing liver viability.

There are other advantages to using lactate in preference to bile production in assessing liver function during NMLP. Firstly, the decrease in lactate in well-functioning livers emerges 30-90 minutes earlier when compared to the bile production. This observation gives lactate concentration a particular advantage for viability assessment and would permit a timely start of LT. Secondly, lactate concentration can be measured immediately on commencement of NMLP and repeated as frequently as required to provide a trend. Additionally, the rate of decline in lactate level concentration (delta lactate) may be a better parameter for characterising the liver function, offering a semi-quantitative description of organ functional capacity compared to single values.

Bile production varied not only in quantity but also in quality. Some livers excreted large volumes of thin, unconcentrated bile whilst some livers excreted haemobilia, though it ws not possibleto provide detailed analysis of the bile. The lack of bile production in some viable grafts may have been exacerbated by a technical issue. This had implications for the assessment of bile production and, on the basis of this study, quality of bile cannot be considered to be a reliable marker of liver function. One accepts that other studies have shown bile analytes that may reflect liver function.[227] In contrast, lactate concentration is a simple value, easily obtained from readily available, standardised and validated point-of-care blood gas analysers. Readings are simple to interpret and the familiarity with this measure improved the engagement and

acceptance in the implementation of NMLP when it was proposed for adoption into clinical practice.

Perfusate liver function tests were also unreliable in providing an assessment of potential viability. Due to haemolysis within the perfusate samples, one was only able to obtain complete sets of perfusate transaminase levels from four of the latter perfusions (numbers 8, 10, 11 and 12). In each case there was a steady increase in ALT over the course of the 6 hour perfusion. Although it is difficult to say with these small numbers whether transaminase levels can be used to determine viability, it is more likely that similar to their use in clinical scenarios, they are better suited as indicators of liver injury. Haemolysis also accounted for the high potassium concentrations recorded for the majority of perfusions.

The O2ER in the two groups were similar after two hours and the end of NMLP. These absolute values in the viable group are in keeping with the normal adult at rest. Graphically higher O2ER values seen in the non-viable group reflects relative tissue hypoxia and has been noted in livers subjected to trauma and haemorrhage after a period of warm ischaemia in animal models, in which more warm ischaemia was associated with higher O2ER levels.

Viability testing are urgently required for high-risk organs where donor under-utilisation is dictated by the risk of PNF and a suboptimal macroscopic appearance of the liver. This data demonstrated that histological findings rarely reflected the impression of the retrieving or transplanting surgeon concerning the possible underlying condition of the liver that led to their discard and these livers are the best organs to be considered for viability testing via NMLP. As a transplant community, we are yet to fully understand and validate this data, but such an approach does show increasing promise for adoption into clinical practice. The objective parameters generated by NMLP technology have the potential to transform the organ selection process and shift boundaries into using high-risk livers or inappropriately declined organs in the future. Many parameters assessed over the course of NMLP can be affected by external intervention. Further research is needed to understand the complexity and the impact of the interventions performed during NMLP and to discover optimal strategies to maximise or even improve the quality of

marginal livers.

With patient safety in mind, composite parameters consisting of multiple variables were developed, based primarily on lactate clearance and bile production. As NMLP attempts to replicate the *in vivo* conditions, parameters of macroscopic graft appearance were also included, as they are generally seen as favourable signs following reperfusion during transplantation of high-risk organs. These criteria have now been adopted in our unit's clinical protocol for the functional assessment of high-risk or discarded livers.

There are limitations to the use of NMLP. There is uncertainty concerning its impact on long-term post-transplant outcome and is yet to be determined by adequately powered prospective clinical trials. It may be possible with future research to refine these parameters and include additional markers that might have an impact on the long-term graft function. The presented viability criteria represent a reference point with which to base future research in this area.

Patient safety is the highest priority in implementing this novel strategy into the future organ selection pathway, hence setting an initial target of meeting criteria within 2 hours of starting NMLP. Some non-viable organs may still be salvaged by delaying the cut-off for viability assessment or by increasing the required trough lactate value. Additional livers might be rescued from a 'grey zone' of organs achieving trough lactate levels of 2.5 – 4 mmol/L within two hours of NMLP by supplementary therapeutic interventions, as NMLP alone may not be sufficient to resuscitate their function. This hypothesis clearly requires further research.

These results demonstrate that lactate clearance and bile production are the most significant parameters. Presence of bile production is widely recognised as a highly sensitive viability marker following transplantation and it was included in the viability criteria. However, it has low specificity as the lack of bile production may be contributed to technical factors, such as cannulae kinking and low pressure in the biliary tree influencing the ability to collect bile, or lack of bile salts in the perfusate. Lactate clearance was found to be a consistent, responsive and readily available parameter confirming liver function. For defining clinically usable via-

bility criteria to assess the high-risk and or discarded livers function, our main objective was to assure transplant recipient safety. A composite measure consisting of lactate clearance and or bile production (major criteria) in combination with additional minor criteria of stable arterial and portal flows, perfusate pH and favourable assessment by the transplant surgeon was designed. Heterogeneous perfusion is a frequent reason for discarding organs. This usually improves shortly after the liver temperature normalises and vascular flows stabilise. Persistent segmental hypoperfusion might suggest vascular damage, thrombi or emboli and, if arterial in origin, it could lead to liver abscess formation and biliary problems. Soft consistency relates to the clinical observation of very marginal grafts becoming stiff soon after implantation. In the transplant community's experience, gradual softening is a reassuring sign observed earlier than any objective parameters of recovering function. Consistent stiffness of the liver during perfusion would be seen as a concerning feature.

2.4.1 The Relationship Between NMLP and the Resuscitation & Reconditioning of Livers for Transplantation

There are a number of different machine perfusion strategies for the assessment and recovery of either ECD or donor livers outside current criteria for transplantation. Despite international growing expertise in machine perfusion, it is remains unclear whether a physiological temperature of 37^oC best promotes initial energy recovery of such livers.[230] Several reports have suggested Hypothermic Machine Perfusion (HMP) attenuates IRI in preclinical experiments subsequently translated in to promising clinical outcomes.[200, 231, 232, 233, 234, 235] In these studies, donor livers are perfused at 4-10^oC with a UW or HTK based solution that can be supplemented with antioxidants and metabolic intermediates.[233, 234] Comparisons with variations of UW and HTK solutions have been performed by Bae *et al* and Stegemann *et al* respectively in rat models, although the two groups are yet to be directly compared in discarded human livers.[234, 236] Oxygenation in HMP has been demonstrated to improve functional recovery with increased bile production at reperfusion, most notably with 100% oxygen administration.[237] A combination of α-ketoglutarate, N-acetylcysteine, prostaglandin E1, ni-

troglyerin, L-arginine and α-tocopherol attenuate transaminases and inflammatory cytokines in a rat model of HMP, however, it is not clear the extent to which prostaglandin E1 contributes to this effect in an *ex vivo* human system.[236]

Normothermic perfusion provides the conditions required to assess donor organ viability, thereby increasing safety in the use of high-risk livers and preventing PNF.[210, 238] To date, oxygenated Williams E media, whole blood or human PRC and FFP have been used in rat, porcine and discarded human models of NMLP respectively.[202, 222, 239] One study investigated oxygenated steen as an acellular fluid in porcine NMLP following a period of SCS, concluding that it enhanced arterial perfusion and reduced bile duct injury compared to SCS alone.[240] However, the efficacy of PRC compared to an acellular fluid is yet to be determined. The rationale for the majority of the components in PRC-based NMLP fluids has not been explored until now. Imber *et al* have demonstrated that taurocholic acid is essential to maintaining bile output in a porcine model of NMLP over 20 hours, hence its initial use in the fluid.[206] However, due to the lack of availability of clinical grade taurocholic acid, it was excluded from NMLPs with the prospect of transplantation. The Oxford group added prostacyclin to their circuit to ensure adequate arterial flows, although the Groningen group did not supplement their NMLP circuits with a vasodilator but still achieved arterial flows of up to 300 ml/min.[202, 222] As no data existed to compare arterial flow rates with and without vasodilators, epoprostenol was incorporated into the fluids to permit higher arterial flows. An extension to these strategies is subnormothermic perfusion, where livers are maintained at 21^{o}C.[241, 242] These circuits to date incorporate either Williams E or a novel acellular oxygen carrier.[241, 242]

This experience suggests that providing an initially untransplantable liver adequate oxygenation with PRC, arterial flows and physiological pH increases the chance of successful NMLP to assess viability. Despite this, some livers are beyond resuscitation with current technology. These fluids provide a tool for facilitating NMLP over a period of up to 18 hours and the delivery of beneficial therapies. Understanding and modulating IRI with NMLP is the next step towards reconditioning currently discarded human donor livers.

In summary, this study introduces specific composite viability assessment criteria including lactate concentration, bile production and vascular flow patterns, that if met may define a Machine Criteria Donor (MCD) which may be integrated into the clinical organ selection pathway. NMLP may lead to considerable expansion of the donor pool available for OLT. The positive effect of NMLP on long-term transplant outcomes is yet to be demonstrated.

CHAPTER 3

EARLY APPLICATIONS FOR THE POTENTIAL FUTURE DIRECTIONS OF NORMOTHERMIC MACHINE LIVER PERFUSION.

3.1 Identification of Novel Hepatic Biomarkers Using Normothermic Machine Perfusion

3.1.1 Introduction

Chapter 2 detailed how the viability of a liver for transplantation could be predicted after 2 hours of NMLP based on absolute criteria and other considerations. Whilst this may potentially represent an advancement in expanding the donor organ pool, such an assessment only leaves a further 4 hours of possible NMLP before the oxygenators reach their maximum specification. During this time, the potential transplant recipient needs to be delivered to the operating theatre complex, anaesthetised along with the insertion of monitoring devices (including but not limited to: arterial line, central line, Swann sheath, oesophageal doppler probe, epidural, urinary catheter), transferred to the operating table, draped, equipment placed and the hepatectomy completed. Potentially, this exposes the donor liver, transplant recipient and clinical team to adverse outcome. Some of these obstacles can be overcome with the upgrading to larger oxygenators with longer specifications or the use of a different normothermic perfusion device. However, to an extent these limitations still exist.

Metabolomics has been utiliised in liver transplantation. Initially, high resolution Nuclear Magnetic Resonance (NMR) was performed to compare the metabolome in a patient that had received a living donor graft that failed which was followed by successful transplantation from a cadaveric donor.[243] This demonstrated 48 metabalolites of which six were consisitent with non-function after the first.[243] The difference in expression of metabolites between 27 DBD and 13 DCD gratfts has been investigated using liver microdialysate samples in both the cold storage and post-reperfusion phase of transplanation.[244] This reveled the potential important role of overexpression of kynurenine in DCD and failed graft.[244] This was translated to liver biopsies taken during static cold storage and post-reperfusion in DBD and DCD liver transplantation, where differences were found between both time points and graft types.[245] Specifically, typtophan/kynurenine metabolism during the cold phase and S-adenosylmethionine post-

reperfusion were of significance.[245]

More specifically, metabolomics analysis has been performed on human cadaveric kidneys subjected to hypothermic machine perfusion to identify markers of immediate and delayed graft function.[246] Furthermore, comparison with human data has demonstrated that porcine kidney hypothermic machine perfusion is a valid model for further human studies, whilst recognising that 3-Hydroxybutyrate is greater in human kidney perfusates.[247] Metabolomic profiling of livers has been documented when subjecting them to subnormic machine perfusion, at temperatures of 21^{o}C.[248] Untargetted metabolomic profiling was able to cluster livers according to steatosis and severe warm ischaeia in this study focussed mainly on 18 DCD compared to 3 DBD livers.[248] In particular, perfusate lactate had been noted to rise within the first hour of perfusion followed by a significant decrease over the following two hours.[248] This was associated with an decrease in glucose-6-phophate and fructose-6-phosphate but an increase in citrate, α-ketoglutarate and succinate throughout perfusion.[248] These suggest there are significant changes in the TCA cycle during even subnormothermic mhacine perfusion of discarded human livers. At the time of this study, metabolomic profiling had not been performed on livers subjected to NMLP in either the preclinical setting or as part of a clinical trial.

In the transplant setting, their is some evidence for the use of serum proteomics in detecting and predicting acute T-cell mediated kidney allograft rejection and the effects of post transplant statin therapy respectively.[249, 250] Within the field of liver transplantation, proteomics on donor liver tissue has identified 36 proteins which are significantly altered during IRI, whilst another study revealed that Ras GTPase-activating-like Protein (IQGAP1) had a protective effect on bile cannuliculi, damage to which is one of the main drivers of post transplant liver dysfunction, particularly after DCD transplatation.[251, 252] However, as with any technology, experimental design is key to being able to answer the specific question in mind, something not even proteomics can overcome even when attempting to identify proteins associated with PNF or chronic kidney disease after liver transplantation.[253, 254] Nevertheless, with a robust approach, proteomics has successfully been used to study the dynamics of hepatitis C medi-

ated liver disease following transplantation, in particular the onset of immune, hepatoprotective and fibrogenic pathways leading to the increase in proinflammatory activity and the impairment of antioxidant processes.[255] Recently, the urinary chemokines CXCL-9 and CXCL-10 as well as protein kidney injury markers in the urine such as Neutrophil Gelatinase-associated Lipocalin (NGAL) and Kidney Injury Molecule-1 (KIM-1) is the focus of clinical validation of proteomics.[256] Ultimately, proteomics may identify novel targets in the pathways leading towards personalised immunosuppresive regimens or direct therapeuric intervention.

To date, metabolomics and proteomics have not been used in the context of NMLP. The aim of this section is to test the hypothesis that metabolomic and proteomic profiling can predict the viability of livers, initially rejected for transplantation, that have been subjected to NMLP prior to 2 hours of perfusion. This will allow earlier decision making regarding the quality of the liver and has the potential to reduce transplant risk to recipients.

3.1.2 Methods

The normothermic perfusion machine, the perfusion fluid, the livers perfused and the sampling protocol are as described in Chapter 2.

Metabolomic Profiling of Perfusates From Discarded Cadaveric Human Donor Livers Subjected to NMLP

Pre- Sample Preparation

Batches of defrosted perfusates were interrogated for metabolomic analysis from snap frozen samples collected at the start of NMLP and then after 1 hours, 2 hours and the end of NMLP as described above. Prior to perfusate sample preparation, Pall Nanosep mwco 3kDa filters were washed in 500μL of warm (38^{o}C) distilled water before being centrifuged at 3000g for 15 minutes. The flow through was then discarded and a further 500μL of warm distilled water was added before centrifugation at 3000g for 15 minutes. Washing was repeated another 4 times and kept damp whilst any samples required defrosting.

Sample Preparation

For Ultra Performance Liquid Chromatography Mass Spectrometry (UPLC-MS) reversed phase analysis, 100 μL of sample was diluted in 300 μL of 3:1 water/methanol followed by vortex mixing (15 seconds) and centrifugation (13,000 g, 15 minutes). The supernatant was transferred to a glass autosampler vial and analysed within 48 hours. For UPLC-MS Hydrophilic Interaction Liquid Chromatography (HILIC) analysis 100 μL of sample was diluted in 300 μL of acetonitrile followed by vortex mixing (15 seconds) and centrifugation (13,000 xg, 15 minutes). The supernatant was transferred to a glass autosampler vial and analysed within 48 hours.

Ultra Performance Liquid Chromatography-Mass Spectrometry

All samples were analysed applying a Ultimate 3000 UPLC system interfaced to an electrospray Q Exactive Focus mass spectrometer (Thermo Fisher Scientific, San Jose, USA). Full scan data were acquired continuously for 15 minutes at a mass resolution of 70,000 (FWHM at m/z 200). Each sample was analysed twice, once in positive ion mode followed by re-analysis in negative ion mode. UPLC-MS reversed phase analysis was performed applying a Hypersil GOLD aQ (100 x 2.1mm, 1.9 μm) operating at 45^{o}C (Thermo Scientific, Runcorn, UK) with a binary gradient elution using solvent A (0.1% formic acid in water (v/v)) and solvent B (0.1% formic acid in acetonitrile (v/v)) operating at a flow rate of 300 μL/min. The following gradient elution was applied: 99% A at 0 minutes, 50% A at 2 minutes, 1% A at 9 minutes and 99% A at 10.5 minutes. UPLC-MS HILIC analysis was performed applying a Accucore 150 Amide HILIC (100 x 2.1mm, 2.6 μm) operating at 35^{o}C (Thermo Scientific, Runcorn, UK) with a binary gradient elution using solvent A (10 mM Ammonium Formate in 95% acetontrile/water + 0.1% formic acid (v/v)) and solvent B (10 mM Ammonium Formate in 50% acetonitrile/water + 0.1% formic acid (v/v)) operating at a flow rate of 500 μL/min. The following gradient elution was applied: 99% A at 0 minutes, 85% A at 3 minutes, 50% A at 6 minutes and 95% A at 10 minutes.

Proteomic Profiling of Perfusates From Discarded Cadaveric Human Donor Livers Subjected to NMLP

Perfusate samples for proteomic analysis were taken from the pre-oxygenator hepatic venous circuit immediately at the start of NMLP, after 2 hours of perfusion and at the end of NMLP. The samples were initially snap frozen in liquid nitrogen before being stored in a -80^{o}C freezer until required for proteomic profiling. A summary of the proteomic workflow is demonstrated in Figure 3.1.

Sample Preparation

Perfusate samples were defrosted before 50μL of the haemolysed sample was added 1:8 (400μL) to HemogloBind (Biotech Support Group, USA) in an Eppendorf and was mixed well for 30 seconds on a vortexer. This sample was further mixed on a rotary mixer for an additional 10 minutes at room temperature, before being centrifuged for 5 minutes at 10,000g. The supernatant was removed to a clean tube and to it was added 10X volume of 1% TCA/Isopropanol, before being mixed on a vortexer for 30 seconds. The sample was subsequently centrifuged at 10,000g (4^{o}C) for 15 minutes. The supernatant was carefully decanted to waste before adding 1ml methanol, mixed for 30 seconds and centrifuged again for 15 minutes, 4^{o}C, at 10,000g. The supernatant was again decanted to waste and the pellets dried at 60^{o}C.

Standard Digestion

The pellet was re-suspended in 50μL 100mM ammonium bicarbonate at 37^{o}C for 10 minutes to encourage the pellet to dissolve. To this was added 25μL Dithiothreitol (DTT) (10mM in 100mM ammonium bicarbonate) and incubated at 60^{o}C for 15 minutes. Subsequently it was cooled to room temperature and 25μL of 2-Iodoacetamide solution (950mM in 100mM ammonium bicarbonate) was added. After incubation at room temperature for 45 minutes in the dark, 500ng Promega Trypsin Gold was added and the mixed well. The solution was incubated overnight at 37^{o}C.

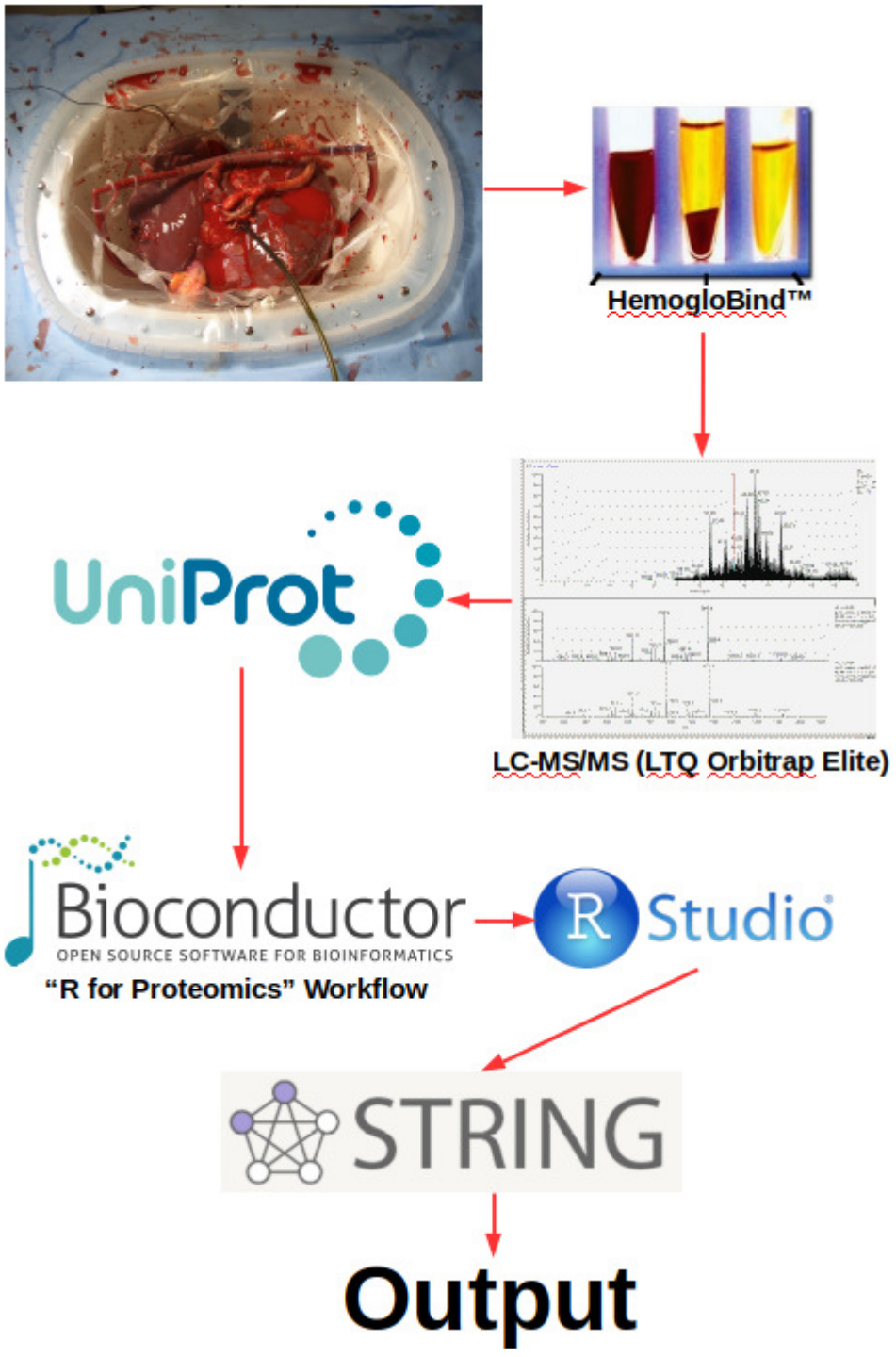

Figure 3.1: Summary of the workflow for acquisition of label-free proteomic data with NMLP. Perfusate analysis at 0, 2 hours and end of NMLP was based on viability in 12 livers subjected to NMLP (n=6 each group). Haemoglobin depletion was completed using HemogloBind.

C18 Zip Tip Preparation to Clean Peptides

Zip tips were pre-wetted with 10μL wetting solution (100% acetonitrile), dispensed to waste and repeated. Aspiration of 10μL equilibration solution (0.1% trifluoroacetic acid in purified H_2O) was followed by dispensing it to waste and the process repeated. Aspiration and dispensation through the entire sample was performed 5 times at which point the sample bound to the matrix. Aspiration of the wash solution (0.1% trifluoroacetic acid in purified H_2O) and dispensation to waste was performed three times. The peptides were eluted by aspirating 10μL of elution solution (1:1, acetonitrile: 0.1% formic acid in H_2O) with repeated pipetting into a clean tube or well without introducing air. After repeating twice the eluates were pooled together. Finally, the tip was discarded and the sample completely dried in a speed vacuum.

LC-MS/MS Experiment

UltiMate 3000 HPLC series (Dionex, Sunnyvale, CA USA) was used for peptide concentration and separation. Samples were trapped on a uPrecolumn Cartridge, Acclaim PepMap 100 C18, 5 μm, 100A 300μm i.d. x 5mm (Dionex, Sunnyvale, CA USA) and separated in Nano Series Standard Columns 75 μm i.d. x 15cm, packed with C18 PepMap100, 3 μm, 100A (Dionex, Sunnyvale, CA USA). The gradient used was from 3.2% to 44% solvent B (0.1% formic acid in acetonitrile) for 30 minutes. Peptides were eluted directly ($\sim$300 nL/min) via a Triversa Nanomate nanospray source (Advion Biosciences, NY) into a LTQ Orbitrap Elite mass spectrometer (ThermoFisher Scientific, Germany). The data-dependent scanning acquisition was controlled by Xcalibur 2.1 software. The mass spectrometer alternated between a full FT-MS scan (m/z 380-1800) and subsequent Collision Induced Dissociation (CID) MS/MS scans of the 7 most abundant ions. Survey scans were acquired in the Orbitrap with a resolution of 120 000 at m/z 400 and Automatic Gain Control (AGC) $1x10^6$. Precursor ions were isolated and subjected to CID in the linear ion trap with AGC $1x10^5$. Collision activation for the experiment was performed in the linear trap using helium gas at normalized collision energy to precursor m/z of 35% and activation Q 0.25. The width of the precursor isolation window was 2 m/z and only multiply-charged precursor ions were selected for MS/MS.

The MS and MS/MS scans were searched against Uniprot database using Sequest algorithm (ThermoFisher PD 1.4). Variable modifications were deamidation (N and Q), oxidation (M) and phosphorylation (S, T and Y). Carbamidomethyl (C) modification was for fixed modification. The precursor mass tolerance was 10 ppm and the MS/MS mass tolerance was 0.8Da. Two missed cleavages were allowed and were accepted as a real hit protein with at least two high confidence peptides.

Analysis of Metabolomic Data

Data was processed applying XCMS, a technique that incorporates nonlinear retention time alignment, matched filtration, peak detection and peak matching, to produce a data matrix of metabolite features (mass-to-charge/retention time pairs) detected in a minimum of one sample with the integrated chromatographic peak area reported for each metabolite feature in each sample.[182] Metabolite annotation was performed applying the software PUTMEDID-LCMS.[257] When the metabolite was not detected NA was reported. The percentage difference in peak areas for each metabolite feature were calculated as follows:

1. Calculate the percentage difference for each sample when comparing time 0 and time 6 hours. The 25 metabolites showing the largest percentage increase at 6 hours and the 25 metabolites showing the largest percentage decrease at 6 hours are reported.

2. Calculate the percentage difference to time 6 hours between sample 1 (positive outcome) and sample 2 (negative outcome). The 25 metabolites showing the largest percentage increase and the 25 metabolites showing the largest percentage decrease are reported.

Analysis of Proteomic Data

Two techniques were used when analysing the perfusate proteomic data, both of which used label-free proteomics, one of which identified unique proteins within the sample, the other quantified proteins within the perfusate.

Unique Proteins Using Label-Free Perfusate Proteomics

Perfusate proteomic data was exported as a spreadsheet from Proteome Discoverer (Thermo Scientific, Runcorn, UK). Accession numbers were available for each NMLP across the collected timepoints. Using conditional formatting in LibreOffice^{TM}Calc (version 5.3.7, The Document Foundation^{TM}, Berlin, Germany), protein accession numbers in 5 out of 6 livers for both viable and non-viable livers at each timepoint were elicited. Inverse conditional formatting between viable and non-viable livers highlighted unique accession numbers at the start of NMLP, T2 and the end of NMLP. Concurrently, protein accession numbers in the perfusate across all timepoints for viable and non-viable livers were determined. Output from the unique and common accession numbers were parsed to the STRING: functional protein association networks database (version 10.5) for identification and functional expression analysis.[258]

Quantitative Label-Free Perfusate Proteomics

Although the raw mass spectrometer data was not available due to logisitic reasons, a quantitative approach to high throughput label-free perfusate proteomic data was adopted using metadata spectral counting, a MS2-level quantitation technique, adapted from statistical techniques used in the analysis of large set microarray gene data.[183, 259, 260] Although not as robust as measuring peptide signal intensities using eXtracted Ion Chromatogram (XIC), MS1-level quatitation techqniue, it can still be used for comparing large datasets.[261] This provided a dynamic assessment of fluctuations in the amount of proteins in perfusates across different timepoints between viable and non-viable livers. Perfusate proteomic data was exported to a spreadsheet as described above. In addition to protein accession numbers, the total number of identified peptide sequences, known as Peptide Spectrum Matches (PSM), for each protein accession number were available. These were summarised by NMLP and timepoint in a pivot table using LibreOffice^{TM}Calc (version 5.3.7, The Document Foundation^{TM}, Berlin, Germany).

Analysis of these PSM was performed using the 'R for Proteomics' packages in Bioconductor. Specifically, the expression data was from the pivot table, with zeroes for missing values, was

arranged with phenotypic feature meta-data and sample meta-data, namely viability, to produce a MSnSet using the 'MSnbase' package.[262] The MSnSet was analysed using negative binomial Generalised Linear Model (GLM) regression technique, that incorporates empirical Bayes methods to share information among features, allowing it to be used with replicates as low as two, and tends towards the Poisson distribution.[263, 264] This produced protein accession numbers, the logarithm of the fold change and the p-values for proteins differentially expressed between viable and non-viable livers at T0, T2 and the end of NMLP. A p-value of less than 0.01 was deemed significant. The output parsed to the STRING: functional protein association networks database (version 10.5) for identification and functional expression analysis.[258]

3.1.3 Results

Perfusate Metabolomic Profiling

Metabolomics was performed in negative and positive ion mode for all timepoints, at the start of NMLP, after 1 hours of NMLP, after 2 hours of NMLP and at the end of NMLP. Principle Component Analysis (PCA) and Partial Least Squares Discriminant Analysis (PLS-DA) was performed to highlight goodness of fit (R^2) and the goodness of prediction (Q^2) of the models (Figures 3.2 and 3.3). The R^2 would increase with the number of Partial Least Squares (PLS) factors. The data demonstrated that, where available, the models accounted for $>80\%$ of the variance (Table 3.1). The Q^2 demonstrated more variability, ranging from 0.50 to 0.73. None of the Q^2 reached higher than the accepted 0.8 for adequate prediction. Overall, metabolomic analysis of NMLP perfusates did not elicit any metabolites that could be used to predict viability consistnely across all timepoints. This is contrary to blood gas analysis in Chapter 2, which clearly demonstrated lactate determining viability. This is possibly a result of sampling, storage and processing techniques including an untargetted metabolomics approach that should be addressed in future studies. Once completed, the response of lactate to time during NMLP could be determined using a metabolomics approach.

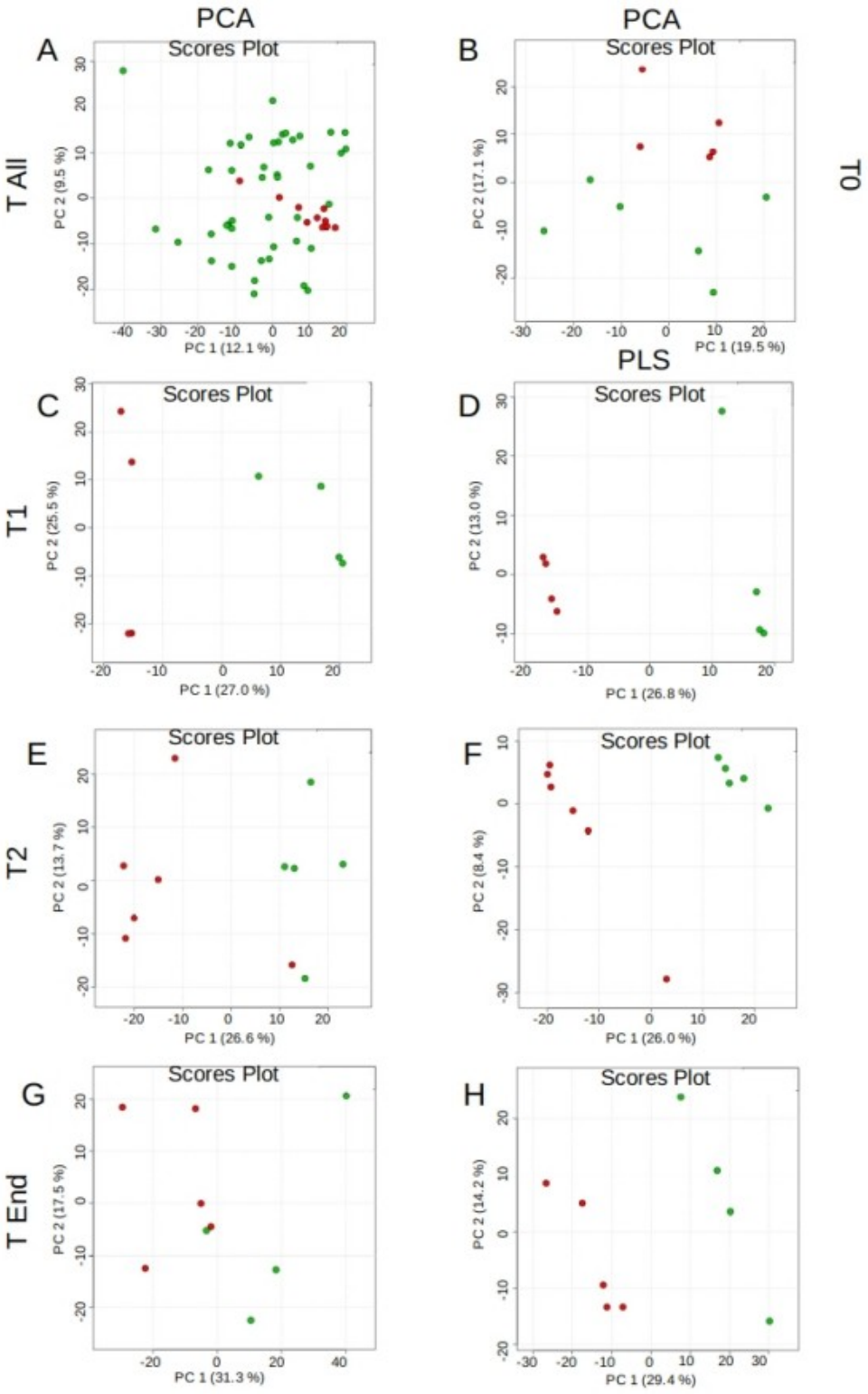

Figure 3.2: PCA and PLS-DA of metabolites identified in negative ion mode during NMLP. PCA, A,B,C,E,G; PLS-DA, D,F,H; Across all timepoints, A; At start of NMLP, B; After 1 hour of NMLP, C,D; After 2 hours of NMLP E,F; At end of NMLP G,H. In A, quality control (red), sample (green). For remaining plots non-viable (red), viable (green). None of the models reached the threshold for goodness of prediction (0.8)

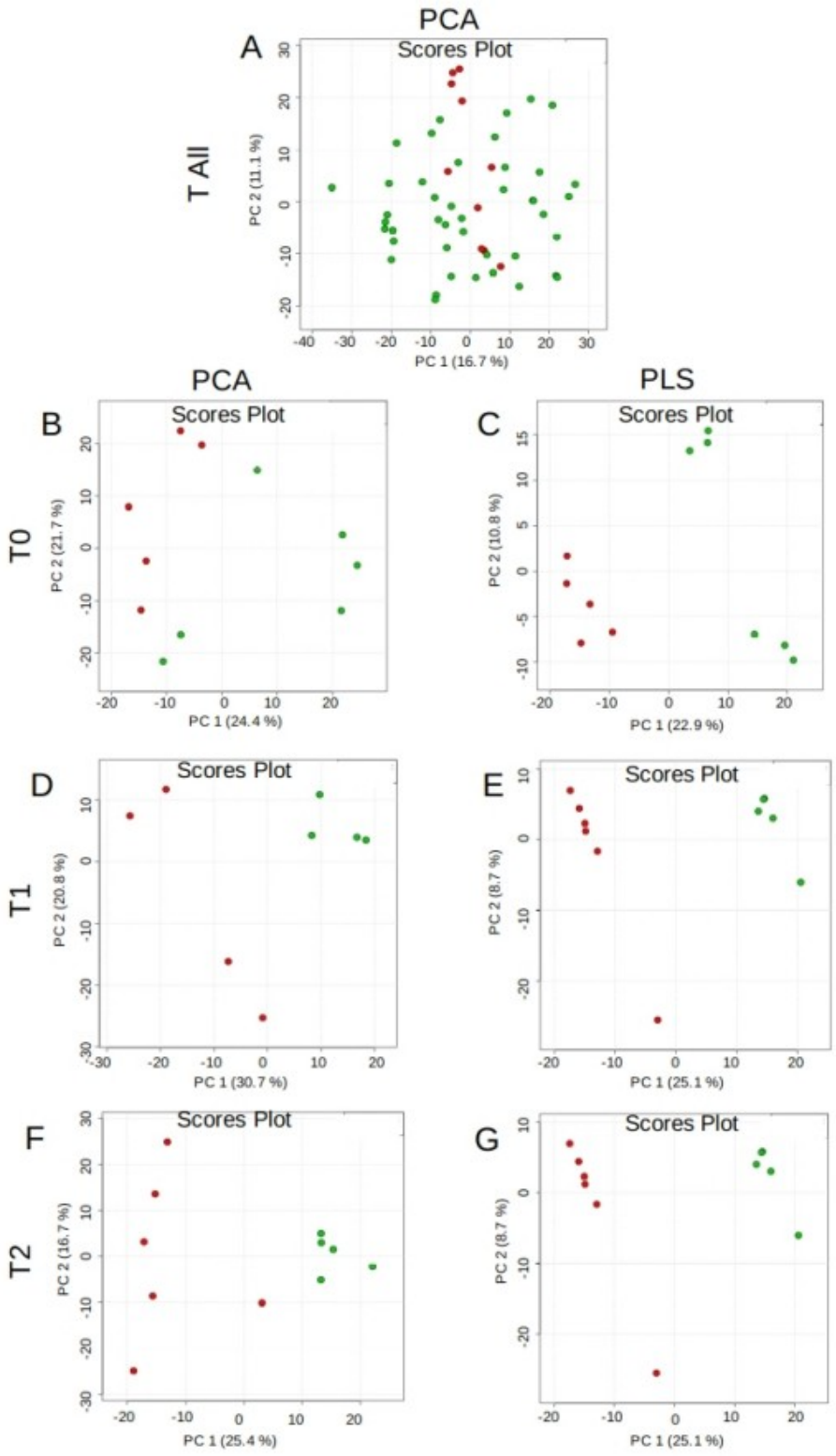

Figure 3.3: PCA and PLS-DA of metabolites identified in positive ion mode during NMLP. PCA and PLS-DA of metabolites identified in negative ion mode during NMLP. PCA, A,B,D,F; PLS-DA, C,E,G; Across all timepoints, A; At start of NMLP, B,C; After 1 hour of NMLP, D,E; After 2 hours of NMLP F,G. Metabolites at the end of NMLP not shown. In A, quality control (red), sample (green). For remaining plots non-viable (red), viable (green). None of the models reached the threshold for goodness of prediction (0.8)

	Negative Ion Mode			Positive Ion Mode		
	#Components	**R^2**	**Q^2**	**#Components**	**R^2**	**Q^2**
All	NA	NA	NA	NA	NA	NA
T0	NA	NA	NA	2	0.98	0.53
T1	2	0.99	0.72	4	0.99	0.70
T2	1	0.85	0.55	4	0.99	0.73
TEnd	4	0.99	0.54	4	0.99	0.50

Table 3.1: Summary of metabolomic analysis in negative and positive ion modes. R^2, goodness of fit, Q^2, goodness of prediction. All, across all timepoints; T0, at start of NMLP; T2, after 2 hours of NMLP; TEnd, at end of NMLP; NA, not available as no valid model.

Proteins Identified Using Label-Free Perfusate Proteomics

The list of all proteins identifed during NMLP using a label-free perfusate proteomics approach, categorised by NMLP, viability and timepoint, can be found at:
https://doi.org/10.5072/eData.bham.00000361

Unique Proteins Identified Using Label-Free Perfusate Proteomics

Label-free perfusate proteomics identified 11 and 13 unique proteins present in the perfusate across all timepoints for non-viable and viable livers respectively (Table 3.2). There were a significantly higher number of Protein-Protein Interaction (PPI) than would have been expected (PPI non-viable 0.00118, viable 0.0336). There were 5 nodal associations in the non-viable group and 14 nodal associations in the viable group including known and predicted interactions (Figures 3.4, 3.5, 3.6).

On commencing NMLP, 15 and 27 unique proteins were present in the perfusate for non-viable and viable livers respectively (Table 3.3). There were a significantly higher number of PPI than would have been expected (PPI non-viable 0.00010, viable $6.72\text{x}10^{-6}$). There were 7 nodal associations in the non-viable group and 27 nodal associations in the viable group including known and predicted interactions (Figures 3.7, 3.8).

After 2 hours of NMLP, 15 and 16 unique proteins were present in the perfusate for non-viable and viable livers respectively (Table 3.4). There were a significantly higher number of PPI than would have been expected in the non-viable group only (PPI non-viable $5.52\text{x}10^{-7}$, viable 0.134). There were 11 nodal associations in the non-viable group and 16 nodal associations in the viable group including known and predicted interactions (Figures 3.9, 3.10).

At the end of NMLP, 13 and 35 unique proteins were present in the perfusate for non-viable and viable livers respectively (Table 3.5). There were a significantly higher number of PPI than would have been expected in the viable group only (PPI non-viable 0.154, viable $3.47\text{x}10^{-9}$). There were 2 nodal associations in the non-viable group and >40 nodal associations in the

Non-Viable		Viable	
PPI	0.00118	**PPI**	0.0336
Node	**Annotation**	**Node**	**Annotation**
APOH	Apolipoprotein H (beta-2-glycoprotein I)	HSPA8	Heat shock 70kDa protein 8
ADH1A	Alcohol dehydrogenase 1A (class I), alpha polypeptide	ACLY	ATP citrate lyase
SDC1	Syndecan 1	GMPR	Guanosine monophosphate reductase
LCAT	Lecithin-cholesterol acyltransferase	FBXO7	F-box protein 7
GALM	Galactose mutarotase (aldose 1-epimerase)	C1RL	Complement component 1, r subcomponent-like
FTH1	Ferritin, heavy polypeptide 1	UBA1	Ubiquitin-like modifier activating enzyme 1
FTCD	Formiminotransferase cyclodeaminase	BPGM	2,3-bisphosphoglycerate mutase
PGM1	Phosphoglucomutase 1	UBC	Ubiquitin C
ALDOB	Aldolase B, fructose-bisphosphate	TGM2	Transglutaminase 2 (C polypeptide, protein-glutamine-gamma-glutamyltransferase)
FTL	Ferritin, light polypeptide	PGK1	Phosphoglycerate kinase 1
ALDH1L1	Aldehyde dehydrogenase 1 family, member L1	GLO1	Glyoxalase I
		ALAD	Aminolevulinate dehydratase
		TSTA3	Tissue specific transplantation antigen P35B

Table 3.2: Identity of unique proteins present in perfusates throughout NMLP by viability.

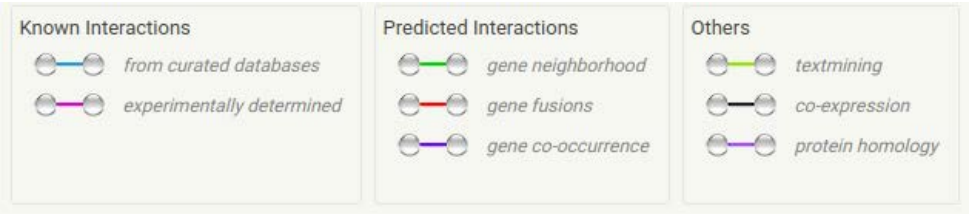

Figure 3.4: Legend for protein node interactions in STRING.

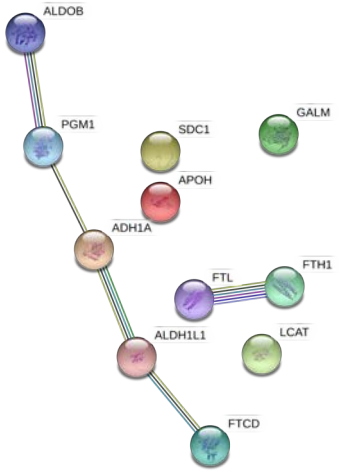

Figure 3.5: Associations of unique proteins identified from non-viable livers throughout NMLP. The 11 identified proteins are unique to non-viable livers and are present at commencing NMLP, after 2 hours and the end of NMLP. The line colour indicates the type of interaction evidence. Filled nodes indicates that some 3-dimensional structure is known or predicted.

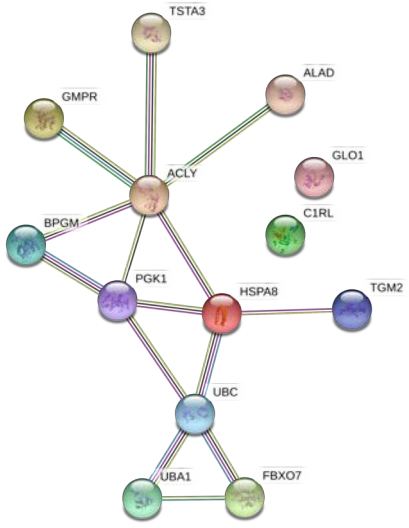

Figure 3.6: Associations of unique proteins identified from viable livers throughout NMLP. The 13 identified proteins are unique to viable livers and are present at commencing NMLP, after 2 hours and the end of NMLP. The line colour indicates the type of interaction evidence. Filled nodes indicates that some 3-dimensional structure is known or predicted.

Non-Viable		Viable	
PPI	0.000102	**PPI**	6.72E-06
Node	**Annotation**	**Node**	**Annotation**
APOH	Apolipoprotein H (beta-2-glycoprotein I)	HSPA8	Heat shock 70kDa protein 8
ADH1A	Alcohol dehydrogenase 1A (class I), alpha polypeptide	HRG	Histidine-rich glycoprotein
SDC1	Syndecan 1	APOA1	Apolipoprotein A-I
LCAT	Lecithin-cholesterol acyltransferase	ACLY	ATP citrate lyase
GALM	Galactose mutarotase (aldose 1-epimerase)	USP15	Ubiquitin specific peptidase 15
FTH1	Ferritin, heavy polypeptide 1	GMPR	Guanosine monophosphate reductase
FTCD	Formiminotransferase cyclodeaminase	IDH1	Isocitrate dehydrogenase 1 (NADP+), soluble
HAAO	3-hydroxyanthranilate 3,4-dioxygenase	SLC4A1	Solute carrier family 4, anion exchanger, member 1 (erythrocyte membrane protein band 3, Diego blood group)
SERPINA6	Serpin peptidase inhibitor, clade A (alpha-1 antiproteinase, antitrypsin), member 6	FBXO7	F-box protein 7
GOT1	Glutamic-oxaloacetic transaminase 1, soluble (aspartate aminotransferase 1)	C1RL	Complement component 1, r subcomponent-like
PGM1	Phosphoglucomutase 1	CA2	Carbonic anhydrase II
ALDOB	Aldolase B, fructose-bisphosphate	DCXR	dicarbonyl/L-xylulose reductase
TPP2	Tripeptidyl peptidase II	UBA1	Ubiquitin-like modifier activating enzyme 1
FTL	Ferritin, light polypeptide	BPGM	2,3-bisphosphoglycerate mutase
ALDH1L1	Aldehyde dehydrogenase 1 family, member L1	UBC	Ubiquitin C
		RNH1	Ribonuclease/angiogenin inhibitor 1
		TGM2	Transglutaminase 2 (C polypeptide, protein-glutamine-gamma-glutamyltransferase)
		ACAT2	acetyl-CoA acetyltransferase 2
		PGK1	Phosphoglycerate kinase 1
		GLO1	Glyoxalase I
		GDI2	GDP dissociation inhibitor 2
		PRPS2	Phosphoribosyl pyrophosphate synthetase 2
		ALAD	Aminolevulinate dehydratase
		TSTA3	Tissue specific transplantation antigen P35B
		GPX1	Glutathione peroxidase 1
		MDH1	Malate dehydrogenase 1, NAD (soluble)
		LDHA	Lactate dehydrogenase A

Table 3.3: Identity of unique proteins present in perfusates on commencing NMLP by viability.

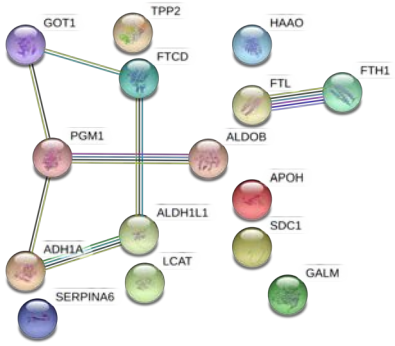

Figure 3.7: Associations of unique proteins identified from non-viable livers on commencing NMLP. The 15 identified proteins are unique to non-viable livers and are present at commencing NMLP only. The line colour indicates the type of interaction evidence. Filled nodes indicates that some 3-dimensional structure is known or predicted.

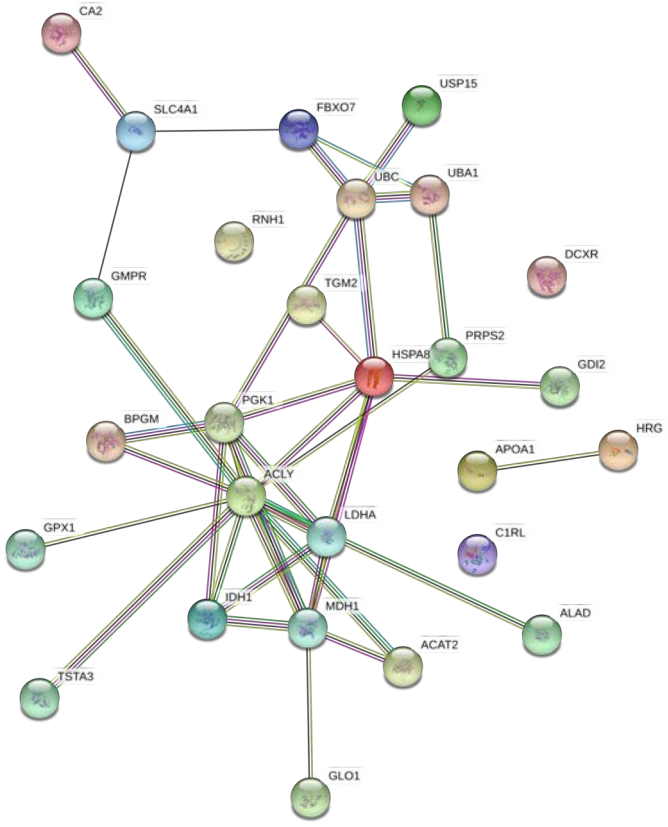

Figure 3.8: Associations of unique proteins identified from viable livers on commencing NMLP. The 29 identified proteins are unique to viable livers and are present at commencing NMLP only. The line colour indicates the type of interaction evidence. Filled nodes indicates that some 3-dimensional structure is known or predicted.

Non-Viable		Viable	
PPI	5.52E-07	**PPI**	0.134
Node	**Annotation**	**Node**	**Annotation**
APOH	Apolipoprotein H (beta-2-glycoprotein I)	MPO	Myeloperoxidase
LDHB	Lactate dehydrogenase B	HSPA8	Heat shock 70kDa protein 8
KRT9	Keratin 9	ACLY	ATP citrate lyase
IDH1	Isocitrate dehydrogenase 1 (NADP+), soluble	ATRN	Attractin
LCAT	Lecithin-cholesterol acyltransferase	C9	Complement component 9
KRT10	Keratin 10	FBXO7	F-box protein 7
FTCD	Formiminotransferase cyclodeaminase	C1RL	Complement component 1, r subcomponent-like
FABP1	Fatty acid binding protein 1, liver	HSPA4	Heat shock 70kDa protein 4
EEF1A1	Eukaryotic translation elongation factor 1 alpha 1	PFAS	Phosphoribosylformylglycinamidine synthase
PGM1	Phosphoglucomutase 1	SERPINA6	Serpin peptidase inhibitor, clade A (alpha-1 antiproteinase, antitrypsin), member 6
TXN	Thioredoxin	UBC	Ubiquitin C
ALDOB	Aldolase B, fructose-bisphosphate	RAD23B	RAD23 homolog B (S. cerevisiae)
FTL	Ferritin, light polypeptide	TGM2	Transglutaminase 2 (C polypeptide, protein-glutamine-gamma-glutamyltransferase)
HBD	Hemoglobin, delta	PGK1	Phosphoglycerate kinase 1
ALDH1L1	Aldehyde dehydrogenase 1 family, member L1	CFB	Complement factor B
		GC	Group-specific component (vitamin D binding protein)

Table 3.4: Identity of unique proteins present in perfusates after 2 hours of NMLP by viability.

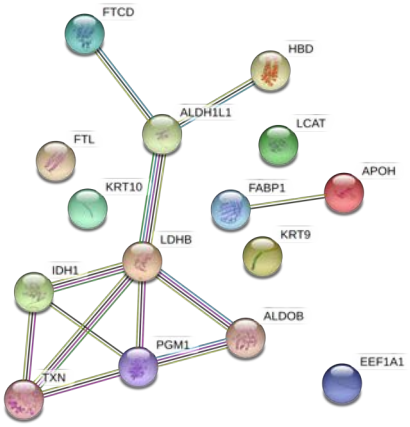

Figure 3.9: Associations of unique proteins identified from non-viable livers after 2 hours of NMLP. The 18 identified proteins are unique to non-viable livers and are present after 2 hours of NMLP only. The line colour indicates the type of interaction evidence. Filled nodes indicates that some 3-dimensional structure is known or predicted.

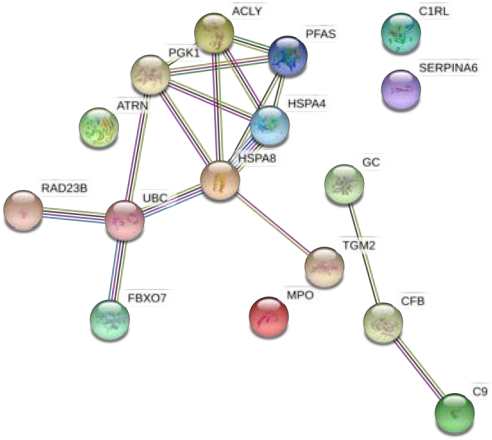

Figure 3.10: Associations of unique proteins identified from viable livers after 2 hours of NMLP. The 17 identified proteins are unique to viable livers and are present after 2 hours of NMLP only. The line colour indicates the type of interaction evidence. Filled nodes indicates that some 3-dimensional structure is known or predicted.

Non-Viable		Viable	
PPI	0.154	**PPI**	3.47E-09
Node	**Annotation**	**Node**	**Annotation**
ADH1A	Alcohol dehydrogenase 1A (class I), alpha polypeptide	VTN	Vitronectin
HRG	Histidine-rich glycoprotein	HSPA8	Heat shock 70kDa protein 8
SDC1	Syndecan 1	USP5	Ubiquitin specific peptidase 5 (isopeptidase T)
KRT10	Keratin 10	ENO1	Enolase 1, (alpha)
GALM	Galactose mutarotase (aldose 1-epimerase)	CAT	Catalase
FTH1	Ferritin, heavy polypeptide 1	C3	Complement component 3
DCXR	dicarbonyl/L-xylulose reductase	H3F3B	H3 histone, family 3B (H3.3B)
SERPINA7	Serpin peptidase inhibitor, clade A (alpha-1 antiproteinase, antitrypsin), member 7	CRP	C-reactive protein, pentraxin-related
EEF1A1	Eukaryotic translation elongation factor 1 alpha 1	APCS	Amyloid P component, serum
PGLYRP2	Peptidoglycan recognition protein 2	GMPR	Guanosine monophosphate reductase
FTL	Ferritin, light polypeptide	FAH	Fumarylacetoacetate hydrolase (fumarylacetoacetase)
AKR1C3	Aldo-keto reductase family 1, member C3 (3-alpha hydroxysteroid dehydrogenase, type II)	FBXO7	F-box protein 7
C11orf54	Chromosome 11 open reading frame 54	LUM	Lumican
		ADH5	Alcohol dehydrogenase 5 (class III), chi polypeptide
		HSPA4	Heat shock 70kDa protein 4
		FGB	Fibrinogen beta chain
		F2	Coagulation factor II (thrombin)
		CLU	Clusterin
		SERPINF2	Serpin peptidase inhibitor, clade F (alpha-2 antiplasmin, pigment epithelium derived factor), member 2
		HSP90AB1	Heat shock protein 90kDa alpha (cytosolic), class B member 1
		UBA1	Ubiquitin-like modifier activating enzyme 1
		BPGM	2,3-bisphosphoglycerate mutase
		UBC	Ubiquitin C
		HIST1H2BK	Histone cluster 1, H2bk
		TGM2	Transglutaminase 2 (C polypeptide, protein-glutamine-gamma-glutamyltransferase)
		GSTO1	Glutathione S-transferase omega 1
		RBP4	Retinol binding protein 4, plasma
		GLO1	Glyoxalase I
		HIST1H2AH	Histone cluster 1, H2ah
		ALAD	Aminolevulinate dehydratase
		TSTA3	Tissue specific transplantation antigen P35B
		ITIH3	Inter-alpha-trypsin inhibitor heavy chain 3
		CFB	Complement factor B
		GC	Group-specific component (vitamin D binding protein)
		RAD23A	RAD23 homolog A (S. cerevisiae)

Table 3.5: Identity of unique proteins present in perfusates at the end of NMLP by viability.

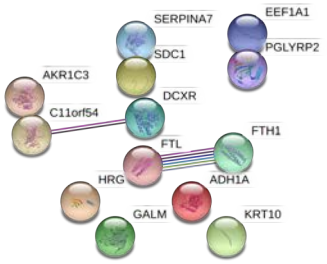

Figure 3.11: Associations of unique proteins identified from non-viable livers at the end of NMLP. The 15 identified proteins are unique to non-viable livers and are present at the end of NMLP only. The line colour indicates the type of interaction evidence. Filled nodes indicates that some 3-dimensional structure is known or predicted.

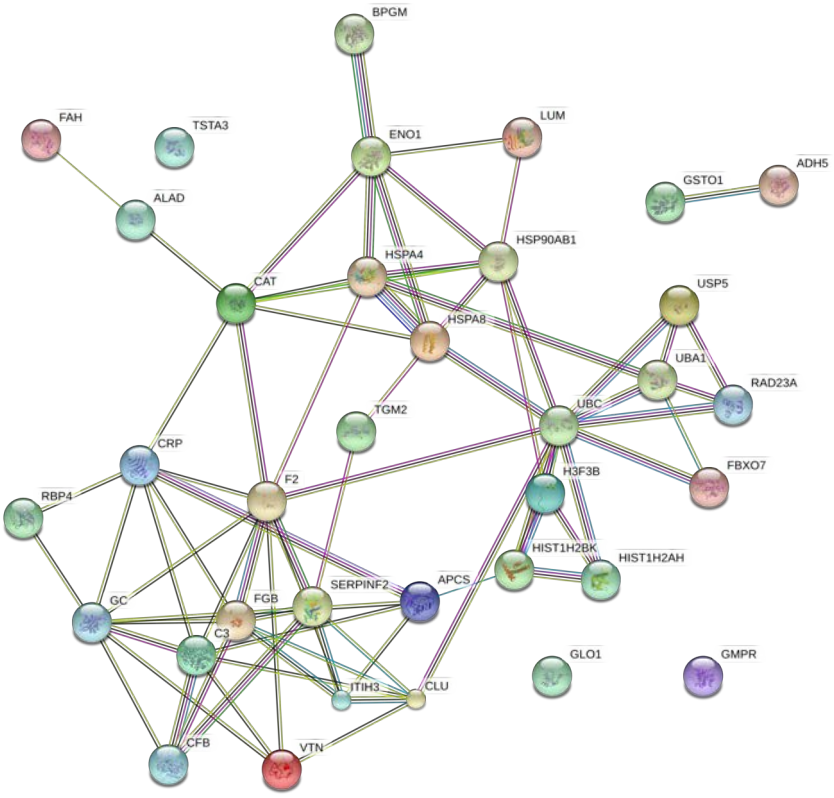

Figure 3.12: Associations of unique proteins identified from viable livers at the end of NMLP. The 36 identified proteins are unique to viable livers and are present at the end of NMLP only. The line colour indicates the type of interaction evidence. Filled nodes indicates that some 3-dimensional structure is known or predicted.

viable group including known and predicted interactions (Figures 3.11, 3.12).

KEGG Pathways of Unique Proteins Identified on Commencing NMLP

At the start of NMLP, 15 and 27 unique proteins were identified in the non-viable and viable livers. To highlight which metabolic pathways might be differentially involved at this timepoint, KEGG pathway analysis was performed. Although both non-viable and viable livers had activation of different parts of the metabolic pathway and biosynthesis of amino acids, significant upregulation of the Tricarboxylic Acid Cycle (TCA) cycle, pyruvate metabolism, glyoxylate cycle in peroxisomes and mitchondria as well as fat digestion and absorption were present in the viable livers (Table 3.6). In contrast, non-viable livers had significant upregulation of glycolysis and gluconeogenesis, pentose phosphate pathway and galactose as well as tyrosine metabolism.

Identification of Significant Proteins Using Quantitative Label-Free Perfusate Proteomics

Quantitative label-free perfusate proteomics identified 24 significantly expressed proteins with both negative (non-viable) and positive (viable) log fold changes across all timepoints (Table 3.7). There was a significantly higher number of PPI than would have been expected (PPI = 0.00305). There were 14 nodal associations including known and predicted interactions (Figure 3.13).

On commencing NMLP, 6 significantly expressed proteins were present in the perfusate (Table 3.8). The proteins APOA1, HSP90AA1, ACTC1 and GPX1 was associated with viability, whilst FTH1 and C4B were associated with non-viable livers. There was not a significantly higher number of PPI than would have been expected (PPI = 0.778). There was 1 nodal association (ACTC1 to HSP90AA1, both attributed to viable livers) including known and predicted interactions (Figure 3.14).

After 2 hours of NMLP, 4 proteins (LTF, CD163, MPO and ZCCHC14) were significantly expressed in the perfusate (Table 3.9). There was a significantly higher number of PPI than would have been expected (PPI = 0.0312). There was 1 nodal association (LTF to MPO, both

Non-Viable				Viable			
Pathway Description	**Observed Gene Count**	**False Discovery Rate**	**Matching Proteins in your Network (Labels)**	**Pathway Description**	**Observed Gene Count**	**False Discovery Rate**	**Matching Proteins in your Network (Labels)**
Glycolysis / Gluconeogenesis	4	2.56E-05	ADH1A,ALDOB,GALM,PGM1	Carbon metabolism	5	5.93E-05	ACAT2,IDH1,MDH1,PGK1,PRPS2
Metabolic pathways	7	0.00115	ADH1A,ALDOB,FTCD,GALM,GOT1,HAAO,PGM1	Metabolic pathways	10	0.000166	ACAT2,ACLY,ALAD,BPGM,DCXR,IDH1,MDH1,PGK1,PRPS2,TSTA3
One carbon pool by folate	2	0.00815	ALDH1L1,FTCD	Citrate cycle (TCA cycle)	3	0.000629	ACLY,IDH1,MDH1
Pentose phosphate pathway	2	0.0116	ALDOB,PGM1	Pyruvate metabolism	3	0.00141	ACAT2,GLO1,MDH1
Galactose metabolism	2	0.0124	GALM,PGM1	Biosynthesis of amino acids	3	0.00607	IDH1,PGK1,PRPS2
Tyrosine metabolism	2	0.0158	ADH1A,GOT1	Proximal tubule bicarbonate reclamation	2	0.0135	CA2,MDH1
Porphyrin and chlorophyll metabolism	2	0.0166	FTH1,FTL	Glyoxylate and dicarboxylate metabolism	2	0.0192	ACAT2,MDH1
Mineral absorption	2	0.0208	FTH1,FTL	Collecting duct acid secretion	2	0.0192	CA2,SLC4A1
Biosynthesis of amino acids	2	0.0375	ALDOB,GOT1	Fat digestion and absorption	2	0.0385	ACAT2,APOA1

Table 3.6: KEGG pathways of unique proteins, with low false discovery rates, identified on commencing NMLP by viability.

attributed to viable livers) including known and predicted interactions (Figure 3.15).

At the end of NMLP, 3 significantly expressed proteins were present in the perfusate (Table 3.10). There was not a significantly higher number of PPI than would have been expected (PPI = 1). There were no nodal associations (Figure 3.16).

Gene Ontology Pathways of Proteins Identified by Quantitative Analysis on Commencing NMLP

KEGG pathway analysis of significantly expressed proteins at the start of NMLP did not reveal any metabolic pathways that were upregulated. Using Gene Ontology (GO) analysis, protein oxidation and tissue migration matched proteins in the network (APOA1, GPX1, ACTC1), both had acceptable false discovery rates (Table 3.11). All of these proteins were associated with viable livers.

3.1.4 Discussion

The use of metabolomics and proteomics in the context of NMLP and predicting viability is novel. In particular, the developed label free proteomic techniques have identified unique and quantitatively significant proteins that can be used to predict viability of discarded human cadaveric livers subjected to NMLP, earlier than non -omic methods previously demonstrated. Furthermore, the analytical techniques have highlighted potential metabolic pathways that are regulated during the phases of ischaemia reperfusion injury in an *ex vivo* human model. Fluxes in these proteins and pathways can then be elicited by proteomic profiling throughout the model. These findings, particularly in proteomics predicting viability, could be translated to clinical practice even with limited investigation, potentially increasing the donor pool for liver transplantation than even the current use of NMLP has permitted.

The main strengths of these results, especially with respect to proteomics, is the use of a label free approach, allowing for more rapid result generation that is important when looking towards

PPI	0.00305		
Node	**Annotation**	**LogFC**	**P-value**
AHSG	alpha-2-HS-glycoprotein	-1.3327452	4.111896E-05
HSP90AA1	Heat shock protein 90kDa alpha (cytosolic), class A member 1	3.4632391	5.215816E-05
PSMA2	Proteasome (prosome, macropain) subunit, alpha type, 2	1.9954656	0.000243474
ALAD	Aminolevulinate dehydratase	1.5638086	0.0003842338
CD163	CD163 molecule	-1.9726252	0.0004022573
BPGM	2,3-bisphosphoglycerate mutase	2.0930184	0.0005269648
GLO1	Glyoxalase I	1.9014504	0.0006264129
MPO	Myeloperoxidase	2.63538	0.001385834
YWHAZ	Tyrosine 3-monooxygenase/tryptophan 5-monooxygenase activation protein, zeta polypeptide	2.020553	0.00147892
LTF	Lactotransferrin	2.5511045	0.00172346
ELANE	Elastase, neutrophil expressed	2.6701343	0.002022424
CUTA	cutA divalent cation tolerance homolog (E. coli)	2.1089956	0.002576786
GALM	Galactose mutarotase (aldose 1-epimerase)	-1.2873115	0.002928171
ADH4	Alcohol dehydrogenase 4 (class II), pi polypeptide	-1.0140271	0.004025853
GPNMB	Glycoprotein (transmembrane) nmb	-2.1779406	0.004046685
FTH1	Ferritin, heavy polypeptide 1	-1.5148082	0.004811478
IGFALS	Insulin-like growth factor binding protein, acid labile subunit	2.0743203	0.004831594
PRDX2	Peroxiredoxin 2	0.8541914	0.005051867
PARK7	Parkinson protein 7	1.8463458	0.00684204
PAPSS2	3'-phosphoadenosine 5'-phosphosulfate synthase 2	-1.8598597	0.007409467
DCXR	dicarbonyl/L-xylulose reductase	-1.1930896	0.007903249
SAA2	Serum amyloid A2	2.1322339	0.007951295
BCHE	Butyrylcholinesterase	1.736627	0.007996761
CDH1	Cadherin 1, type 1, E-cadherin (epithelial)	-2.2045025	0.00872516

Table 3.7: Identity of proteins present in perfusates throughout NMLP by quantitative analysis.

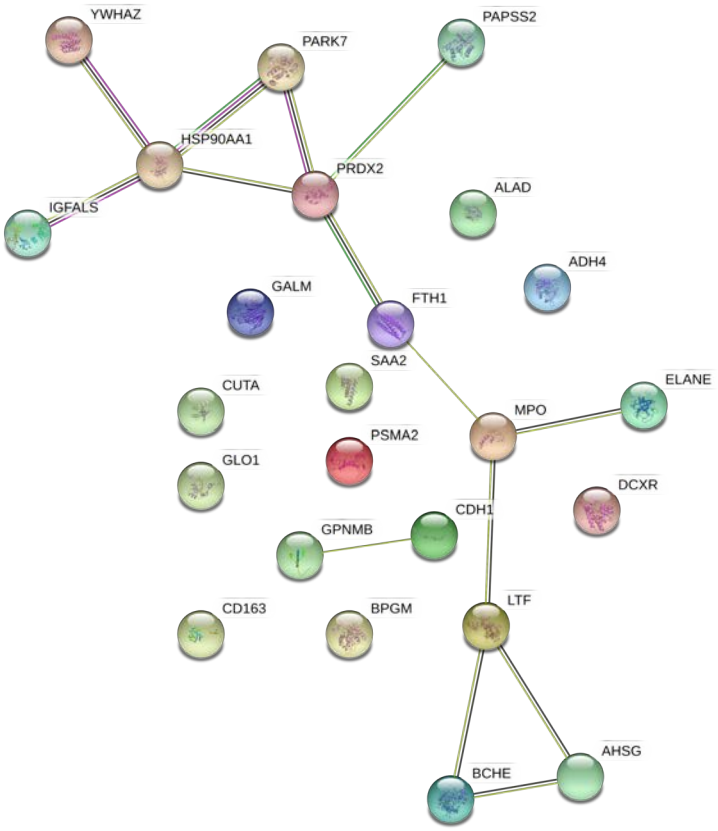

Figure 3.13: Associations of proteins identified by quantitative analysis throughout NMLP. The 24 identified proteins have the most significant fold changes on commencing NMLP, after 2 hours and the end of NMLP. The line colour indicates the type of interaction evidence. Filled nodes indicates that some 3-dimensional structure is known or predicted.

PPI	0.778		
Node	**Annotation**	**LogFC**	**P-value**
APOA1	Apolipoprotein A-I	4.392446	0.0003664732
HSP90AA1	Heat shock protein 90kDa alpha (cytosolic), class A member 1	4.334253	0.0007877133
ACTC1	Actin, alpha, cardiac muscle 1	4.629109	0.0011665981
FTH1	Ferritin, heavy polypeptide 1	-2.642914	0.0055252898
C4B	Complement component 4B (Chido blood group)	-4.550921	0.008651977
GPX1	Glutathione peroxidase 1	3.17337	0.0087903235

Table 3.8: Identity of proteins present in perfusates on commencing NMLP by quantitative analysis.

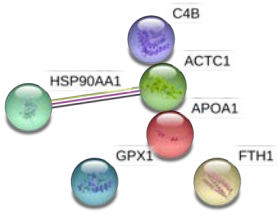

Figure 3.14: Associations of proteins identified by quantitative analysis on commencing NMLP. The 6 identified proteins have the most significant fold changes on commencing NMLP. The line colour indicates the type of interaction evidence. Filled nodes indicates that some 3-dimensional structure is known or predicted.

PPI	0.0312		
Node	**Annotation**	**LogFC**	**P-value**
LTF	Lactotransferrin	3.332166	0.001773611
CD163	CD163 molecule	-1.964989	0.005445518
MPO	Myeloperoxidase	2.153964	0.005654576
ZCCHC14	Zinc finger, CCHC domain containing 14	-3.481443	0.008660559

Table 3.9: Identity of proteins present in perfusates after 2 hours of NMLP by quantitative analysis.

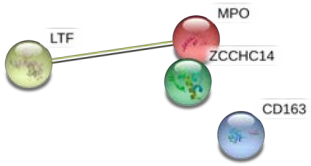

Figure 3.15: Associations of proteins identified by quantitative analysis after 2 hours of NMLP. The 4 identified proteins have the most significant fold changes after 2 hours of NMLP. The line colour indicates the type of interaction evidence. Filled nodes indicates that some 3-dimensional structure is known or predicted.

PPI	1		
Node	**Annotation**	**LogFC**	**P-value**
AHSG	alpha-2-HS-glycoprotein	-1.902466	0.003648839
HSP90AA1	Heat shock protein 90kDa alpha (cytosolic), class A member 1	3.713159	0.007913096
ELANE	Elastase, neutrophil expressed	3.809979	0.008965856

Table 3.10: Identity of proteins present in perfusates at the end of NMLP by quantitative analysis.

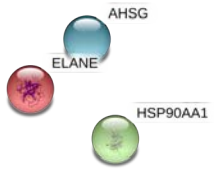

Figure 3.16: Associations of proteins identified by quantitative analysis at the end of NMLP. The 3 identified proteins have the most significant fold changes on commencing NMLP. There are no interactions. Filled nodes indicates that some 3-dimensional structure is known or predicted.

Pathway Description	Observed Gene Count	False Discovery Rate	Matching Proteins in your Network (Labels)
protein oxidation	2	0.0104	APOA1,GPX1
tissue migration	3	0.0104	ACTC1,APOA1,GPX1

Table 3.11: Pathways of significant proteins at the start of NMLP by quantitative analysis using Gene Ontology.

clinical translation, as well as incorporating two different techniques that have generated related lists of proteins. The fact that these results have been acquired despite the heterogeneity of the discarded human livers that have become available, can also be seen as a strength when considering clinical translation.

Nevertheless, the relatively low number of perfused livers in combination with the use of HaemagloBind to overcome the effects of haemolysis seen during NMLP can be seen as potential obstacles to future adoption. The commencement of the VITTAL Trial, towards which results from Chapter 2 onwards generated the preliminary data for the successful Wellcome Trust grant application, has allowed time to reflect upon and refine the methodology from sample protocol to analytical techniques. This should have an impact on the identification of potential proteins important for predicting viability using a proteomic approach. This may also influence the ability to generate significant metabolomic results by using a targetted approach to lactate and confirm the role of lactate metabolism in the viability assessment of discarded human livers subject to NMLP over the course of perfusion.

The use of metabolomics and proteomics in NMLP is novel for ischaemia reperfusion models of the liver. It has been utilised in a pig and discarded human kidney model using hypothermic machine perfusion.[246, 247] However, although promising, the results of this are awaiting to be translated to clinical practice.

Future research must include increasing the numbers over a broader range of livers that have sustained differing amounts of pre-existing injury prior to commencing NMLP, thus ensuring that these proteomic results are replicated. To overcome technical biases, samples should be sent to collaborating laboratories to confirm the results, even by the use of different mass-spectrometry techniques. More detailed and possibly accurate analysis can be performed by utilising the vast quantities of data within the raw mass-spectrometry data. The sensitivity and specificity of spectral counting could be increased by incorporating XIC methods to calculate the area under the curve of raw data files. Once these challenges have been overcome, the prospect of clinical translation is increasingly promising.

3.2 Acellular Perfusion Fluid and Its Potential Application in NMLP

3.2.1 Introduction

The shortage of suitable donor livers remains a limiting factor in the attempt to transplant an increasing number of patients with end-stage liver disease. This has led to an increase in the use of ECD that encompass organs from donors of increased age, higher Body Mass Index (BMI) and DCD. However, ECD livers are at increased risk of graft dysfunction, primary graft non-function and increased susceptibility to IRI. One potential method of improving the quality of ECD livers is by the utilisation of machine perfusion, in particular, NMLP. It is well known that the main injurious agent during liver IRI is the generation of ROS. During NMLP the liver is exposed to oxygen and nutrients supporting intrinsic metabolic activity. Currently, devices used for NMLP in pre-clinical and limited clinical settings perfuse the livers with group specific packed red cells from the blood bank. However, this has disadvantages including potential immune-mediated phenomena, disruption of the liver micro-circulation, red blood cell mediated cell death, haemolysis and the logistical planning for gaining access to the crossmatched blood. Acellular perfusion fluids, such as Hemopure, allow oxygenation of donor livers during NMLP without the logistic and cell-mediated issues discussed above. Hemopure or HBOC-201 is a bovine haemoglobin-based oxygen carrier. The aim fo this section is to test the effec of Hemopure on liver parenchymal cells *in vitro* and in the NMLP.

3.2.2 Methods & Materials

Isolation of Human Sinusoidal Endothelial Cells

Liver tissue was obtained via the Hepatobiliary and Liver Transplant surgery program at the Queen Elizabeth Hospital, Birmingham UK, from consenting adult patients undergoing transplantation, hepatic resection for liver metastasis, hepatic resection for benign liver disease or normal donor tissue surplus to surgical requirements. Ethical approval for the study was grant

by the Local Research Ethics Committee (LREC) (reference number 06/Q702/61). HSEC were isolated from human liver tissue as previously described. Briefly, parenchymal cells were collected after collagenase digestion of mechanically disaggregated liver and were further purified by density gradient centrifugation over Percoll. Endothelial cells were isolated from the resultant heterogeneous cell mixture by positive immunomagnetic selection using antibodies raised against CD31 (Clone JC70A, Dako, Denmark) and magnetic beads (Dynal) conjugated with goat anti-mouse antibody according to the manufacturer's protocol. All endothelial cells were maintained in complete media comprising Human Endothelial-SFM basal growth medium (Invitrogen) containing 104 U/ml penicillin and 10 μL/ml streptomycin, 10 ng/ml epidermal growth factor (R & D Systems, Abingdon, UK), 10 μg/ml hydrocortisone (Sigma-Aldrich, UK), and either 10% heat-inactivated human serum (TCS Biologicals). All endothelial cells were plated out into collagen-coated culture flasks (Sigma-Aldrich, UK) and maintained at 37°C in a humidified 5% CO_2 incubator until confluent. The endothelial cells were used only up to passage 6, and phenotypic identity as well as purity were confirmed by staining for endothelial markers.

Isolation of Biliary Epithelial Cells

Biliary epithelial cells were isolated from liver tissue as described. Liver (30g) was finely diced and incubated with collagenase type 1A (Sigma, St. Louis, MO). The digest was layered onto a 33% and 77% iso-osmotic Percoll gradient and centrifuged at 500 g for 30 minutes. The interface layer was collected, washed three times in PBS and incubated with the Biliary Epithelial Cells (BEC)-specific mouse anti-human monoclonal antibody to Human Epithelial Antigen 125 (HEA125) (TCS Biologicals Ltd., Botolph Claydon, Bucks, UK). BEC were positively selected by incubating with anti-mouse IgG1-coated Dynabeads (Dynal) and by magnetic separation. The cells were cultured in plating media comprising Hams F12, Dulbecco's Eagle medium (Sigma-Aldrich, UK) containing 10% heat-inactivated fetal calf serum (TCS Biologicals), 104 U/ml penicillin, 10 μL/ml streptomycin, 2 mM glutamine, 10ng/ml epidermal growth factor (R & D Systems), 2 g/ml hydrocortisone (Sigma-Aldrich, UK), 10 ng/ml choleratoxin, 2 nM

tri-iodo-thyronine, 0.124 iu/ml insulin. After 1–2 days in culture, the medium was exchanged for media containing 5% fetal calf serum and 10 ng/ml hepatocyte growth factor (R&D Systems, Abingdon, UK). In all subsequent experiments, cells were used between passage 2 and 5 depending on the initial yield of the primary isolate.

In vitro Model of Ischaemia Reperfusion Injury

Cells were incubated in standard media or 50:50 mix of media with Hemopure. In experiments, HSEC and BEC were grown for 2 days at 37^{o}C, 5% CO_2 in the media described above in 6-well, rat type 1 collagen-coated plates. We utilised a model of warm *in vitro* IRI that described previously. HSEC and BEC were either incubated in normoxia, or hypoxia (0.1%) for 24 hours, or in hypoxia for 24 hours followed by 24 hours of reoxygenation, known as Hypoxia-Reperfusion (H-R). Hypoxia was achieved by placing cells in an airtight incubator (RS Mini Galaxy A incubator, Wolf Laboratories, UK) flushed with 5% CO_2 and 95% N_2 until oxygen content in the chamber reached 0.1%, as verified by a dissolved oxygen monitor (DOH-247-KIT, Omega Engineering, UK). Media was pre-incubated in the hypoxic chamber in a sterile container, allowing gas equilibration, for 8 hours before experiments were conducted. This resulted in a final oxygen concentration of $<$0.1%. Where appropriate, after 24 hours of hypoxia media was aspirated and replaced with fresh, warmed, oxygenated medium, with the cells subsequently returned to normoxic conditions. This was defined as the beginning of reoxygenation.

Assessment of ROS Production, Apoptosis and Necrosis

ROS production, apoptosis and necrosis were determined using a three-colour assay. Apoptosis was determined by labelling cells with Annexin-V (Molecular Probes, Paisley, UK) which detects exposed phosphatidylserine on the cell membrane. ROS accumulation was determined using the fluorescent probe 2',7'-Dichlorodihydrofluorescein (DCF) diacetate (Merck, Nottingham, UK,). This probe is cell permeable and once intracellular, is cleaved by intracellular esterases to 2',7'-DCF that is then rendered cell impermeable. DCF is then able to react with intracellular ROS, specifically hydrogen peroxide, to give a fluorescent signal detectable on the

Fluorescein Isothiocyanate (FITC) channel. The signal is directly proportional to the level of intracellular ROS present. 7-Aminoactinomycin D (7-AAD) (Molecular Probes, Paisley, UK) only enters cells once the cell membrane is disrupted during necorsis and is a vital dye that intercalates with high affinity to GC-rich regions of Deoxyribose Nucleic Acid (DNA).

To ensure consistency of flow cytometric data, each human preparation was labelled with DCF alone, Annexin-V alone and 7-AAD alone to ensure that cells had become labelled and that the flow cytometry data could be compensated for crossover of fluorophore emission spectra. The same flow cytometer protocol, including voltages for all markers, was used for all experiments shown in the study, ensuring internal consistency of experiments.

Following appropriate treatment of cells, media was aspirated and replaced with HBSS (Gibco) without calcium and magnesium. DCF (30 μM) was added and the cells were incubated for 20 minutes in the dark at 37^{o}C. Cells were then trypinsed and washed extensively in FACs buffer (Phosphate-buffered saline pH 7.2) with 10% heat inactivated foetal calf serum (Gibco). Cells were subsequently labelled with Annexin-V and 7-AAD for 15 minutes whilst on ice before immediate flow cytometry. At least 20,000 events were recorded within the gated region of the flow cytometer for each human cell preparation in each experimental condition. Only the cells within the gated regions were used to calculate Median Fluorescent Intensity (MFI).

Preparation of the Donor Liver

Two human livers deemed not suitable for clinical transplantation were included in the study. They were procured by one of the teams from UK NORS, with the intention of transplantation using nationally agreed surgical protocols. In-situ ice cooling and perfusion via the hepatic artery and portal vein was performed using University of Wisconsin (UW; SPS-1, Organ Recovery Systems, USA or Belzer UW Cold Storage Solution, Bridge to Life, USA) preservation fluid at 4^{o}C. Donor livers were packed in preservation fluid filled sterile bags and placed on crushed ice immediately prior to transportation.

Consent for academic research was granted either directly by the donor when joining the UK ODR or by the donor's family during consent for procurement utilising a SNOD. Ethical approval was granted by University Hospitals Birmingham NHS Foundation Trust, as well as Loco-Regional and NHSBT Ethics Committees.

Each liver was initially prepared for NMLP analagous to clinical transplantation. The inferior vena cava was dissected and the phrenic veins ligated. The portal vein was dissected to its bifurcation. The aortic patch was trimmed and the hepatic artery was dissected to the gastroduodenal artery. Curved and straight Medos cannulae were inserted in to the coeliac trunk and the portal vein respectively before being secured with silk ligatures. Livers were then flushed with 2 litres of 10% dextrose solution. The cannulae were primed with perfusion fluid and connected to the normothermic perfusion machine.

Normothermic Machine Liver Perfusion

Upon arrival at the transplant centre, the cold preserved liver was prepared on the back table as described previously [13]. NMLP was initiated using a CE marked (Liver Assist, Organ Assist b.v., Groningen, The Netherlands) device that enables dual perfusion via both the hepatic artery and the portal vein in a semi-closed circuit. Two rotary pumps provided pulsatile flow to the hepatic artery and a continuous flow to the portal vein. The pressure for each system was set independently. Measured flow rates and calculated resistances were shown in real-time on a liquid crystal display. Oxygen was supplied to two polypropylene, rheoparin® coated, microporous hollow fibre membrane oxygenators with integrated heat exchangers, that also removed CO_2. Pressure was limited to a mean of 50 mmHg in the hepatic artery and 10 mmHg in the portal vein. The temperature was set to 37^oC. Before connecting the liver to the device, the perfusion fluid was primed with the addition of an 8.4% sodium bicarbonate solution to obtain a stable physiological pH. The liver was perfused for 6 hours with Hemopure or PRC.

Assessment of Hepatobiliary Injury Using Histological Evaluation

Biopsies were obtained from the donor liver immediately before as well as after 3 and 6 hours of NMLP. Biopsies were fixed in formalin for histological evaluation. Paraffin-embedded slides of liver biopsies were prepared for H&E staining and assessed in a semi-quantitatively for the presence of endotheial and biliary ductule apoptosis and necrosis using light microscopy.

Statistical Analysis

All data was analysed using R version 3.3.0 within RStudio version 0.99.896 (RStudio Inc., Boston, MA, USA) Integrated Development Environment. Graphs were compiled using the 'ggplot2' package whilst statistics were performed using the 'stats' and 'psych' packages. Numerical data is presented as median and range with data assumed to be homoscedastic. Factoral 2-way (2x3 design) ANOVA was performed to compare the effect of culture media, oxygenation and their interaction on MFI. A p-value of < 0.05 was deemed to be significant.

3.2.3 Results

Hemopure Does Not Alter ROS Production in HSEC and BEC During *In Vitro* IRI

There was no significant effect of Hemopure on ROS production in HSEC *in vitro*, F(1,30) = 0.046, p = 0.831 (Figure 3.17 A). There was also no effect of oxygenation on ROS production, F(2,30) = 0.075, p = 0.928. Similarly, there was no effect of either Hemopure, F(1,18) = 0.717, p = 0.408, or oxygenation, F(2,18) = 1.722, p = 0.207, on ROS production in BEC *in vitro* (Figure 3.17 B).

Hemopure Does Not Increase Apoptosis or Necrosis in HSEC and BEC Necrosis During *In Vitro* IRI

Previous work has shown that increases in intracellular ROS increase cell death in parenchymal liver cells primarily via apoptosis but also necrosis. There was no effect of Hemopure on apoptosis in HSEC *in vitro*, F(1,30) = 0.319, p = 0.712 (Figure 3.18 A). Whilst there was a trend for

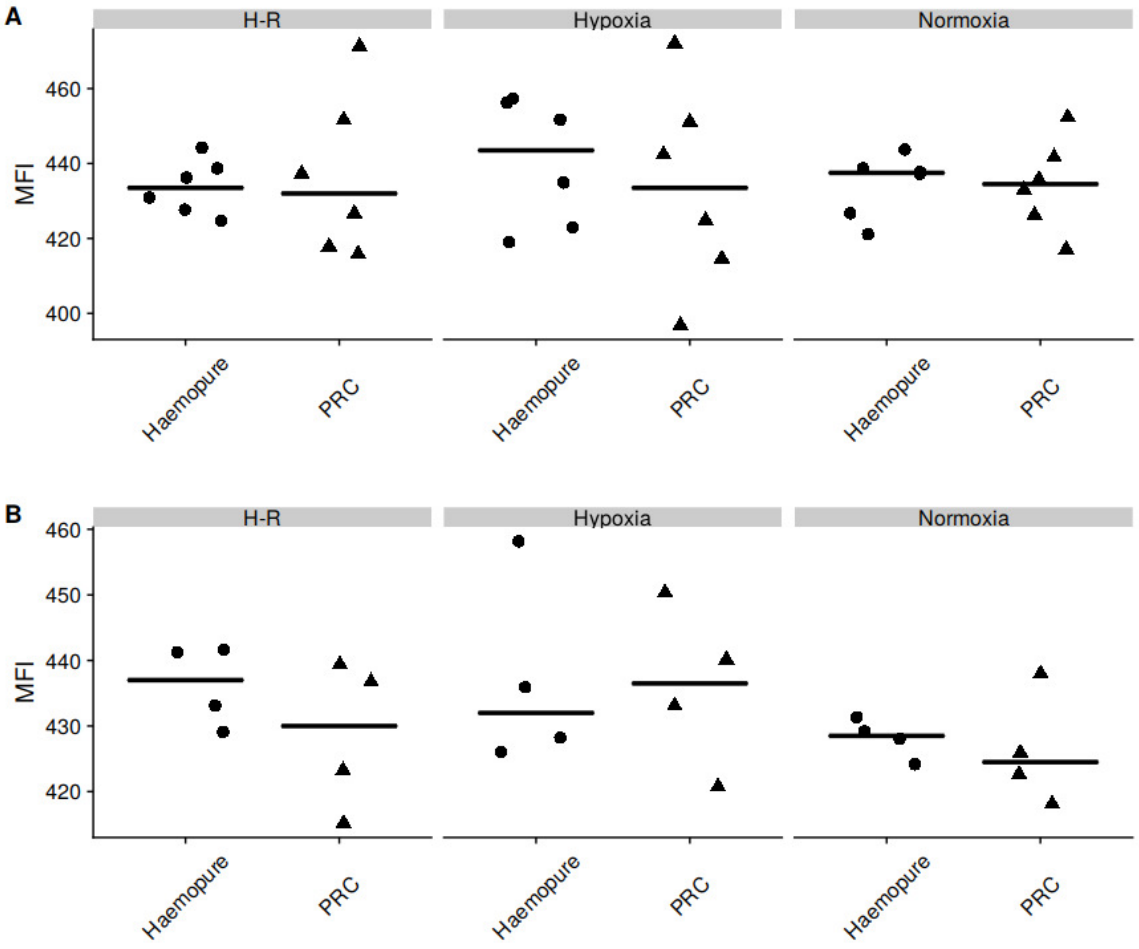

Figure 3.17: ROS production in HSEC (A) and BEC (B) using Hemopure and PRC during *in vitro* IRI. There was no significant effect of either Hemopure or oxygenation on ROS production in either HSEC (A) or BEC (B) *in vitro*.

more apoptosis with hypoxia (M = 5.1, SD = 1.3) compared to normoxia (M = 4.4, SD = 0.5) and H-R (M = 4.3, SD = 0.5), this did not reach significance, $F(2,30) = 2.53$, $p = 0.096$. In BEC, there was no effect of either Hemopure, $F(1,18) = 0.00$, $p = 1.000$, or oxygenation, $F(2,18) = 0.00$, $p = 1.000$, on apoptosis *in vitro* (Figure 3.18 B). When cultured in either standard media or Hemopure, HSEC and BEC did not undergo necrosis (data not shown).

Hemopure Does Not Increase Cell Death During NMLP

In the present study, the liver used for NMLP using PRC infusion was procured from a 60 year old female with a BMI 36.4. CIT was 491 minutes and the liver was discarded due to macroscopic steatosis. The liver used for NMLP using Hemopure was retrieved from a 70 year old male. The CIT was 359 minutes and the liver was also discarded due to macroscopic steatosis. Both donor livers showed mild to moderate steatosis onH&E staining prior to NMLP (Figure 3.19). After 6 hours of perfusion, the liver perfused with PRC showed a slight reduction in steatosis and showed very little cell death with maintenance of liver architecture and intact biliary cells. In comparison, the donor liver perfused with Hemopure also did not demonstrate any increased hepatocellular cell death and also maintained biliary and endothelial cell integrity.

Hemopure Does Not Adversely Affect Perfusion Parameters During NMLP

The duration of NMLP was 431 minutes. Homogenous perfusion was noted on the surface of the liver after 3 minutes of NMLP which was maintained throughout perfusion.

At the start of NMLP, arterial and portal venous flow rates were 386 ml/min and 980 ml/min respectively. Flow rates increased rapidly, with an arterial zenith of 650 ml/min after 120 minutes whilst the portal flow increased more steadily, reaching 1270 ml/min after 230 minutes of NMLP (Figure 3.20 A). Flow rates at the end of NMLP were 575 ml/min for the artery and 1300 ml/min for the portal vein. Arterial and portal venous pressures were maintained within physiological thresholds. After an initial decrease, resistances in the artery and portal vein remained low. The initial reservoir temperature was 32^{o}C, reaching 36^{o}C after 36 minutes of NMLP.

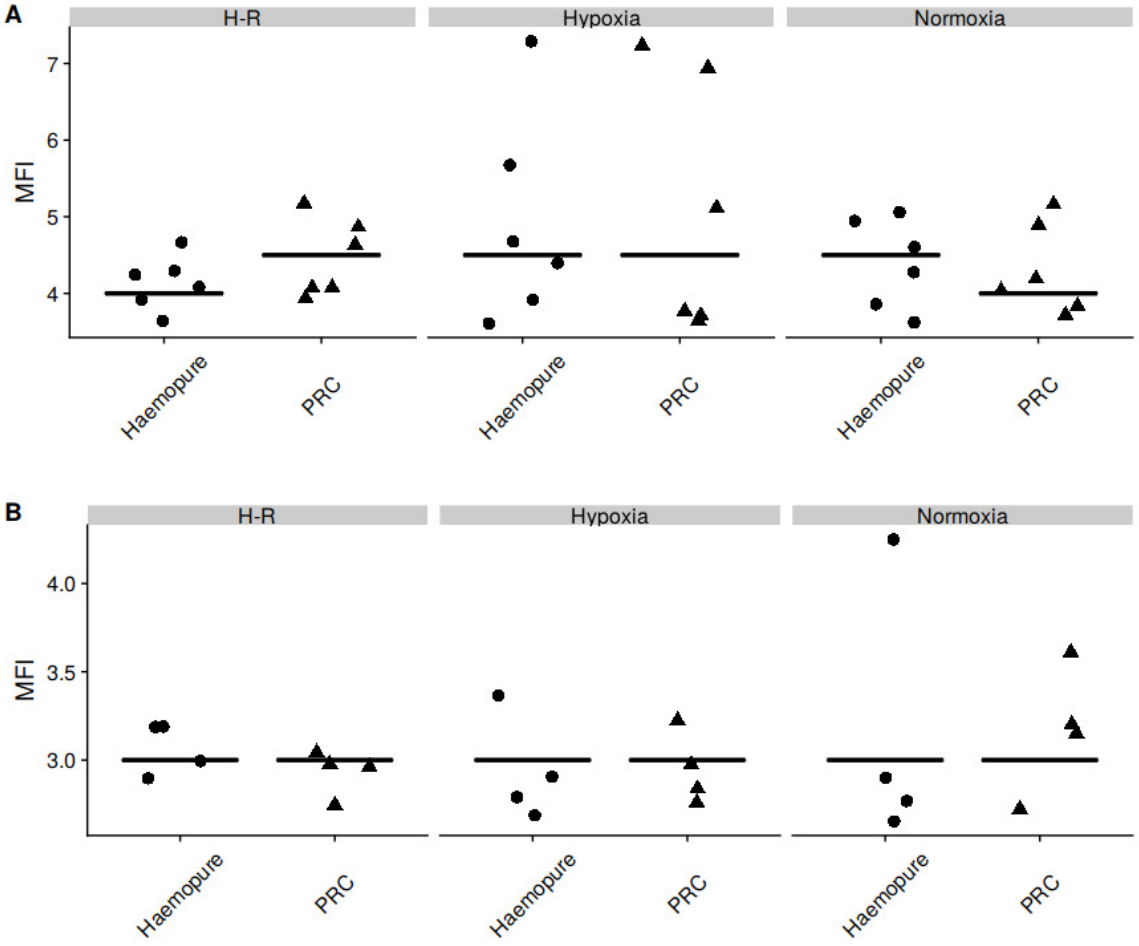

Figure 3.18: Apoptosis in HSEC (A) and BEC (B) using Hemopure and PRC during *in vitro* IRI. There was no effect of either Hemopure or oxygenation on apoptosis in HSEC (A) or BEC (B) *in vitro*. When cultured in either standard media or Hemopure, HSEC and BEC did not undergo necrosis (data not shown).

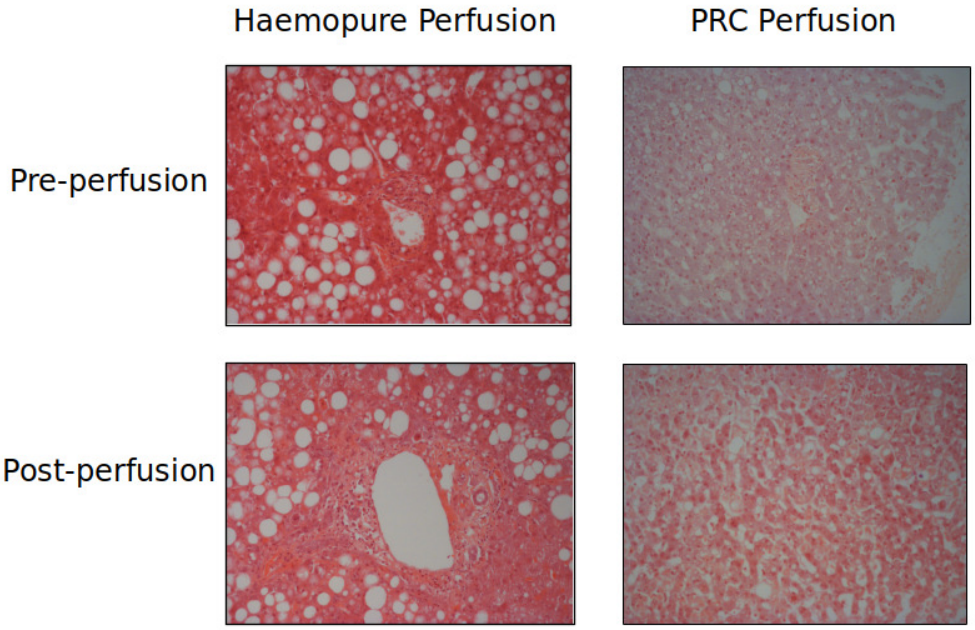

Figure 3.19: H&E staining before and at the end of NMLP using Hemopure and PRC. After 6 hours, PRC perfusion showed a slight reduction in steatosis, very little cell death and maintenance of liver architecture and intact biliary cells. The liver perfused with Hemopure did not demonstrate any increased hepatocellular cell death and also maintained biliary and endothelial cell integrity.

The initial lactate of 8.1 mmol/L decreased steadily (Figure 3.20 B). After 3 hours of NMLP, the lactate was 3.8 mmol/L. There was an increase to 6.2 mmol/L by 4.5 hours, after which it decreased to 5.3 mmol/L at the end of NMLP. The liver utilised glucose during NMLP, commencing at 37.2 mmol/L and reaching 19.0 mmol/L at the end of perfusion (Figure 3.20 C). Bile was produced throughout perfusion. These results are comparable to similar livers subjected to NMLP in Chapter 2.

3.2.4 Discussion

Machine perfusion of donor livers is receiving increasing attention as experimental studies have suggested that this method can afford protection from IRI and improve allograft function. One of the putative protective mechanisms of NMLP is the reduction in IRI. There is clear evidence that during IRI, ROS accumulation is central to the necro-apoptosis observed in allografts after liver transplantation. In addition, NMLP allows the possibility of viability testing of a donor organs prior to transplantation. However, one potential barrier to the widespread clinical adoption of NMLP is the requirement for group-specific PRC with which to perfuse the donor liver. This has clear logistical and potential safety implications. The use of an acellular perfusion fluid, such as Hemopure, would negate many of these issues and potentially increase the wider clinical application of NMLP by obviating the need for PRC in the perfusion fluid. Its use is particularly attractive in the NMLP setting given the potential risk of patient sensitisation and disruption of the liver micro-circulation from red cell trapping. There are some reports in animal models purporting to the advantage of acellular fluids in models of trauma, brain injury and haemorrhage.[265, 266, 267] Unfortunately, these promising pre-clinical results with acellular fluids have not translated into improved patient outcome when used clinically.[268] The effects upon cardiovascular system, including nitric oxide scavenging and subsequent higher vascular resistance, have been suggested to underlie the adverse effects seen in patients although more recent randomized studies suggest there no increased risk with acellular fluids.[269] Limited studies have assessed the use of acellular perfusion fluids in the setting of liver injury. In a porcine model of liver injury Hemopure improved early mortality and in rodent models of IRI

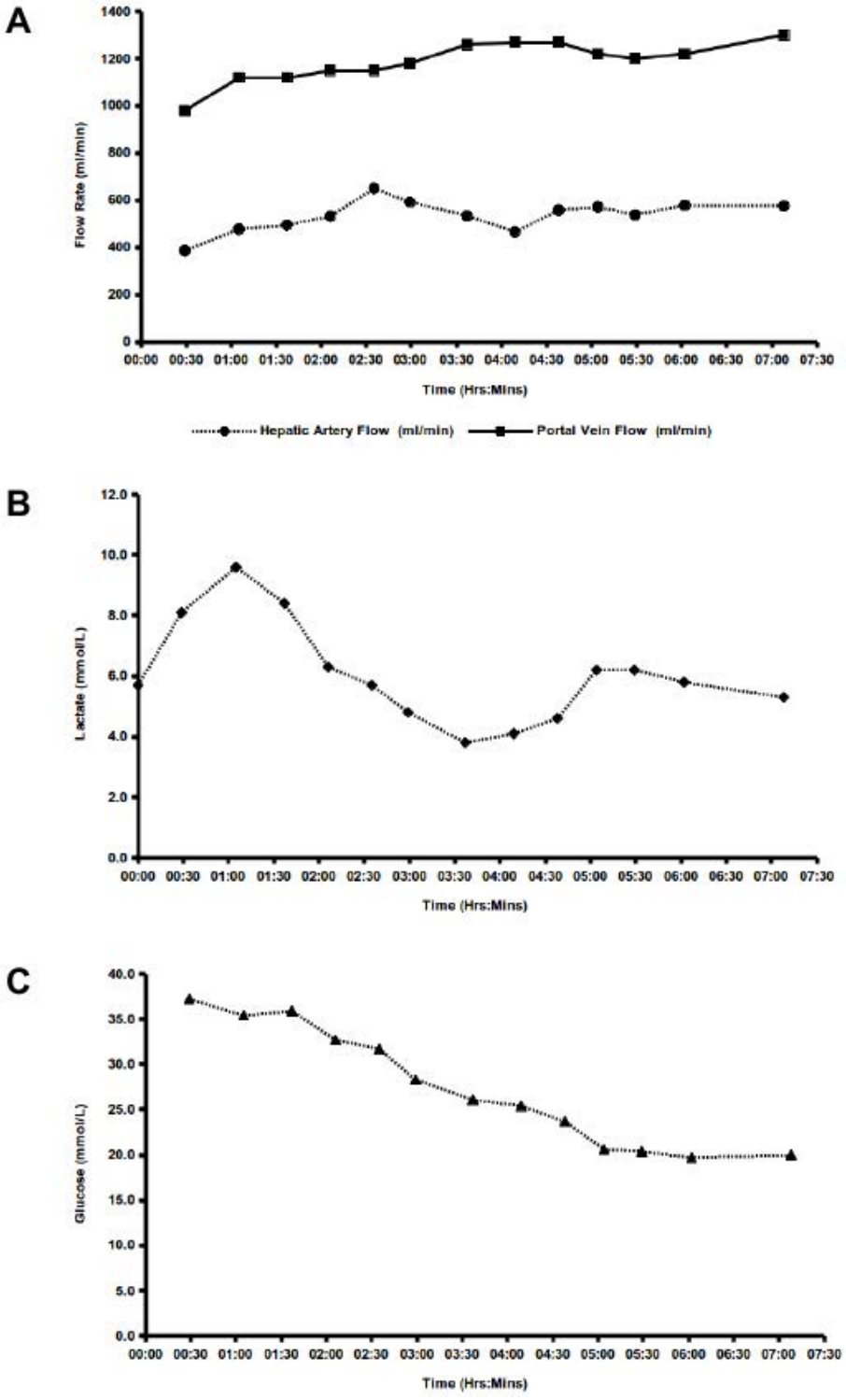

Figure 3.20: A: Hepatic arterial and portal venous flow parameters during NMLP with Hemopure. B: The decrease in lactate concentration during NMLP with Hemopure. C: Utilisation of glucose during NMLP with Hemopure. These results are comparable to those presented in the previous chapter.

Hemopure improved oxygenation in post-reperfusion liver tissue.[270, 271]

This *in vitro* data shows that under normoxia, hypoxia and H-R HSEC and BEC have a high basal intracellular ROS content. Exposure to Hemopure *in vitro* IRI did not alter intracellular ROS levels in BEC or HSEC significantly. Furthermore, during *in vitro* IRI neither HSEC nor BEC show increases in either apoptosis or necrosis. When HSEC and/or BEC cultured in Hemopure are exposed to the same *in vitro* model of IRI they did not alter intracellular ROS production significantly. Interestingly, there was no reduction in intracellular ROS when using Hemopure during IRI. The reasons for this remain the focus of on-going research in the laboratory. Importantly Hemopure did not induce cell death in HSEC or BEC during IRI. These observations suggest that *in vitro* Hemopure is not toxic to human liver cells. When used in the NMLP setting, Hemopure demonstrated no increase in hepatocellular apoptosis and necrosis when compared to PRC perfusion. In this study both donor livers showed maintenance of biliary duct integrity and relatively normal liver morphology. Although Hemopure has been used in only one perfusion, the results from this suggest that adequate levels of oxygen can be delivered the liver tissues in the absence of packed red cells.

In conclusion, this preliminary study suggests that there is potential to expand the use acellular perfusion fluids in the setting of NMLP. Haempoure both *in vitro* and *in vivo* does not appear to be toxic to liver cells and further studies are required to assess fully the potential for its use in clinical setting of NMLP.

3.3 Proof of Concept: Liver Splitting During Normothermic Machine Perfusion

3.3.1 Introduction

Each year 15% of patients on the liver transplant waiting list in the UK either have died or been removed.[107] One strategy to increase numbers of available livers is splitting, performed

either *in situ* or *ex situ*. The most common approach is the "classical" left lateral + right trisegmentectomy split providing left grafts for children. The less frequently performed full left-right split can provide livers for two adults but this is technically complex and questions remain over vascular and biliary outcomes.[272]

Normothermic machine perfusion of the liver was developed to attenuate IRI and improve organ utilisation, early data are encouraging. A viability protocol was developed and subsequently validated by transplantation.[224, 273] Here, viability testing and resuscitation of a donor liver followed by left lateral + right trisegmentectomy splitting with concurrent NMLP is reported.

3.3.2 Methods

Donor

A DCD liver from a 69 year-old female with a body mass index of 34.3 kg/m^2 and DRI of 3.053, who sustained an irrecoverable hypoxic brain injury following an out-of-hospital cardiac arrest and had been admitted to the ITU for 7 days, was initially accepted for transplantation. Withdrawal of life sustaining treatment was conducted in ITU according to UK standard practice and 34 minutes later dual arterial and porto-venous liver perfusion commenced with UW perfusion fluid at 4^{o}C, using the established super-rapid technique. On back-table inspection the liver was described as being mildly steatotic with an iatrogenic 2.5cm superficial laceration to the left lobe and atherosclerosis to the coeliac patch. There was normal extrahepatic vascular anatomy. The liver was deemed unsuitable for transplantation by the initial allocated transplanting centre, was offered to the national pool but rejected, and then accepted by the Liver Unit at the Queen Elizabeth Hospital Birmingham for reseach.

After transportation on static cold storage, the liver experienced a CIT of 9 hours 43 minutes. It was inspected but subsequently declined for transplantation. It was decided to subject the liver to NMLP for viability testing.

Normothermic Machine Liver Perfusion

The liver was prepared for modified piggyback transplantation. The IVC was dissected to permit unobstructed drainage, portal vein to its bifurcation, hepatic artery to the gastroduodenal artery and the common bile duct was identified. NMLP commenced with a PRC based fluid at 37^{o}C using the Liver Assist device (Organ Assist, The Netherlands) via hepatic artery and portal vein cannulae. Oxygenated pulsatile flow (pressure 50 mmHg) and non-pulsatile flow (pressure 10 mmHg) perfused the liver via hepatic artery and portal vein respectively, before recirculating via the open circuit reservoir.

During NMLP, flow parameters, blood gases and bile production were assessed every 30 minutes. Homogenous perfusion, stable flow parameters, lactate concentration of $<$ 2.0 mmol/L and evidence of bile production after 2 hours fulfilled criteria for viability.

Splitting

'Classical' left lateral + right trisegmentectomy split was performed with an integrated bipolar and ultrasonic device (Thunderbeat, Olympus, UK) for dissection with simultaneous ligation. Splitting was conducted in the reservoir with concurrent NMLP throughout (Figure 3.21 A & B), maintaining inflow and outflow for both 'grafts'.

Flow parameters and perfusate analysis were recorded during post-hilar and post-parenchymal phases from left and right hepatic arteries, portal veins and IVC. Post-procedure blood flow was confirmed using Doppler ultrasound (CX50 CompactXtreme, Philips, The Netherlands), in each lobe.

Histology

Specimens taken 3 hourly and on completion of NMLP from each lobe were examined by H&E and PAS staining. Blinded assessment was performed by a qualified pathologist.

3.3.3 Results

Prior to Splitting

The liver weighed 1650g. Duration of pre-splitting NMLP was 6 hours 28 minutes. Within 3 minutes of commencing NMLP, homogenous perfusion was noted. At the start of NMLP, arterial and portal venous flow rates were 116 ml/min and 630 ml/min respectively. Flow rates increased rapidly, reaching of 573 ml/min (artery) and 1500 ml/min (portal vein) after 3 hours of NMLP (Figure 3.21 A). Flow rates at the end of NMLP prior to splitting were 500 ml/min for the artery and 1510 ml/min for the portal vein. Arterial and portal venous pressures were maintained within physiological thresholds. After an initial decrease, resistances in the artery and portal vein remained low. The initial reservoir temperature was 26^{o}C, reaching 36^{o}C after 47 minutes.

Prior to NMLP, lactate concentration of the perfusion fluid was $>$20.0 mmol/L. The initial lactate of 13.9 mmol/L decreased rapidly (Figure 3.21 B). After 2 hours of NMLP, when viability was assessed, lactate concentration was 1.0 mmol/L. It continued to decrease to 0.9 mmol/L at 2 hours 30 minutes, after which it increased to 3.0 mmol/L by the end of pre-splitting NMLP. Bile was initially collected 2 hours 30 minutes after starting perfusion (Figure 3.21 C) and in total 11 grammes were excreted. NMLP was associated with a reduction in perfusate glucose concentration from a maximum of 46.9 mmol/L to 16.5 mmol/L without the adminstration of exogenous insulin (Figure 3.21 D).

Pre-Parenchymal, Post-Hilar Dissection and Post-Parenchymal Transection

The duration of splitting with concurrent NMLP was 71 minutes. Total duration of NMLP was 8 hours 22 minutes. No additional PRC were required for the circuit during NMLP. The splitting procedure resulted in a dry transection surface and extrahepatic vasculature.

During the pre-hilar phase, flow in the hepatic arteries and portal veins decreased despite maintaining the pre-splitting pressures (hepatic arterial median pressure 55 [53-56] mmHg, flow

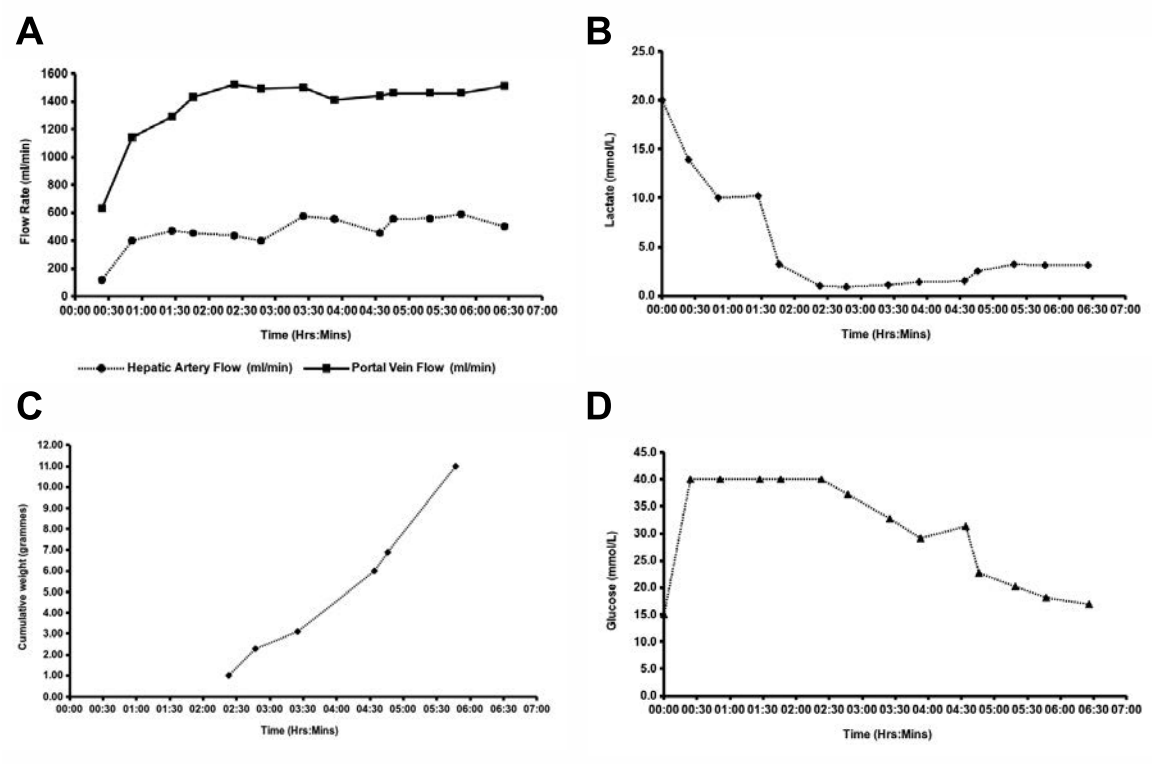

Figure 3.21: (A) Hepatic arterial and portal venous flow rates; (B) Lactate concentrations; (C) Cumulative bile production; (D) Glucose concentrations.

447 [441-448] ml/min; portal venous median pressure 10 [10-11] mmHg, flow 750 [720-770] ml/min). After parenchymal splitting and maintaining previous differential pressures (median 54 [54-55] mmHg), total hepatic arterial flow remained just below pre-hilar rates (median 429 [424-450] ml/min). The total portal venous flow rate increased to near pre-splitting rates (median 1250 [1230-1260] ml/min) whilst maintaining physiological pressures (median 9 [8-10] mmHg).

Lactate concentrations at the end of the hilar phase were similar in the left and right hepatic arteries and portal veins as well as in the effluent from the IVC (Table 3.12). Post-parenchymal phase lactate concentrations in the hepatic arteries and portal veins were unchanged. Lactate concentration in the inferior vena cava increased by 0.3 mmol/L compared to the pre-hilar phase. Bile production continued throughout splitting. Doppler ultrasound demonstrated expected hepatic arterial, portal venous and inferior vena cava waveforms in both lobes after splitting (Figure 3.22).

Histological Assessment

Moderate sinusoidal vasodilatation, equivalent to one hepatocyte width, was noted throughout NMLP although it was milder after splitting (Figure 3.23 A, C, E, G). There was no evidence of hepatocyte necrosis during the first 3 hours of NMLP (Figure 3.23 A, C). Mild periportal necrosis (Figure 3.23 E, $< 20\%$) was noted only in the left lobe after 6 hours of NMLP however, there were no necrotic hepatocytes after parenchymal splitting (Figure 3.23 G). Macrovesicular steatosis was low ($< 10\%$) on the biopsy taken immediately prior to NMLP (Figure 3.23 A). The distribution of both macro- and microsteatosis remained the same at completion of splitting (Figure 3.23 G). There was no evidence of intrahepatic bile duct injury either before or after splitting. There was patchy PAS staining throughout NMLP prior to and on completion of splitting as we frequently observe with donor organs initially thought to be un-transplantable (Figure 3.23 B, D, F). Nevertheless, there was a trend for increasing PAS staining by the end of splitting (Figure 3.23 H).

	Pre-Parenchymal, Post Hilar Dissection					Post-Parenchymal Transection				
	Left		Right		IVC	Left		Right		IVC
	HA	PV	HA	PV		HA	PV	HA	PV	
pH	7.439	7.432	7.442	7.448	7.387	7.416	7.405	7.439	7.403	7.369
pCO2 (kPa)	4.04	4.22	4.1	4.06	4.83	3.96	4.29	3.74	4.32	4.93
pO2 (kPa)	10.07	6.8	9.47	7.02	4.67	7.94	5.83	10.21	6.28	3.48
BE (mmol/L)	-3.6	-3.2	-3.1	-2.9	-3.3	-5.2	-4.5	-4.9	-4.4	-4
HCO3- (mmol/L)	20	20.6	20.5	20.6	21.3	18.7	19.7	18.6	19.8	20.9
tHb (g/L)	76.5	78.2	76.7	77.5	81	78.1	78.4	79.5	79	76.1
Hct (%)	17.2	17.6	17.6	17.4	18.3	16.6	17	16.8	17	16.8
Glucose (mmol/L)	13.7	14	14.1	13.8	14.4	15.3	15.8	16.6	15.8	15.6
Lactate (mmol/L)	2.7	2.7	2.8	2.6	2.6	2.6	2.7	2.8	2.7	2.9

Table 3.12: Table of flow rates and blood gas results prior to, during and after completion of splitting with concurrent NMLP.

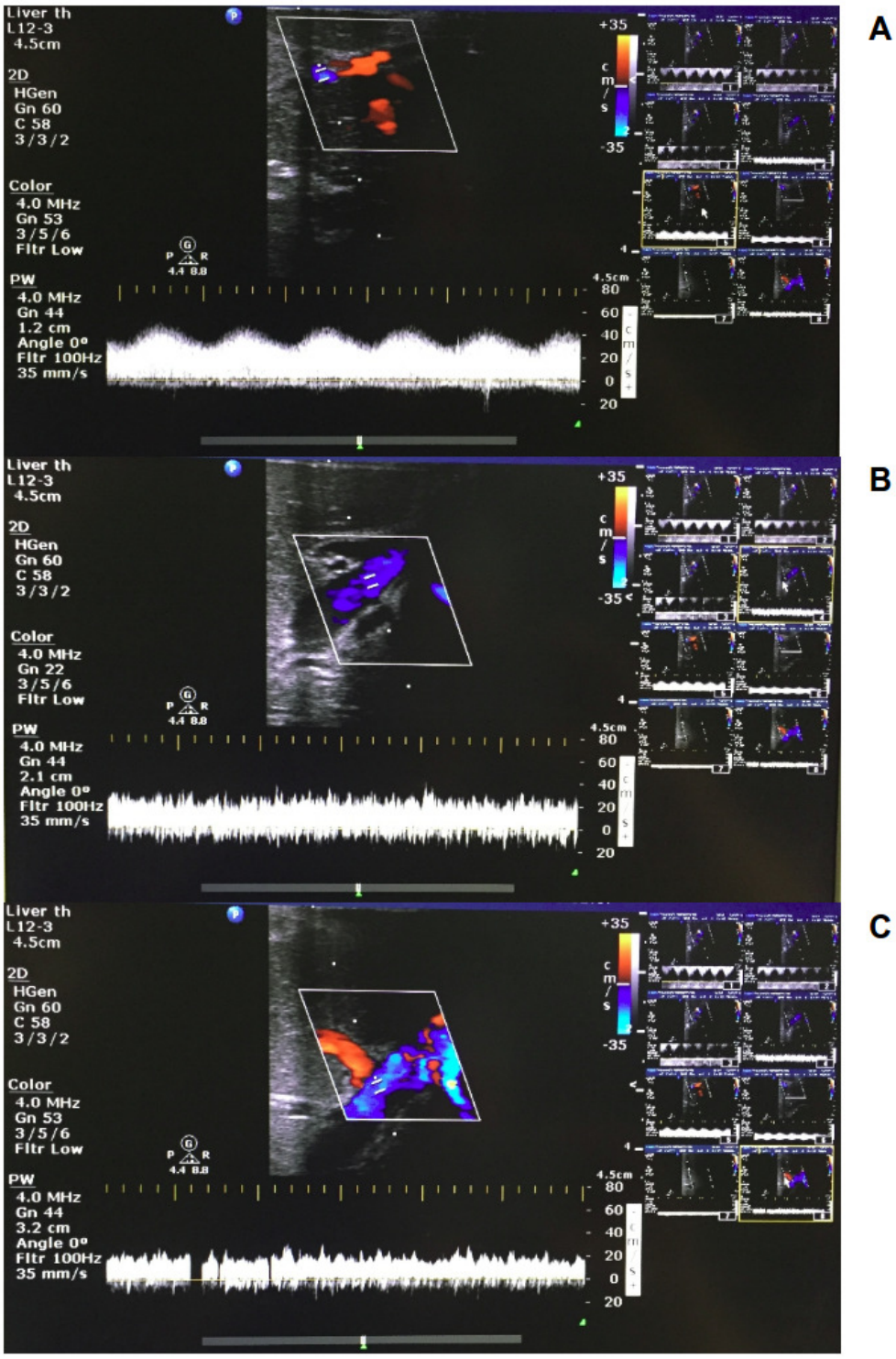

Figure 3.22: (A) Hepatic arteriolar waveform; (B) Portal venous waveform; (C) Hepatic venous waveform.

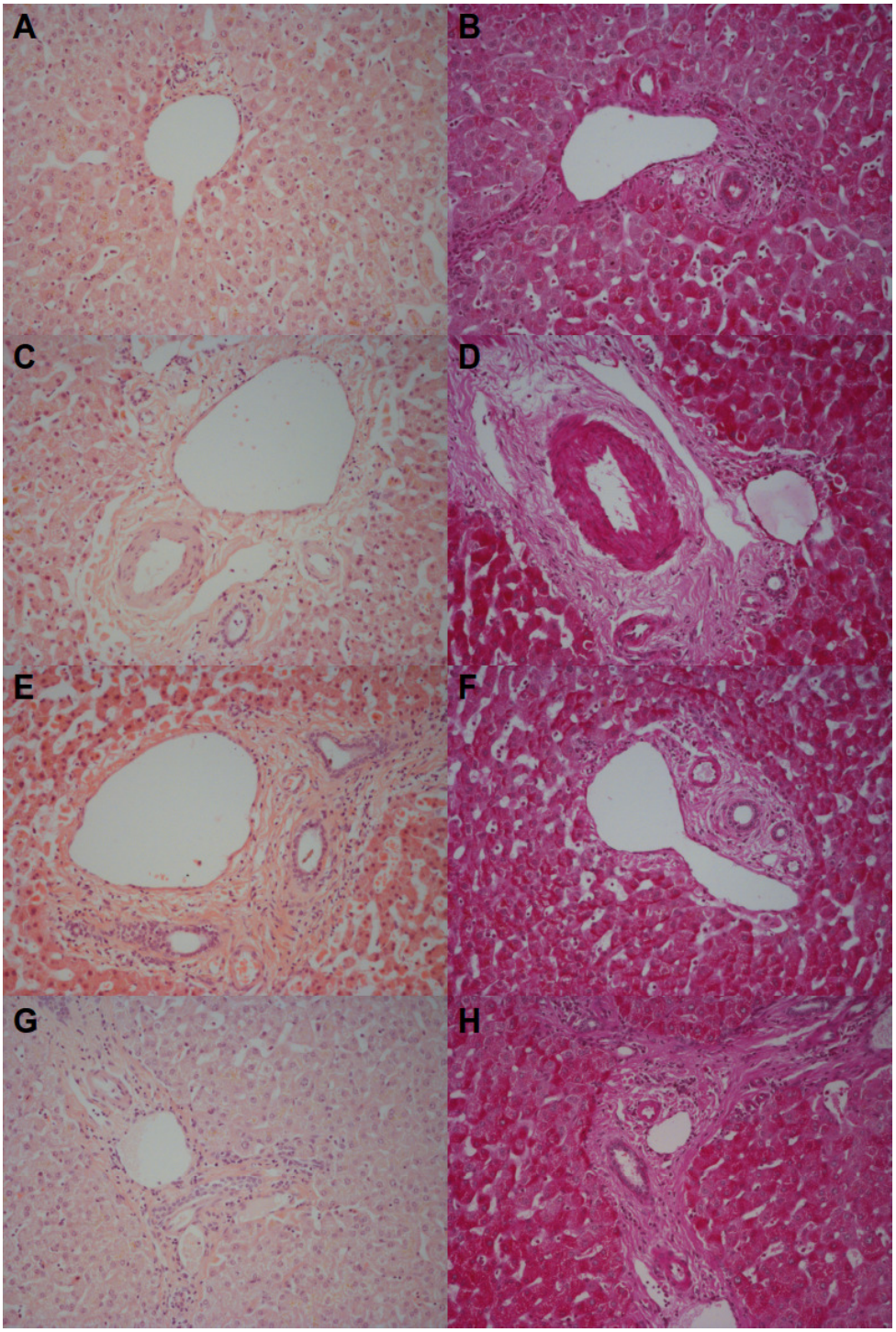

Figure 3.23: Representative histological samples to assess architectural integrity and necrosis by H&E staining (A,C,E,G) as well as glycogen content using Periodic acid-Schiff staining (B,D,F,H). Samples taken prior to commencement of NMLP (A,B), after 3 hours of NMLP (C,D), after 6 hours of NMLP (E,F) and after parenchymal splitting with concurrent NMLP (G,H).

3.3.4 Discussion

This is the first study demonstrating that splitting a liver with concurrent NMLP throughout is feasible and viability is maintained. Furthermore, this has been achieved in a liver unsuitable for transplantation. No studies to date have investigated liver splitting with concurrent NMLP throughout splitting using either normothermic, subnormothermic or hypothermic strategies.

This technique presents advantages over existing *ex situ* or *in situ* methods. There is no increasing temperature and rewarming under ischaemic conditions seen with cold *ex situ* splitting. Whilst possible during *in situ* splitting, concurrent NMLP provides *ex situ* direct visualisation of perfused segments. Throughout and after splitting the cut surface can be inspected and vessels ligated to ensure haemostasis. Continuation of NMLP permits continuous viability assessment. This may contribute to recipient selection, aid informed decision-making and facilitate logistics of transplanting two grafts by preventing long CIT. This study has shown that *ex situ* splitting is feasible in extended criteria donor livers performed in combination with NMLP, and results in pre-transplant biochemical, histological and Doppler findings that are compatible with transplantation.

Liver splitting during NMLP has been described using the OrganOx metra® device. Due to the closed circuit, a hanging procedure was implemented to facilitate dissection whilst minimising fluid loss from the cut surface. Here perfusion was paused for six minutes to separate the grafts and yielded only an extended right segment still perfused.[274] Specific advantages of an open circuit include: Superior manipulation; reduced risk of compromised flow; potential to perform and assess integrity of vascular reconstruction; the ability to perform the complete splitting procedure with concurrent NMLP.

Ex-situ splitting with NMLP allows exploration of splitting ECD livers and may increase the donor pool enabling two recipients to be transplanted from a single donor. This apparatus also could facilitate training in liver splitting and providing controls for experimental research.

In summary, classical left lateral + right trisegmentectomy liver splitting entirely with concur-

rent NMLP is feasible, maintaining viability of both lobes, combining 'normal' physiological conditions with reduced CIT with the ease of *ex situ* splitting, without impacting on organ retrieval. Future work will allow improved monitoring and facilitate logistics of liver splitting.

CHAPTER 4

TWEAK/FN14 IN HUMAN DISEASED LIVER AND ITS RELATIONSHIP TO BILIARY EPITHELIAL CELLS

4.1 Introduction

The potential role of Fn14 in the liver was initially described at the start of the millennium. Fn14 expression was mapped to chromosome 16 by fluorescent *in situ* hybridisation and its presence was demonstrated in both human and murine models of hepatocellular carcinoma.[275] Fn14 is highly expressed in the developing murine foetal liver and up-regulated during murine and rat adult hepatic injury.[84, 85, 276] Fn14 is expressed on Liver Progenitor Cell (LPC), hepatocytes and cholangiocytes in human and murine models.[84, 85, 276] Fn14 is expressed on murine CD 24+, Sca-1 high, Thymocyte Differentiation Antigen-1 (Thy-1) low progenitor cells and its activation results in proliferation and the formation of duct-like structures in foetal rat liver.[277] Further evidence of Fn14 on LPCs has been provided by a more direct evaluation of Fn14 and TWEAK in a survey of human liver and their role in HSCs.[278] Recently, transcription of Fn14 in human hepatocellular carcinoma may be mediated by alpha-fetoprotein.[279] Translational studies have focussed on Fn14 being a potential therapeutic target in alcoholic hepatitis.[280, 281] TWEAK expression was shown to be up-regulated in human and murine models of hepatocellular carcinoma and detected on Thy-1+ cells in the regenerating liver.[282, 283] More recently, in a murine model of fibrosis, macrophage-derived TWEAK promoted liver progenitor population expansion and improvements in fibrosis.[284] Translational studies of TWEAK therapy are yet to be conducted and to date, there are no studies investigating the role of Fn14 and TWEAK subsequent to liver transplantation.

The presence of high levels of Fn14 on cholangiocytes in areas of ductular regeneration and the presence of surrounding myeloid cells expressing high levels of TWEAK during inflammation would be consistent with a major role for this receptor-ligand pair in ductular remodelling. The aim of this chapter is to test the hypothesis that the Fn14/TWEAK receptor-ligand systems plays a role in intra-hepatic biliary epithelial cell biology using established *in vitro* modelling.

The aim of this chapter is to test the hypothesis that the Fn14/TWEAK receptor-ligand systems plays a role in intra-hepatic biliary epithelial cell biology using established *in vitro* modelling.

4.2 Materials & Methods

4.2.1 Ethical Approval

Human tissue sections and cultured primary human cholangiocytes were isolated from slices of normal donor tissue not required for transplantation and explanted diseased livers obtained from the Queen Elizabeth Hospital Birmingham liver transplant programme. The study was granted ethical approval by the University of Birmingham Local Regional Ethics Committee (reference number 06/Q702/61). Consent to use donor tissues for research was obtained by SNOD from the donor's next of kin during consent for organ donation. None of the organ donors were from a vulnerable population. All donors, next of kin freely or liver transplant recipients freely provided written informed consent.

4.2.2 Determining Fn14 in the Liver by Immunohistochemistry & Immunofluorescence

Immunohistochemistry was performed using standard techniques on human tissue sections obtained from blocks of snap frozen tissue that had been stored at -80^{o}C. Briefly, sections were cut using a cryostat by an experienced laboratory scientist on to poly-L-lyseine coated glass slides before being fixed in acetone for 5 minutes. Sections were washed in PBS prior to being stored at -20^{o}C. When required, sections were defrosted in a humidifying chamber, the tissue demarcated with a wax pen, labelled and washed in PBS. The peroxide activity of the tissue sections was quenched by bathing the sections in 0.3% hydrogen peroxide before further washing in PBS then immunoglobulin blocked with 10% normal horse serum (S2000, Vector Laboratories Ltd., Peterborough, UK) for 30 minutes. In all immunohistochemical and immunofluorescent experiments, no primary and relevant concentration-matched isotype immunoglobulin controls were used. The primary antibodies Fn14 (mP4A8, kindly supplied by Dr. Linda Burkley, Biogen Idec.) and HEA125 were diluted to their appropriate concentrations, 37 ng/ml and 5 μg/ml respectively, in 10% normal horse serum buffer and incubated at room temperature for

1 hour. Sections were washed in PBS before rabbit anti-mouse secondary antibody (MP7500, Vector Laboratories Ltd., Peterborough, UK) was applied and incubated for a further 1 hour. After further washing in PBS, the sections were incubated with either ImmPACT AEC (3-amino-9-ethylcarbazole, SK4205, Vector Laboratories Ltd., Peterborough, UK) for 30 minutes or ImmPACT DAB (diaminobenzidine, SK4105, Vector Laboratories Ltd., UK) for 3 minutes. Washing in PBS was followed by haematoxylin counterstaining for 30 seconds before washing and mounting in aqueous mountant.

Immunofluorescence was performed in a similar manner however the blocking and antibody buffer used was PBS with 10% foetal calf serum and 1% sodium azide. Washes were perforemd twice in PBS for 10 minutes each time. The secondary and substrate steps were replaced by a single application of fluorescent secondary conjugates incubated in the dark. These were either FITC or Texas Red (TXRD). The counterstain used 4',6-diamidino-2-phenylindole (DAPI) that had been incubated with the slides for 2 minutes. Sections were mounted using an immunofluorescent mountant and stored in foil at 4^oC. Images of fluorescent stained sections were taken using an fluorescent microscope (Axioskope 40, Carl Zeiss Ltd., Cambridge, UK) within 7 days.

4.2.3 Isolation of Human Cholangiocytes

Primary human cholangiocytes were isolated from donor tissue either not required for transplantation or from the hepatectomy during transplantation. Specimens were processed by a University Hospital Birmingham Pathology Department approved scientist. The method to isolate human cholangiocytes was commenced within 24 hours of the specimen becoming available to the laboratory. In summary, the isolation involved a collagenase digestion for 30 minutes followed by serial centrifugation before purification with a 77%:33% Percoll 25 minute centrifugation step. This was followed by extraction of the pellet and further centrifugation before immunomagnetic separation using mouse-antihuman HEA125 and Dynal beads. Once separated the cholangiocytes were plated on to rat-tail collagen-coated 25cm^3 flasks and fed with

sterile supplemented Dulbecco's Modified Eagle's Medium (DMEM):Ham's-F12 based media. Flasks were incubated at 37^{o}C and the media changed every other day. Once at least 70% confluent, cholangiocytes were passaged using trypsin to a 75cm^3 rat-tail collagen-coated flask for further incubation to expand the cholangiocyte population.

4.2.4 Human Cholangiocyte Cell Lines

The viability of primary human cholangiocytes is known to be dependent upon the liver disease from which the cholangiocytes were isolated. For this reason contiguous experiments were conducted on non-malignant and malignant cell lines. None of these cell lines are Simian Vacuolating Virus 40 (SV40) transformed. The Andreas K Nussler-1 (AKN-1) cell line, initially described in 1999, was derived from a 10 year old boy and characterises non-malignant biliary epithelial cells.[285] The CC-LP-1 and CC-SW-1 cell lines, described together in 1992, were derived from moderately differentiated adenocarcinomae and characterise intrahepatic cholangiocarcinoma.[286] All of the cell lines are plastic adherent and do not require the flasks to be coated with rat-tail collagen. Cells were incubated with a supplemented DMEM media.

4.2.5 Phenotyping of Cultured Human Cholangiocytes and Cell Lines

Once primary human cholangiocytes or the cell lines became at least 70% confluent in the 75cm^3 flasks, the cells could be trypsinised and cultured in a 24 well plate at 5x10^4 cells per well. Once these were 70% confluent the cells could be phenotyped by either immunohistochemistry/immunofluorescence after being cytospun to poly-L-lysine coated slides or by flow cytometry using standard techniques. The cellular phenotype was determined using a variety of different antibodies including but not exclusively the following: Epithelial Cell Adhesion Molecule (EpCAM), also known as HEA125, a surface cholangiocyte marker; Cytokeratin (CK)18, an intracellular hepatocyte and cholangiocyte marker; CK19, an intracellular cholangiocyte marker); CD 31 also known as Platelet Endothelial Cell Adhesion Molecule-1 (PECAM-1), a surface endothelial cell maker; CD 90, also known as Thy-1, surface fibroblast

marker. Additionally, no primary and relevant concentration matched immunoglobulin isotype control samples were tested to ensure specificity of the phenotyping antibodies.

4.2.6 Determining Trypsin Sensitivity of Fn14

Trypsin can disrupt the glycocalyx immediately surrounding the cell. The use of trypsin to dissociate cells from flasks or culture plates may therefore cleave the extracellular domains of Fn14 and render it inactive. The sensitivity of the cultured cell lines to trypsin was investigated by subjecting the cells to either trypsin or cell dissociation buffer immediately prior to preparation for flow cytometry to determine Fn14 expression. For each dissociation method, the experiment was repeated three times.

4.2.7 Determining Expression of Fn14 on Cultured Cholangiocytes and Cell Lines

Cholangiocytes and cell lines were cultured in a 24 well plated at $50x10^5$ cells per well. After incubation for 24 hours cells were either left to continue being cultured in standard media or were stimulated with either TNF-α (10 μg/ml), IFN-γ (50 ng/ml) or Fibroblast Growth Factor-basic (FGF-b)(0.05 ng/ml) for 24 hours. Cells were then trypsinised off the 24 well plate and either cytospun for immunohistochemistry/immunofluorescence or prepared for flow cytometry using standard methods. Fn14 was determined by FITC emission on the 488 nm laser.

4.2.8 Determining Expression of Fn14 on Cultured Cell Lines Using Cell Surface Proteomics

This method was developed over 6 months to maximise on yield of peptides from the cell surface proteome being was delivered to the mass spectrometer. The final experiment was performed three times once the protocol was optimised.

Biotinylation

Four T75 flasks 95% confluent with CC-SW-1 intra-hepatic cholangiocarcinoma cell line were used for determining Fn14 expression by cell surface proteomics. The T75 flasks were placed on ice, the media removed before being washed twice with 8ml of ice-cold PBS per flask. The PBS was quickly removed to prevent rounding and detachment of the cells. The contents of one vial of EZ-Link Sulfo-NHS-SS-Biotin (Thermo Scientific, UK) was dissolved in 48ml of ice-cold PBS, before 10ml of the biotin solution was added to each flask. The EZ-Link Sulfo-NHS-SS-Biotin is a sulfosuccinimidyl-2-(biotinamido)ethyl-1,3-dithiopropionate that has accessible lysine residues which can covalently bind to primary amines at the sulfo end (Figure 4.1). Subsequently, the flasks were placed on a rocking platform or an orbital shaker and gently agitated for 30 minutes at 4^{o}C to ensure even coverage of the cells with labelling solution. The flasks were washed three times with ice-cold PBS to remove all labelling solution, after which 500μL of Quenching Solution was added to each flask to stop the reaction. The cells were subsequently scraped gently in to solution and transferred to a single 50ml conical tube. This was centrifuged at 500x g for 3 minutes and the supernatant discarded. Finally, 5ml of Tris Buffered Saline (TBS) was added to the cell pellet to suspend it before centrifugation at 500x g for 3 minutes with the supernatant again discarded.

Cell Lysis

The supplied protease inhibitor was added to 500μL of lysis buffer and added to the cells and, after gentle suspension, disrupted by sonicating on ice for 1-second bursts. The cells were then incubated on ice, vortexing every 5 minutes for 5 seconds. Additional sonications were performed during incubation as necessary. The lysate was then centrifuged at 10,000x g for 2 minutes at 4^{o}C after which the clarified supernatant was transferred to a new tube.

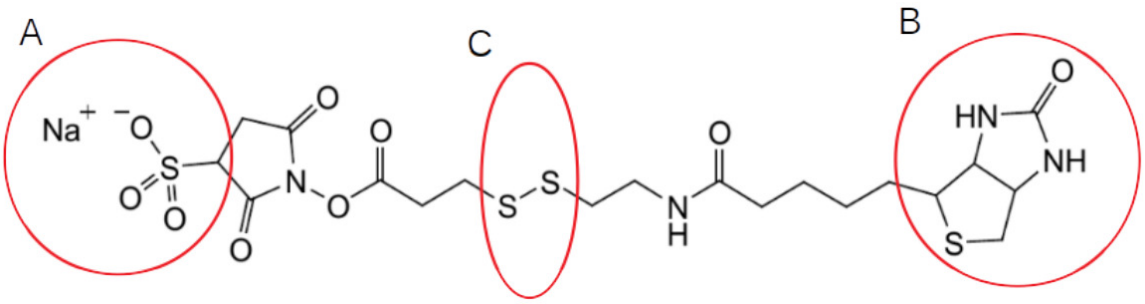

Figure 4.1: Biotinylation of cell surface proteins in preparation for cell surface proteomics. The EZ-Link Sulfo-NHS-SS-Biotin covalently binds to primary amines of cell surface proteins at (A), with the attached Biotin captured on a NeutrAvidin gel (B). The disulfide bridge (C) is cleaved to release the proteins for peptide processing. Figure adapted from Thermo Scientific EZ-Link Sulfo-NHS-SS-Biotin product information.

Isolation of Labelled Proteins

An even suspension of the supplied NeutrAvidin Agarose was added to a collecting column that had been capped. This was centrifuged for 1 minute at 1000x g and the flow-through discarded before being repeated twice. The bottom cap was applied, the clarified cell lysate added to the gel and the top cap applied. The capped column was incubated for 60 minutes at room temperature with end-over-end mixing using a rotator. The column was uncapped and centrifuged for 1 minute at 1000x g before 500μL of 1M sodium chloride was added. Following two further centrifugations, 25μL of the supplied protease inhibitors was added to 2.5ml of wash buffer, from which 500μL was added to the column that had been placed in the collection tube. Centrifugation for 1 minute at 1000x g was conducted 4 times before the bottom cap was replaced.

Protein Elution

A 0.5M preparation of DTT was prepared by weighing 77.1mg of DTT in a 1.5ml Eppendorf, adding 900μL of Chromanorm H_2O and 100μL of Tetraethylammonium Bromide (TEAB). To 450μL of a 2% solution of Sodium-deoxycholate (SDC) in 100mM of TEAB, 23.7μL of 0.5M DTT was added to make sample buffer. From this, 400μL of the sample buffer was pipetted to the gel and the column capped. Incubation of the reaction occurred for 60 minutes at room temperature with end-over-end mixing on a rotator. The sample was then centrifuged in to a new column for 2 minutes at 1000x g to yield the eluted protein.

Protein Digestion

To defrosted 20μg of sequencing grade trypsin (Promega UK, Southampton, Hampshire, UK), 100μL of 100mM TEAB was added and mixed thoroughly. From this 50μL was added to the protein solution which was then placed on a shaker overnight at room temperature to complete digestion of the eluted cell surface proteins.

Peptide Enrichment

To the peptide solution, 50μL of pure Trifluoroacetic Acid (TFA) was added to precipitate the SDC. After vortexing for 1 minute, the sample was cetrifuged for 3 minutes at 13,000g. A 50μL aliquot of 1M iodoacetamide in 100mM of TEAB was added to 500μL of the peptide solution. This was incubated at room temperature for 60 minutes in the dark.

Purification of Labelled Peptides

To a 15ml conical tube, a SUPEL C18 cartridge was inserted and subsequently washed with 1ml of acetylnitrile/1% TFA, leaving a disc of fluid following low pressure suction to the cartridge. The SUPEL C18 cartridge was then washed with 1ml Chromanorm/1% TFA, again leaving a disc of fluid following low pressure suction. The peptide samples were rolled, added to the SUPEL C18 cartridge and allowed to drip in to a new 15ml conical tube. Any residual sample was washed with 1ml Chromanorm/1% TFA for 5-10 minutes. The purified peptides were eluted by adding 1ml acetylnitrile/1% TFA to the C18 cartridge. Sample quality was checked by taking 100μL from the peptide sample for SDS-PAGE banding. The remaining purified sample was dried over 1-2 hours and stored as appropriate at -20^{o}C.

Peptide Fractionation and Mass Spectrometry

The dried sample was reconstituted in 105μL of 0.03% Triethylamine in water before being fractionated in to 22 low-binding Eppendorfs, each being a 3 minute fractionation. The fractionated samples were then dried for 2 hours with centrifugation. After drying, 40μL pf 1% formic acid was added to each fraction, sonicated for 2 minutes, vortexed then centrifuged for 3 minutes. Finally, 20μL of each reconstituted fraction was placed in to a microvial and transferred to the cooling rack in preparation for fragmentation in to the 8 most abundant peptides per fraction by tandem mass spectrometry (MS/MS) with an Electrospray Ionisation (ESI) interface using a maXis impact UHR-TOF mass spectrometer and its associated software ProteinScape (both Bruker Daltonics, Bremen, Germany). Subsequent analysis of collision induced dissoci-

ation was performed against NCBInr using the Mascot search algorithm to generate Swiss-Prot accession numbers to identify corresponding proteins using the STRING: functional protein association networks database (version 10.5) for functional expression analysis.[258] Immunohistochemistry was performed on paraffin-embedded sections with a peroxidase detection technique, with 3,3'-Diaminobenzidine (DAB) as the substrate, previously described.

4.2.9 Determining Functional Outcome of Fn14 Activation by TWEAK

To determine the functional outcome of Fn14 activation by TWEAK, unstimulated and stimulated cells as described above were exposed to either no TWEAK, a low concentration of TWEAK (10 ng/ml) or a high concentration of TWEAK (100 ng/ml) for a further 24 hours. Cells were then prepared for flow cytometry to determine apoptosis, autophagy, ROS and necrosis activity using a 4 colour assay developed by the Afford Group. In summary, apoptosis was tested using Annexin-V (Molecular Probes, Paisley, UK) emitting in the pacific blue channel on the 405 nm laser. Autophagy was investigated using Monodansylcadaverine (MDC) (Sigma-Aldrich, UK),that binds to autophagic vacuoles and emits in the pacific orange channel on the 405 nm laser. The ROS production was determined using DCF diacetate (Merck, Nottingham, UK,) that recognises a number of species including peroxides, super oxides and nitric oxide, with emission is via the FITC channel on the 488 nm laser, once cleaved by intracellular esterases to 2',7'-DCF whichrenderd it cell impermeable. Necrosis was quantified using 7-AAD (Molecular Probes, Paisley, UK) that intercalates with high affinity to GC-rich regions of DNA, with emission in the PE-Cy-5 channel on the 488 nm laser. Appropriate compensation of the 4 colour assay was determined by permeabilising the cells of 4 wells and attaching the fluorochromes in the above channels to CK19. The compensation matrix was calculated prior to the 4 colour assay being conducted on different experiments.

4.3 Results

As determined by immunohistochemistry, using DAB as the substrate, Fn14 is expressed mainly on diseased tissue (Figure 4.2). There is a very low expression of Fn14 in donor tissue not required for transplantation (Figure 4.2 A), whilst the diseased tissues stain at a stronger intensity. In ALD (Figure 4.2 B) Fn14 expression is limited to the ductular reactive regions around the Canals of Hering as located by the arrow. In PBC (Figure 4.2 C), overall there is a more widespread ductular reaction which stains with a higher intensity for Fn14 compared to ALD. In contrast, Fn14 expression in chronic rejected organs is more widespread and is seen not only in areas of ductular reaction, as demarcated by the arrows, but also on hepatocytes peripheral to the stroma.

4.3.1 Phenotyping of Cultured Human Primary Cholangiocytes and Cell Lines

Phenotyping of the cultured human primary cholangiocytes and cell lines is used to determine if the cells cultured are adequate model of those seen in tissue. Representative gating strategies for primary cholangiocytes (Passage 4 PBC) and the AKN-1 cell line are shown (Figure 4.3 A & B respectively). The forward:side scatters of the primary cholangiocytes are more diverse compared to the AKN-1 cell line suggesting a more heterogeneous population. The forward scatter:pulse width of the primary cholangiocytes are more tightly grouped, demonstrating that a higher proportion of the primary cells are singlets compared to the AKN-1.

Quantitatively, the differences between the different cell types are shown in Figure 4.4. The primary cells are cholangiocytes from: passage 2 (P2) NASH; P4 PBC; P5 PBC; P5 ALD; P6 ALD; P6 Donor. Generally, all cell types are CD31 low, CD90 low, CK18 high and CK19 high. However, there are differences between cell types or each marker. There is a higher amount of CD31 in the primary cells compared to the AKN-1 cell line (MFI Primary 11.54 cf. AKN-1 7.81, $p < 0.05$), however there is no such difference between the primary cells and the cholangiocarcinoma cell-line CC-SW-1. Additionally, there is a higher amount of CD90 in the

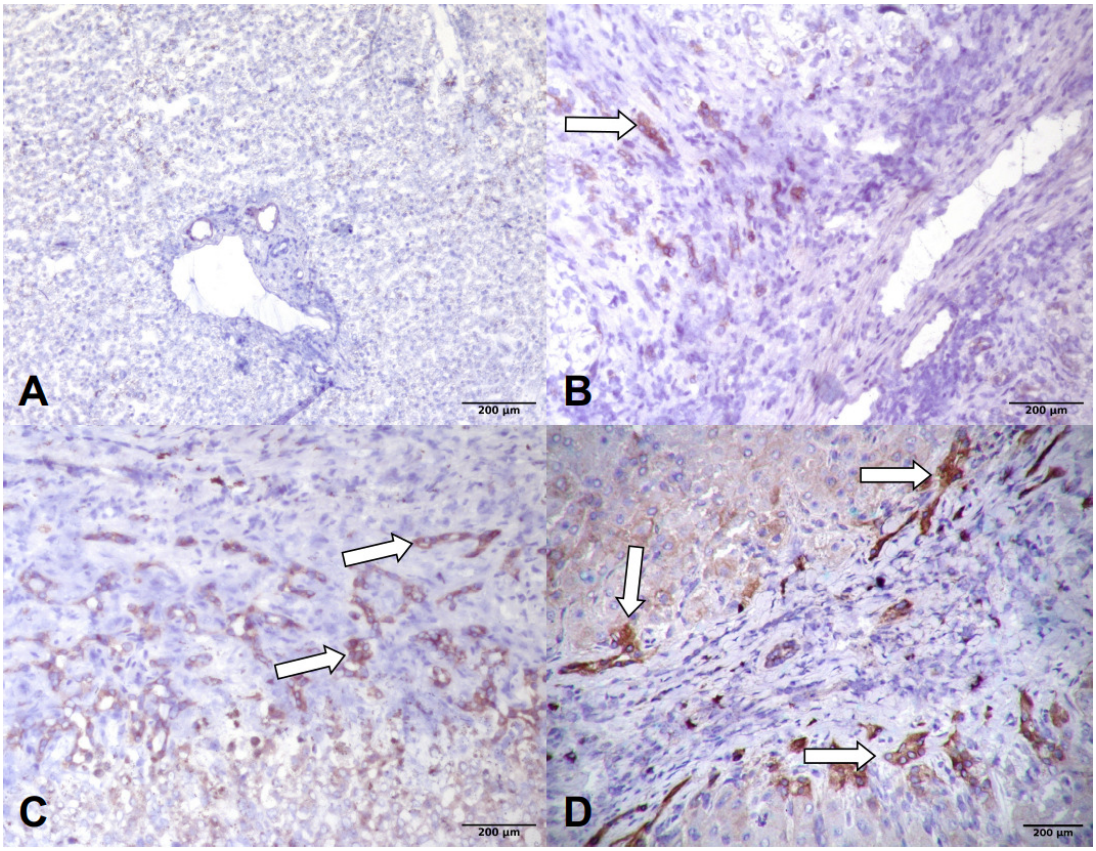

Figure 4.2: Expression of Fn14 in normal and diseased tissue by immunohistochemistry. (A) Donor tissue, (B) ALD, (C) PBC, (D) chronic rejection. Staining uses DAB as a substrate and haematoxylin as the counterstain. Arrows indicate areas of ductular reaction around the Canals of Hering.

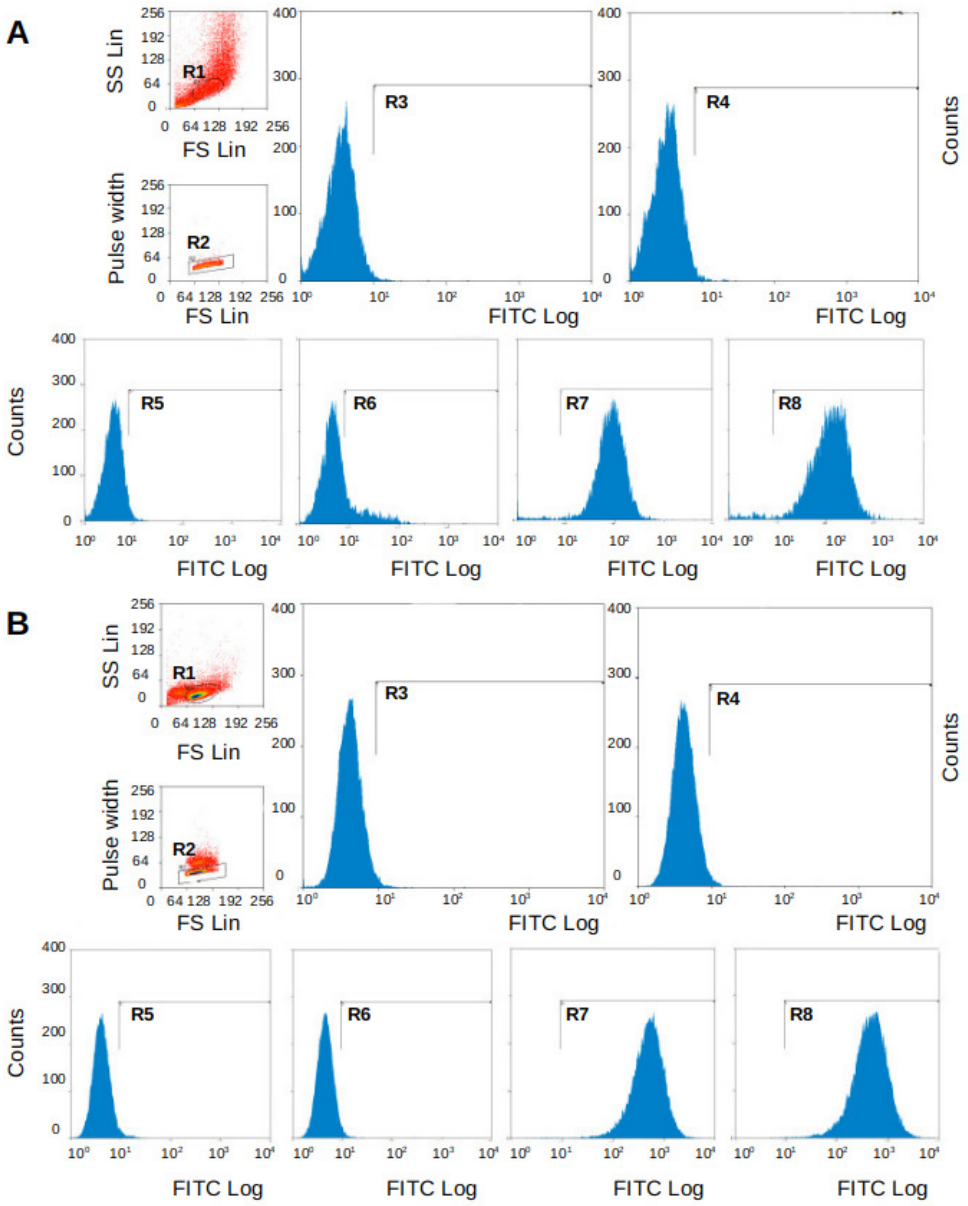

Figure 4.3: Phenotype of cultured human cells by flow cytometry. (A) Passage 4, primary cholangiocytes from a PBC liver, (B) AKN-1 cell line, N = 4 for each cell type. Gating strategy: R1, Forward:Side Scatters gating to R2, Forward Scatter:Pulse Width. Histograms are log fluorescent intensity versus event count gated from R2, Forward Scatter:Pulse Width. R3, Cells only; R4, 2% positive cells for IgG1; R5, CD31; R6, CD90; R7, CK18; R8, CK19. R5-8 same FITC Log as R4.

primary cells compared to the AKN-1 cell line (MFI Primary 26.20 cf. AKN-1 7.98, $p < 0.05$). Again, no difference exists between the primary cells and the CC-SW-1 cell line. There appears to be differences in the CK18 and CK19 contents between cell types but this is not statistically different.

4.3.2 Fn14 Expression *In Vitro* by Immunohistochemistry and Immunofluorescence

Using immunohistochemistry, primary human cholangiocytes (P6 ALD) that were cytospun on to poly-L-lyseine coated slides are a heterogeneous group of cells as shown by the variability in cellular size on haematoxylin staining (Figure 4.5). CK19 staining, demonstrating mature cholangiocytes, is expressed at a higher intensity on the smaller diameter cells. In contrast, Fn14 is expressed on these cells at a higher intensity on the larger cells.

Immunofluorescence on cytospun primary cholangiocytes demonstrates Fn14 is present on the majority of the cholangiocytes (Figure 4.6). Fn14 is distributed across the plasma membrane of cholangiocytes and within the cytoplasm. Additionally, there are areas of much higher intensity within the cytoplasm, suggesting storage of Fn14.

4.3.3 Determining Optimum Concentration of Fn14 Antibody for Flow Cytometry

The optimum concentration of the Fn14 antibody is demonstrated using the titration by doubling dilutions (Figure 4.7). The overlay histograms generated by flow cytometry in the AKN-1 cell line show a decrease in the percentage positivity of the cells with low concentrations of the Fn14 mouse anti-human antibody (Figure 4.7 A). A 2% positivity for the IgG1 isotype control antibody was used to ensure that positivity of the Fn14 antibody was more than two standard deviations away from the mean of the isotype control, hence this could not be a result of chance. Quantitatively, the percentage of AKN-1 cells positive for Fn14 was 79.02%, 78.03%, 74.97%, 65.73%, 59.16% and 37.32% when titrated to 1:25 (148 ng/ml), 1:50 (74 ng/ml), 1:100 (37

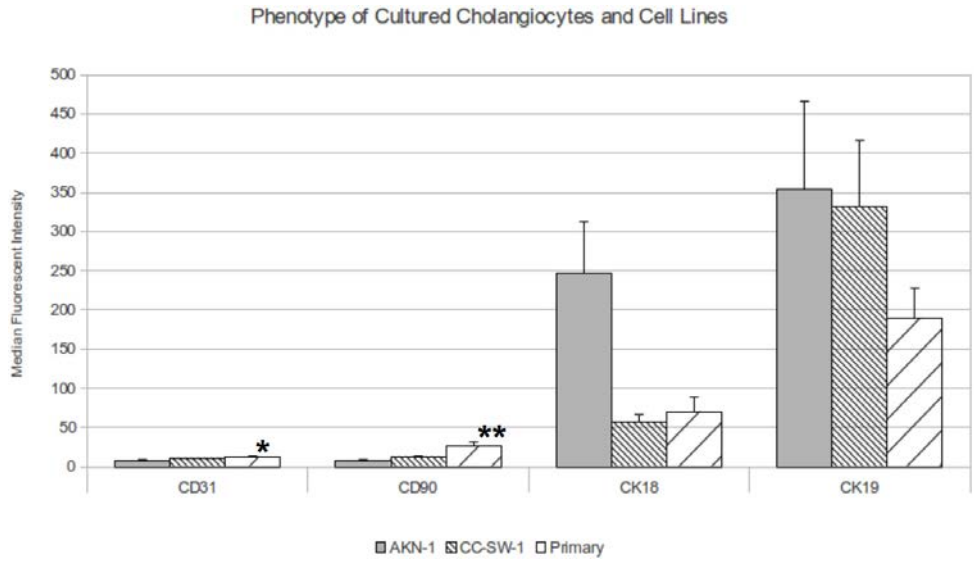

Figure 4.4: Phenotype of primary cholangiocytes, AKN-1 cell line and CC-SW-1 cell line expressed as MFI. Left to right CD31, CD90, CK18, CK19. AKN-1 represented by grey bars, cholangiocarcinoma cell line CC-SW-1 represented by tight hatched bar, primary cholangiocytes represented by wide hatched bars, N = 4 for each cell type. Error bars indicate standard error. * and ** indicate statistical difference from AKN-1 cell line using two-tailed students' T-test, with $p < 0.05$.

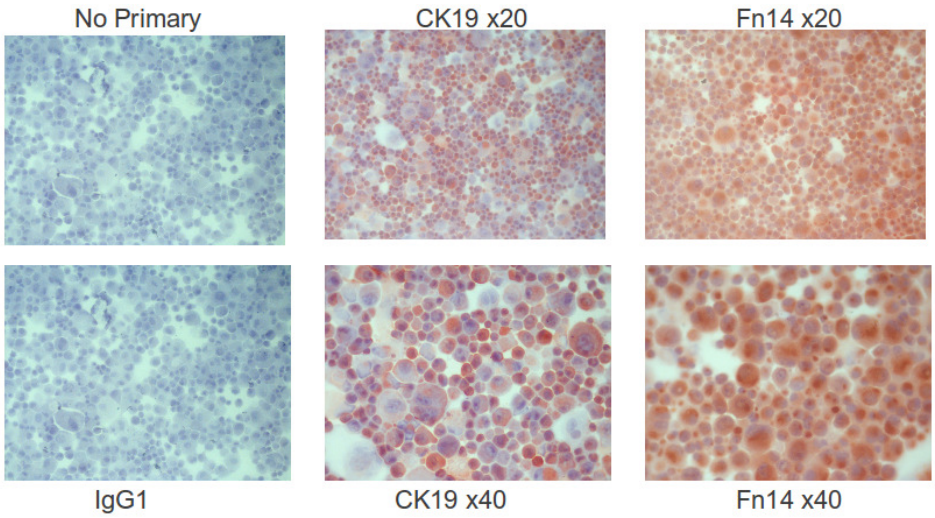

Figure 4.5: Fn14 expression on primary cholangiocytes by immunohistochemistry. Cytospun primary human cholangiocytes (P6 ALD) stained for CK19 and Fn14, imaged with 20x and 40x objective. No primary and concentration matched isotype controls also shown. Counterstaining with haematoxylin.

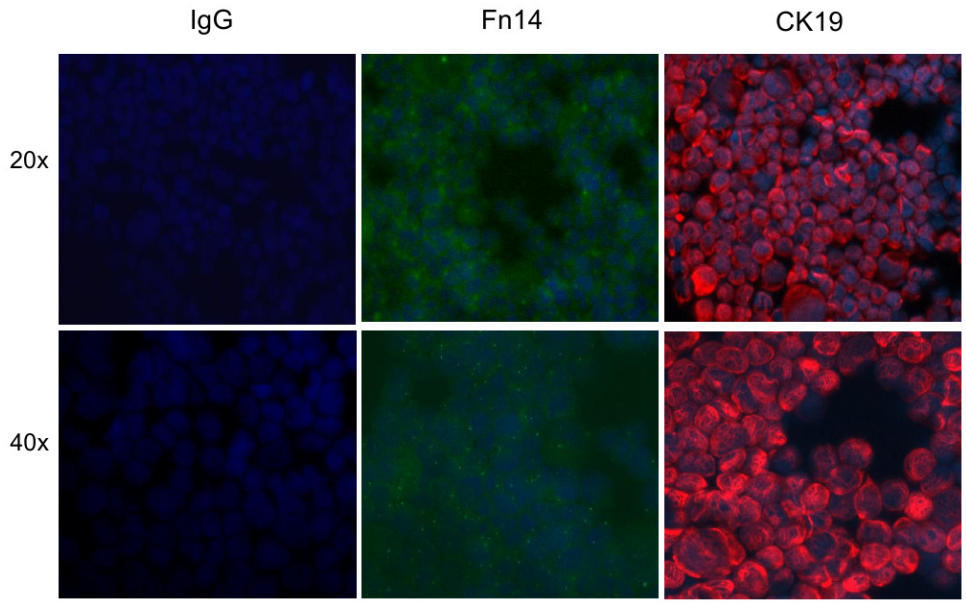

Figure 4.6: Fn14 expression on primary cholangiocytes by immunofluorescence. Cytospun cholangiocytes stained using DAPI nuclear stain (blue) and isotype control (left), Fn14 (centre, FITC) and cholangiocyte marker CK19 (right, TXRD).

ng/ml), 1:250 (14.8 ng/ml), 1:500 (7.4 ng/ml) and 1:1000 (3.7 ng/ml) respectively (Figure 4.7 B). A similar pattern in the decrease of percentage positive cells at different dilutions was seen in the CC-LP-1 and CC-SW-1 cholangiocarcinoma cell lines. For further flow cytometry a dilution of 1:100 (37 ng/ml) was considered to be appropriate.

4.3.4 Trypsin Sensitivity of Fn14

Although the smallest of the TNF receptor superfamily, the extracellular domains of the Fn14 receptor exist in the extracellular glycocalyx. The forward:side scatters demonstrate that the AKN-1 cells dissociated from the coated flasks using Cell Dissociation Buffer (CDB) generated more debris compared to using trypsin (Figure 4.8 A1 & B1). Using CDB prevented the AKN-1 cells from forming couplets or triplets, as shown by a higher proportion of cells within the singlet gate on the forward scatter: pulse width compared to cells dissociated with trypsin (Figure 4.8 A2 & B2). However, there was no difference between Fn14 expression using the different dissociation methods (Percentage postitive cells Trypsin 80.33% cf. CDB 73.39%, p = 0.239)(Figure 4.8 A3 & B3). Similar results are seen with the other cell lines CC-LP-1 and CC-SW-1.

4.3.5 Surface and Intracellular Expression of Fn14

Surface and intracellular expression of Fn14 by different cell types was investigated quantitatively (Figure 4.9). The primary cells were cholangiocytes from: P2 NASH; P4 PBC; P5 PBC; P5 ALD; P6 ALD; P6 Donor. The AKN-1 and CC-SW-1 cell lines were also used. Generally, for all models there was a higher expression of Fn14 intracellularly compared to the cell surface. There was a higher amount of Fn14 intracellularly compared to the cell surface for CC-SW-1 cholangiocarcinoma cell line (Percentage positive cells Intracellular 81.48% cf. Surface 69.02%, $p < 0.05$). Although there was a trend for the intracellular expression of Fn14 to be higher compared to the surface in the primary cells (Percentage positive cells Intracellular 80.54% cf. Surface 53.57%) and the AKN-1 cell line (Percentage positive cells Intracellular

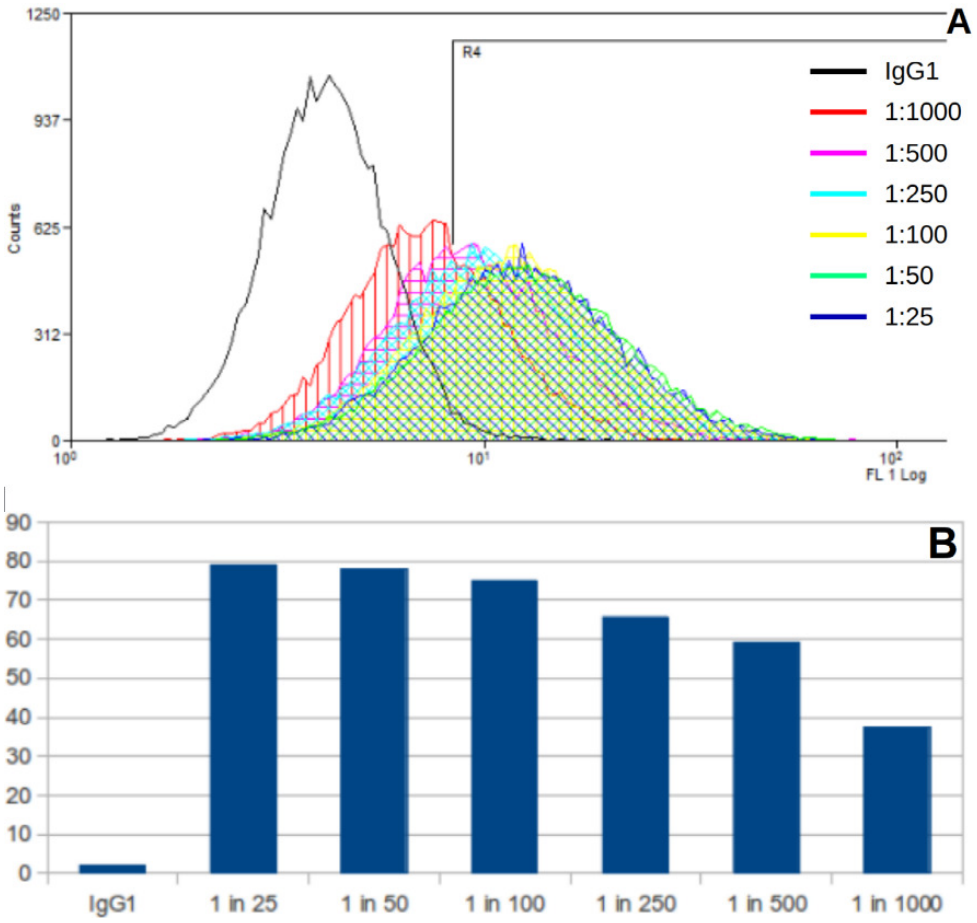

Figure 4.7: Determining optimum Fn14 antibody concentration by doubling dilutions. Overlay histograms demonstrating Fn14 expression in cultured AKN-1 cholangiocytes by flow cytometry (A). Unfilled histogram represents IgG1. Other histograms, from left to right, represent expression using progressively higher Fn14 antibody concentrations, 1:1000, 1:500, 1:250, 1:100, 1:50 and 1:25. Region R4 based on 2% positivity for IgG1 cells. Percentage positive cells for different concentrations of Fn14 antibody based on region R4 (B).

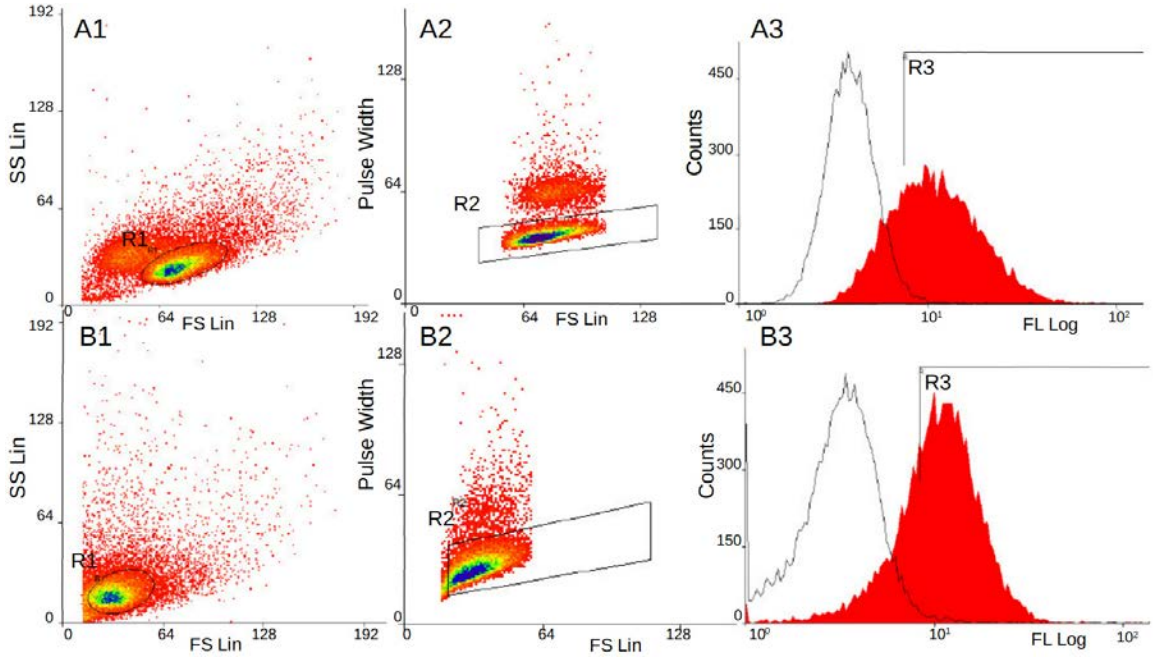

Figure 4.8: Determining the trypsin sensitivity Fn14. Flow cytometry of AKN-1 cell line dissociated from collagen coated flasks using trypsin (A) and CDB (B). From left to right, Forward v side scatter (1), forward scatter v pulse width (2) and log FITC v event count (3). MFI for trypsin and CDB dissociated cells not statistically different. Figure representative of N = 4 experiments.

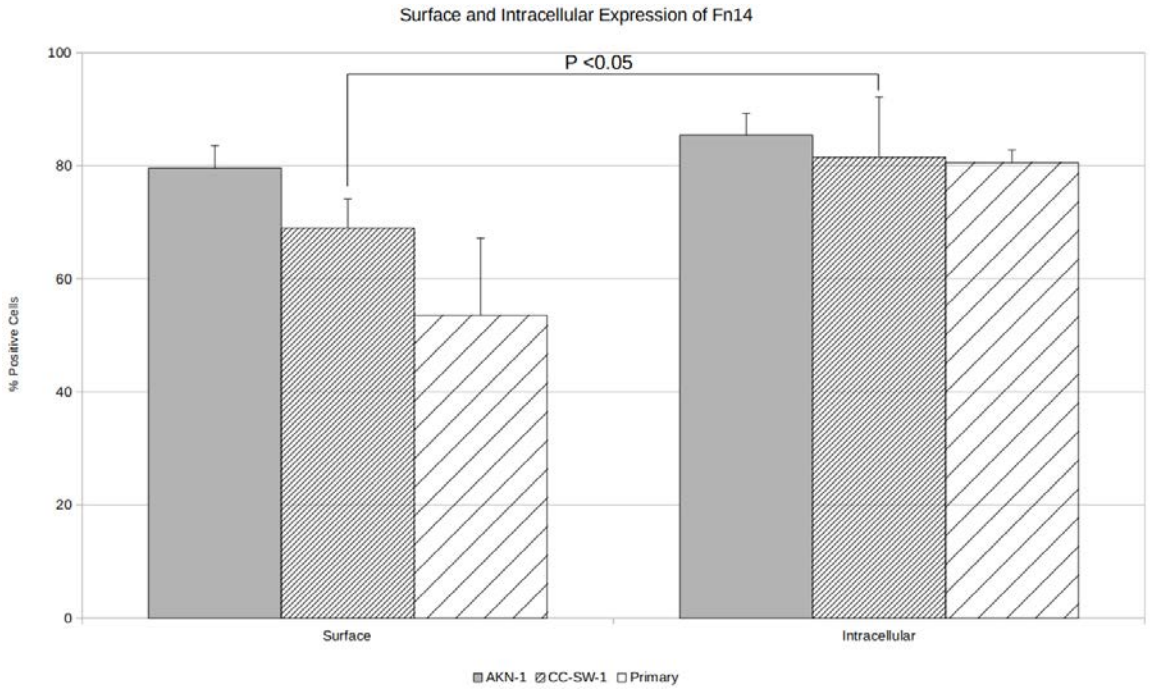

Figure 4.9: Surface and intracellular expression on Fn14. Summary of quantitative flow cytometry for surface and intracellular expression of Fn14 on primary cholangiocytes (wide hatched bars), AKN-1 cell line (grey bars) and CC-SW-1 cholangiocarcinoma (narrow hatched bars) cell line. N=4 for each cell type. Error bars indicate standard error. Line indicates higher intracelleular expression of Fn14 from cell surface in the CC-SW-1 cell line expression using two-tailed students' T-test, with $p < 0.05$.

85.41% cf. 79.60%), it does not reach statistical significance.

4.3.6 Expression of Fn14 Stimulation After 24 Hours of Cytokine Stimulation

The expression of Fn14 changed when the different models were exposed to cytokine stimulation for 24 hours (Figure 4.10). In the AKN-1 cell line, Fn14 expression, based upon MFI increased after exposure to TNF-α stimulation (1.07; 95% CI=1.05-1.09; $p < 0.05$) and FGF-b (1.29; 95% CI = 1.25-1.34; $p < 0.01$) relative to no stimulation at 24hrs. There was no decrease in Fn14 expression after 24 hours of IFN-γ stimulation in the AKN-1 cell line. Again, the primary cells are cholangiocytes from: P2 NASH; P4 PBC; P5 PBC P5 ALD; P6 ALD; P6 Donor. Although there was a decrease in Fn14 surface expression at 24 hours of IFN-γ stimulation (0.84; 95% CI = 0.76-0.91; $p < 0.05$), there was no decrease in Fn14 expression after 24 hours of TNF-α and FGF-b stimulation.

4.3.7 Expression of Fn14 on Cholangiocarcinoma Is Confirmed by Mass Spectrometry

Confirmation of extraction of the cell surface proteome was confirmed by gel electrophoresis using SDS-PAGE (Figure 4.11). The intensity of the cell surface peptides in the gel was in keeping as a proportion of the whole cell peptides that demonstrated a greater intensity on the gel. Mass spectrometry yielded spectra that highlighted abundant peptides (Figure 4.12). In total, 862 cell surface enriched proteins were common to all three of the final samples that had maximised their yield over the course of the protocol development (Figure 4.13). Further analysis revealed that of the 862 proteins identified, 271 (31.4%) were components of the plasma membrane, with gene products having a moiety embedded in the membrane. Most (135 proteins) were integral to the plasma membrane, having gene products that penetrate at least one leaflet of the bilipid layer (Figure 4.14). The cell surface proteins could also be categorised according to their preclinical and clinical applications. From this, it could be seen that markers used in the clinical staging of cholangiocarcinoma, such as CK19, as well as cancer stem

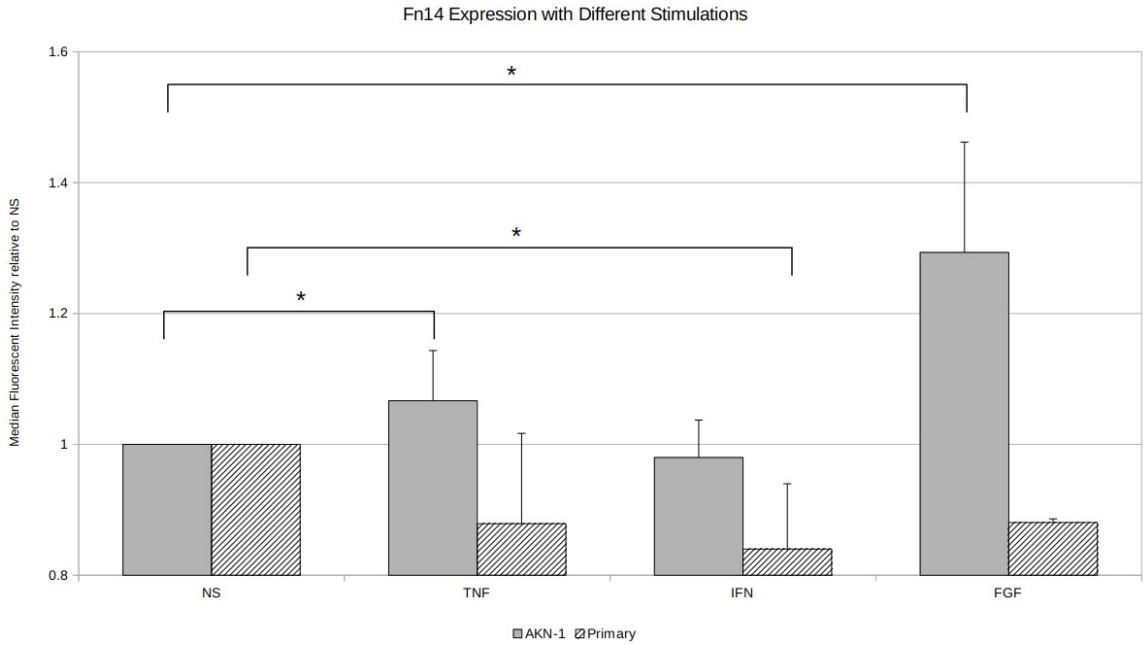

Figure 4.10: Surface expression of Fn14 after 24 hours of cytokine stimulation on cholangiocytes. Flow cytometry for surface expression of Fn14 after 24 hours of cytokine stimulation on primary cholangiocytes (narrow hatched bars) and AKN-1 cell line (grey bars). Results expressed as median fluorescent intensity relative to unstimulated cells for each cell type (N=6). Error bars indicate standard error. Asterisk and double asterisk indicates statistical difference from expression on unstimulated cells using two-tailed students' T-test, with $p < 0.05$. NS = no stimulation.

cell markers (EpCAM, Neural Cell Adhesion Molecule (NCAM)) in addition to differentiation markers (Frizzled-2, -6 and NOTCH-2, -3) and Fn14, also kown as TNFRSF12A (Figure 4.15). Further verification of the presence of Fn14 in cholangocarcinoma was provided by immunohistochemical staining of tissue as well as that of CK19 (Figures 4.16 & 4.17). A list of all cell surface proteins identified in the cholangiocarcinoma cell line for each experiment, those that were shared with all experiments and categorised by cellular location can be found at: https://doi.org/10.5072/eData.bham.00000362

4.3.8 Functional Outcome of Fn14 Activation by Recombinant TWEAK

The gating strategy adopted for investigating the functional outcome of Fn14 activation by TWEAK on the CC-LP-1 cholangiocarcinoma cell line is shown in Figure 4.18. After 24 hours of cytokine stimulation, followed by a further 24 hours of cytokine stimulation and exposure to TWEAK, the forward:side scatter and forward:pulse width are similar to that of unstimulated cells. There is a demarcated population of cells, the majority of which form singlets.

The quantitative summary of the functional outcome of Fn14 activation by TWEAK in the CC-LP-1 cholangiocarcinoma cell line is shown in Figure 4.19. In general, the apoptosis response and ROS production are similar as are the autophagy and necrosis responses. For each cytokine stimulation, the sum of the percentage positivity for the different functional outcomes approaches 100%. In all cytokine stimulation models, the majority of the response to Fn14 activation is apoptosis and is at least 60%.

In the unstimulated, TNF-α stimulated and IFN-γ stimulated cells, exposure to TWEAK increases ROS production and apoptosis whilst decreasing autophagy and necrosis. However, in the FGF-b stimulated cells that up-regulates Fn14 receptor expression, exposure to TWEAK decreases apoptosis but increases autophagy and necrosis. Despite graphical appearances, statisitcally this is not proven, with the exception of autophagy, where all values are less ($p < 0.05$) than the reference of no stimulation and no TWEAK.

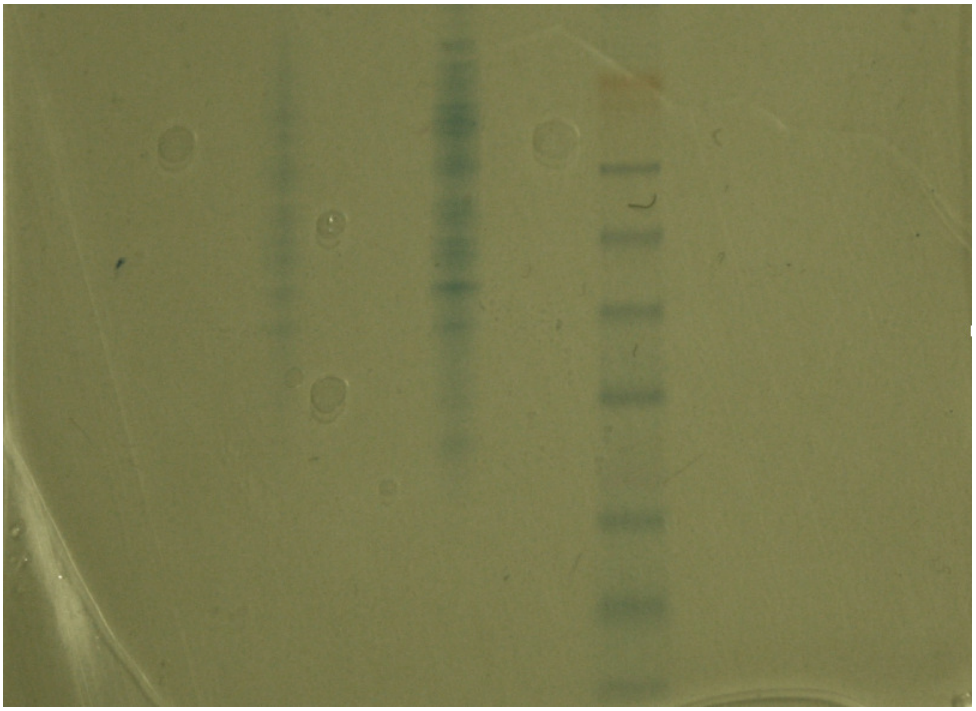

Figure 4.11: Gel electrophoresis confirming presence of the cell surface proteome. From left to right, surface peptides, whole cell peptides, standard ladder. The extent of the cell surface peptides is in keeping as a proportion of the whole cell peptides (middle).

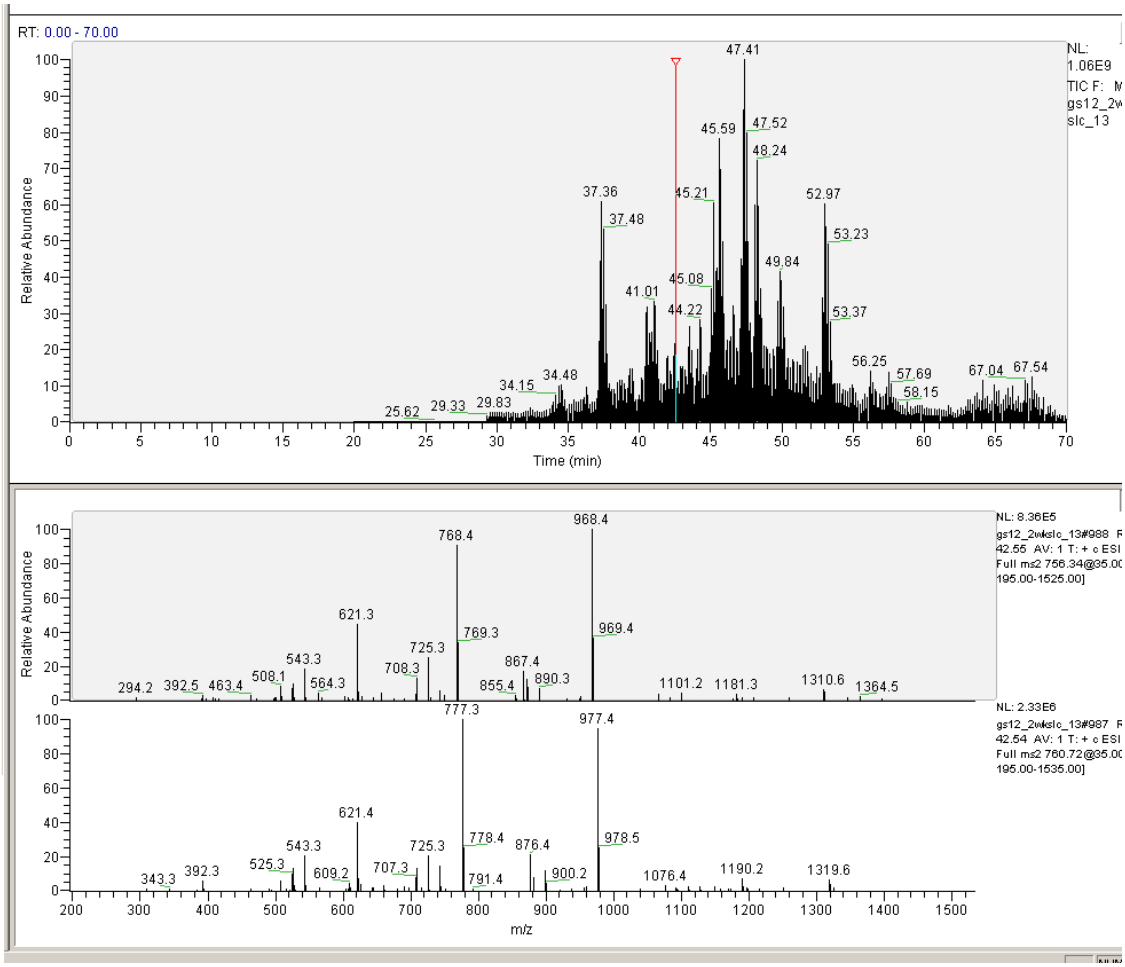

Figure 4.12: Typical spectrum obtained during ESI tandem mass spectrometry of cell surface peptides. The 8 most abundant peptides from the top spectrum were fragmented to enable analysis of collision induced dissociation against NCBInr using the Mascot search algorithm.

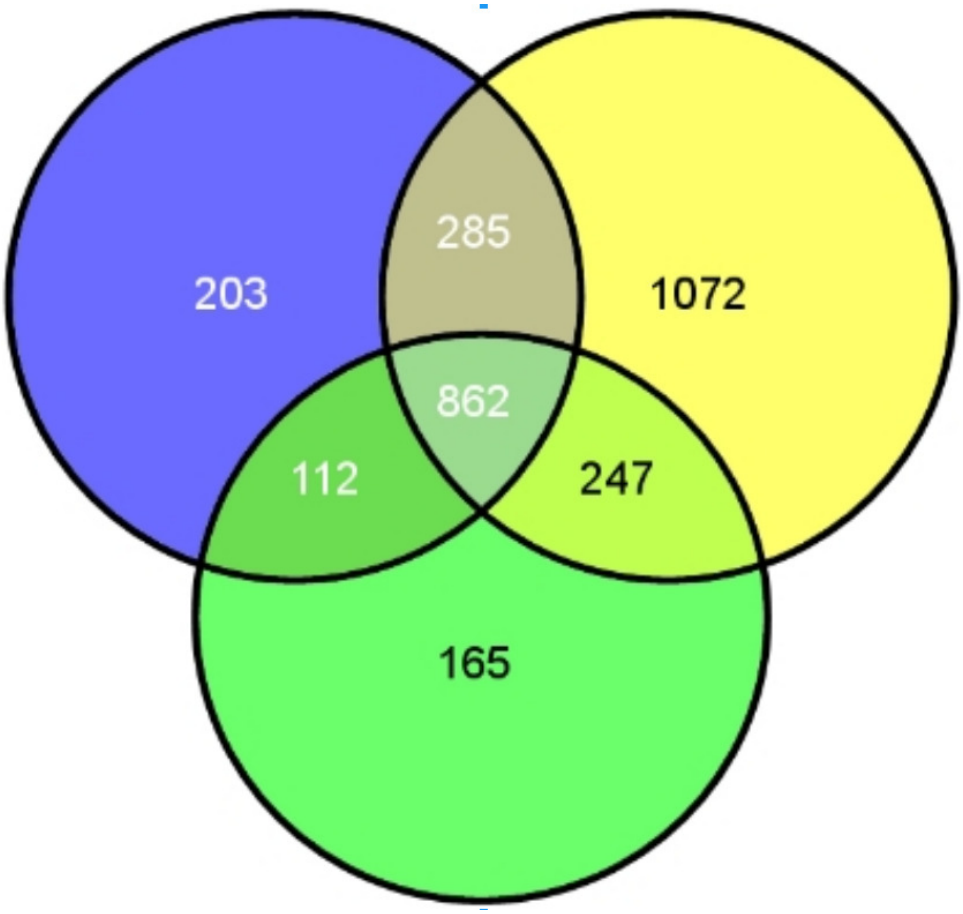

Figure 4.13: Venn diagram of cholangiocarcinoma cell surface proteins by cell surface proteomics. Each circle represents a single experiment of N=3. Despite optimising the yield of cell surface proteins, there was considerable disparity between the number of proteins detected on the cell surface proteome between each experiment. A total of 862 proteins were common to the three experiments, the basis of further analysis.

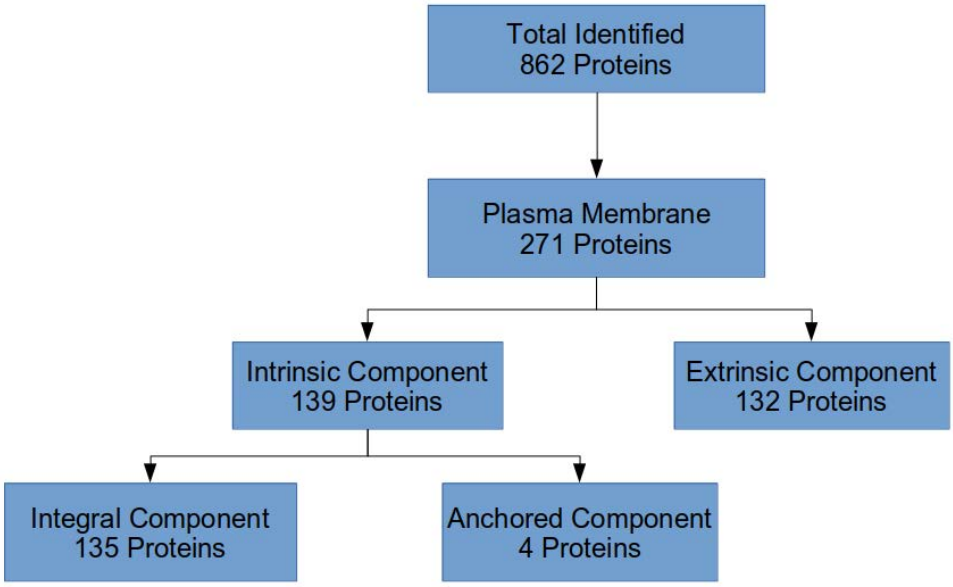

Figure 4.14: Location of identified proteins by cellular component. 135 of the 271 plasma membrane proteins identified from three experiments were integral components of the plasma membrane, having at least one gene product penetrating one leaflet of the bilipid membrane.

Clinical Staging of Cholangiocarcinoma	Cancer Stem Cell Markers	Differentiation Markers	TNF Receptors
KRT19	EPCAM	FZD2	TNFRSF12A
	NCAM1	FZD6	TNFSF10
	NCAM2	NOTCH2	
	PROM2	NOTCH3	

Figure 4.15: Categorisation of CC-SW-1 cell surface enriched proteins by application. Selected proteins categorised according to preclinical and clinical use. KRT = Cytokeratin; EPCAM = Epithelial Cell Adhesion Molecule; NCAM = Neural Cell Adhesion Molecule; PROM = Promonin; FZD = Fizzled; TNFRSF = Tumour Necrosis Factor Receptor Superfamily; TNFSF = Tumour Necrosis Factor Superfamily.

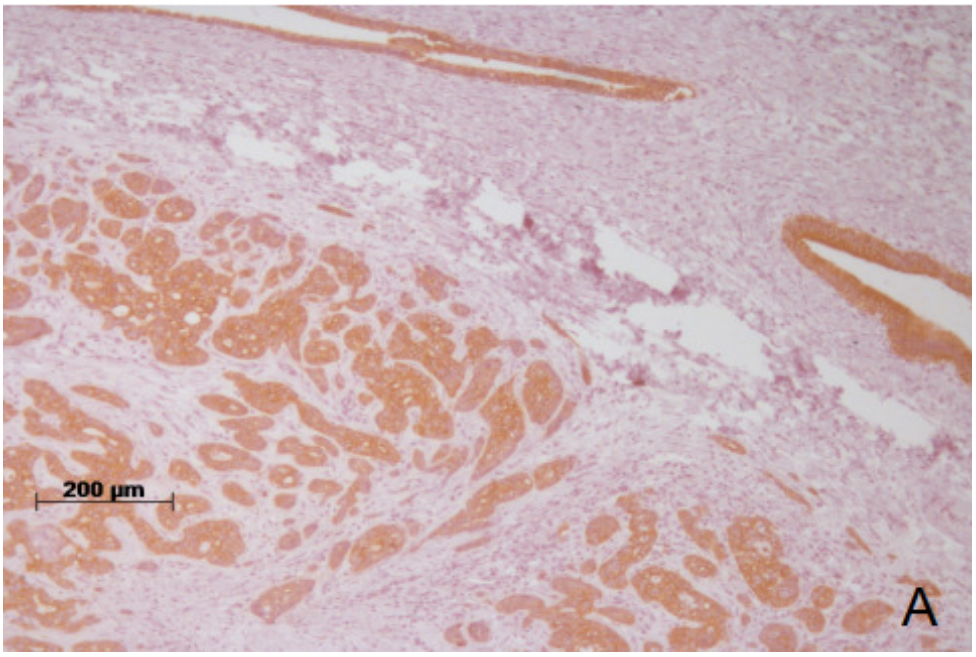

Figure 4.16: Confirmation of presence of CK19 on cholangiocarcinoma by immunohistochemistry. Immunohistochemistry of formalin fixed paraffin embedded an intrahepatic cholangiocarcinoma specimen for CK19, used to clinically stage disease, by DAB staining photographed at 10x objective.

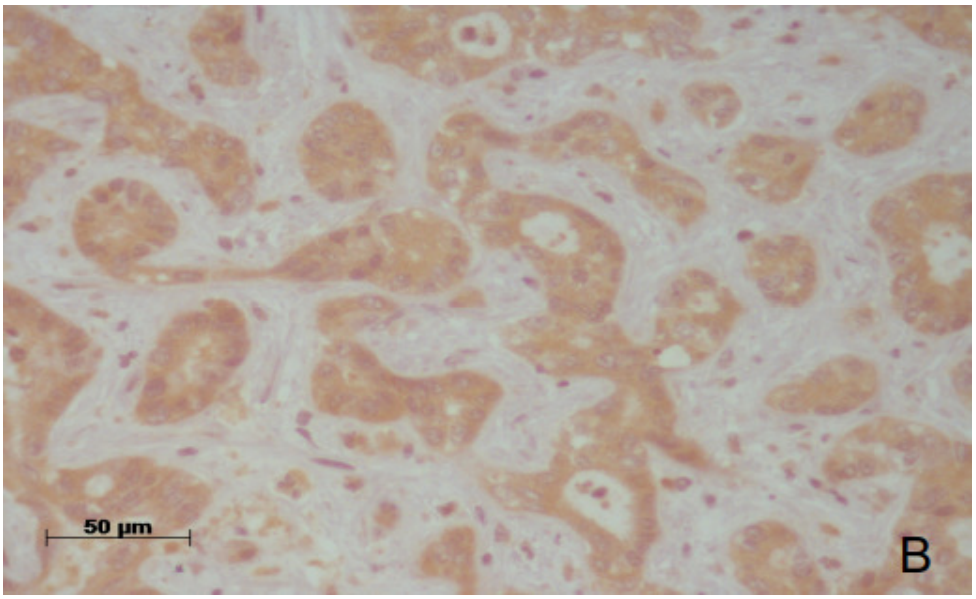

Figure 4.17: Confirmation of presence of Fn14 on cholangiocarcinoma by immunohistochemistry. Immunohistochemistry of sections from same formalin fixed paraffin embedded specimen as Figure 4.16 for Fn14, by DAB staining using earlier described method, photographed with 40x objective.

With the exception of unstimulated cells, a higher concentration of TWEAK results in lower ROS production and a decrease in apoptosis. In contrast and again with the exception of unstimulated cells, a higher concentration of TWEAK is associated with increased autophagy and necrosis.

4.4 Discussion

The principal findings of this project investigating the role of the Fn14/TWEAK receptor ligand in ductular reactive cell differentiation and bile ductule neogenesis during hepatic inflammation and repair are that:

1. Fn14 is expressed in diseased liver tissue and that the extent of expression is dependent on liver pathology.

2. Isolated and cultured primary human cholangiocytes from various liver diseases as well as the non-malignant AKN-1 cholangiocyte cell line and the cholangiocarcinoma CC-LP-1 and CC-SW-1 cell lines express Fn14.

3. Fn14 is not cleaved by trypsin but it remains to seen the functional impact that typsin has on Fn14.

4. Fn14 not only exists on the cell surface but also that considerable amounts of Fn14 exist within the cytoplasm of the different cholangiocyte models.

5. The expression of Fn14 is dependent on the inflammatory cytokines to which the cultured cholangiocyte are exposed and that the response varies depending on the cholangiocyte model used.

6. In FGF-b stimulated cholangiocarcinoma cell line, exposure to TWEAK decreases apoptosis but increases autophagy and necrosis in contrast to other cytokine stimulations.

7. A higher concentration of TWEAK tends towards a lower ROS production and a decrease in

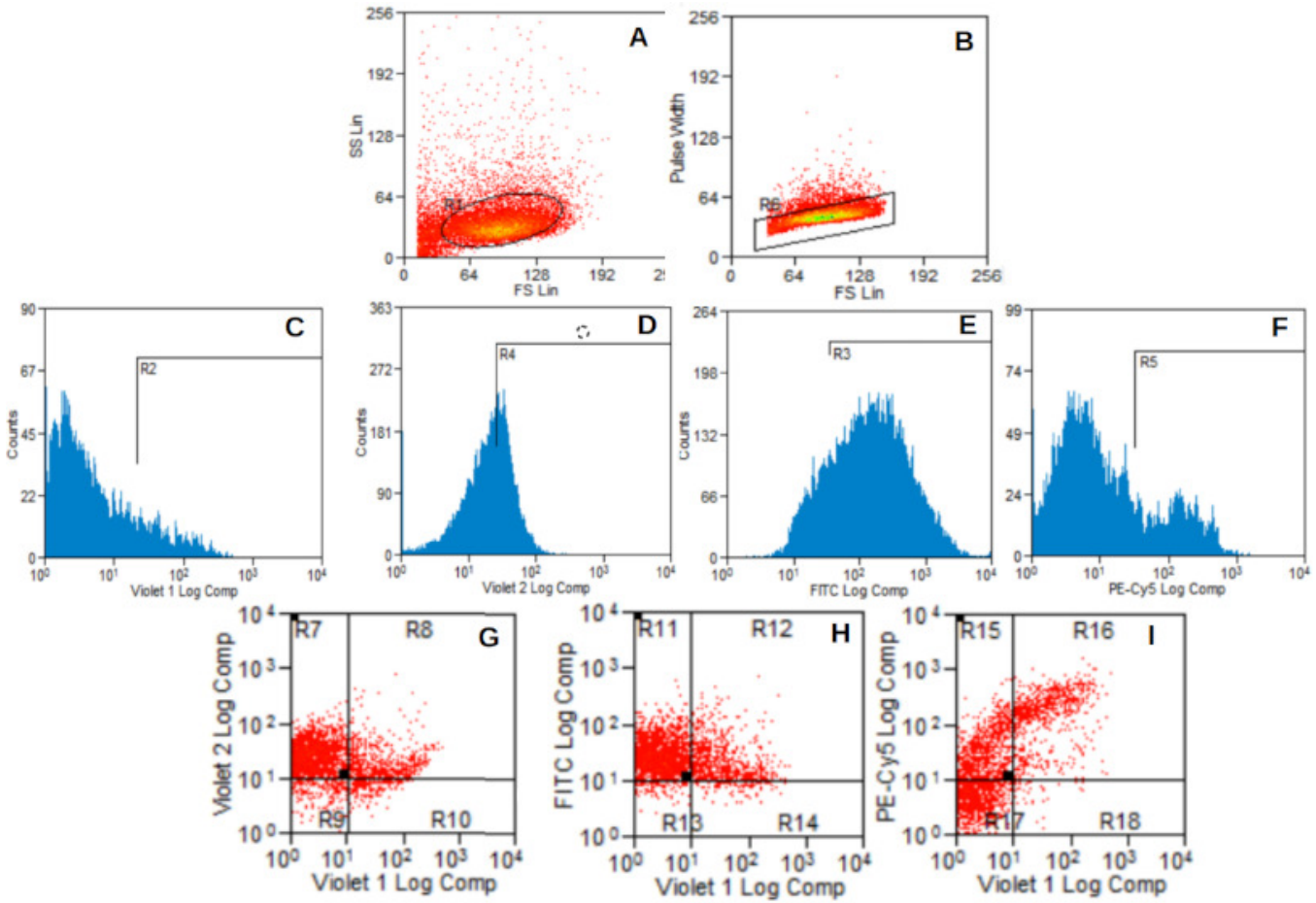

Figure 4.18: Gating strategy determining functional outcome of Fn14 activation in CC-LP-1 cholangiocarcinoma cell line after exposure to TWEAK for 24 hours. Gating strategy: A, Forward:Side Scatter gating to; B, Forward Scatter:Pulse. Histograms are log fluorescent intensity v event count gated from Forward Scatter:Pulse Width. Histograms: C, apoptosis; D, autophagy; E, ROS production; D, necrosis. Regions R2 to R5 determined by 2% positive cells of IgG1 population. Plots used in compensation based on fluorescent labelled CK19, compensation plots G-I.

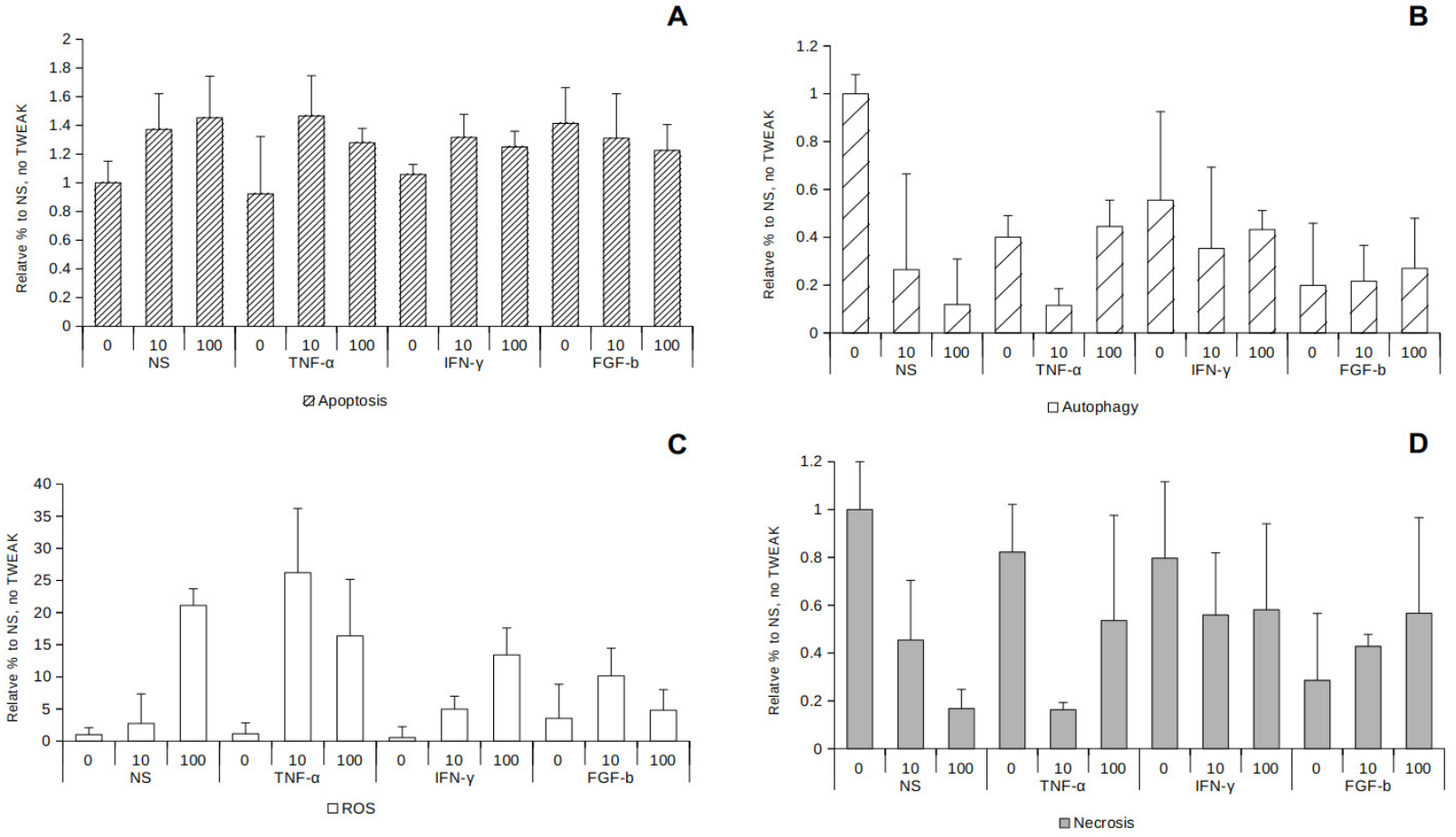

Figure 4.19: Functional outcome of Fn14 activation in cytokine stimulated CC-LP-1 cholangiocarcinoma cell line after exposure to TWEAK for 24 hours. Percentage positive cells for: A, apoptosis; B, autophagy; C, ROS production and; D, necrosis in 48 hour cytokine (TNF-a, IFN or FGF) stimulated cells exposed to either no TWEAK, low TWEAK (10 ng/ml) or high TWEAK (100 ng/ml) for the previous 24 hours, experiments N = 3.

apoptosis but is associated with increased autophagy and necrosis.

A particular strength is the use of cultured cholangiocytes isolated from human diseased livers. This is only possible as a result of the availability of human liver tissue from the adjacent Queen Elizabeth Hospital liver transplantation programme that has the highest transplant activity in the United Kingdom. Clearly, this is a highly valuable resource without which much of the project would not be possible.

Additionally, this project makes use of the non-malignant non-SV40 transformed AKN-1 cell line. The availability of the AKN-1 cell line means firstly that experiments can be optimised prior to investigations on the primary human cholangiocytes that are regarded as a precious commodity. Secondly, by demonstrating that the AKN-1 cell line is an appropriate model for primary isolated human cholangiocytes, these results can inform other groups to conduct experiments that would not otherwise be possible without access to human tissue. This ultimately means that data and knowledge can be assimilated more quickly that allow for translational research to be conducted earlier so that therapies may become available for the treatment of patients.

Confirming the presence of Fn14 on the cell surface proteome was designed to demonstrate improvements over more traditional methods such as Western Blotting, especially by reducing potential errors in processing. The fact that there was considerable variation in the number of proteins in the experiments demonstrates that in its current state, although it has a role in protein discovery, cell surface proteomics is still prone to significant errors using this particular cell surface enrichment technique. Other stages of the experimental design are more established. As the enrichment technique evolves, hopefully the variation in the end result will be attenuated. There is potential for this technique to contribute towards the construction of the protein atlas especially for relatively rare diseases, such as cholangiocarcinoma, where access to primary human tissue is limited.

Finally, by demonstrating that the phenotype of the cell lines CC-LP-1 and CC-SW-1 are not dissimilar to that of primary human cholangiocytes, further investigation may inform of the role of the Fn14/TWEAK receptor-ligand system cholangiocarcinoma, a disease that also has a high morbidity and mortality for which there are very few treatment options for patients. Detailed investigation of the differences in Fn14 expression between the primary cells and cell lines after 24 hours of cytokine expression needs to be conducted in the context of similar broad phenotype. The results from this data may be a funcion of the elements of the phenotype not investigated or an issue with the cell lines themselves. More detailed phenotype analysis is warranted.

Currently, there are a number of weaknesses in the data presented from this project to date. Most notable are the experimental numbers for the primary human cholangiocytes. Importantly, although the total number is adequate, experiments have been conducted on a number of different diseases, ranging from NASH, PBC, ALD and donor livers. The expression of Fn14 varies considerably between these diseases and therefore increases the standard deviation for these experiments. This subsequently influences any of the statistics that are conducted on the primary cholangiocytes and largely explains the lack of significance that might be expected from the results presented. This is a considerable sample bias. By stratifying Fn14 expression by type of liver disease, a true indication of Fn14 expression will be revealed.

A further issue with the use of the primary cholangiocytes is the variability in the passage number for the samples, ranging from P2 to P6. It is not known if Fn14 expression changes with passage number per disease type and therefore must be considered a considerable bias that also contributes to the high standard deviation values seen in results for experiments conducted on the primary cholangiocytes. This could be overcome by investigating Fn14 expression on cells in serial passages.

Although the activation of Fn14 by TWEAK has been investigated at 10 ng/ml and 100 ng/ml, further elucidation of the response should be investigated at the 1 ng/ml and 1000 ng/ml concentrations to allow for the formation of a dose-response curve. There have been reports of a

bipotent response (Burkly, unpublished data) at different concentrations of TWEAK however, this requires further clarification. Statistical analysis is further hampered by the low experimental number when investigating the effect of different doses of TWEAK on functional outcome of already cytokine stimulated cells. Due to the high number of variables, a student's T-test or even non-parametric equivalent are not robust enough to accept or reject any hypothesis using an experimental number of three, despite the graphical representations. The solution, is to use factorial ANOVA, ideally incorporating time as a factor to provide a repeated measures approach.

Following on from the above, it is not clear from the data at what time point TWEAK initiates its effect and if the cellular response is dependent on the prolonged activation of the Fn14 receptor. Evaluating the response to TWEAK using repeated serial time course experiments in the cholangiocytes and the various cell lines may provide further evidence of the reported bipotent response. This would give insight to the potential signalling mechanisms that could be investigated. This requires considerable numbers of samples within the experimental design and should include positive controls for apoptosis, such as the use of hydrogen peroxide or etoposide.[287, 288]

The functional outcome of Fn14 activation by different concentrations of TWEAK has been investigated by flow cytometry for apoptosis, autophagy, ROS production and necrosis. However, the extent of cellular proliferation after Fn14 activation by TWEAK has not been investigated. This is due to delays in developing the technique for the consistent assessment of proliferation by flow cytometry. Such issues are now almost overcome and further functional experiments will include proliferation as an output, so as to provide a more complete assessment. Additionally, the stage of the cell cycle after exposure to TWEAK could be investigated by flow cytometry.

There is a paucity of publications investigating the role of Fn14 in the liver. Those that exist relate mainly to the role of Fn14 in either murine and human models of hepatocellular carcinoma or its potential role in murine liver progenitor cells.[84, 85, 275, 282, 284] Additionally, Fn14

has been suggested to be a potential therapeutic target after transcriptome analysis revealed that it was up-regulated in patients with alcoholic hepatitis and predicted 90-day mortality and the severity of portal hypertension.[280] However, to date there are no publications directly addressing the role of Fn14 either cholangiocytes or cholangiocarcinoma or the cholangiopathies.

Studies in other organ systems have provided some insight in to the function of the Fn14/TWEAK receptor-ligand system. These show highly variable effects in renal, cardiac and rheumatic diseases. There has been some work investigating the signalling pathways involved in these other systems. Pathways implicated include JAK-STAT, EGFR, JNK and NF-kappa-B.[79] As yet my data neither addresses the intracellular signalling pathways involved nor the role that the scavenger receptor CD163 plays nor the effect of blocking the FGF-b signalling pathway on the Fn14/TWEAK receptor-ligand system. Currently, it is not clear if these signalling pathways are conserved between organ systems. Therefore, it would be disingenuous to speculate on the mechanisms through which Fn14 signalling in the liver is occurring.

Furthermore, despite some studies published purporting to investigate the role of this receptor-ligand system on murine liver progenitor cells, as yet there are no published techniques to isolate a pure liver progenitor cell populations in either the murine or the human models. Once this methodological technique has been established, the role of the Fn14/TWEAK receptor-ligand system in ductular reactive cell differentiation in human liver can be characterised.

CHAPTER 5

THE ROLE OF FN14/TWEAK DURING NORMOTHERMIC MACHINE LIVER PERFUSION

5.1 Introduction

To date, studies in to the role of Fn14 and TWEAK both *in vivo* and *in vitro*, as with many other systems, have been limited by the model used or the methods incorporated. *In vivo*, this includes but is not limited to the of use animal models that may not truly reflect the human biological system, whilst *in vitro* the cellular isolation technique and microenvironment might not result in a representative phenotype, despite best efforts.[85, 278, 289, 290] One approach that has been gaining traction is the use of microfluidic devices, in which cultured cells have a culture medium perfused over them in an attempt to mimic the *in vivo* environment.[291] Whilst this approach was oringially conceived to allow more accurate investigation of human physiology, it has since developed into a drug discovery tool as organ/body-on-a-chip.[292] This has been expanded to the development of bioreactor systems that have been assessed in human tumour models, an example being in breast cancer.[293] Direct comparison within the same microfluid chip based culture system of both animal and human tissue concurrently further allows assesment of potential drug candidates and towards the goal of personalised medicine.[294] Examples exist of bioprinted liver-on-a-chip systems for drug screening that incorporate hepatocyte organoids withina hydrogel scaffold to model the 3-dimensional environment of the liver.[295] [296] [297] [298] To date, this has been scaling up development from *in vitro* cell culture systems. Since the time of commencing this thesis, although a number of groups are reporting to be investigating the role of NMLP in studying liver disease, published data is awaited. It could be anticipated that relatively helathy donor livers, still rejected for transplantation, would be good candidates for such testing prior to attempts at perfusing resected liver specimen containing, for example, cancer. Nevertheless, NMLP might provide a more robust model to study disease and modulate biological systems, including the ability to administer novel therapeutics, whilst overcoming the potential issues surrounding animal testing. As a means that, one tested the hypothesis that NMLP could be used to investigate the role of the Fn14/TWEAK receptor ligand system in an *ex vivo* human model.

5.2 Materials & Methods

The normothermic machine, the perfusion fluid, the 12 livers used, the sampling protocol, spectral analysis and the machine, fluids, livers, sampling protocol, slide scanner methodology, spectral analysis and statistical techniques using 2-way repeated measures factorial ANOVA have been described in Chapter 2. The rabbit anti-human Fn14 antibody and the method for immunohistochemical staining of generated specimens using the semi-automated Sequenza®rack and Coverplate^{TM}system (Thermo Scientific, Runcorn, UK) have been described in Chapters 4 and 2.

The rationale for using Van Gieson (VG) was to demonstrate collagen within with the specimens. Once batches of sections had been taken to water, they were stained with Celestine Blue (Sigma Aldrich, Gillingham, UK) for 5 minutes. After washing in a water bath for 2 minutes, repeated twice, they were stained in Harris Haematoxylin (PFM Medical, Poynton, UK) for 4 minutes, followed by a further wash in water for 2 minutes. Subsequently, slides were dipped in 1% Acid Alcohol for 30 seconds followed by a water bath for 2 minutes. Following a wash in Scott's Tap Water Substitute for 30 seconds and another wash in water for 2 minutes, slides were stained with VG solution (PFM Medical, Poynton) for 3 minutes. Excess stain was rinsed off using alcohol before slides were taken back to Xylene and mounted in DPX using glass coverslips as previously described. Any collagen in the tissue would then be seen as bright red, nuclei blue or black and cytoplasm yellow.

A one-way Analysis of Covariance (ANCOVA) was performed to determine a statistically significant difference between intensity density staining of Fn14 and VG, controlling for viability and testing for unbalanced data using Type II sum of squares. This was accomplished using the 'car' R package.

5.3 Results

Titrations of the anti-human Fn14 antibody were performed to confirm the correct dilution to be used. Sections from the same PSC specimen were used with dilutions ranging from 1:50 to 1:400, N = 3 for each dilution, after which sections were subjected to spectral analysis via the slide scanner (Figure 5.1). This confirmed that 1:100 was the most appropriate dilution, balancing adequate chromagen staining, whilst ensuring that a range of chromagen intensities across the section could be observed (Figures 5.2 and 5.3) This was congruent with the concentration of the anti-human Fn14 antibody utilised for manual staining as described in Chapter 4.

Sections stained with anti-human Fn14 antibody were categorised according to viability across different NMLP timepoints (Figure 5.3). Both non-viable (n=5, Figure 5.3 A,C,E) and viable (n=3, Figure 5.3 B,D,F) appeared to have higher intensity staining at the end of NMLP (Figure 5.3 E & F respectively), with non-viable at the start of NMLP higher than viable livers (Figure 5.3 A & B respectively). At higher resolution, the differences between viable and non-viable livers becomes more apparent, with increased staining in the viable group and a possible morphological ductular reaction noted at 3 hours of NMLP and beyond (Figure 5.4).

Spectral analysis of intensity density against perfusion time and viability was performed (Figure 5.5). Graphically, there appeared to be a trend towards higher intensity density in viable livers towards the end of NMLP compared to non-viable livers. However, repeated measures ANOVA demonstrated the main effect for viability yielded a F value of $F = 0.162$, $p > 0.05$, indicating that the effect for viability was not significant. The main effect for perfusion time yielded a F value of $F = 2{,}574$, $p > 0.05$, indicating that the effect for NMLP time was not significant. The interaction effect was insignificant, $F = 0.952$, $p > 0.05$.

Sections stained with VG were categorised according to viability across different NMLP timepoints (Figure 5.6). Viable livers (n=3, Figure 5.6 B,D,F) appeared to have higher intensity staining at the end of NMLP compared to non-viable (n=5, Figure 5.6 A,C,E) Viable livers appeared to have less staining intensity for VG at the start of NMLP compared to non-viable livers

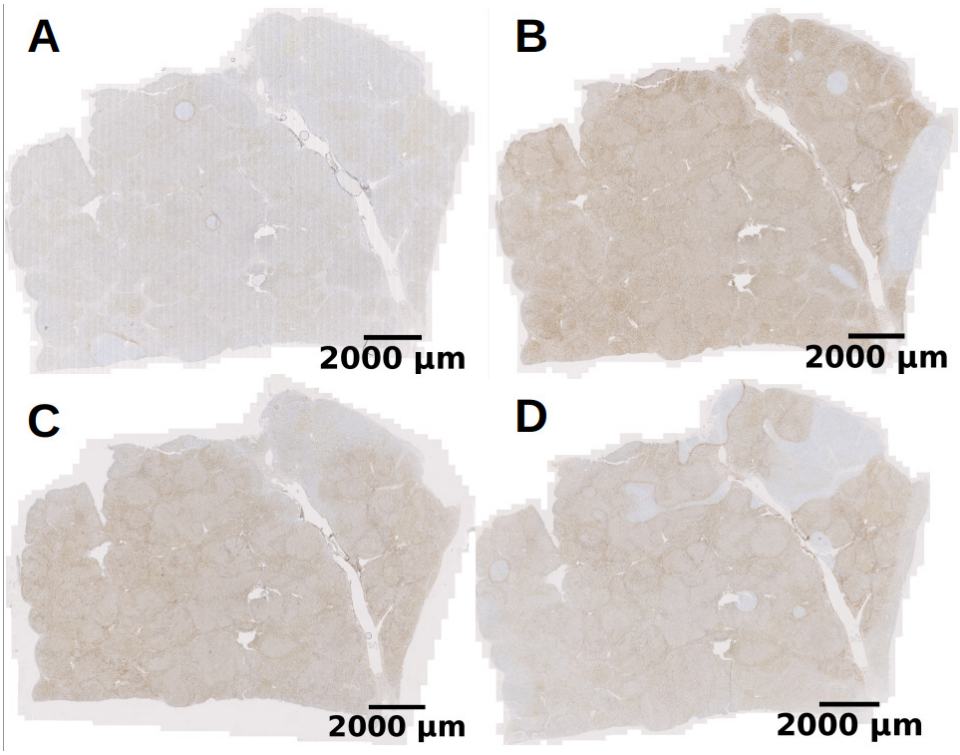

Figure 5.1: Representative immunohistochemistry of Fn14 antibody titrations for use with the slide scanner. Sections from the same PSC specimen subjected to titrations of anti-human Fn14 antibody as previously described. A, control; B, 1:50; C, 1:100; D, 1:400

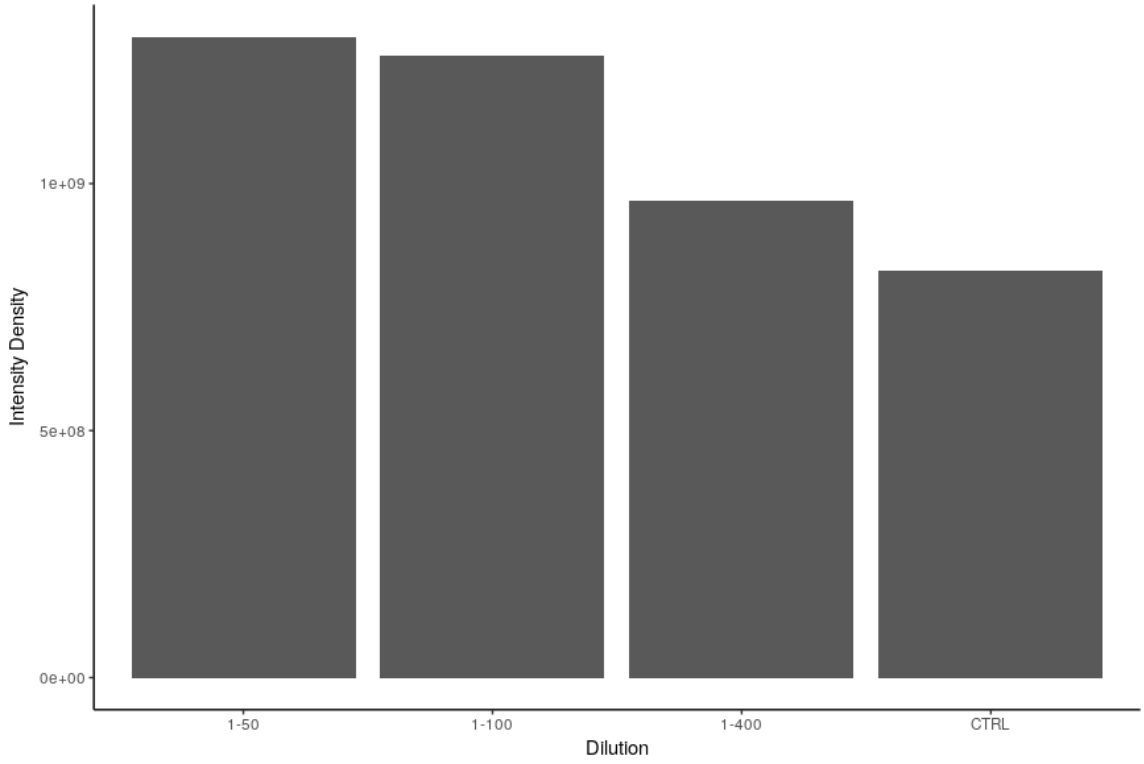

Figure 5.2: Titrations of Fn14 antibody for use with the slide scanner. Sections from the same PSC specimen were subjected to titrations of anti-human Fn14 antibody as previous described, to ascertain the best concentration to use for slide scanning.

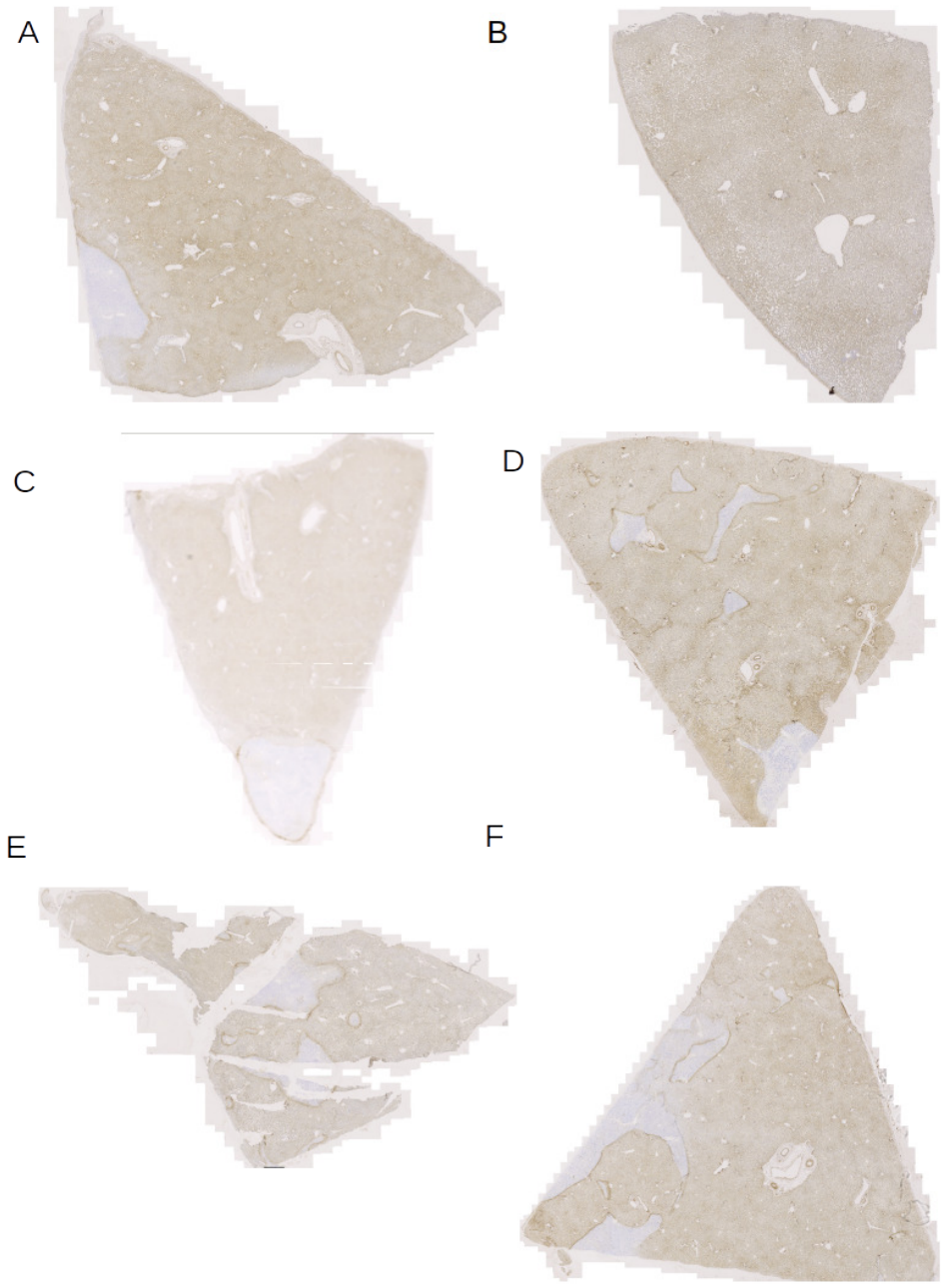

Figure 5.3: Fn14 staining in livers subjected to NMLP by viability. A,C,E non-viable; B,D,F viable; A,B at start of NMLP; C,D after 3 hours of NMLP; E,F at end of NMLP. All photographs using the Axio Scan Z1 (Zeiss, GmBH).

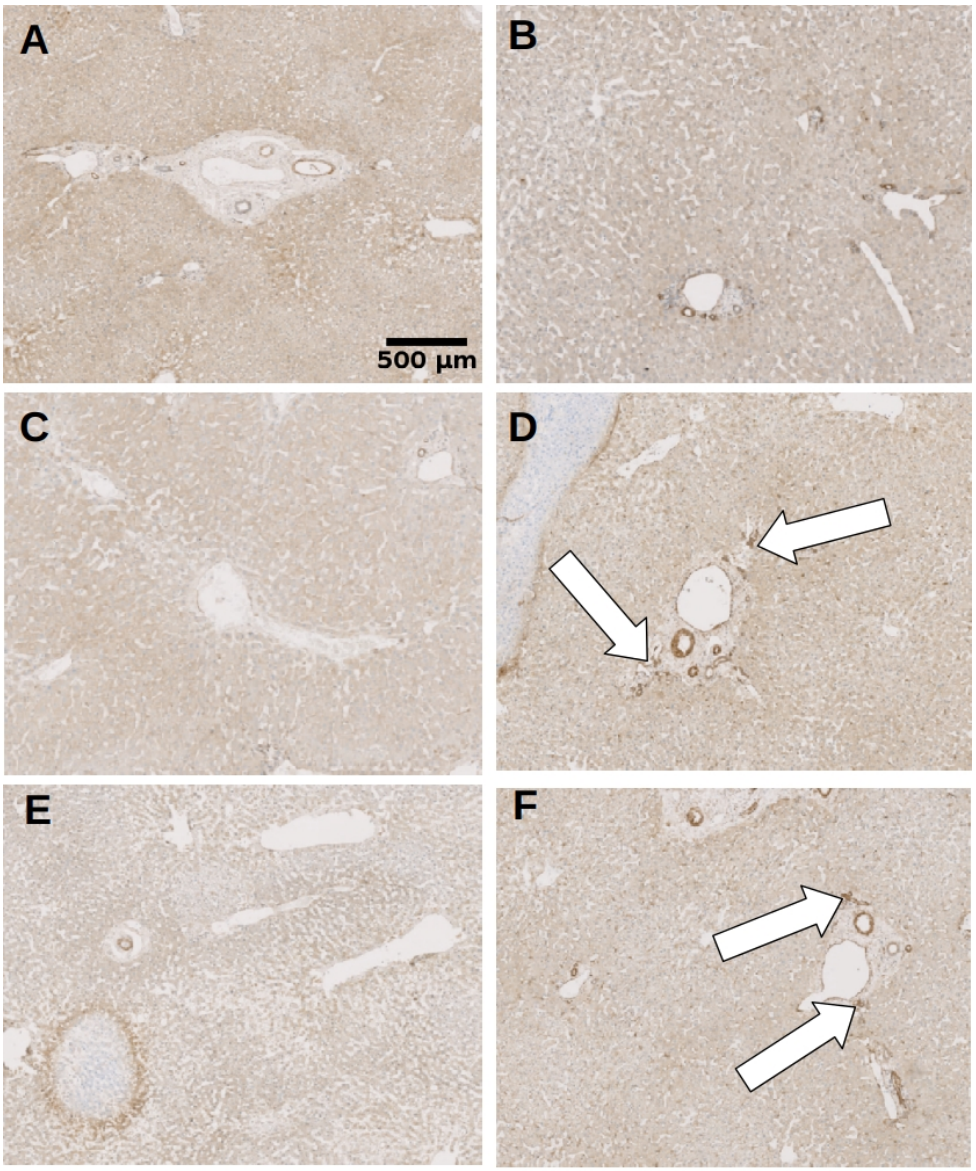

Figure 5.4: Higher resolution Fn14 staining in livers subjected to NMLP by viability. A,C,E non-viable; B,D,F viable; A,B at start of NMLP; C,D after 3 hours of NMLP; E,F at end of NMLP. All photographs using the Axio Scan Z1 (Zeiss, GmBH). Arrows in D and F indicate morphological ductular reaction asociated with intense Fn14 staining.

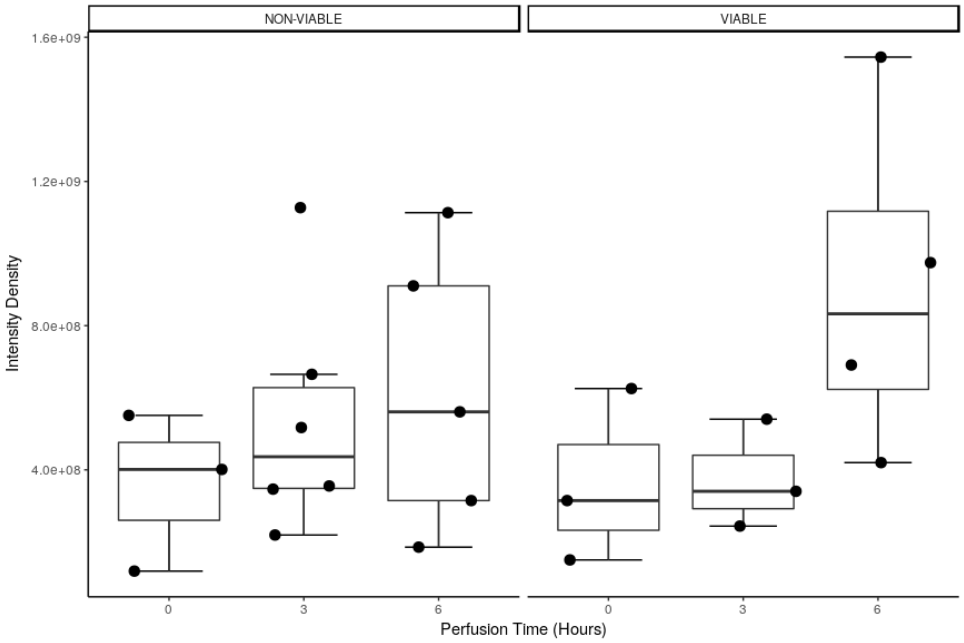

Figure 5.5: Intensity density of Fn14 staining by perfusion time in livers subjected to NMLP by viability. Graphical representation is made by combining dot and box plot to demonstrate sample results. Horizontal bar within box plot is median intensity density.

(Figure 5.3 A & B) and so a more pronounced increase in VG staining with longer perfusion time.

Spectral analysis of intensity density against perfusion time and viability was performed (Figure 5.7). Graphically, there appeared to be a trend towards higher intensity density in viable livers towards the end of NMLP compared to non-viable livers, with a more marked increase over NMLP time. However, repeated measures ANOVA demonstrated the main effect for viability yielded a F value of F = 0.162, $p > 0.05$, indicating that the effect for viability was not significant. The main effect for perfusion time yielded a F value of F = 2.142, $p > 0.05$, indicating that the effect for NMLP time was not significant. The interaction effect was insignificant, F = 1.048, $p > 0.05$.

Intensity density of Fn14 and VG across all timepoints of NMLP was performed to ascertain if there was any correlation (Figure 5.8). This demonstrated a reasonable positive association between Fn14 and VG with a R^2 of 0.775. However, when interrogating if any relationship was present according to viability, a stronger positive correlation was seen in the viable group (R^2 of 0.938) compared to the non-viable group (R^2 of 0.600)(Figure 5.9). Analysis using one-way ANCOVA with Fn14 as the dependent variable confirmed a significant effect of VG on Fn14 F(1,21) = 73.159, $p < 0.001$ after eliminating the effect of viability. Viability was not a significant covariate F(1,21) = 0.250, p = 0.623. Replacing VG as the dependent variable confirmed a significant effect of Fn14 on VG F(1,21) = 73.159, $p < 0.001$ after eliminating the effect of viability. Again, viability was not a significant covariate F(1,21) = 0.739, p = 0.400 however, there did exist an interaction between Fn14 and viability F(1,21) = 5.425, p = 0.030.

5.4 Discussion

This is the first study to demonstrate Fn14 in human cadaveric donor livers rejected from transplantation and subjected to NMLP. The results suggest that Fn14 content changes over time and that there is possibly a more positive correlation between Fn14 and collagen deposition in

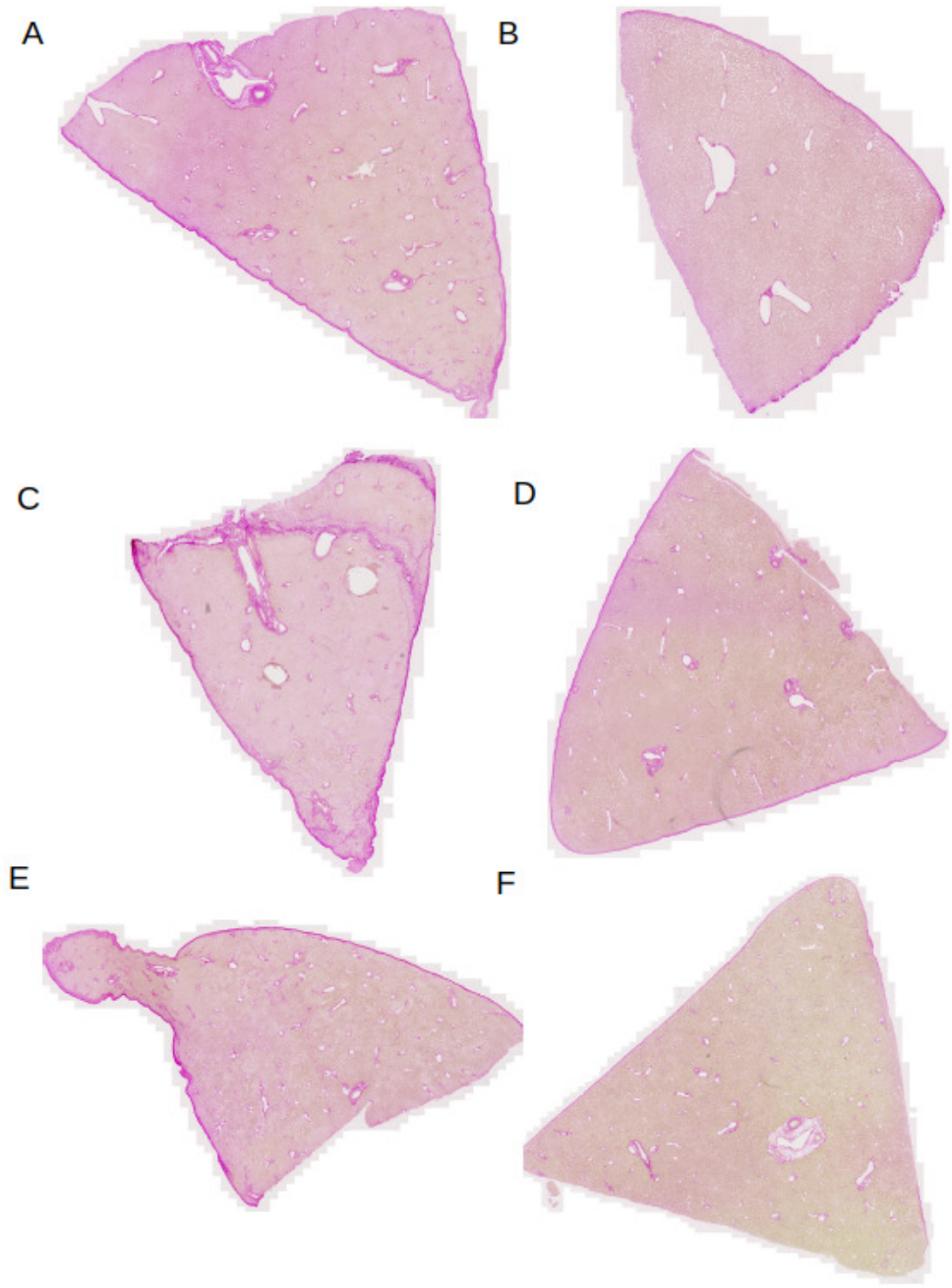

Figure 5.6: Van Gieson staining in livers subjected to NMLP by viability. A,C,E non-viable; B,D,F viable; A,B at start of NMLP; C,D after 3 hours of NMLP; E,F at end of NMLP. All photographs using the Axio Scan Z1 (Zeiss, GmBH).

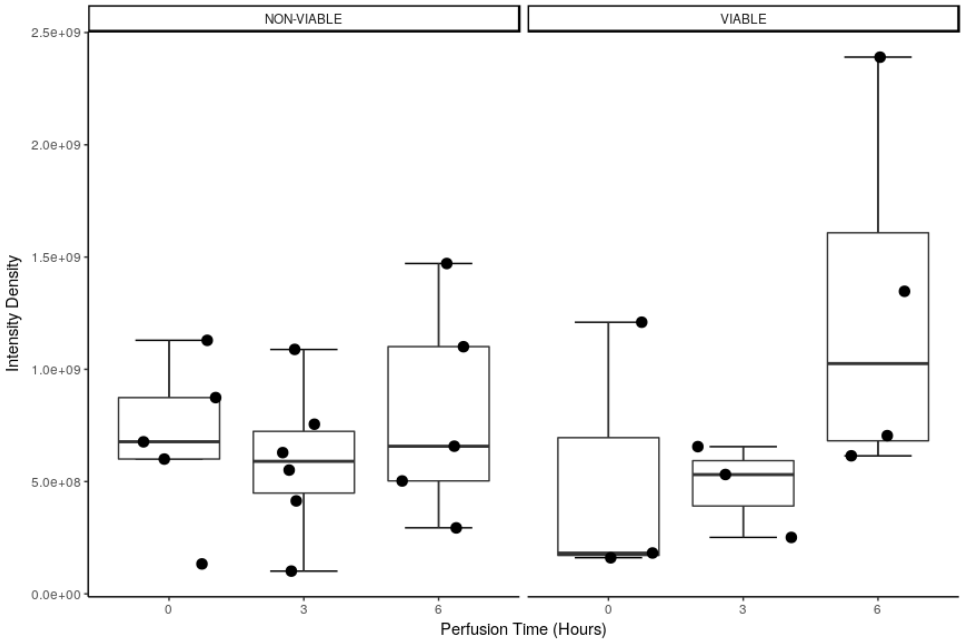

Figure 5.7: Intensity density of Van Gieson staining by perfusion time in livers subjected to NMLP by viability. Graphical representation is made by combining dot and box plot to demonstrate sample results. Horizontal bar within box plot is median intensity density.

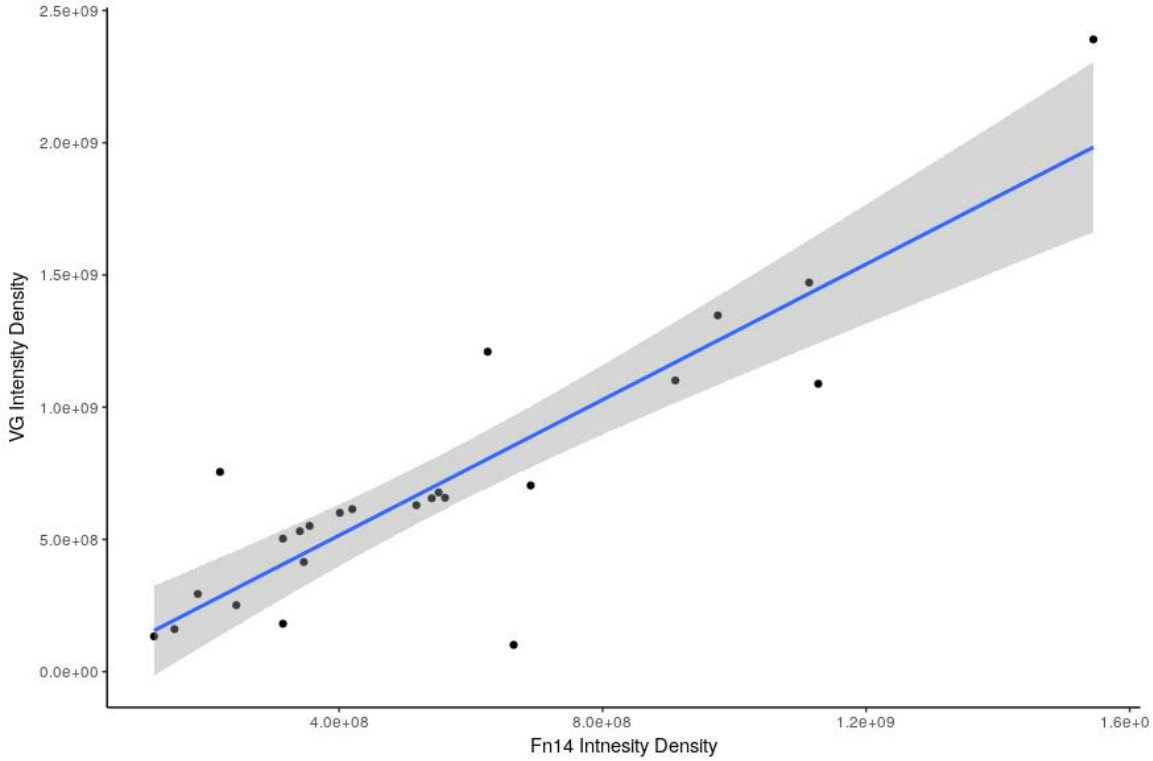

Figure 5.8: Correlation between intensity density of Fn14 and VG staining across all perfusion times. Regression analysis revealed a positive correlation with a R^2 of 0.779.

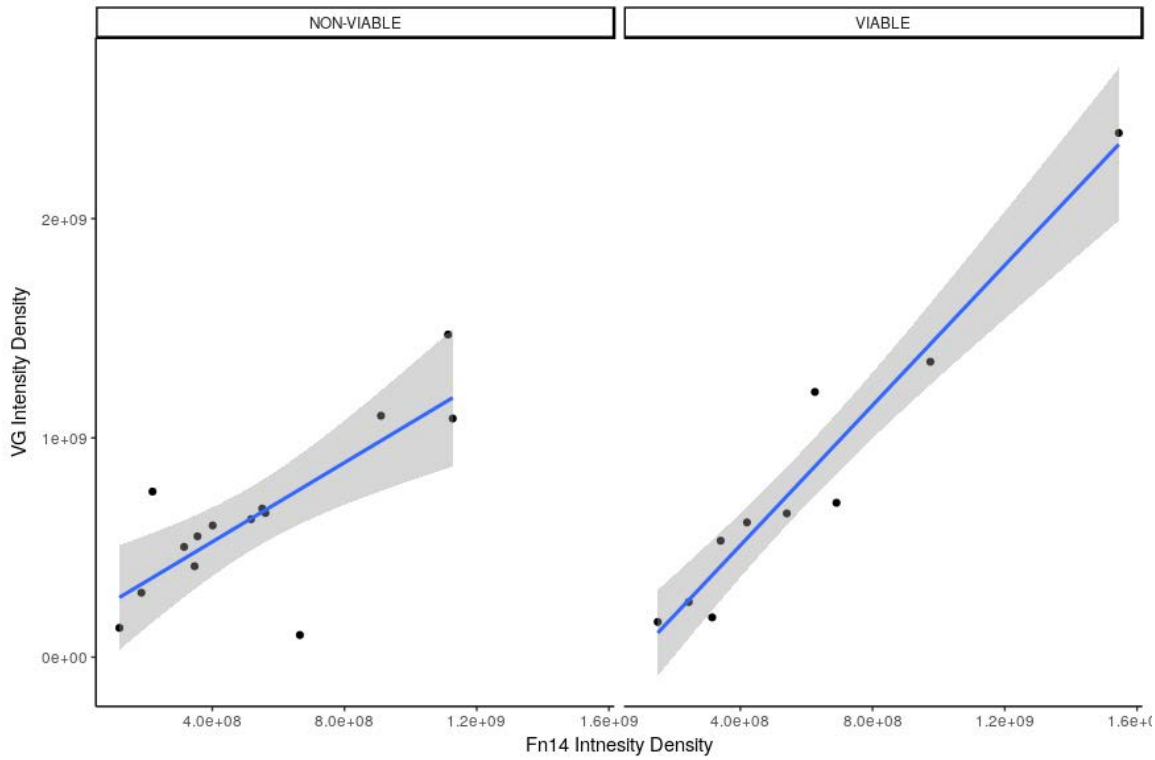

Figure 5.9: Correlation between intensity density of Fn14 and Van Gieson staining by viability across all perfusion times. Regression analysis revealed positive correlations for both non-viable and viable livers with R^2s of 0.600 and 0.938 repsectively.

viable livers compared to non-viable livers. The reason for any increase is yet to be determined. One possibilty is that it is a response to inflammation associated with non-resident immune cells however, as the model employs a perfusion circuit, it would be expected for these immune cells to be washout. Addition of a leukocyte filter to the circuit would remove these cells from the circuit and help ascertain an explanation. An alternative is that Fn14 is upregulated as part of a regenerative response on either HSCs or epithelial cells of the liver including the bipotent liver progenitor cells. This would seem less likely given the duration of NMLP however, early morphological evidence associated with Fn14 staining in the viable group after 3 hours of NMLP. Further extensive studies are required.

The main strengths of these results are that this is an *ex vivo* human model of ischaemia reperfusion injury and so more likely to represent biological action in humans compared to other animal models. The method presented also provide the advantage of reducing technical, assessor and interpretation bias during immunohistochemistry, as each section is subjected to the same light intensity during scanning, there is an assessment of the whole slide rather than possibly random areas within each section and the output is a numerical intensity density.

Despite these advantages, a number of weaknesses still exist. Each of the sections were scanned at a 5x objective rather than standard 20x or 40x objective due to the file sizes involved. Consequently, the resolution available for spectral analysis was lower, so might have missed variations in intensity that otherwise exist. this is particularly important for the VG staining which heterogenously distributed in the liver and is dependent on the specimen of tissue sampled. To overcome this would require repeated sectins to be scanned within the same block of tissue. Additionally, the size of the section scanned influenced the quality of the image. Some of the sections, particularly in the viable group, were small as the livers were destined for transplantation. In these livers only 16G needle biopsies were performed to reduced the risk of haematoma and bile leak in the transplant recipient. Sections from these biopsies were especially susceptible to light washout in which the slide scanner was unable to differentiate between different intensities of staining on the section. Immunohistochemical staining makes a number of assumptions

regarding antibody binding to antigen, particularly the Beer-Lambert law of intensity of stain is directly proportional to amount of antigen present. However, it is known that is not the case when using chromagens such as DAB.[299, 300]. Finally, although the Sequenza®rack and Coverplate®system reduces technical bias compared to manual immunohistochemical techniques, a fully automated system, subject to calibration, would provide an advantage.

The results demonstrate that there is a positive correlation between Fn14 and collagen deposition over perfusion time for all livers, independent of viability. Whilst statistically not significant, the positive correlation between VG as a function of Fn14, including an interaction with viability, is in keeping with data demonstrating that Fn14 is upregulated in acute human liver injury and that Fn14 gene expression is significantly upregulated in CCl_4 murine models of hepatic injury.[278]. That the interaction with viability occurs when VG is the dependent variable suggests, in this small series of relatively short perfusions, a mechanism in which increases in ECM and collagen deposition is a result of activation of Fn14 in stellate cells rather than the commencement of a cellular regenerative response and that this is more pronounced in viabile livers.

Future research should initially start with improving this ischaemia reperfusion injury model. This would include increasing the numbers and length of perfusions, improving the staining techniques possibly by the use of fluorescent microscopy to adhere more closely to the Beer-Lambert law, as well as incorporating better slide scanner and spectral analysis workflows. Further studies understanding the distribution and mechanism of Fn14 activation, including the role of its cognate ligand by extraneous administration of TWEAK and the role of circulating immune cells, in this exciting new model of ischaemia reperfusion injury, especially with extended perfusion times combined with concurrent liver splitting, are paramount.

CHAPTER 6

CONCLUSION

6.1 Overview

The initial aim of the project was to identify the functional significance of the Fn14/TWEAK system in cholangiocytes and ductular reactive cells during hepatic inflammation and repair. Although it could be established that Fn14 is present on cholangiocytes and ductular reactive cells as well as cholangiocarcinoma demonstrated by existing immunohistochemical and a newly established cell surface proteomic technique there are clearly severe limitations in the *in vitro* modelling that was available at that time. The issue largely revolves around the micro environment of cell culturing which is not representative of its *in vivo* environment. Differentiators between the two models include: The extracellular matrix onto which cells isolated from human liver; whether resected, explanted or surplus to transplantation are cultured; the constituents of the culture media itself; the relative hyperoxia that cells are exposed to when being incubated. This is before considering that *in vivo* cells are within a three-dimensional environment compared to *in vitro* where they are largely within a two-dimensional plane. This is assuming one has prospectively isolated, or isolated with a media selective technique, the specific cells that are of structural and functional significance to ones research.

Considering the previous paragraph, the opportunity became available to establish, evaluate and validate a new *ex vivo* human model. Not only could this system be used for the original intention of viability testing *ex vivo* human livers using normothermic machine perfusion and, specifically for this project, livers that had been declined for transplantation by all UK Transplant Centres that has helped to define the MCD, but also it could be used for translational and clinical research. To this end, this model of normothermic machine liver perfusion has been used to make an early evaluation of a bovine-based artificial oxygen carrier instead of the standard packed red cells, which are expensive and of limited resource, and that potentially it can be used to expand the donor pool, by evaluating livers that may be split with a left lobe being transplanted into either a child or small adult and the right lobe being transplanted into an adult. Furthermore, there has been an early demonstration of this *ex vivo* model being established in preclinical research as a novel ischaemia-reperfusion injury model, which will

not only help directly with interrogating existing adjuncts to transplantation but also to evaluate novel therapies. This would establish NMLP as a method of improving the efficiency of the current bench to bedside translational research pathways. Excitingly, this project has allowed for the significant development and establishing of a number of new techniques many of which are still in their early phases. As NMLP becomes more widely accepted, hopefully the scientific community will see this as a valuable resource.

6.2 Future Work

1. Development of existing *in vitro* modelling and prospective isolation of small populations of resident hepatic cells are of paramount importance. It is quite possible that there is a different role for more immature cells, for example the bipotent liver progenitor cells compared to more mature intra-hepatic cholangiocytes, when exposed to the correct conditions. Furthermore there needs to be an evolution of cell surface proteomics. In its current form the requirement for large numbers of cells for the assay to work limits its application defining small populations of cells where its application would be most appreciated. Additionally there needs to be better *in vitro* modelling as elicited in the overview.

2. In its current format normothermic machine perfusion could be improved. Defining the mechanism of viability is key to the future of all normothermic machine liver perfusion strategies. Additionally, further work can be conducted on perfusion fluid design such as artifical oxygen carriers, temperature strategies for specific donor organs for example DCD and steatotic livers, as well as understanding the potential role for interventions by drugs for defatting, viral vector or cellular therapy. These studies are currently being undertaken. Further studies can be conducted on splitting for clinical and preclinical research purposes as described above and with regards to using explanted and resected specimens.

3. Overall this would allow for a much better comparison of the specific role of the Fn14/TWEAK

receptor ligand system both *in vivo* and *ex vivo* allowing for more rapid, safe translation of future work.

For *ex vivo* NMLP to be a success it is absolutely imperative that there is intellectual, preclinical, translational, clinical and moral robustness and integrity in the design and application of research projects utilising this valuable resource. There must be rigour in definitions of viability assessment, resuscitation and reconditioning in addition to the use of controls, whether scientific or clinically orientated, specifically when using NMLP to intervene with drug, viral, cellular, vesicular or nucleic acid therapy. To that end the splitting of livers with concurrent NMLP is an exciting prospect for the future of preclinical liver research and its translation to everyday clinical practice.

Appendices

APPENDIX A

PUBLICATIONS

Manuscripts and Papers

Stephenson BTF *et al*. Label-free proteomics identifies proteins determining viability of discarded human livers resuscitated by normothermic machine perfusion. In preparation.

Stephenson BTF *et al*. Quantitative assessment of the cell surface proteome could identify novel therapeutics targets in cholangiocarcinoma. In preparation.

Mergental H*, **Stephenson BTF***, Laing RW, Kirkham AJ, Neil DAH, Wallace LL, Boteon YL, Widmer J, Bhogal RH, Perera MTPR, Smith A, Reynolds GM, Yap C, Hübscher SG, Mirza DF, Afford SC. Development of Clinical Criteria for Functional Assessment to Predict Primary Nonfunction of High-Risk Livers Using Normothermic Machine Perfusion. *Liver Transplantation*. 2018 Oct;24(10):1453-1469.

Bhogal RH, Weston CJ, Velduis S, G D Leuvenink H, Reynolds GM, Davies S, Nyguet-Thin L, Alfaifi M, Shepard EL, Boteon Y, Wallace L, Oo YH, Adams DH, Mirza DF, Mergental H, Muirhead G, **Stephenson BTF**, Afford SC. The Reactive Oxygen Species-Mitophagy Signaling Pathway Regulates Liver Endothelial Cell Survival During Ischemia/Reperfusion Injury. *Liver Transplantation*. 2018 Oct;24(10):1437-1452.

Stephenson BTF, Bonney GK, Laing RW, Bhogal RH, Marcon F, Neil DAH, Perera MTPR, Afford SC, Mergental H, Mirza DF. Proof of concept: liver splitting during normothermic machine perfusion. *Journal of Surgical Case Reports*. 2018 Mar 28;2018(3).

Laing RW, Bhogal RH, Wallace L, Boteon Y, Neil DAH, Smith A, **Stephenson BTF**, Schlegel A, Hübscher SG, Mirza DF, Afford SC, Mergental H. The use of an acellular oxygen carrier in a

human liver model of normothermic machine perfusion. *Transplantation*. 2017 Nov;101(11):2746-2756.

Mergental H, Perera MT, Laing RW, Muiesan P, Isaac JR, Smith A, **Stephenson BT**, Cilliers H, Neil DA, Hübscher SG, Afford SC, Mirza DF. Transplantation of declines liver allografts following normothermic ex-situ evaluation. *American Journal of Transplantation*. 2016 Nov;16(11):3235-3245.

Perera T, Mergental H, **Stephenson B**, Roll GR, Cilliers H, Liang R, Angelico R, Hübscher S, Neil DA, Reynolds G, Isaac J, Adams DA, Afford S, Mirza DF, Muiesan P. First human liver transplantation using a marginal allograft resuscitated by normothermic machine perfusion. *Liver Transplantation*. 2016 Jan;22(1):120-4.

Parker R, Armstrong MA, Bruns T, Hodson J, Rowe IA, Corbett CD, Reuken PA, Gunson BK, Houlihan DD, **Stephenson B**, Malessa C, Lester W, Ferguson JW. Reticulocyte count and haemaglobin concentration predict survival in candidates for liver transplantation. *Transplantation*. 2014 Feb;97(4):463-9.

Letters to the Editor

Boteon YL, **Stephenson BTF**, Neil DAH, Mirza DF, Afford SC, Mergental H. Lipid metabolism and functional assessment of discarded human livers with steatosis undergoing 24 hours of normothermic machine perfusion. *Liver Transplantation*. 2018 May;24(5):708-709.

Bhogal R, **Stephenson BT**, Afford SC. Preoperative fasting protects mice against hepatic is-

chemia/reperfusion injury: Mechanisms and Effects on liver regeneration. *Liver Transplantation*. 2011 Nov;17(11):1364.

Book Chapter

Bhogal RH, **Stephenson BTF**, Afford SC. Immune Cell Communication in Liver Disease and Liver Regeneration. In: Dufour J-F, Clavien PA, (eds.) *Signalling Pathways in Liver Diseases*. 2nd Edition. New York: Springer, 2016.

APPENDIX B

AWARDS AND PRIZES

Awards

Direct Funding

Full Bursary to attend and give 3 poster presentations at the International Symposium: Liver Transplantation & Liver Research in Birmingham.
University of Birmingham, September 2017.

Quantitative assessment of the liver extracellular matrix can identify components required for the engraftment of liver stem cells necessary in regenerative cellular therapy.
College Research and Development Fund Preliminary Data Award, College of Medical and Dental Studies, University of Birmingham, February 2014, £4961.

Quantitative assessment of the surface proteome can distinguish between distal cholangiocarcinoma and pancreatic carcinoma and identify new therapeutic targets.
College Research and Development Fund Preliminary Data Award, College of Medical and Dental Studies, University of Birmingham, February 2014, £4998.

The Isolation of Human Adult Bipotent Hepatic Stem and Lineage Committed Cholangiocyte Progenitor Cells to Study Functional Outcomes of Fn14/TWEAK Interaction.
College Research and Development Fund Preliminary Data Award, College of Medical and Dental Studies, University of Birmingham, October 2013, £2000.

Normothermic Machine Liver Perfusion in discarded human livers (application based on personal preliminary data).
University Hospital Birmingham NHS Foundation Trust, June 2013, £10,000.

EASL Young Investigator Full Bursary to attend and give an oral presentation at the International Liver Congress (EASL), Amsterdam, The Netherlands, April 2013, €650.

The Functional Significance of the Fn14/TWEAK Receptor-Ligand System in Ductular Reactive Cell Differentiation and Bile Ductule Neogenesis.
Medical Research Council UK Clinical Research Training Fellowship, May 2012, £213,348.

Indirect Funding

Provided preliminary data for the Viability Testing and Transplantation of Marginal Livers (VITTAL) study. Chief Investigator Professor Darius Mirza.
The Wellcome Trust, January 2016, £850,000.

Prizes

Bhogal RH, Weston C, Laing R, Alfaifi M, Nguyet T-L, Buteon Y, **Stephenson BTF**, Schlegel A, Wallace L, Mergental H, Afford SC. Reactive oxygen species mediated activation of autophagy in liver sinusoidal endothelial cells is a key regulator of liver ischaemia-reperfsion injury. David Adams Basic Science Prize. International Symposium: Liver Transplantation & Liver Research in Birmingham; University of Birmingham, UK; 6th September 2017.

Stephenson BTF, Widmer J, Laing R, Smith A, Hübscher S, Neil D, Perera T, Muiesan P, Mirza DF, Afford SC, Mergental H. Normothermic machine liver perfusion: a tool to assess the viability of human donor livers. Best Abstract Presentation. National Transplant Society Meeting of Ireland; Titanic Centre, Belfast, NI; 11th September 2015.

Stephenson BTF, Widmer J, Laing R, Smith A, Hübscher S, Neil D, Perera T, Muiesan P, Mirza DF, Afford SC, Mergental H. Normothermic machine liver perfusion: a tool to assess the viability of human donor livers. Sankey Research Prize. Sankey Clinico-Pathological Club; Queen Elizabeth Hospital, Birmingham, UK; 2nd July 2015.

Stephenson BTF, Widmer J, Humphreys E, Perera T, Fear J, Smith A, Laing R, Muiesan P, Hübscher S, Neil D, Mirza D, Afford S, Mergental H. Normothermic machine liver perfusion in the ex-vivo assessment of discarded human donor livers. Best Oral Presentation. Midlands Gastroenterological Society Autumn Conference (91st Meeting); Royal Wolverhampton Hospitals, UK; 14th November 2014.

Part of winning team from NIHR BRU and Centre for Liver Research, specifically presenting Normothermic Machine Liver Perfusion. Queen Elizabeth Hospital Showcase Day; 2014 May 20; Birmingham, UK.

LIST OF REFERENCES

[1] Gray H, Williams PL, Gray H. Gray's Anatomy. 37th ed. Edinburgh ; New York: C. Livingstone; 1989.

[2] Moore KL, Dalley AF. Clinically Oriented Anatomy. 4th ed. Philadelphia: Lippincott Williams & Wilkins; 1999.

[3] Whitaker RH, Borley NR. Instant Anatomy. 2nd ed. Oxford ; Boston: Blackwell Science; 2000.

[4] Fasel JHD, Schenk A. Concepts for Liver Segment Classification: Neither Old Ones nor New Ones, but a Comprehensive One. Journal of Clinical Imaging Science. 2013 Oct;3:48.

[5] Sibulesky L. Normal Liver Anatomy. Clinical Liver Disease. 2013 Mar;2(Suppl 1):S1–S3.

[6] Bismuth H. Surgical Anatomy and Anatomical Surgery of the Liver. World Journal of Surgery. 1982 Jan;6(1):3–9.

[7] Dufour JF, Clavien PA, editors. Signaling Pathways in Liver Diseases. Third edition ed. Chichester, West Sussex, UK ; Hoboken, NJ, USA: John Wiley & Sons, Ltd; 2016.

[8] Stevens A, Lowe JS. Human Histology. 2nd ed. London: Mosby; 1997. OCLC: 833097505.

[9] Adams DH, Eksteen B. Aberrant Homing of Mucosal T Cells and Extra-Intestinal Manifestations of Inflammatory Bowel Disease. Nature Reviews Immunology. 2006 Mar;6(3):244–251.

[10] Lamers WH, Hilberts A, Furt E, Smith J, Jonges GN, van Noorden CJ, et al. Hepatic Enzymic Zonation: A Reevaluation of the Concept of the Liver Acinus. Hepatology (Baltimore, Md). 1989 Jul;10(1):72–76.

[11] Jung J, Zheng M, Goldfarb M, Zaret KS. Initiation of Mammalian Liver Development from Endoderm by Fibroblast Growth Factors. Science (New York, NY). 1999 Jun;284(5422):1998–2003.

[12] Rossi JM, Dunn NR, Hogan BL, Zaret KS. Distinct Mesodermal Signals, Including BMPs from the Septum Transversum Mesenchyme, Are Required in Combination for Hepatogenesis from the Endoderm. Genes & Development. 2001 Aug;15(15):1998–2009.

[13] Wandzioch E, Zaret KS. Dynamic Signaling Network for the Specification of Embryonic Pancreas and Liver Progenitors. Science (New York, NY). 2009 Jun;324(5935):1707–1710.

[14] Kyrmizi I, Hatzis P, Katrakili N, Tronche F, Gonzalez FJ, Talianidis I. Plasticity and Expanding Complexity of the Hepatic Transcription Factor Network during Liver Development. Genes & Development. 2006 Aug;20(16):2293–2305.

[15] Macchiarelli G, Motta PM. The Three-Dimensional Microstructure of the Liver. A Review by Scanning Electron Microscopy. Scanning Electron Microscopy. 1986;(Pt 3):1019–1038.

[16] Crocenzi FA, Mottino AD, Roma MG. Regulation of Synthesis and Trafficking of Canalicular Transporters and Its Alteration in Acquired Hepatocellular Cholestasis. Experimental Therapeutic Strategies for Its Prevention. Current Medicinal Chemistry. 2004 Feb;11(4):501–524.

[17] Seseke FG, Gardemann A, Jungermann K. Signal Propagation via Gap Junctions, a Key Step in the Regulation of Liver Metabolism by the Sympathetic Hepatic Nerves. FEBS letters. 1992 Apr;301(3):265–270.

[18] Braet F, De Zanger R, Baekeland M, Crabbé E, Van Der Smissen P, Wisse E. Structure and Dynamics of the Fenestrae-Associated Cytoskeleton of Rat Liver Sinusoidal Endothelial Cells. Hepatology (Baltimore, Md). 1995 Jan;21(1):180–189.

[19] Fraser R, Dobbs BR, Rogers GW. Lipoproteins and the Liver Sieve: The Role of the Fenestrated Sinusoidal Endothelium in Lipoprotein Metabolism, Atherosclerosis, and Cirrhosis. Hepatology (Baltimore, Md). 1995 Mar;21(3):863–874.

[20] Braet F, Spector I, De Zanger R, Wisse E. A Novel Structure Involved in the Formation of Liver Endothelial Cell Fenestrae Revealed by Using the Actin Inhibitor Misakinolide. Proceedings of the National Academy of Sciences of the United States of America. 1998 Nov;95(23):13635–13640.

[21] Shetty S, Weston CJ, Adams DH, Lalor PF. A Flow Adhesion Assay to Study Leucocyte Recruitment to Human Hepatic Sinusoidal Endothelium under Conditions of Shear Stress. Journal of Visualized Experiments: JoVE. 2014 Mar;(85).

[22] Sakamoto S, Okanoue T, Itoh Y, Sakamoto K, Nishioji K, Nakagawa Y, et al. Intercellular Adhesion Molecule-1 and CD18 Are Involved in Neutrophil Adhesion and Its Cytotoxicity to Cultured Sinusoidal Endothelial Cells in Rats. Hepatology (Baltimore, Md). 1997 Sep;26(3):658–663.

[23] Wise C, Pilanthananond M, Perry BF, Alpini G, McNeal M, Glaser SS. Mechanisms of Biliary Carcinogenesis and Growth. World Journal of Gastroenterology. 2008 May;14(19):2986–2989.

[24] Gaudio E, Franchitto A, Pannarale L, Carpino G, Alpini G, Francis H, et al. Cholangiocytes and Blood Supply. World Journal of Gastroenterology. 2006 Jun;12(22):3546–3552.

[25] Zong Y, Panikkar A, Xu J, Antoniou A, Raynaud P, Lemaigre F, et al. Notch Signaling Controls Liver Development by Regulating Biliary Differentiation. Development (Cambridge, England). 2009 May;136(10):1727–1739.

[26] Antoniou A, Raynaud P, Cordi S, Zong Y, Tronche F, Stanger BZ, et al. Intrahepatic Bile Ducts Develop According to a New Mode of Tubulogenesis Regulated by the Transcription Factor SOX9. Gastroenterology. 2009 Jun;136(7):2325–2333.

[27] Blomhoff R, Wake K. Perisinusoidal Stellate Cells of the Liver: Important Roles in Retinol Metabolism and Fibrosis. FASEB journal: official publication of the Federation of American Societies for Experimental Biology. 1991 Mar;5(3):271–277.

[28] Pinzani M. Liver Fibrosis. Springer Seminars in Immunopathology. 1999;21(4):475–490.

[29] Gaça MDA, Zhou X, Issa R, Kiriella K, Iredale JP, Benyon RC. Basement Membrane-like Matrix Inhibits Proliferation and Collagen Synthesis by Activated Rat Hepatic Stellate Cells: Evidence for Matrix-Dependent Deactivation of Stellate Cells. Matrix Biology: Journal of the International Society for Matrix Biology. 2003 May;22(3):229–239.

[30] Sica A, Invernizzi P, Mantovani A. Macrophage Plasticity and Polarization in Liver Homeostasis and Pathology. Hepatology (Baltimore, Md). 2014 May;59(5):2034–2042.

[31] Martinez FO, Sica A, Mantovani A, Locati M. Macrophage Activation and Polarization. Frontiers in Bioscience: A Journal and Virtual Library. 2008 Jan;13:453–461.

[32] Liaskou E, Zimmermann HW, Li KK, Oo YH, Suresh S, Stamataki Z, et al. Monocyte Subsets in Human Liver Disease Show Distinct Phenotypic and Functional Characteristics. Hepatology (Baltimore, Md). 2013 Jan;57(1):385–398.

[33] Marastoni S, Ligresti G, Lorenzon E, Colombatti A, Mongiat M. Extracellular Matrix: A Matter of Life and Death. Connective Tissue Research. 2008;49(3):203–206.

[34] Roskams T. Different Types of Liver Progenitor Cells and Their Niches. Journal of Hepatology. 2006 Jul;45(1):1–4.

[35] Mokdad AA, Lopez AD, Shahraz S, Lozano R, Mokdad AH, Stanaway J, et al. Liver Cirrhosis Mortality in 187 Countries between 1980 and 2010: A Systematic Analysis. BMC medicine. 2014 Sep;12:145.

[36] Koyama Y, Brenner DA. Liver Inflammation and Fibrosis. The Journal of Clinical Investigation. 2017 Mar;127(1):55–64.

[37] Burt AD. Primary Biliary Cirrhosis and Other Ductopenic Diseases. Clinics in Liver Disease. 2002 May;6(2):363–380, vi.

[38] Desmet VJ. Histopathology of Chronic Cholestasis and Adult Ductopenic Syndrome. Clinics in Liver Disease. 1998 May;2(2):249–264, viii.

[39] Roskams TA, Theise ND, Balabaud C, Bhagat G, Bhathal PS, Bioulac-Sage P, et al. Nomenclature of the Finer Branches of the Biliary Tree: Canals, Ductules, and Ductular Reactions in Human Livers. Hepatology (Baltimore, Md). 2004 Jun;39(6):1739–1745.

[40] Mederacke I, Hsu CC, Troeger JS, Huebener P, Mu X, Dapito DH, et al. Fate Tracing Reveals Hepatic Stellate Cells as Dominant Contributors to Liver Fibrosis Independent of Its Aetiology. Nature Communications. 2013;4:2823.

[41] Duffield JS, Forbes SJ, Constandinou CM, Clay S, Partolina M, Vuthoori S, et al. Selective Depletion of Macrophages Reveals Distinct, Opposing Roles during Liver Injury and Repair. The Journal of Clinical Investigation. 2005 Jan;115(1):56–65.

[42] Ding BS, Cao Z, Lis R, Nolan DJ, Guo P, Simons M, et al. Divergent Angiocrine Signals from Vascular Niche Balance Liver Regeneration and Fibrosis. Nature. 2014 Jan;505(7481):97–102.

[43] Michalopoulos GK, DeFrances MC. Liver Regeneration. Science (New York, NY). 1997 Apr;276(5309):60–66.

[44] Seki E, De Minicis S, Osterreicher CH, Kluwe J, Osawa Y, Brenner DA, et al. TLR4 Enhances TGF-Beta Signaling and Hepatic Fibrosis. Nature Medicine. 2007 Nov;13(11):1324–1332.

[45] Radaeva S, Sun R, Jaruga B, Nguyen VT, Tian Z, Gao B. Natural Killer Cells Ameliorate Liver Fibrosis by Killing Activated Stellate Cells in NKG2D-Dependent and Tumor Necrosis Factor-Related Apoptosis-Inducing Ligand-Dependent Manners. Gastroenterology. 2006 Feb;130(2):435–452.

[46] Hellerbrand C, Jobin C, Licato LL, Sartor RB, Brenner DA. Cytokines Induce NF-kappaB in Activated but Not in Quiescent Rat Hepatic Stellate Cells. The American Journal of Physiology. 1998 Aug;275(2):G269–278.

[47] Friedman SL. Hepatic Stellate Cells: Protean, Multifunctional, and Enigmatic Cells of the Liver. Physiological Reviews. 2008 Jan;88(1):125–172.

[48] Canbay A, Feldstein AE, Higuchi H, Werneburg N, Grambihler A, Bronk SF, et al. Kupffer Cell Engulfment of Apoptotic Bodies Stimulates Death Ligand and Cytokine Expression. Hepatology (Baltimore, Md). 2003 Nov;38(5):1188–1198.

[49] Zhan SS, Jiang JX, Wu J, Halsted C, Friedman SL, Zern MA, et al. Phagocytosis of Apoptotic Bodies by Hepatic Stellate Cells Induces NADPH Oxidase and Is Associated with Liver Fibrosis in Vivo. Hepatology (Baltimore, Md). 2006 Mar;43(3):435–443.

[50] Syal G, Fausther M, Dranoff JA. Advances in Cholangiocyte Immunobiology. American Journal of Physiology Gastrointestinal and Liver Physiology. 2012 Nov;303(10):G1077–1086.

[51] He Y, Wu GD, Sadahiro T, Noh SI, Wang H, Talavera D, et al. Interaction of CD44 and Hyaluronic Acid Enhances Biliary Epithelial Proliferation in Cholestatic Livers. American Journal of Physiology Gastrointestinal and Liver Physiology. 2008 Aug;295(2):G305–312.

[52] Xie G, Wang X, Wang L, Wang L, Atkinson RD, Kanel GC, et al. Role of Differentiation of Liver Sinusoidal Endothelial Cells in Progression and Regression of Hepatic Fibrosis in Rats. Gastroenterology. 2012 Apr;142(4):918–927.e6.

[53] Pellicoro A, Ramachandran P, Iredale JP, Fallowfield JA. Liver Fibrosis and Repair: Immune Regulation of Wound Healing in a Solid Organ. Nature Reviews Immunology. 2014 Mar;14(3):181–194.

[54] Melhem A, Muhanna N, Bishara A, Alvarez CE, Ilan Y, Bishara T, et al. Anti-Fibrotic Activity of NK Cells in Experimental Liver Injury through Killing of Activated HSC. Journal of Hepatology. 2006 Jul;45(1):60–71.

[55] Jeong WI, Park O, Suh YG, Byun JS, Park SY, Choi E, et al. Suppression of Innate Immunity (Natural Killer Cell/Interferon-γ) in the Advanced Stages of Liver Fibrosis in Mice. Hepatology (Baltimore, Md). 2011 Apr;53(4):1342–1351.

[56] Krämer B, Körner C, Kebschull M, Glässner A, Eisenhardt M, Nischalke HD, et al. Natural Killer p46High Expression Defines a Natural Killer Cell Subset That Is Potentially Involved in Control of Hepatitis C Virus Replication and Modulation of Liver Fibrosis. Hepatology (Baltimore, Md). 2012 Oct;56(4):1201–1213.

[57] Moles A, Murphy L, Wilson CL, Chakraborty JB, Fox C, Park EJ, et al. A TLR2/S100A9/CXCL-2 Signaling Network Is Necessary for Neutrophil Recruitment in Acute and Chronic Liver Injury in the Mouse. Journal of Hepatology. 2014 Apr;60(4):782–791.

[58] McHedlidze T, Waldner M, Zopf S, Walker J, Rankin AL, Schuchmann M, et al. Interleukin-33-Dependent Innate Lymphoid Cells Mediate Hepatic Fibrosis. Immunity. 2013 Aug;39(2):357–371.

[59] Anstee QM, Dhar A, Thursz MR. The Role of Hypercoagulability in Liver Fibrogenesis. Clinics and Research in Hepatology and Gastroenterology. 2011 Sep;35(8-9):526–533.

[60] Seki E, Schwabe RF. Hepatic Inflammation and Fibrosis: Functional Links and Key Pathways. Hepatology. 2015 Mar;61(3):1066–1079.

[61] Jagavelu K, Routray C, Shergill U, O'Hara SP, Faubion W, Shah VH. Endothelial Cell Toll-like Receptor 4 Regulates Fibrosis-Associated Angiogenesis in the Liver. Hepatology (Baltimore, Md). 2010 Aug;52(2):590–601.

[62] Affò S, Morales-Ibanez O, Rodrigo-Torres D, Altamirano J, Blaya D, Dapito DH, et al. CCL20 Mediates Lipopolysaccharide Induced Liver Injury and Is a Potential Driver of Inflammation and Fibrosis in Alcoholic Hepatitis. Gut. 2014 Nov;63(11):1782–1792.

[63] Gieling RG, Wallace K, Han YP. Interleukin-1 Participates in the Progression from Liver Injury to Fibrosis. American Journal of Physiology Gastrointestinal and Liver Physiology. 2009 Jun;296(6):G1324–1331.

[64] Tarrats N, Moles A, Morales A, García-Ruiz C, Fernández-Checa JC, Marí M. Critical Role of Tumor Necrosis Factor Receptor 1, but Not 2, in Hepatic Stellate Cell Proliferation, Extracellular Matrix Remodeling, and Liver Fibrogenesis. Hepatology (Baltimore, Md). 2011 Jul;54(1):319–327.

[65] Meng F, Wang K, Aoyama T, Grivennikov SI, Paik Y, Scholten D, et al. Interleukin-17 Signaling in Inflammatory, Kupffer Cells, and Hepatic Stellate Cells Exacerbates Liver Fibrosis in Mice. Gastroenterology. 2012 Sep;143(3):765–776.e3.

[66] Kong X, Feng D, Wang H, Hong F, Bertola A, Wang FS, et al. Interleukin-22 Induces Hepatic Stellate Cell Senescence and Restricts Liver Fibrosis in Mice. Hepatology (Baltimore, Md). 2012 Sep;56(3):1150–1159.

[67] Kronenberger B, Rudloff I, Bachmann M, Brunner F, Kapper L, Filmann N, et al. Interleukin-22 Predicts Severity and Death in Advanced Liver Cirrhosis: A Prospective Cohort Study. BMC medicine. 2012 Sep;10:102.

[68] Dooley S, ten Dijke P. TGF-β in Progression of Liver Disease. Cell and Tissue Research. 2012 Jan;347(1):245–256.

[69] Baeck C, Wei X, Bartneck M, Fech V, Heymann F, Gassler N, et al. Pharmacological Inhibition of the Chemokine C-C Motif Chemokine Ligand 2 (Monocyte Chemoattractant Protein 1) Accelerates Liver Fibrosis Regression by Suppressing Ly-6C(+) Macrophage Infiltration in Mice. Hepatology (Baltimore, Md). 2014 Mar;59(3):1060–1072.

[70] Seki E, De Minicis S, Gwak GY, Kluwe J, Inokuchi S, Bursill CA, et al. CCR1 and CCR5 Promote Hepatic Fibrosis in Mice. The Journal of Clinical Investigation. 2009 Jul;119(7):1858–1870.

[71] Karlmark KR, Zimmermann HW, Roderburg C, Gassler N, Wasmuth HE, Luedde T, et al. The Fractalkine Receptor CX_3CR1 Protects against Liver Fibrosis by Controlling Differentiation and Survival of Infiltrating Hepatic Monocytes. Hepatology (Baltimore, Md). 2010 Nov;52(5):1769–1782.

[72] Pradere JP, Kluwe J, De Minicis S, Jiao JJ, Gwak GY, Dapito DH, et al. Hepatic Macrophages but Not Dendritic Cells Contribute to Liver Fibrosis by Promoting the Survival of Activated Hepatic Stellate Cells in Mice. Hepatology (Baltimore, Md). 2013 Oct;58(4):1461–1473.

[73] Luedde T, Schwabe RF. NF-κB in the Liver–Linking Injury, Fibrosis and Hepatocellular Carcinoma. Nature Reviews Gastroenterology & Hepatology. 2011 Feb;8(2):108–118.

[74] Kluwe J, Pradere JP, Gwak GY, Mencin A, De Minicis S, Osterreicher CH, et al. Modulation of Hepatic Fibrosis by C-Jun-N-Terminal Kinase Inhibition. Gastroenterology. 2010 Jan;138(1):347–359.

[75] Seki E, Brenner DA, Karin M. A Liver Full of JNK: Signaling in Regulation of Cell Function and Disease Pathogenesis, and Clinical Approaches. Gastroenterology. 2012 Aug;143(2):307–320.

[76] Ware CF. The TNF Receptor Super Family in Immune Regulation. Immunological Reviews. 2011;244(1):5–8.

[77] Bodmer JL, Schneider P, Tschopp J. The Molecular Architecture of the TNF Superfamily. Trends in Biochemical Sciences. 2002 Jan;27(1):19–26.

[78] Locksley RM, Killeen N, Lenardo MJ. The TNF and TNF Receptor Superfamilies: Integrating Mammalian Biology. Cell. 2001 Feb;104(4):487–501.

[79] Burkly LC, Michaelson JS, Zheng TS. TWEAK/Fn14 Pathway: An Immunological Switch for Shaping Tissue Responses. Immunological reviews. 2011;244(1):99–114.

[80] Croft M, Benedict CA, Ware CF. Clinical Targeting of the TNF and TNFR Superfamilies. Nature Reviews Drug Discovery. 2013 Feb;12(2):147–168.

[81] Ward-Kavanagh LK, Lin WW, Šedý JR, Ware CF. The TNF Receptor Superfamily in Co-Stimulating and Co-Inhibitory Responses. Immunity. 2016 May;44(5):1005–1019.

[82] Etemadi N, Holien JK, Chau D, Dewson G, Murphy JM, Alexander WS, et al. Lymphotoxin α Induces Apoptosis, Necroptosis and Inflammatory Signals with the Same Potency as Tumour Necrosis Factor. The FEBS journal. 2013 Nov;280(21):5283–5297.

[83] Cheung TC, Steinberg MW, Oborne LM, Macauley MG, Fukuyama S, Sanjo H, et al. Unconventional Ligand Activation of Herpesvirus Entry Mediator Signals Cell Survival. Proceedings of the National Academy of Sciences of the United States of America. 2009 Apr;106(15):6244–6249.

[84] Jakubowski A, Ambrose C, Parr M, Lincecum JM, Wang MZ, Zheng TS, et al. TWEAK Induces Liver Progenitor Cell Proliferation. The Journal of Clinical Investigation. 2005 Sep;115(9):2330–2340.

[85] Tirnitz-Parker JEE, Viebahn CS, Jakubowski A, S Klopcic BR, Olynyk JK, Yeoh GCT, et al. Tumor Necrosis Factor-like Weak Inducer of Apoptosis Is a Mitogen for Liver Progenitor Cells. Hepatology. 2010 Mar;p. n/a–n/a. Cited by 0038.

[86] Chicheportiche Y, Bourdon PR, Xu H, Hsu YM, Scott H, Hession C, et al. TWEAK, a New Secreted Ligand in the Tumor Necrosis Factor Family That Weakly Induces Apoptosis. Journal of Biological Chemistry. 1997;272(51):32401.

[87] Kaduka Y, Takeda K, Nakayama M, Kinoshita K, Yagita H, Okumura K. TWEAK Mediates Anti-Tumor Effect of Tumor-Infiltrating Macrophage. Biochemical and Biophysical Research Communications. 2005 Jun;331(2):384–390.

[88] Burkly LC, Dohi T. The TWEAK/Fn14 Pathway in Tissue Remodeling: For Better or for Worse. Advances in Experimental Medicine and Biology. 2011;691:305–322.

[89] Urbonaviciene G, Martin-Ventura JL, Lindholt JS, Urbonavicius S, Moreno JA, Egido J, et al. Impact of Soluble TWEAK and CD163/TWEAK Ratio on Long-Term Cardiovascular Mortality in Patients with Peripheral Arterial Disease. Atherosclerosis. 2011 Sep;.

[90] Van Gorp H, Delputte PL, Nauwynck HJ. Scavenger Receptor CD163, a Jack-of-All-Trades and Potential Target for Cell-Directed Therapy. Molecular Immunology. 2010 Apr;47(7-8):1650–1660. Cited by 0077.

[91] Moreno JA, Dejouvencel T, Labreuche J, Smadja DM, Dussiot M, Martin-Ventura JL, et al. Peripheral Artery Disease Is Associated With a High CD163/TWEAK Plasma Ratio. Arteriosclerosis, Thrombosis, and Vascular Biology. 2010 Mar;30(6):1253–1262.

[92] Girgenrath M, Weng S, Kostek CA, Browning B, Wang M, Brown SAN, et al. TWEAK, via Its Receptor Fn14, Is a Novel Regulator of Mesenchymal Progenitor Cells and Skeletal Muscle Regeneration. The EMBO journal. 2006;25(24):5826–5839.

[93] Dogra C, Hall SL, Wedhas N, Linkhart TA, Kumar A. Fibroblast Growth Factor Inducible 14 (Fn14) Is Required for the Expression of Myogenic Regulatory Factors and Differentiation of Myoblasts into Myotubes: EVIDENCE FOR TWEAK-INDEPENDENT FUNCTIONS OF Fn14 DURING MYOGENESIS. Journal of Biological Chemistry. 2007 Mar;282(20):15000–15010.

[94] Mustonen E, Säkkinen H, Tokola H, Isopoussu E, Aro J, Leskinen H, et al. Tumour Necrosis Factor-like Weak Inducer of Apoptosis (TWEAK) and Its Receptor Fn14 during Cardiac Remodelling in Rats. Acta Physiologica (Oxford, England). 2010 May;199(1):11–22.

[95] Dharmapatni AA, Smith MD, Crotti TN, Holding CA, Vincent C, Weedon HM, et al. TWEAK and Fn14 Expression in the Pathogenesis of Joint Inflammation and Bone Erosion in Rheumatoid Arthritis. Arthritis Research & Therapy. 2011;13(2):R51. Cited by 0016.

[96] Liu YP, Yu GR, Li K, Yuan F. Is There Another Possible Approach to Inhibit Wear Particles-Induced Inflammatory Osteolysis? Medical Hypotheses. 2011 Feb;76(2):280–282.

[97] Justo P, Sanz AB, Sanchez-Nino MD, Winkles JA, Lorz C, Egido J, et al. Cytokine Cooperation in Renal Tubular Cell Injury: The Role of TWEAK. Kidney Int. online 2006;70(10):1750–1758.

[98] Gao HX, Campbell SR, Burkly LC, Jakubowski A, Jarchum I, Banas B, et al. TNF-like Weak Inducer of Apoptosis (TWEAK) Induces Inflammatory and Proliferative Effects in Human Kidney Cells. Cytokine. 2009 Apr;46(1):24–35. Cited by 0059.

[99] Zhao Z, Burkly LC, Campbell S, Schwartz N, Molano A, Choudhury A, et al. TWEAK/Fn14 Interactions Are Instrumental in the Pathogenesis of Nephritis in the Chronic Graft-versus-Host Model of Systemic Lupus Erythematosus. The Journal of Immunology. 2007;179(11):7949.

[100] Donohue PJ, Richards CM, Brown SAN, Hanscom HN, Buschman J, Thangada S, et al. TWEAK Is an Endothelial Cell Growth and Chemotactic Factor That Also Potentiates FGF-2 and VEGF-A Mitogenic Activity. Arterioscler Thromb Vasc Biol. 2003 Apr;23(4):594–600.

[101] Brown SAN, Richards CM, Hanscom HN, Feng SLY, Winkles JA. The Fn14 Cytoplasmic Tail Binds Tumour-Necrosis-Factor-Receptor-Associated Factors 1, 2, 3 and 5 and Mediates Nuclear Factor-kappaB Activation. Biochemical Journal. 2003;371(Pt 2):395.

[102] Roos C, Wicovsky A, M\üller N, Salzmann S, Rosenthal T, Kalthoff H, et al. Soluble and Transmembrane TNF-Like Weak Inducer of Apoptosis Differentially Activate the Classical and Noncanonical NF-$appa$B Pathway. The Journal of Immunology. 2010;185(3):1593.

[103] Officer CM. Annual Report of the Chief Medical Officer 2001 [Publication];. This annual report highlights selected health issues from 2001 and the actions taken to overcome health problems. http://www.dh.gov.uk/en/Publicationsandstatistics/Publications/AnnualReports/DH_4005607.

[104] Williams J, Roberts S, Ali F, Cheung WY, Cohen D, Demery G, et al. Gastroenterology Services in the UK. The Burden of Disease, and the Organisation and Delivery of Services for Gastrointestinal and Liver Disorders: A Review of the Evidence. Gut. 2007 Feb;56(suppl_1):1–113. Cited by 0052.

[105] Williams R, Ashton K, Aspinall R, Bellis MA, Bosanquet J, Cramp ME, et al. Implementation of the Lancet Standing Commission on Liver Disease in the UK. The Lancet. 2015;386(10008):2098–2111.

[106] Williams R, Aspinall R, Bellis M, Camps-Walsh G, Cramp M, Dhawan A, et al. Addressing Liver Disease in the UK: A Blueprint for Attaining Excellence in Health Care and Reducing Premature Mortality from Lifestyle Issues of Excess Consumption of Alcohol, Obesity, and Viral Hepatitis. The Lancet. 2014;384(9958):1953–1997.

[107] Activity_report_2016_17.Pdf;. https://nhsbtdbe.blob.core.windows.net/umbraco-assets-corp/4657/activity_report_2016_17.pdf.

[108] Annual_liver_transplantation_report_2017.Pdf;. https://nhsbtdbe.blob.core.windows.net/umbraco-assets-corp/5007/annual_liver_transplantation_report_2017.pdf.

[109] NHSBT - ODT Clinical Site - Annual Activity Report;. http://www.odt.nhs.uk/uk-transplant-registry/annual-activity-report/.

[110] Detry O, Le Dinh H, Noterdaeme T, De Roover A, Honoré P, Squifflet JP, et al. Categories of Donation After Cardiocirculatory Death. Transplantation Proceedings. 2012 Jun;44(5):1189–1195.

[111] Andrews PA, Burnapp L, Manas D. Summary of the British Transplantation Society Guidelines for Transplantation from Donors After Deceased Circulatory Death:. Transplantation Journal. 2014 Feb;97(3):265–270.

[112] Summers DM, Counter C, Johnson RJ, Murphy PG, Neuberger JM, Bradley JA. Is the Increase in DCD Organ Donors in the United Kingdom Contributing to a Decline in DBD Donors?:. Transplantation. 2010 Dec;90(12):1506–1510.

[113] Annual-Pda-Report-2016-17.Pdf;. https://nhsbtdbe.blob.core.windows.net/umbraco-assets-corp/14010/annual-pda-report-2016-17.pdf.

[114] NHSBT - Organ Donation - Activity Report;. 00000. http://www.organdonation.nhs.uk/statistics/transplant_activity_report/.

[115] Pol195_7-Liver-Selection-Policy.Pdf;. https://nhsbtdbe.blob.core.windows.net/umbraco-assets-corp/9440/pol195_7-liver-selection-policy.pdf.

[116] O'Grady JG, Alexander GJ, Hayllar KM, Williams R. Early Indicators of Prognosis in Fulminant Hepatic Failure. Gastroenterology. 1989 Aug;97(2):439–445.

[117] Fujita S, Mizuno S, Fujikawa T, Reed AI, Kim RD, Howard RJ, et al. Liver Transplantation from Donation after Cardiac Death: A Single Center Experience. Transplantation. 2007 Jul;84(1):46–49.

[118] Foley DP, Fernandez LA, Leverson G, Chin LT, Krieger N, Cooper JT, et al. Donation after Cardiac Death: The University of Wisconsin Experience with Liver Transplantation. Annals of Surgery. 2005 Nov;242(5):724–731.

[119] Chan EY, Olson LC, Kisthard JA, Perkins JD, Bakthavatsalam R, Halldorson JB, et al. Ischemic Cholangiopathy Following Liver Transplantation from Donation after Cardiac Death Donors. Liver Transplantation: Official Publication of the American Association for the Study of Liver Diseases and the International Liver Transplantation Society. 2008 May;14(5):604–610.

[120] Muiesan P, Girlanda R, Jassem W, Melendez HV, O??Grady J, Bowles M, et al. Single-Center Experience With Liver Transplantation From Controlled Non-Heartbeating Donors: A Viable Source of Grafts. Annals of Surgery. 2005 Nov;242(5):732–738. 00143.

[121] Dubbeld J, Hoekstra H, Farid W, Ringers J, Porte RJ, Metselaar HJ, et al. Similar Liver Transplantation Survival with Selected Cardiac Death Donors and Brain Death Donors. The British Journal of Surgery. 2010 May;97(5):744–753.

[122] Jay CL, Lyuksemburg V, Ladner DP, Wang E, Caicedo JC, Holl JL, et al. Ischemic Cholangiopathy after Controlled Donation after Cardiac Death Liver Transplantation: A Meta-Analysis. Annals of Surgery. 2011 Feb;253(2):259–264. Cited by 0033.

[123] Foley DP, Fernandez LA, Leverson G, Anderson M, Mezrich J, Sollinger HW, et al. Biliary Complications after Liver Transplantation from Donation after Cardiac Death Donors: An Analysis of Risk Factors and Long-Term Outcomes from a Single Center. Annals of Surgery. 2011 Apr;253(4):817–825. Cited by 0054.

[124] Jay C, Ladner D, Wang E, Lyuksemburg V, Kang R, Chang Y, et al. A Comprehensive Risk Assessment of Mortality Following Donation after Cardiac Death Liver Transplant - an Analysis of the National Registry. Journal of Hepatology. 2011 Oct;55(4):808–813.

[125] Ho KJ, Owens CD, Johnson SR, Khwaja K, Curry MP, Pavlakis M, et al. Donor Postextubation Hypotension and Age Correlate with Outcome after Donation after Cardiac Death Transplantation. Transplantation. 2008 Jun;85(11):1588–1594.

[126] Bernat JL, D'Alessandro AM, Port FK, Bleck TP, Heard SO, Medina J, et al. Report of a National Conference on Donation after Cardiac Death. American Journal of Transplantation: Official Journal of the American Society of Transplantation and the American Society of Transplant Surgeons. 2006 Feb;6(2):281–291.

[127] Mateo R, Cho Y, Singh G, Stapfer M, Donovan J, Kahn J, et al. Risk Factors for Graft Survival after Liver Transplantation from Donation after Cardiac Death Donors: An Analysis of OPTN/UNOS Data. American Journal of Transplantation: Official Journal of the American Society of Transplantation and the American Society of Transplant Surgeons. 2006 Apr;6(4):791–796.

[128] Kamath PS, Wiesner RH, Malinchoc M, Kremers W, Therneau TM, Kosberg CL, et al. A Model to Predict Survival in Patients with End-Stage Liver Disease. Hepatology (Baltimore, Md). 2001 Feb;33(2):464–470.

[129] Wiesner R, Edwards E, Freeman R, Harper A, Kim R, Kamath P, et al. Model for End-Stage Liver Disease (MELD) and Allocation of Donor Livers. Gastroenterology. 2003 Jan;124(1):91–96.

[130] Barber K, Madden S, Allen J, Collett D, Neuberger J, Gimson A, et al. Elective Liver Transplant List Mortality: Development of a United Kingdom End-Stage Liver Disease Score. Transplantation. 2011 Aug;92(4):469–476.

[131] Neuberger J, Gimson A, Davies M, Akyol M, O'Grady J, Burroughs A, et al. Selection of Patients for Liver Transplantation and Allocation of Donated Livers in the UK. Gut. 2008 Feb;57(2):252–257.

[132] Feng S, Goodrich NP, Bragg-Gresham JL, Dykstra DM, Punch JD, DebRoy MA, et al. Characteristics Associated with Liver Graft Failure: The Concept of a Donor Risk Index. American Journal of Transplantation: Official Journal of the American Society of Transplantation and the American Society of Transplant Surgeons. 2006 Apr;6(4):783–790.

[133] Flores A, Asrani SK. The Donor Risk Index: A Decade of Experience. Liver Transplantation. 2017 Sep;23(9):1216–1225.

[134] Blok JJ, Braat AE, Adam R, Burroughs AK, Putter H, Kooreman NG, et al. Validation of the Donor Risk Index in Orthotopic Liver Transplantation within the Eurotransplant Region. Liver Transplantation: Official Publication of the American Association for the Study of Liver Diseases and the International Liver Transplantation Society. 2012 Jan;18(1):112–119.

[135] Collett D, Friend PJ, Watson CJE. Factors Associated With Short- and Long-Term Liver Graft Survival in the United Kingdom: Development of a UK Donor Liver Index. Transplantation. 2017 Apr;101(4):786–792.

[136] Halldorson JB, Bakthavatsalam R, Fix O, Reyes JD, Perkins JD. D-MELD, a Simple Predictor of Post Liver Transplant Mortality for Optimization of Donor/Recipient Matching. American Journal of Transplantation. 2009 Feb;9(2):318–326. 00100.

[137] Kim WR, Lake JR, Smith JM, Skeans MA, Schladt DP, Edwards EB, et al. OPTN/SRTR 2015 Annual Data Report: Liver. American Journal of Transplantation: Official Journal of the American Society of Transplantation and the American Society of Transplant Surgeons. 2017 Jan;17 Suppl 1:174–251.

[138] Dutkowski P, Oberkofler CE, Slankamenac K, Puhan MA, Schadde E, Müllhaupt B, et al. Are There Better Guidelines for Allocation in Liver Transplantation? A Novel Score Targeting Justice and Utility in the Model for End-Stage Liver Disease Era. Annals of Surgery. 2011 Nov;254(5):745–753; discussion 753.

[139] Schrem H, Focken M, Gunson B, Reichert B, Mirza D, Kreipe HH, et al. The New Liver Allocation Score for Transplantation Is Validated and Improved Transplant Survival Benefit in Germany but Not in the United Kingdom. Liver Transplantation: Official Publication of the American Association for the Study of Liver Diseases and the International Liver Transplantation Society. 2016 Jun;22(6):743–756.

[140] Rice P, Drummond C. The Price of a Drink: The Potential of Alcohol Minimum Unit Pricing as a Public Health Measure in the UK. The British Journal of Psychiatry: The Journal of Mental Science. 2012 Sep;201(3):169–171.

[141] Sheron N, Chilcott F, Matthews L, Challoner B, Thomas M. Impact of Minimum Price per Unit of Alcohol on Patients with Liver Disease in the UK. Clinical Medicine (London, England). 2014 Aug;14(4):396–403.

[142] Holmes J, Meng Y, Meier PS, Brennan A, Angus C, Campbell-Burton A, et al. Effects of Minimum Unit Pricing for Alcohol on Different Income and Socioeconomic Groups: A Modelling Study. Lancet (London, England). 2014 May;383(9929):1655–1664.

[143] Gill J, Black H, Rush R, O'May F, Chick J. Heavy Drinkers and the Potential Impact of Minimum Unit Pricing-No Single or Simple Effect? Alcohol and Alcoholism (Oxford, Oxfordshire). 2017 Nov;52(6):722–729.

[144] Boniface S, Scannell JW, Marlow S. Evidence for the Effectiveness of Minimum Pricing of Alcohol: A Systematic Review and Assessment Using the Bradford Hill Criteria for Causality. BMJ open. 2017 Jun;7(5):e013497.

[145] Thomas-Meyer M, Mytton O, Adams J. Public Responses to Proposals for a Tax on Sugar-Sweetened Beverages: A Thematic Analysis of Online Reader Comments Posted on Major UK News Websites. PloS One. 2017;12(11):e0186750.

[146] Briggs ADM, Mytton OT, Kehlbacher A, Tiffin R, Rayner M, Scarborough P. Overall and Income Specific Effect on Prevalence of Overweight and Obesity of 20% Sugar Sweetened Drink Tax in UK: Econometric and Comparative Risk Assessment Modelling Study. BMJ (Clinical research ed). 2013 Oct;347:f6189.

[147] Briggs ADM, Mytton OT, Kehlbacher A, Tiffin R, Elhussein A, Rayner M, et al. Health Impact Assessment of the UK Soft Drinks Industry Levy: A Comparative Risk Assessment Modelling Study. The Lancet Public Health. 2017 Jan;2(1):e15–e22.

[148] Current UK NSC Recommendations;. https://legacyscreening.phe.org.uk/screening-recommendations.php.

[149] Matthews PC, Jeffery K, Klenerman P, Barnes E, Cooke G. Screening and Treatment for Hepatitis C: A Balanced Perspective. BMJ (Clinical research ed). 2015 Feb;350:h644.

[150] Hepatitis B Vaccine Overview; 31 Jul 2019, 10:37 a.m. https://www.nhs.uk/conditions/vaccinations/hepatitis-b-vaccine/.

[151] Nhsbt_organ_donor_strategy_summary.Pdf;. https://nhsbtdbe.blob.core.windows.net/umbraco-assets-corp/4241/nhsbt_organ_donor_strategy_summary.pdf.

[152] Odt-Organ-Utilisation-Strategy.Pdf;. https://nhsbtdbe.blob.core.windows.net/umbraco-assets-corp/3579/odt-organ-utilisation-strategy.pdf.

[153] Rithalia A, McDaid C, Suekarran S, Myers L, Sowden A. Impact of Presumed Consent for Organ Donation on Donation Rates: A Systematic Review. BMJ (Clinical research ed). 2009 Jan;338:a3162.

[154] Matesanz R, Marazuela R, Coll E, Mahíllo B, Domínguez-Gil B. About the Opt-Out System, Live Transplantation, and Information to the Public on Organ Donation in Spain ...

Y Olé! American Journal of Transplantation: Official Journal of the American Society of Transplantation and the American Society of Transplant Surgeons. 2017 Jun;17(6):1695–1696.

[155] Tot2020-Mid-Point-Review.Pdf;. https://nhsbtdbe.blob.core.windows.net/umbraco-assets-corp/7884/tot2020-mid-point-review.pdf.

[156] Busuttil RW, editor. Transplantation of the Liver. 3rd ed. Philadelphia, PA: Elsevier Saunders; 2015. OCLC: 931517082.

[157] Rana A, Hardy MA, Halazun KJ, Woodland DC, Ratner LE, Samstein B, et al. Survival Outcomes Following Liver Transplantation (SOFT) Score: A Novel Method to Predict Patient Survival Following Liver Transplantation. American Journal of Transplantation: Official Journal of the American Society of Transplantation and the American Society of Transplant Surgeons. 2008 Dec;8(12):2537–2546.

[158] Low PS, Bada JL, Somero GN. Temperature Adaptation of Enzymes: Roles of the Free Energy, the Enthalpy, and the Entropy of Activation. Proceedings of the National Academy of Sciences of the United States of America. 1973 Feb;70(2):430–432.

[159] Engerson TD, McKelvey TG, Rhyne DB, Boggio EB, Snyder SJ, Jones HP. Conversion of Xanthine Dehydrogenase to Oxidase in Ischemic Rat Tissues. The Journal of Clinical Investigation. 1987 Jun;79(6):1564–1570.

[160] Ikeda T, Yanaga K, Kishikawa K, Kakizoe S, Shimada M, Sugimachi K. Ischemic Injury in Liver Transplantation: Difference in Injury Sites between Warm and Cold Ischemia in Rats. Hepatology (Baltimore, Md). 1992 Aug;16(2):454–461.

[161] Jaeschke H, Bautista AP, Spolarics Z, Spitzer JJ. Superoxide Generation by Kupffer Cells and Priming of Neutrophils during Reperfusion after Hepatic Ischemia. Free Radical Research Communications. 1991;15(5):277–284.

[162] Tsung A, Klune JR, Zhang X, Jeyabalan G, Cao Z, Peng X, et al. HMGB1 Release Induced by Liver Ischemia Involves Toll-like Receptor 4 Dependent Reactive Oxygen Species Production and Calcium-Mediated Signaling. The Journal of Experimental Medicine. 2007 Nov;204(12):2913–2923.

[163] Leifeld L, Cheng S, Ramakers J, Dumoulin FL, Trautwein C, Sauerbruch T, et al. Imbalanced Intrahepatic Expression of Interleukin 12, Interferon Gamma, and Interleukin 10

in Fulminant Hepatitis B. Hepatology (Baltimore, Md). 2002 Oct;36(4 Pt 1):1001–1008.

[164] Hanschen M, Zahler S, Krombach F, Khandoga A. Reciprocal Activation between CD4+ T Cells and Kupffer Cells during Hepatic Ischemia-Reperfusion. Transplantation. 2008 Sep;86(5):710–718.

[165] Luedde T, Assmus U, Wüstefeld T, Meyer zu Vilsendorf A, Roskams T, Schmidt-Supprian M, et al. Deletion of IKK2 in Hepatocytes Does Not Sensitize These Cells to TNF-Induced Apoptosis but Protects from Ischemia/Reperfusion Injury. The Journal of Clinical Investigation. 2005 Apr;115(4):849–859.

[166] Colletti LM, Kunkel SL, Walz A, Burdick MD, Kunkel RG, Wilke CA, et al. Chemokine Expression during Hepatic Ischemia/Reperfusion-Induced Lung Injury in the Rat. The Role of Epithelial Neutrophil Activating Protein. The Journal of Clinical Investigation. 1995 Jan;95(1):134–141.

[167] Kuboki S, Shin T, Huber N, Eismann T, Galloway E, Schuster R, et al. Hepatocyte Signaling through CXC Chemokine Receptor-2 Is Detrimental to Liver Recovery after Ischemia/Reperfusion in Mice. Hepatology (Baltimore, Md). 2008 Oct;48(4):1213–1223.

[168] Granger DN, Kubes P. The Microcirculation and Inflammation: Modulation of Leukocyte-Endothelial Cell Adhesion. Journal of Leukocyte Biology. 1994 May;55(5):662–675.

[169] Hasegawa T, Malle E, Farhood A, Jaeschke H. Generation of Hypochlorite-Modified Proteins by Neutrophils during Ischemia-Reperfusion Injury in Rat Liver: Attenuation by Ischemic Preconditioning. American Journal of Physiology Gastrointestinal and Liver Physiology. 2005 Oct;289(4):G760–767.

[170] Weston CJ, Shepherd EL, Claridge LC, Rantakari P, Curbishley SM, Tomlinson JW, et al. Vascular Adhesion Protein-1 Promotes Liver Inflammation and Drives Hepatic Fibrosis. The Journal of Clinical Investigation. 2015 Feb;125(2):501–520.

[171] Ji SG, Juran BD, Mucha S, Folseraas T, Jostins L, Melum E, et al. Genome-Wide Association Study of Primary Sclerosing Cholangitis Identifies New Risk Loci and Quantifies the Genetic Relationship with Inflammatory Bowel Disease. Nature Genetics. 2017 Feb;49(2):269–273.

[172] Chung BK, Guevel BT, Reynolds GM, Gupta Udatha DBRK, Henriksen EKK, Stamataki Z, et al. Phenotyping and Auto-Antibody Production by Liver-Infiltrating B Cells in Primary Sclerosing Cholangitis and Primary Biliary Cholangitis. Journal of Autoimmunity. 2017 Feb;77:45–54.

[173] Patten DA, Kamarajah SK, Rose JM, Tickle J, Shepherd EL, Adams DH, et al. SCARF-1 Promotes Adhesion of CD4+ T Cells to Human Hepatic Sinusoidal Endothelium under Conditions of Shear Stress. Scientific Reports. 2017 Dec;7(1):17600.

[174] Jeffery HC, van Wilgenburg B, Kurioka A, Parekh K, Stirling K, Roberts S, et al. Biliary Epithelium and Liver B Cells Exposed to Bacteria Activate Intrahepatic MAIT Cells through MR1. Journal of Hepatology. 2016 May;64(5):1118–1127.

[175] Bhogal RH, Weston CJ, Curbishley SM, Adams DH, Afford SC. Activation of CD40 with Platelet Derived CD154 Promotes Reactive Oxygen Species Dependent Death of Human Hepatocytes during Hypoxia and Reoxygenation. PLoS ONE. 2012 Jan;7(1):e30867.

[176] King A, Houlihan DD, Kavanagh D, Haldar D, Luu N, Owen A, et al. Sphingosine-1-Phosphate Prevents Egress of Hematopoietic Stem Cells From Liver to Reduce Fibrosis. Gastroenterology. 2017 Jul;153(1):233–248.e16.

[177] Lu WY, Bird TG, Boulter L, Tsuchiya A, Cole AM, Hay T, et al. Hepatic Progenitor Cells of Biliary Origin with Liver Repopulation Capacity. Nature Cell Biology. 2015 Aug;17(8):971–983.

[178] Wang Y, Lanzoni G, Carpino G, Cui CB, Dominguez-Bendala J, Wauthier E, et al. Biliary Tree Stem Cells, Precursors to Pancreatic Committed Progenitors: Evidence for Possible Life-Long Pancreatic Organogenesis. Stem cells (Dayton, Ohio). 2013 Sep;31(9):1966–1979. 00001.

[179] Sampaziotis F, de Brito MC, Madrigal P, Bertero A, Saeb-Parsy K, Soares FAC, et al. Cholangiocytes Derived from Human Induced Pluripotent Stem Cells for Disease Modeling and Drug Validation. Nature Biotechnology. 2015 Aug;33(8):845–852.

[180] Wiggins BG, Aliazis K, Davies SP, Hirschfield G, Lalor PF, Reynolds G, et al. In Vitro and Ex Vivo Models to Study T Cell Migration Through the Human Liver Parenchyma. Methods in Molecular Biology (Clifton, NJ). 2017;1591:195–214.

[181] Sampaziotis F, Justin AW, Tysoe OC, Sawiak S, Godfrey EM, Upponi SS, et al. Reconstruction of the Mouse Extrahepatic Biliary Tree Using Primary Human Extrahepatic Cholangiocyte Organoids. Nature Medicine. 2017 Aug;23(8):954–963.

[182] Dunn WB, Broadhurst D, Brown M, Baker PN, Redman CWG, Kenny LC, et al. Metabolic Profiling of Serum Using Ultra Performance Liquid Chromatography and the LTQ-Orbitrap Mass Spectrometry System. Journal of Chromatography B. 2008 Aug;871(2):288–298.

[183] Mallick P, Kuster B. Proteomics: A Pragmatic Perspective. Nature Biotechnology. 2010 Jul;28(7):695.

[184] Bajaj JS, Heuman DM, Sanyal AJ, Hylemon PB, Sterling RK, Stravitz RT, et al. Modulation of the Metabiome by Rifaximin in Patients with Cirrhosis and Minimal Hepatic Encephalopathy. PloS One. 2013;8(4):e60042.

[185] Stiuso P, Scognamiglio I, Murolo M, Ferranti P, De Simone C, Rizzo MR, et al. Serum Oxidative Stress Markers and Lipidomic Profile to Detect NASH Patients Responsive to an Antioxidant Treatment: A Pilot Study. Oxidative Medicine and Cellular Longevity. 2014;2014:169216.

[186] Dong S, Zhan ZY, Cao HY, Wu C, Bian YQ, Li JY, et al. Urinary Metabolomics Analysis Identifies Key Biomarkers of Different Stages of Nonalcoholic Fatty Liver Disease. World Journal of Gastroenterology. 2017 Apr;23(15):2771–2784.

[187] Mindikoglu AL, Opekun AR, Putluri N, Devaraj S, Sheikh-Hamad D, Vierling JM, et al. Unique Metabolomic Signature Associated with Hepatorenal Dysfunction and Mortality in Cirrhosis. Translational Research: The Journal of Laboratory and Clinical Medicine. 2018 May;195:25–47.

[188] He T. Implementation of Proteomics in Clinical Trials. Proteomics Clinical Applications. 2019 Mar;13(2):e1800198.

[189] Argilés Á, Siwy J, Duranton F, Gayrard N, Dakna M, Lundin U, et al. CKD273, a New Proteomics Classifier Assessing CKD and Its Prognosis. PloS One. 2013;8(5):e62837.

[190] Kuznetsova T, Mischak H, Mullen W, Staessen JA. Urinary Proteome Analysis in Hypertensive Patients with Left Ventricular Diastolic Dysfunction. European Heart Journal. 2012 Sep;33(18):2342–2350.

[191] Gatto L, Breckels LM, Naake T, Gibb S. Visualization of Proteomics Data Using R and Bioconductor. Proteomics. 2015 Apr;15(8):1375–1389.

[192] Zhang J, Liang R, Wei J, Ye J, He Q, ChunlingYuan n, et al. Identification of Candidate Biomarkers in Malignant Ascites from Patients with Hepatocellular Carcinoma by iTRAQ-Based Quantitative Proteomic Analysis. BioMed Research International. 2018;2018:5484976.

[193] Yeh CC, Hsu CH, Shao YY, Ho WC, Tsai MH, Feng WC, et al. Integrated Stable Isotope Labeling by Amino Acids in Cell Culture (SILAC) and Isobaric Tags for Relative and Absolute Quantitation (iTRAQ) Quantitative Proteomic Analysis Identifies Galectin-1 as a Potential Biomarker for Predicting Sorafenib Resistance in Liver Cancer. Molecular & cellular proteomics: MCP. 2015 Jun;14(6):1527–1545.

[194] Shi Y, Deng X, Zhan Q, Shen B, Jin X, Zhu Z, et al. A Prospective Proteomic-Based Study for Identifying Potential Biomarkers for the Diagnosis of Cholangiocarcinoma. Journal of Gastrointestinal Surgery: Official Journal of the Society for Surgery of the Alimentary Tract. 2013 Sep;17(9):1584–1591.

[195] Morofuji N, Ojima H, Onaya H, Okusaka T, Shimada K, Sakamoto Y, et al. Macrophage-Capping Protein as a Tissue Biomarker for Prediction of Response to Gemcitabine Treatment and Prognosis in Cholangiocarcinoma. Journal of Proteomics. 2012 Feb;75(5):1577–1589.

[196] Devitt EJ, Power KA, Lawless MW, Browne JA, Gaora PO, Gallagher WM, et al. Early Proteomic Analysis May Allow Noninvasive Identification of Hepatitis C Response to Treatment with Pegylated Interferon α-2b and Ribavirin. European Journal of Gastroenterology & Hepatology. 2011 Feb;23(2):177–183.

[197] Elaffandi AH, Bonney GK, Gunson B, Scalera I, Mergental H, Isaac JR, et al. Increasing the Donor Pool: Consideration of Prehospital Cardiac Arrest in Controlled Donation After Circulatory Death for Liver Transplantation: Increasing the Donor Pool. Liver Transplantation. 2014 Jan;20(1):63–71. 00003.

[198] Perera MTPR, Richards DA, Silva MA, Ahmed N, Neil DA, Murphy N, et al. Comparison of Energy Metabolism in Liver Grafts from Donors after Circulatory Death and Donors after Brain Death during Cold Storage and Reperfusion. The British Journal of Surgery. 2014 Jun;101(7):775–783.

[199] Guarrera JV, Estevez J, Boykin J, Boyce R, Rashid J, Sun S, et al. Hypothermic Machine Perfusion of Liver Grafts for Transplantation: Technical Development in Human Discard and Miniature Swine Models. Transplantation Proceedings. 2005 Jan;37(1):323–325.

[200] Dutkowski P, Schlegel A, de Oliveira M, Müllhaupt B, Neff F, Clavien PA. HOPE for Human Liver Grafts Obtained from Donors after Cardiac Death. Journal of Hepatology. 2014 Apr;60(4):765–772. 00025.

[201] Ravikumar R, Leuvenink H, Friend PJ. Normothermic Liver Preservation: A New Paradigm? Transplant International. 2015 Apr;p. n/a–n/a.

[202] op den Dries S, Karimian N, Weeder PD, Porte RJ. Normothermic Acellular Machine Perfusion and Bile Duct Injury in Pig Livers Retrieved After Cardiac Death. American Journal of Transplantation. 2013 Dec;13(12):3289–3289.

[203] NHSBT - Organ Donation - Monthly Statistics;. http://www.organdonation.nhs.uk/ukt/statistics/latest_statistics/monthly.jsp.

[204] O'Neill S, Roebuck A, Khoo E, Wigmore SJ, Harrison EM. A Meta-Analysis and Meta-Regression of Outcomes Including Biliary Complications in Donation after Cardiac Death Liver Transplantation. Transplant International. 2014 Nov;27(11):1159–1174. 00002.

[205] Sakamoto S, Nakazawa A, Shigeta T, Uchida H, Kanazawa H, Fukuda A, et al. Devastating Outflow Obstruction after Pediatric Split Liver Transplantation: **Outflow Obstruction after Pediatric LT**. Pediatric Transplantation. 2013 Feb;17(1):E25–E28.

[206] Imber CJ, St Peter SD, Cenarruzabeitia D, Lopez I, Lemonde H, Rees M, et al. Optimisation of Bile Production during Normothermic Preservation of Porcine Livers. American Journal of Transplantation. 2002;2(7):593–599. 00030.

[207] Ali JM, Davies SE, Brais RJ, Randle LV, Klinck JR, Allison MED, et al. Analysis of Ischemia/Reperfusion Injury in Time-Zero Biopsies Predicts Liver Allograft Outcomes: Time-Zero Liver Transplant Biopsy IRI. Liver Transplantation. 2015 Apr;21(4):487–499. 00000.

[208] Briceño J, Ciria R, de la Mata M, Rufián S, López-Cillero P. Prediction of Graft Dysfunction Based on Extended Criteria Donors in the Model for End-Stage Liver Disease Score Era. Transplantation. 2010 Sep;90(5):530–539. 00037.

[209] Tariciotti L, Rocha C, Perera MTPR, Gunson BK, Bramhall SR, Isaac J, et al. Is It Time to Extend Liver Acceptance Criteria for Controlled Donors after Cardiac Death? Transplantation. 2011 Nov;92(10):1140–1146. 00013.

[210] Vogel T, Brockmann JG, Coussios C, Friend PJ. The Role of Normothermic Extracorporeal Perfusion in Minimizing Ischemia Reperfusion Injury. Transplantation Reviews. 2012 Apr;26(2):156–162. 00034.

[211] Fondevila C, Hessheimer AJ, Maathuis MHJ, Muñoz J, Taurá P, Calatayud D, et al. Superior Preservation of DCD Livers with Continuous Normothermic Perfusion. Annals of Surgery. 2011 Dec;254(6):1000–1007. 00080.

[212] Serviddio G, Bellanti F, Tamborra R, Rollo T, Capitanio N, Romano AD, et al. Uncoupling Protein-2 (UCP2) Induces Mitochondrial Proton Leak and Increases Susceptibility of Non-Alcoholic Steatohepatitis (NASH) Liver to Ischaemia-Reperfusion Injury. Gut. 2008 Jul;57(7):957–965.

[213] Ruiz-Ramírez A, Chávez-Salgado M, Peñeda-Flores JA, Zapata E, Masso F, El-Hafidi M. High-Sucrose Diet Increases ROS Generation, FFA Accumulation, UCP2 Level, and Proton Leak in Liver Mitochondria. American Journal of Physiology Endocrinology and Metabolism. 2011 Dec;301(6):E1198–1207.

[214] Schindelin J, Arganda-Carreras I, Frise E, Kaynig V, Longair M, Pietzsch T, et al. Fiji: An Open-Source Platform for Biological-Image Analysis. Nature Methods. 2012 Jun;9(7):676–682.

[215] Ruifrok AC, Johnston DA. Quantification of Histochemical Staining by Color Deconvolution. Analytical and Quantitative Cytology and Histology. 2001 Aug;23(4):291–299.

[216] Picture Thresholding Using an Iterative Selection Method. IEEE Transactions on Systems, Man, and Cybernetics. 1978 Aug;8(8):630–632.

[217] Marzella L, Yu Q, Mergner W, Trump BF. Unbuffered Osmium Staining of Cell Organelles: Alterations Induced by Cell Injury. Virchows Archiv B, Cell Pathology Including Molecular Pathology. 1984;45(3):273–287.

[218] Yoshizumi T, Gondolesi GE, Bodian CA, Jeon H, Schwartz ME, Fishbein TM, et al. A Simple New Formula to Assess Liver Weight. Transplantation Proceedings. 2003 Jun;35(4):1415–1420.

[219] Team RC. R: A Language and Environment for Statistical Computing. Vienna, Austria; 2017. R Foundation for Statistical Computing.

[220] Kaufman L, Rousseeuw P. Finding Groups in Data: An Introduction To Cluster Analysis; 1990.

[221] version) JPS, to 2007) DBu, to 2002) SDu, to 2005) DSu, authors (src/rs f) E, fixed sigma) SHA, et al.. Nlme: Linear and Nonlinear Mixed Effects Models; 2017.

[222] St Peter SD, Imber CJ, Lopez I, Hughes D, Friend PJ. Extended Preservation of Non-Heart-Beating Donor Livers with Normothermic Machine Perfusion. British journal of surgery. 2002;89(5):609–616. 00128.

[223] Barle H, Nyberg B, Essén P, Andersson K, McNurlan MA, Wernerman J, et al. The Synthesis Rates of Total Liver Protein and Plasma Albumin Determined Simultaneously in Vivo in Humans. Hepatology (Baltimore, Md). 1997 Jan;25(1):154–158.

[224] Mergental H, Perera MTPR, Laing RW, Muiesan P, Isaac JR, Smith A, et al. Transplantation of Declined Liver Allografts Following Normothermic *Ex-Situ* Evaluation. American Journal of Transplantation. 2016 Jul;.

[225] Faitot F, Besch C, Battini S, Ruhland E, Onea M, Addeo P, et al. Impact of Real-Time Metabolomics in Liver Transplantation: Graft Evaluation and Donor-Recipient Matching. Journal of Hepatology. 2018 Apr;68(4):699–706.

[226] Sutton ME, op den Dries S, Karimian N, Weeder PD, de Boer MT, Wiersema-Buist J, et al. Criteria for Viability Assessment of Discarded Human Donor Livers during Ex Vivo Normothermic Machine Perfusion. PLoS ONE. 2014 Nov;9(11):e110642.

[227] Watson CJE, Kosmoliaptsis V, Randle LV, Gimson AE, Brais R, Klinck JR, et al. Normothermic Perfusion in the Assessment and Preservation of Declined Livers Before Transplantation: Hyperoxia and Vasoplegia-Important Lessons From the First 12 Cases. Transplantation. 2017 May;101(5):1084–1098.

[228] Liu Q, Nassar A, Buccini L, Iuppa G, Soliman B, Pezzati D, et al. Lipid Metabolism and Functional Assessment of Discarded Human Livers with Steatosis Undergoing 24 Hours of Normothermic Machine Perfusion. Liver Transplantation: Official Publication of the American Association for the Study of Liver Diseases and the International Liver Transplantation Society. 2018 Feb;24(2):233–245.

[229] Nath J, Smith T, Hollis A, Ebbs S, Canbilen SW, Tennant DA, et al. (13)C Glucose Labelling Studies Using 2D NMR Are a Useful Tool for Determining Ex Vivo Whole Organ Metabolism during Hypothermic Machine Perfusion of Kidneys. Transplantation Research. 2016;5:7.

[230] Weeder PD, van Rijn R, Porte RJ. Machine Perfusion in Liver Transplantation as a Tool to Prevent Non-Anastomotic Biliary Strictures: Rationale, Current Evidence and Future Directions. Journal of Hepatology. 2015 Mar;.

[231] Guarrera JV, Henry SD, Samstein B, Odeh-Ramadan R, Kinkhabwala M, Goldstein MJ, et al. Hypothermic Machine Preservation in Human Liver Transplantation: The First Clinical Series. American Journal of Transplantation. 2010 Feb;10(2):372–381. 00175.

[232] Henry SD, Nachber E, Tulipan J, Stone J, Bae C, Reznik L, et al. Hypothermic Machine Preservation Reduces Molecular Markers of Ischemia/Reperfusion Injury in Human Liver Transplantation: Liver Machine Perfusion Reduces Ischemia/Reperfusion Injury. American Journal of Transplantation. 2012 Sep;12(9):2477–2486.

[233] Guarrera JV, Henry SD, Samstein B, Reznik E, Musat C, Lukose TI, et al. Hypothermic Machine Preservation Facilitates Successful Transplantation of "Orphan" Extended Criteria Donor Livers: Machine Preservation of ECD Livers. American Journal of Transplantation. 2015 Jan;15(1):161–169. 00000.

[234] Stegemann J, Hirner A, Rauen U, Minor T. Use of a New Modified HTK Solution for Machine Preservation of Marginal Liver Grafts. Journal of Surgical Research. 2010 May;160(1):155–162.

[235] Dutkowski P, Furrer K, Tian Y, Graf R, Clavien PA. Novel Short-Term Hypothermic Oxygenated Perfusion (HOPE) System Prevents Injury in Rat Liver Graft From Non-Heart Beating Donor:. Annals of Surgery. 2006 Dec;244(6):968–977. 00087.

[236] Bae C, Pichardo EM, Huang H, Henry SD, Guarrera JV. The Benefits of Hypothermic Machine Perfusion Are Enhanced With Vasosol and α-Tocopherol in Rodent Donation After Cardiac Death Livers. Transplantation Proceedings. 2014 Jun;46(5):1560–1566.

[237] Lüer B, Koetting M, Efferz P, Minor T. Role of Oxygen during Hypothermic Machine Perfusion Preservation of the Liver. Transplant International. 2010 Feb;.

[238] Graham JA, Guarrera JV. "Resuscitation" of Marginal Liver Allografts for Transplantation with Machine Perfusion Technology. Journal of hepatology. 2014;61(2):418–431. 00010.

[239] Tolboom H, Milwid JM, Izamis ML, Uygun K, Berthiaume F, Yarmush ML. Sequential Cold Storage and Normothermic Perfusion of the Ischemic Rat Liver. Transplantation Proceedings. 2008 Jun;40(5):1306–1309.

[240] Boehnert MU, Yeung JC, Bazerbachi F, Knaak JM, Selzner N, McGilvray ID, et al. Normothermic Acellular Ex Vivo Liver Perfusion Reduces Liver and Bile Duct Injury of Pig Livers Retrieved after Cardiac Death. American Journal of Transplantation. 2013;13(6):1441–1449.

[241] Bruinsma BG, Yeh H, Özer S, Martins PN, Farmer A, Wu W, et al. Subnormothermic Machine Perfusion for *Ex Vivo* Preservation and Recovery of the Human Liver for Transplantation: Subnormothermic Machine Perfusion of Human Livers. American Journal of Transplantation. 2014 Jun;14(6):1400–1409. 00000.

[242] Fontes P, Lopez R, van der Plaats A, Vodovotz Y, Minervini M, Scott V, et al. Liver Preservation With Machine Perfusion and a Newly Developed Cell-Free Oxygen Carrier Solution Under Subnormothermic Conditions: MP at 21°C With an Oxygen Carrier Solution. American Journal of Transplantation. 2015 Feb;15(2):381–394. 00000.

[243] Serkova NJ, Zhang Y, Coatney JL, Hunter L, Wachs ME, Niemann CU, et al. Early Detection of Graft Failure Using the Blood Metabolic Profile of a Liver Recipient. Transplantation. 2007 Feb;83(4):517–521.

[244] Perera MTPR, Higdon R, Richards DA, Silva MA, Murphy N, Kolker E, et al. Biomarker Differences between Cadaveric Grafts Used in Human Orthotopic Liver Transplantation as Identified by Coulometric Electrochemical Array Detection (CEAD) Metabolomics. Omics: A Journal of Integrative Biology. 2014 Dec;18(12):767–777.

[245] Hrydziuszko O, Perera MTPR, Laing R, Kirwan J, Silva MA, Richards DA, et al. Mass Spectrometry Based Metabolomics Comparison of Liver Grafts from Donors after Circulatory Death (DCD) and Donors after Brain Death (DBD) Used in Human Orthotopic Liver Transplantation. PloS One. 2016;11(11):e0165884.

[246] Guy AJ, Nath J, Cobbold M, Ludwig C, Tennant DA, Inston NG, et al. Metabolomic Analysis of Perfusate during Hypothermic Machine Perfusion of Human Cadaveric Kidneys. Transplantation. 2015 Apr;99(4):754–759.

[247] Nath J, Guy A, Smith TB, Cobbold M, Inston NG, Hodson J, et al. Metabolomic Perfusate Analysis during Kidney Machine Perfusion: The Pig Provides an Appropriate Model for Human Studies. PloS One. 2014;9(12):e114818.

[248] Bruinsma BG, Sridharan GV, Weeder PD, Avruch JH, Saeidi N, Özer S, et al. Metabolic Profiling during Ex Vivo Machine Perfusion of the Human Liver. Scientific Reports. 2016 Mar;6:22415.

[249] van der Zwan M, Hesselink DA, Clahsen-van Groningen MC, Baan CC. Targeted Proteomic Analysis Detects Acute T Cell-Mediated Kidney Allograft Rejection in Belatacept-Treated Patients. Therapeutic Drug Monitoring. 2019 Apr;41(2):243–248.

[250] Pérez V, Navarro-Muñoz M, Mas S, Bayés B, Pastor MC, Martínez-Cáceres E, et al. Proteomic Approach to the Study of Statin Pleiotropy in Kidney Transplant Patients. Pharmacology. 2011;87(3-4):161–168.

[251] Vascotto C, Cesaratto L, D'Ambrosio C, Scaloni A, Avellini C, Paron I, et al. Proteomic Analysis of Liver Tissues Subjected to Early Ischemia/Reperfusion Injury during Human Orthotopic Liver Transplantation. Proteomics. 2006 Jun;6(11):3455–3465.

[252] Emadali A, Muscatelli-Groux B, Delom F, Jenna S, Boismenu D, Sacks DB, et al. Proteomic Analysis of Ischemia-Reperfusion Injury upon Human Liver Transplantation Reveals the Protective Role of IQGAP1. Molecular & cellular proteomics: MCP. 2006 Jul;5(7):1300–1313.

[253] Kornasiewicz O, Bojarczuk K, Bugajski M, Golab J, Krawczyk M. Application of a Proteomic Approach to Identify Proteins Associated with Primary Graft Non-Function after Liver Transplantation. International Journal of Molecular Medicine. 2012 Oct;30(4):755–764.

[254] Milongo D, Bascands JL, Huart A, Esposito L, Breuil B, Moulos P, et al. Pretransplant Urinary Proteome Analysis Does Not Predict Development of Chronic Kidney Disease after Liver Transplantation. Liver International: Official Journal of the International Association for the Study of the Liver. 2015 Jul;35(7):1893–1901.

[255] Diamond DL, Krasnoselsky AL, Burnum KE, Monroe ME, Webb-Robertson BJ, McDermott JE, et al. Proteome and Computational Analyses Reveal New Insights into the Mechanisms of Hepatitis C Virus-Mediated Liver Disease Posttransplantation. Hepatology (Baltimore, Md). 2012 Jul;56(1):28–38.

[256] Christians U, Klawitter J, Klawitter J. Biomarkers in Transplantation–Proteomics and Metabolomics. Therapeutic Drug Monitoring. 2016 Apr;38 Suppl 1:S70–74.

[257] Brown M, Wedge DC, Goodacre R, Kell DB, Baker PN, Kenny LC, et al. Automated Workflows for Accurate Mass-Based Putative Metabolite Identification in LC/MS-Derived Metabolomic Datasets. Bioinformatics. 2011 Apr;27(8):1108–1112.

[258] Szklarczyk D, Franceschini A, Wyder S, Forslund K, Heller D, Huerta-Cepas J, et al. STRING V10: Protein–Protein Interaction Networks, Integrated over the Tree of Life. Nucleic Acids Research. 2015 Jan;43(Database issue):D447–D452.

[259] The MicroArray Quality Control (MAQC)-II Study of Common Practices for the Development and Validation of Microarray-Based Predictive Models. Nature Biotechnology. 2010 Aug;28(8):827–838.

[260] Neilson KA, Ali NA, Muralidharan S, Mirzaei M, Mariani M, Assadourian G, et al. Less Label, More Free: Approaches in Label-Free Quantitative Mass Spectrometry. PROTEOMICS. 2011 Feb;11(4):535–553.

[261] Lindemann C, Thomanek N, Hundt F, Lerari T, Meyer HE, Wolters D, et al. Strategies in Relative and Absolute Quantitative Mass Spectrometry Based Proteomics. Biological Chemistry. 2017 Jan;398(5-6):687–699.

[262] Genolini C. A (Not So) Short Introduction to S4; 2008.

[263] Gregori J, Sanchez A, Villanueva J. msmsTests: LC-MS/MS Differential Expression Tests; 2013. R package version 1.14.0.

[264] Robinson MD, McCarthy DJ, Smyth GK. edgeR: A Bioconductor Package for Differential Expression Analysis of Digital Gene Expression Data. Bioinformatics. 2010 Jan;26(1):139–140.

[265] Stern S, Rice J, Philbin N, McGwin G, Arnaud F, Johnson T, et al. Resuscitation with the Hemoglobin-Based Oxygen Carrier, HBOC-201, in a Swine Model of Severe Uncontrolled Hemorrhage and Traumatic Brain Injury. Shock (Augusta, Ga). 2009 Jan;31(1):64–79.

[266] Manning JE, Katz LM, Brownstein MR, Pearce LB, Gawryl MS, Baker CC. Bovine Hemoglobin-Based Oxygen Carrier (HBOC-201) for Resuscitation of Uncontrolled, Exsanguinating Liver Injury in Swine. Carolina Resuscitation Research Group. Shock (Augusta, Ga). 2000 Feb;13(2):152–159.

[267] McNeil CJ, Smith LD, Jenkins LD, York MG, Josephs MJ. Hypotensive Resuscitation Using a Polymerized Bovine Hemoglobin-Based Oxygen-Carrying Solution (HBOC-201) Leads to Reversal of Anaerobic Metabolism. The Journal of Trauma. 2001 Jun;50(6):1063–1075.

[268] Natanson C. Incomplete Financial Disclosure in a Study of Cell-Free Hemoglobin-Based Blood Substitutes and Risks of Myocardial Infarction and Death. JAMA. 2008 Sep;300(11):1300.

[269] Van Hemelrijck J, Levien LJ, Veeckman L, Pitman A, Zafirelis Z, Standl T. A Safety and Efficacy Evaluation of Hemoglobin-Based Oxygen Carrier HBOC-201 in a Randomized, Multicenter Red Blood Cell Controlled Trial in Noncardiac Surgery Patients. Anesthesia and Analgesia. 2014 Oct;119(4):766–776.

[270] Katz LM, Manning JE, McCurdy S, Pearce LB, Gawryl MS, Wang Y, et al. HBOC-201 Improves Survival in a Swine Model of Hemorrhagic Shock and Liver Injury. Resuscitation. 2002 Jul;54(1):77–87.

[271] Zapletal C, Bode A, Lorenz MW, Gebhard MM, Golling M. Effects of Hemodilution with a Hemoglobin-Based Oxygen Carrier (HBOC-201) on Ischemia/Reperfusion Injury in a Model of Partial Warm Liver Ischemia of the Rat. Microvascular Research. 2009 Dec;78(3):386–392.

[272] Zambelli M, Andorno E, De Carlis L, Rossi G, Cillo U, De Feo T, et al. Full-Right-Full-Left Split Liver Transplantation: The Retrospective Analysis of an Early Multicenter Experience Including Graft Sharing: **Full-Right-Full-Left SLT**. American Journal of Transplantation. 2012 Aug;12(8):2198–2210.

[273] Perera T, Mergental H, Stephenson B, Roll GR, Cilliers H, Liang R, et al. First Human Liver Transplantation Using a Marginal Allograft Resuscitated by Normothermic Machine Perfusion. Liver Transplantation. 2016 Jan;22(1):120–124.

[274] Brockmann JG, Vogel T, Coussios C, Friend PJ. Liver Splitting during Normothermic Organ Preservation: Liver Splitting During Normothermic Organ Preservation. Liver Transplantation. 2017 May;23(5):701–706.

[275] Feng SLY, Guo Y, Factor VM, Thorgeirsson SS, Bell DW, Testa JR, et al. The Fn14 Immediate-Early Response Gene Is Induced during Liver Regeneration and Highly Expressed in Both Human and Murine Hepatocellular Carcinomas. American Journal of Pathology. 2000;156(4):1253.

[276] Yovchev MI, Grozdanov PN, Zhou H, Racherla H, Guha C, Dabeva MD. Identification of Adult Hepatic Progenitor Cells Capable of Repopulating Injured Rat Liver. Hepatology. 2008 Feb;47(2):636–647.

[277] Qiu Q, Hernandez JC, Dean AM, Rao P, Darlington G. CD24 Positive Cells from Normal Adult Mouse Liver Are Hepatocyte Progenitor Cells. Stem Cells and Development. 2011 Mar;.

[278] Wilhelm A, Shepherd EL, Amatucci A, Munir M, Reynolds G, Humphreys E, et al. Interaction of TWEAK with Fn14 Leads to the Progression of Fibrotic Liver Disease by Directly Modulating Hepatic Stellate Cell Proliferation: TWEAK as a Regulator of Liver Fibrogenesis. The Journal of Pathology. 2016 May;239(1):109–121.

[279] Wang S, Jiang W, Chen X, Zhang C, Li H, Hou W, et al. Alpha-Fetoprotein Acts as a Novel Signal Molecule and Mediates Transcription of Fn14 in Human Hepatocellular Carcinoma. Journal of Hepatology. 2012 Apr;.

[280] Affo S, Dominguez M, Lozano JJ, Sancho-Bru P, Rodrigo-Torres D, Morales-Ibanez O, et al. Transcriptome Analysis Identifies TNF Superfamily Receptors as Potential Therapeutic Targets in Alcoholic Hepatitis. Gut. 2012 May;.

[281] Schnabl B, Brenner DA. Fibroblast Growth Factor Inducible 14 as Potential Target in Patients with Alcoholic Hepatitis. Gut. 2012 Jun;.

[282] Kawakita T, Shiraki K, Yamanaka Y, Yamaguchi Y, Saitou Y, Enokimura N, et al. Functional Expression of TWEAK in Human Hepatocellular Carcinoma: Possible Implication in Cell Proliferation and Tumor Angiogenesis. Biochemical and Biophysical Research Communications. 2004 Jun;318(3):726–733.

[283] Yovchev MI, Zhang J, Neufeld DS, Grozdanov PN, Dabeva MD. Thymus Cell Antigen-1-expressing Cells in the Oval Cell Compartment. Hepatology. 2009 Aug;50(2):601–611.

[284] Thomas JA, Pope C, Wojtacha D, Robson AJ, Gordon-Walker TT, Hartland S, et al. Macrophage Therapy for Murine Liver Fibrosis Recruits Host Effector Cells Improving Fibrosis, Regeneration and Function. Hepatology (Baltimore, Md). 2011 Mar;Cited by 0043.

[285] Nussler AK, Vergani G, Gollin SM, Dorko K, Morris SM Jr, Demetris AJ, et al. Isolation and Characterization of a Human Hepatic Epithelial-like Cell Line (AKN-1) from a Normal Liver. In Vitro Cellular & Developmental Biology Animal. 1999 Apr;35(4):190–197. Cited by 0022.

[286] Shimizu Y, Demetris AJ, Gollin SM, Storto PD, Bedford HM, Altarac S, et al. Two New Human Cholangiocarcinoma Cell Lines and Their Cytogenetics and Responses to Growth Factors, Hormones, Cytokines or Immunologic Effector Cells. International journal of cancer Journal international du cancer. 1992 Sep;52(2):252–260.

[287] Lennicke C, Rahn J, Lichtenfels R, Wessjohann LA, Seliger B. Hydrogen Peroxide - Production, Fate and Role in Redox Signaling of Tumor Cells. Cell communication and signaling: CCS. 2015 Sep;13:39.

[288] Nemade H, Chaudhari U, Acharya A, Hescheler J, Hengstler JG, Papadopoulos S, et al. Cell Death Mechanisms of the Anti-Cancer Drug Etoposide on Human Cardiomyocytes Isolated from Pluripotent Stem Cells. Archives of Toxicology. 2018 Apr;92(4):1507–1524.

[289] Karaca G, Xie G, Moylan C, Swiderska-Syn M, Guy CD, Krüger L, et al. Role of Fn14 in Acute Alcoholic Steatohepatitis in Mice. American Journal of Physiology - Gastrointestinal and Liver Physiology. 2015 Feb;308(4):G325–G334.

[290] Tirnitz-Parker JE, Olynyk JK, Ramm GA. Role of TWEAK in Coregulating Liver Progenitor Cell and Fibrogenic Responses. Hepatology. 2014;59(3):1198–1201.

[291] Hung PJ, Lee PJ, Sabounchi P, Lin R, Lee LP. Continuous Perfusion Microfluidic Cell Culture Array for High-Throughput Cell-Based Assays. Biotechnology and Bioengineering. 2005 Jan;89(1):1–8.

[292] Kimura H, Sakai Y, Fujii T. Organ/Body-on-a-Chip Based on Microfluidic Technology for Drug Discovery. Drug Metabolism and Pharmacokinetics. 2018 Feb;33(1):43–48.

[293] Marshall LE, Goliwas KF, Miller LM, Penman AD, Frost AR, Berry JL. Flow-Perfusion Bioreactor System for Engineered Breast Cancer Surrogates to Be Used in Preclinical Testing: Flow-Perfusion Bioreactor System for Engineered Breast Cancer Surrogates. Journal of Tissue Engineering and Regenerative Medicine. 2017 Apr;11(4):1242–1250.

[294] Astolfi M, Péant B, Lateef MA, Rousset N, Kendall-Dupont J, Carmona E, et al. Micro-Dissected Tumor Tissues on Chip: An Ex Vivo Method for Drug Testing and Personalized Therapy. Lab on a Chip. 2016;16(2):312–325.

[295] Knowlton S, Tasoglu S. A Bioprinted Liver-on-a-Chip for Drug Screening Applications. Trends in Biotechnology. 2016 Sep;34(9):681–682.

[296] Zeilinger K, Schreiter T, Darnell M, Söderdahl T, Lübberstedt M, Dillner B, et al. Scaling Down of a Clinical Three-Dimensional Perfusion Multicompartment Hollow Fiber Liver Bioreactor Developed for Extracorporeal Liver Support to an Analytical Scale Device Useful for Hepatic Pharmacological *In Vitro* Studies. Tissue Engineering Part C: Methods. 2011 May;17(5):549–556.

[297] Vernetti LA, Senutovitch N, Boltz R, DeBiasio R, Ying Shun T, Gough A, et al. A Human Liver Microphysiology Platform for Investigating Physiology, Drug Safety, and Disease Models. Experimental Biology and Medicine. 2016 Jan;241(1):101–114.

[298] van Midwoud PM, Verpoorte E, Groothuis GMM. Microfluidic Devices for in Vitro Studies on Liver Drug Metabolism and Toxicity. Integrative Biology. 2011;3(5):509.

[299] van der Loos CM. Multiple Immunoenzyme Staining: Methods and Visualizations for the Observation with Spectral Imaging. Journal of Histochemistry & Cytochemistry. 2008;56(4):313–328.

[300] van der Loos CM. Chromogens in Multiple Immunohistochemical Staining Used for Visual Assessment and Spectral Imaging: The Colorful Future. Journal of Histotechnology. 2010;33(1):31–40. 00015.

'One learns three axioms during research: The subject to which you are fundamentally dedicating intellectual perseverence; oneself as the conduit of this endeavour, in particular one's resilience and self-determination; chiefly, you learn the most about other people.'

— Barney Stephenson, December 2017

'Illegitimis non carborundum.'

— Anon, during The Great War